9-4-2012

Shallow Thrust and Outer Rise Earthquakes in Northwestern Pacific Subduction Zones and their Role in Subduction Zone Water Budgets with Special Focus on the Mariana Islands

Erica Lynn Emry
Washington University in St. Louis

WASHINGTON UNIVERSITY IN ST. LOUIS

Department of Earth and Planetary Sciences

Dissertation Examination Committee:
Douglas A. Wiens, chair
Philip V. Bayly
Philip Skemer
Viatcheslav S. Solomatov
Linda A. Warren
Michael E. Wysession

Shallow Thrust and Outer Rise Earthquakes in Northwestern Pacific Subduction Zones and their Role in Subduction Zone Water Budgets with Special Focus on the Mariana Islands

by

Erica L. Emry

A dissertation presented to the
Graduate School of Arts and Sciences
of Washington University in
partial fulfillment of the
requirements for the degree
of Doctor of Philosophy

August 2012
Saint Louis, Missouri

ABSTRACT OF THE DISSERTATION

Shallow Thrust and Outer Rise Earthquakes in Northwestern
Pacific Subduction Zones and their Role in Subduction Zone Water Budgets
with Special Focus on the Mariana Islands

by

Erica Lynn Emry

Doctor of Philosophy in Earth and Planetary Sciences

Washington University in St. Louis, 2012

Professor Douglas Wiens, Chairman

This dissertation utilizes accurate earthquake locations and focal mechanisms to examine two distinct regions within shallow subduction zones: the shallow plate interface and the subduction zone trench and outer rise. In particular, I focus on the shallow plate interface and outer rise of the Mariana Subduction Zone and then expand the focus to examine the outer rise at other Northern and Western Pacific Subduction Zones. By understanding where earthquakes occur in these regions, we hope to obtain a better understanding of the cycling of water through subduction zones, mineralogical changes in the presence of water, and the effects of water and hydrous minerals on faulting processes within the shallow subduction zone. The first project is focused on the Northern Mariana shallow plate interface and reveals that small plate interface earthquakes occur at greater depths than previously thought. I show that the earthquake magnitude varies with depth, which may reveal varying conditions of stress, hydration, structure, or mineralogy along the fault. For the second and third projects, I focus on the subduction outer

rise; at this setting, extensional earthquakes near the top of the bending, incoming oceanic plate are thought to provide pathways for water to enter and hydrate the plate. The stresses within the plate may also be impacted by locking along the subduction plate interface. At the Mariana subduction zone, I observe differences in stress distributions within the incoming plate between the Southern and Central regions; this difference may be related to greater locking along the Southern Mariana plate interface. Our results for the Northern and Western Pacific show that extensional outer rise earthquakes occur to ~10-15 km within the incoming plate mantle at most subduction zones. If this entire depth range is hydrated, as much as ~10^{9}-10^{10} Tg/Myr of water may be subducted at the Northwestern Pacific; however, lateral heterogeneities in outer rise faulting would result in reduced concentrations of input water.

Acknowledgements

I would like to acknowledge all of those who have supported me during the writing of this dissertation. My advisor Doug Wiens has provided me with resources to learn about the field of seismology and to become an active member of a research community, while always having an open door and a willingness to answer questions. I am very appreciative of my faculty mentors, Slava Solomatov, Linda Warren, and Diane Doser who have helped to demystify the academic experience and have encouraged me during difficult times. I am very appreciative of all of the members of the seismology community at Washington University who have aided in the technical aspects of my research. In particular special thanks are due to Garrett Euler, David Heeszel, Patrick Shore, and Hugh Chou. I would like to acknowledge the hard work of field teams who installed and serviced the Mariana SUBFAC array so that I could have access to quality data. I am very grateful for the funding I received through NSF which enabled me to complete this research, and I would like to thank the GeoPRISMs, Earthscope, and CIDER programs, which have provided me with funds and opportunities to participate in many workshops and meetings.

I could not have completed this dissertation without the support of many friends and family member, including Joe and Chris Emry, Kathleen Eurek, Selby Cull, Kim Lichtenberg, Garrett Euler, Liz Hasenmueller, and Aaron Keegan who have patiently tolerated the ups and downs of graduate school with me and have contributed immensely to my success. Most importantly, I'd like to thank my parents who have been supportive of my education throughout my whole life; I am very lucky to have parents who encourage me to continue learning.

Table of Contents

List of Tables and Figures

CHAPTER 1

INTRODUCTION

The input of water at subduction zones impacts generation of subduction arc and back-arc volcanics [*Gill*, 1981; *Plank and Langmuir*, 1993], slip along the shallow plate interface [*Moore and Vrolijk*, 1992; *Audet et al*, 2009], nucleation of intermediate depth earthquakes [*Raleigh and Paterson*, 1965; *Meade and Jeanloz*, 1991], the composition of the deep mantle [*Thompson*, 1992; *Hirschmann*, 2006], and initiation of plate tectonics [*O'Neill et al*, 2007]. The relative amounts of water stored within each of the layers of the subducting plate prior to subduction will impact these processes to different extents, depending on the physical state of the plate prior to subduction [*Jarrard*, 2003; *Hacker*, 2008; *Van Keken et al*, 2011]. While some studies have been able to directly measure the water content of materials within the top of the oceanic sediments and crust [e.g. *Plank and Langmuir*, 1993; *Plank and Langmuir*, 1998; *Jarrard*, 2003], there exists very little constraint on the amount of water that may be stored within deeper layers of the lower crust and upper mantle [e.g. *Jarrard*, 2003; *Rüpke et al*, 2004; *Hacker*, 2008; *Van Keken et al*, 2011].

The presence of water and/or hydrous minerals, such as serpentinites, is thought to impact the earthquake nucleation process at shallow depths within the subduction zone [*Reinen et al*, 1991; *Moore and Vrolijk*, 1992; *Shelly et al*, 2006; *Audet et al*, 2009; *Moore and Lockner*, 2007]. The shallow plate interface at the Mariana Subduction Zone, which is thought to be a particularly water rich system [e.g. *Fryer et al*, 1999; *Fryer and Salisbury*, 2006; *Hyndman et al*, 2007; *Tibi et al*, 2008; *Pozgay et al*, 2009; *Pyle et al*, 2010], is enigmatic in that it has not produced any unequivocally great plate interface

earthquakes during the period of time for which instrumental records exist [*Uyeda and Kanamori*, 1979; *Pacheco et al*, 1993; *Hyndman et al*, 2007]. However, the causes for this apparent aseismicity remain elusive.

This dissertation presents research which contributes to our understanding of the cycling of water through subduction zones, mineralogical changes in the presence of water, and the effects of water and hydrous minerals on faulting processes within the shallow subduction zone.

Chapter 2 – Seismogenic characteristics of the Northern Mariana Subduction Zone

The historical record of great, destructive plate interface earthquakes at the Mariana Subduction Zone is not well constrained. During the past century, no great earthquakes have been recorded here, and this lack of great earthquakes has led to the perception that the Mariana Subduction Zone is "decoupled" or incapable of producing a great earthquake [*Uyeda and Kanamori*, 1979]. One previously hypothesized reason for this lack of seismicity is that presence of serpentinite minerals within the subduction zone mantle wedge significantly narrows the boundary along which earthquakes can nucleate, thereby inhibiting the production of large earthquakes [*Hyndman*, 2007]. In this project, I analyzed small earthquakes which were recorded on a regional seismic deployment, consisting of both standard, broadband seismometers located on the nearby Mariana Islands and ocean-bottom seismometers which were located throughout the Northern Mariana subduction forearc, arc, and backarc. The locations and the type of slip which were recorded on these seismometers indicates that plate interface earthquakes occur throughout the mantle wedge – the region in which serpentinites have been proposed to

inhibit earthquake nucleation. I further discuss the characteristics of the Northern Mariana subduction zone and put it into the context of what is currently known about earthquake nucleation along subduction zone plate boundaries.

This chapter has previously been published in the academic journal *Geochemistry Geophysics Geosystems*, and is the effort of authors E.L. Emry, D.A. Wiens, H. Shiobara, and H. Sugioka [*Emry et al*, 2011]. All of the data analysis, writing and interpretation was the work of the first author E.L. Emry (the author of this dissertation). Co-authors D.A. Wiens, H. Shiobara, and H. Sugioka provided input and feedback on the written manuscript and methods used in the study.

Chapter 3 – Faulting within the Mariana Outer Rise

The Mariana Subduction Zone is commonly referred to as a water-rich setting; however our understanding of the overall water budget of the subduction zone is limited by the fact that the amount of water stored within the subducting slab mantle is not constrained for this region. In order to better understand the hydration state of the subducting slab, I analyze global, broadband seismic records of moderately-sized earthquakes occurring within the Mariana outer rise to more accurately determine the depth of extensional faulting, which results from high stresses produced by oceanic plate bending at the outer rise. I find that the depth of extensional faulting varies along the length of the Mariana subduction zone outer rise, a characteristic which likely reflects a change in the curvature of plate bending as well as differences in the regional tectonic stress. I propose that the occurrence of deeper extension at the central region of the Mariana outer rise results in increased amounts of hydrated and serpentinized mantle

materials. I further discuss the state of stress along the subduction plate interface and the implications on the water budget of the Mariana Subduction Zone.

Chapter 4 – Outer Rise Faulting within the Northwestern Pacific Subduction Zones

The transport of water through mantle serpentinites in the subduction slab is suggested to be a major contributor to subduction zone and deep Earth water budgets; however the total amount of water subducted within serpentinites is unconstrained for most subduction zones. Because extensional outer rise faulting is a likely mechanism by which water can enter into the slab prior to subduction and serpentinize the slab mantle, and because old, cold oceanic plates are thought to be partly responsible for deep subduction of serpentinites (and therefore water), I study the depth of extensional outer rise earthquakes for the entire Northern and Western Pacific Basin Subduction Zones. By determining more accurate depths for the moderately-sized earthquakes throughout Northwestern Pacific Subduction Zones, I am able to provide a first-constraint on the state of stress within the outer rise as well as the potential for slab hydration in these regions. I find that although the distribution of earthquakes within the outer rise of Northern and Western Pacific subduction zones may vary in some regions, the overall distribution of extensional earthquakes continues down to 10-15 km at almost all of the subduction zones. I provide a more thorough discussion of water subduction and its implications on water budgets, as well as discuss the implications to the whole Earth water cycle.

References

Audet, P., M.G. Bostock, N.I. Christensen, and S.M. Peacock (2009), Seismic evidence for overpressured subducted oceanic crust and megathrust fault sealing, *Nature*, *457*(7225), 76-78, doi: 10.1038/nature07650.

Emry, E.L., D.A. Wiens, H. Shiobara, and H. Sugioka (2011) Seismogenic characteristics of the Northern Mariana shallow thrust zone from local array data, *Geochem. Geophys. Geosyst., 12*(12), Q12008, doi:10.1029/2011GC003853.

Fryer, P. B., and M. H. Salisbury (2006), Leg 195 synthesis: Site 1200 - Serpentinite seamounts of the Izu-Bonin/Mariana convergent plate margin (ODP Leg 125 and 195 drilling results), in *Proc. ODP, Sci. Results,* vol. 195, edited by M. Shinohara et al., pp.1-30, Ocean Drilling Program, College Station, TX, doi: 10.2973/odp.proc.sr.195.112.2006.

Fryer, P., C.G. Wheat, and M.J. Mottl (1999), Mariana blueschist mud volcanism: Implications for conditions within the subduction zone, *Geology*, *27*(2), 103-106, doi: 10.1130/0091-7613(1999)027<0103:MBMVIF>2.3.CO;2.

Gill, J. B. (1981), *Orogenic Andesites and Plate Tectonics*, 390 pp., Springer, New York.

Hacker, B.R. (2008), H2O subduction beyond arcs, *Geochem. Geophys. Geosyst., 9*, Q03001, doi: 10.1029/2007GC001707.

Hirschmann, M.M. (2006) Water, melting, and the deep Earth H_2O cycle, *Annu. Rev. Earth Planet. Sci., 34*, 629-653, doi: 10.1146/annurev.earth.34.031405.125211.

Hyndman, R. D. (2007), What we know and don't know, in *The Seismogenic Zone of Subduction Thrust Faults*, edited by T. H. Dixon and J. C. Moore, pp. 15-40, Columbia University Press, New York

Jarrard, R.D. (2003), Subduction fluxes of water, carbon dioxide, chlorine, and potassium, *Geochem. Geophys. Geosyst., 4*(5), 8905, doi: 10.1029/2002GC000392.

Meade, C. and R. Jeanloz (1991), Deep-focus earthquakes and recycling of water into the Earth's mantle, *Science, 252*(5002), 68-72, doi: 10.1126/science.252.5002.68.

Moore, D. E., and D. A. Lockner (2007), Comparative deformation behavior of minerals in serpentinized ultramafic rock: Application to the slab-mantle interface in subduction zones, *International Geology Review*, *49*(5), 401-415, doi: 10.2747/0020-6814.49.5.401.

Moore, J. C. and P. Vrolijk (1992), Fluids in accretionary prisms, *Rev. Geophys., 30*(2), 113-135.

O'Neill, C., A. M. Jellinek, and A. Lenardic (2007), Conditions for the onset of plate tectonics on terrestrial planets and moons, *Earth Planet. Sci. Lett., 261*, 20-32, doi:10.1016/j.epsl.2007.05.038.

Pacheco, J. F., L.R. Sykes, and C.H. Scholz (1993), Nature of Seismic Coupling Along Simple Plate Boundaries of the Subduction Type, *Journal of Geophysical Research-Solid Earth, 98*(B8), 14133-14159, doi: 10.1029/93JB00349.

Plank, T. and C. H. Langmuir (1993), Tracing trace elements from sediment input to volcanic output at subduction zones, *Nature, 362*, 739-743.

Plank, T. and C.H. Langmuir (1998), The chemical composition of subducting sediment and its consequences for the crust and mantle, *Chem. Geo., 145*, 325-394.

Pozgay, S., D.A. Wiens, J.A. Conder, H. Shiobara, and H. Sugioka (2009), Seismic attenuation tomography of the Mariana arc: Implications for thermal structure,

volatile distribution, and dynamics, *Geochem. Geophys. Geosystems*, *10*, Q04X05, doi: 10.1029/2008GC002313.

Pyle, M., D.A. Wiens, D.S. Weeraratne, P.J. Shore, H. Shiobara, and H. Sugioka (2010), Shear velocity structure of the Mariana mantle wedge from Rayleigh wave phase velocities, *J Geophys. Res.*, *115*, B11304, doi: 10.1029/2009JB006976.

Raleigh, C.B. and M.S. Paterson (1965), Experimental deformation of serpentinite and its tectonic implications, *J. Geophys. Res.*, *70*(16), 3965-3985.

Reinen, L. A., J.D. Weeks, and T.E. Tullis (1991), The frictional behavior of serpentinite - Implications for aseismic creep on shallow crustal faults, *Geophysical Research Letters*, *18*(10), 1921-1924, doi: 10.1029/91GL02367.

Rüpke, L.H., J. Phipps Morgan, M. Hort, and J.A.D. Connolly (2004), Serpentine and the subduction zone water cycle, *Earth Planet. Sci. Lett.*, *223*(1-2), 17-34, doi:10.1016/j.epsl.2004.04.018.

Shelly, D. R., G.C. Beroza, S. Ide, and S. Nakamula (2006), Low-frequency earthquakes in Shikoku, Japan, and their relationship to episodic tremor and slip, *Nature*, *442*(7099), 188-191, doi: 10.1038/nature04931.

Thompson, A.B. (1992), Water in the Earth's upper mantle, *Nature*, *358*(6384), 295-302, doi:10.1038/358295a0.

Tibi, R., D.A. Wiens, and X.H. Yuan (2008), Seismic evidence for widespread serpentinized forearc mantle along the Mariana convergent margin, *Geophys. Res. Lett.*, *35*(13), L13303, doi: 10.1029/2008GL034163.

Uyeda, S., and H. Kanamori (1979), Back-arc opening and the mode of subduction, *J. Geophys. Res.*, *84*(B3), 1049-1061, doi: 10.1029/JB084iB03p01049.

Van Keken, P.E., B.R. Hacker, E.M. Syracuse, G.A. Abers (2011), Subduction factory: 4. Depth-dependent flux of H_2O from subducting slabs worldwide, *J. Geophys. Res., 116*, B01401, doi:10.1029/2010JB007922.

CHAPTER 2

SEISMOGENIC CHARACTERISTICS OF THE NORTHERN MARIANA SHALLOW THRUST ZONE FROM LOCAL ARRAY DATA

* Previously published in *Geochemistry Geophysics Geosystems, 12*(12), Q12008

Abstract

The Northern Mariana seismogenic zone has no shallow thrust earthquakes larger than Ms 7.4 in the historical seismological record and is traditionally considered ‘decoupled’ or 'aseismic'. During the 2003-2004 Mariana Subduction Factory Imaging Experiment, we recorded local shallow earthquakes throughout the central and northern regions of the Mariana forearc using an array of terrestrial broadband and ocean bottom seismographs. Accurate locations for both the 2003-2004 local seismicity as well as earthquakes with Global Centroid Moment Tensor (GCMT) solutions from 1976-2008 were obtained using the hypocentroidal decomposition relocation method and a local velocity model. Additionally, focal mechanisms for the largest 2003-2004 earthquakes were determined using regional waveform inversion. Thrust faulting earthquakes occur along the Mariana megathrust between depths of 20-60 km, showing that the lack of great shallow thrust earthquakes does not result from a narrow seismogenic zone and that most seismicity occurs where the down-going plate contacts the overriding mantle wedge. Clusters of small plate interface earthquakes with Ml 1.6-4.7 occur within patches 100-120 km west of the trench at depths of 30-45 km. Furthermore, the larger GCMT earthquakes (Mw 4.9-5.8) occur mostly up-dip and down-dip of the patches of smaller earthquakes recorded by our local array and is suggestive of changes in the fault properties with depth. Clusters of small, forearc earthquakes occur discontinuously along

the length of the Mariana subduction zone, showing that Northern Mariana is variable both along the strike of the margin and with depth along the seismogenic zone. We propose that the lack of great (Mw > 8) thrust faulting earthquakes is due in part to the variable frictional heterogeneity along the megathrust.

1. Introduction

The Mariana subduction zone is commonly considered to be the aseismic end member on a spectrum of subduction zones, with the opposite end represented by the Chilean and Alaskan margins, where megathrust earthquakes approaching Mw 9.5 are feasible [*Kanamori,* 1977; *Uyeda and Kanamori*, 1979]. To date, no great (Mw > 8.0) shallow thrust earthquakes have been recorded and accurately located in the Mariana subduction zone, although historical records do contain evidence for infrequent moderate-sized (Mw > 7.0) shallow events and large earthquakes for which magnitude estimates are absent or unreliable (Table 1). In a global study comparing seismic slip coefficients, the Mariana Islands was determined to have a seismic coupling coefficient of 0.002, meaning that only 0.2% of the slip between the Pacific and Philippine plates could be accounted for by historical records of large thrust earthquakes [*Pacheco et al.*, 1993]. The results imply that either a large percentage of interplate slip is accommodated through stable, aseismic slip or that the subduction zone is due for a giant earthquake every hundred years.

Recent devastating magnitude nine earthquakes in regions previously thought to have little potential for great earthquakes have caused reassessment of such

seismic/aseismic classifications. Sumatra, for example, had a coupling coefficient of 0.007 determined by *Pacheco et al.* [1993], yet produced a Mw ~9.1 earthquake in 2004 [e.g. *Lay et al.*, 2005]. The recent 2011 Northeast Japan earthquake also occurred in a region where magnitude nine earthquakes were thought to be impossible. Clearly a much better understanding of the factors controlling the seismic characteristics of the subduction zone thrust interface is needed.

Previous studies present two main hypotheses to explain the lack of large earthquakes in the Mariana and other 'aseismic' subduction zones. The first suggests that the shallow intersection of the plate interface with a serpentinized mantle wedge narrows the seismogenic width so that large earthquakes are not possible [*Hyndman et al.*, 1997; *Peacock and Hyndman*, 1999; *Hyndman*, 2007]. This idea proposes that seismic slip is limited to where the underthrusting plate contacts the overriding forearc crust, which occurs in the Central and Northern Mariana Islands at a depth of about 15 km [*Takahashi et al.,* 2007]. The second hypothesis for lack of large earthquakes in Mariana is that the plate interface is very weakly coupled due to the geometry of the subduction zone and predominance of horizontal tensional tectonic stresses in the region, as evidenced by sea floor spreading in the back arc [*Scholz and Campos*, 1995].

In the absence of large underthrusting earthquakes, the depth extent of the seismogenic zone may be identified through use of microseismicity or by geodesy [*Schwartz and DeShon*, 2007]. Seismic studies are the most feasible option in an island arc setting, given that the geodetic signal of plate coupling and strain accumulation occurs offshore, where geodetic studies require extremely expensive ocean-bottom GPS technology. Through seismic studies, we can examine the pattern of seismic release

along the thrust zone and obtain a rough estimate of how much surface area could rupture seismically if it were all to slip at once.

In this paper we use shallow earthquake locations and focal mechanisms for small earthquakes recorded by a temporary local array of land and ocean bottom seismographs deployed during 2003-2004 to better understand the Northern Mariana shallow thrust region [*Pozgay et al.,* 2007]. Previously, the Northern Mariana subduction zone had only been studied using larger earthquakes detectable teleseismically, since there are few permanent seismic stations in this region. The local recordings provide for study of much smaller earthquakes with much greater location precision, allowing us to answer basic questions about the characteristics of this unusual subduction zone.

2. Background

2.1 Geological setting

2.1.1 Tectonic setting and history

The Mariana-Izu-Bonin system is a young subduction zone extending from Japan in the north to Guam in the south that first formed about 43 Ma [*Stern et al.*, 2003]. The Mariana Islands are the southern portion of the island chain, where a strong, outward curvature of the arc separates it from the mostly North-South Izu-Bonin section. Throughout the history of the Mariana Islands, the volcanic arc has split twice – the remnant arcs from these rifting events constitute the Kyushu-Palau ridge and the West Mariana Ridge [*Stern et al.*, 2003]. Evidence from paleomagnetism suggests the

orientation of the Izu-Bonin-Mariana system was originally East-West and gradually rotated clockwise to its current North-South orientation [*Hall et al.*, 1995; *Hall*, 2002]. The convergence rate between the Pacific plate and the forearc of the Mariana subduction zone from GPS measurements at stations along the island arc and forearc rise show that the arc and forearc are moving east relative to the rest of the Philippine Sea plate, due to active extension in the back-arc basin [*Kato et al.*, 2003]. The rate of subduction beneath the northern part of the Mariana Islands near Agrihan is 35-45 mm/yr, while the rate of subduction in the south near Guam is 60-70 mm/yr [*Kato et al.*, 2003]. The angle of convergence of the Pacific plate beneath the Mariana forearc is 83° West of North (Figure 1) [*Kato et al.*, 2003].

2.1.2 Forearc Morphology

The western portion of the forearc in our study region is flat, covered in volcaniclastic and pelagic sediments, and spans about 2/3 of the forearc seafloor. The region is cut by normal faults that run roughly parallel to the trend of the volcanic arc and the trench, the presence of which indicate that the Mariana forearc is under tension [*Stern and Smoot*, 1998]. The eastern portion of the forearc is cut by numerous, small normal faults in a mostly southwest to northeast orientation [*Stern and Smoot*, 1998]. In this highly deformed part of the forearc, a number of large serpentinite seamounts, unique to the Izu-Bonin-Mariana subduction zone are present [*Stern et al.*, 2003]. The serpentinite seamounts in the Mariana forearc are located at 15-90 km distance from the trench and are formed through serpenitite mud volcanism. The minerals ejected reflect increasing

pressure as distance from the trench increases, suggesting that materials are being ejected from progressively deeper depths [*Fryer and Salisbury*, 2006]. The Big Blue seamount is located at 70 km to the west of the trench [*Oakley et al.*, 2007] and is the largest seamount located on the Mariana forearc. The tectonic instability of the Mariana forearc is responsible for the presence of the active serpentinite seamounts, as fluids expelled during subduction are able to move upward through the extensively faulted forearc and erupt at the surface [*Fryer et al.*, 1999; *Stern et al.*, 2003; *Fryer and Salisbury*, 2006].

The presence of serpentinite mud volcanoes is frequently used as evidence that the underlying Mariana mantle wedge is serpentinized. Geochemical work from *Benton et al.* [2004] found that expelled fluids were not derived directly from the slab, but rather, had interacted with mantle wedge materials prior to being emitted from the seamount. Receiver functions calculated beneath Saipan and Tinian Islands further to the south reveal a pronounced low velocity layer in the mantle wedge at 40-55 km depth, leading to the conclusion that mantle serpentinization is prevalent at these depths [*Tibi et al.*, 2008]. *Pozgay et al*. [2009] suggest mantle serpentinization in the forearc beneath the seamounts as an explanation for an observed zone of high attenuation. Results from surface wave phase velocities in the Northern Mariana Islands also showed a low velocity anomaly in the forearc between Celestial and Big Blue Seamounts [*Pyle et al.*, 2010], postulated to be mantle serpentinization. Similarly, P and S velocity tomography by *Barklage* [2010] revealed a region of an unusually high 1.95-2.0 Vp/Vs ratio; this combined with modeling by *Hacker et al*. [2003] suggests that the forearc mantle wedge is ~30-60% serpentinized. While the evidence for a serpentinized mantle wedge in Mariana is

substantial, its spatial distribution is not well constrained and its relation to shallow forearc seismicity is not completely understood.

2.2 Seismicity

The most recent, large, shallow thrust earthquakes have occurred in the Southern Mariana Islands near Guam (Figure 2; Table 1, Rows 14-16) and began with a Mw 7.7 earthquake on August 8, 1993 [*Campos et al.,* 1996]. Depth estimates for this earthquake vary from 41.5 km [*Campos et al.,* 1996] to 74.5 km [*Harada and Ishibashi,* 2008], and the focal mechanism is consistent with a shallow dipping thrust earthquake [*Campos et al.,* 1996]. In 2001 and 2002, two large Mw 7.0 earthquakes occurred nearby the location of the large 1993 earthquake. The large 1993 Guam earthquake was initially interpreted as rupture along the plate interface [*Campos et al.,* 1996] and supported the interpretation that the Southern Mariana plate interface is more strongly coupled than the Northern plate interface [*Scholz and Campos*, 1995]. However, more recent studies suggest that 1993, 2001, and 2002 Guam earthquakes occurred in the subducting Pacific plate and thus do not represent seismic slip along the megathrust [*Tanioka et al.,* 1995; *Harada and Ishibashi,* 2008].

A number of potentially shallow thrust earthquakes with magnitudes greater than 7.0 occurred from 1900-1950. Many of these events, listed by *Gutenberg and Richter* [1954] as shallow or intermediate depth earthquakes, have revised magnitudes between Ms 7.0-7.4 [*Abe and Kanamori,* 1979; *Abe*, 1981; *Pacheco and Sykes,* 1992] and occur along the entire length of the Mariana forearc (Figure 2; Table 1, Rows 6-13). Although

some of these events are classified as intermediate depth earthquakes, and a few are located in the outer rise of the Pacific slab, they are included in the record due to the possibility of poor event locations in the early 1900's – up to 1° laterally and 30 km in depth for the best-located events, with earthquakes at 40-100 km depth being particularly problematic [*Gutenberg and Richter*, 1954]. In addition to uncertainty in earthquake locations and depths, magnitude estimates for these events have been calculated and revised numerous times [*Gutenberg and Richter,* 1954; *Gutenberg,* 1956; ; *Richter*, 1958; *Abe and Kanamori*, 1979; *Abe,* 1981; *Abe and Noguchi*, 1983; *Pacheco and Sykes,* 1992]; the most recent magnitude revisions are listed in Table 1.

During 1825-1892, four large earthquakes and tsunamis are known to have affected the island of Guam. Estimates for the intensity of shaking on the island of Guam as compiled by *Maso* [1910] are included for all earthquakes occurring in 1825-1902 (Figure 2; Table 1, Rows 1-5), but earthquake location, depth, and slip are unknown for the earliest events. Large, shallow thrust earthquakes often create tsunamis; however large extensional earthquakes in the bending Pacific plate at the Mariana trench have also produced tsunamis [*Satake et al.,* 1992; *Yoshida et al.*, 1992]. Therefore although significant damage and records of tsunamis on Guam exist, these tsunamis may not have been generated by shallow thrust earthquakes.

The seismic record used by *Pacheco et al.* [1993] to compute seismic coupling coefficients along this margin included only two large events: 1902 Ms 7.4 occurring near 18°N, 146°E and 1934 Ms 7.1 occurring near 22.5°N, 144°E (Figure 2; Table 1, Rows 5,10). No shallow thrust earthquakes larger than Ms 7.4 have been recorded and clearly located in the central and northern parts of the Mariana Islands during 1897 to

2010 [*Gutenberg and Richter*, 1954; *Abe and Kanamori*, 1979; *Abe*, 1981; *Pacheco and Sykes*, 1992]. Given the relationship for seismic coupling and fault parameters used by *Pacheco et al.* [1993], the absence of earthquakes larger than Ms 7.4 over the last ~110 years requires that a giant earthquake the size of the great Chilean or Alaskan earthquakes (Mw > 9) occur in order to seismically release the accumulated strain (Table 2, Row 1). Even assuming that every earthquake listed in Table 1 is a shallow thrust earthquake, the resulting seismic coupling coefficient is 0.0076 and requires that a Mw 9.39 earthquake occur every ~110 years in order to seismically release all accumulated strain (Table 2, Row 2). Although it is difficult to preclude this, most previous studies assume that the absence of earthquakes results from aseismic slip rather than an impending great megathrust earthquake [e.g. *Uyeda and Kanamori*, 1979].

2.3 The Marianas Seismogenic Zone and Aseismic Slip

The two proposed explanations for Mariana aseismicity represent inherently different physical processes: reduction of normal force between the plates [*Scholz and Campos*, 1995] or reduced frictional strength between the plates due to rheological or fault zone properties [*Hyndman et al.*, 1997; *Peacock and Hyndman*, 1999; *Hyndman*, 2007]. In this section we review what is known about the Mariana shallow thrust zone in the context of the proposed explanations for the absence of great earthquakes.

2.3.1 Up-dip Limit of Seismogenic Zone

Very little is known about the location of the up-dip limit in the Mariana seismogenic zone – previous studies of coupling have assumed a 10 km up-dip limit depth for all subduction zones [*Pacheco et al.*, 1993]. The onset of seismogenesis in continental subduction zones is classically perceived to begin near the base of the accretionary wedge, due to the compaction and cementation of sediments or presence of stronger crustal materials [*Byrne et al.*, 1988; *Marone and Scholz*, 1988; *Byrne and Fisher*, 1990; *Moore and Saffer*, 2001]. However, the Mariana island arc lacks an accretionary wedge. Hypotheses that the up-dip limit could be controlled by the phase transition of weak smectite clays to stronger illite clays [*Vrolijk, 1990; Moore and Saffer*, 2001] were found to not strongly affect onset of seismogenesis [*Saffer and Marone*, 2003]. More recently, the up-dip limit is thought to be controlled by decreasing pore pressure and fluid flux with depth as fluid producing diagenetic changes, such as the opal to quartz, smectite to illite, or hydrocarbon maturation cease [*Oleskevich et al.,* 1999; *Moore and Saffer*, 2001; *Spinelli and Saffer*, 2004]. Other diagenetic and low-grade metamorphic processes, such as pressure solution with subsequent quartz cementation, and zeolite-facies metamorphism with resulting cementation, are thought to strengthen the down-going slab sediments [*Moore and Saffer,* 2001].

Regardless of the underlying physical cause for the up-dip limit, there appears to be a correlation between the 100-150°C isotherm and the onset of thrust seismicity in subduction zones [*Hyndman and Wang*, 1993; *Oleskevich et al.*, 1999], although it is unclear whether the transition results directly from temperature or from other factors [*Saffer and Marone*, 2003]. In Costa Rica, a change in the age and temperature of the

subducting seafloor correlates with a measurable offset in the location of the up-dip limit [*Harris and Wang,* 2002; *Newman et al.*, 2002; *DeShon et al.,* 2006; *Schwartz and Deshon*, 2007]. In the Mariana Islands, recent geochemical work by *Hulme et al.* [2010] estimates the temperature conditions beneath Big Blue Seamount to be greater than 200°C. Given this and our current understanding of the initiation of seismogenesis, the up-dip limit should occur east of Big Blue Seamount [*Hyndman and Wang,* 1993; *Oleskevich et al,* 1999].

2.3.2 Down-dip Limit of Seismogenic Zone

The transition from unstable slip producing earthquakes to ductile deformation beyond the down-dip limit of the seismogenic zone has traditionally been interpreted as due to increasing temperature [*Hyndman and Wang*, 1993; *Tichelaar and Ruff*, 1993; *Hyndman et al.*, 1995; *Hyndman et al.*, 1997; *Harris and Wang*, 2002]. In continental subduction settings, the down-dip limit was suggested to correspond to the 350-400°C isotherm with a transitional region of stable slip extending to 450°C [*Hyndman et al.*, 1995]. The down-dip limit in regions such as the Mariana Islands, where the overriding plate has a thin crust and the downgoing plate contacts the forearc mantle is suggested to correspond to higher temperatures, near 550°C [*Tichelaar and Ruff*, 1993].

An alternate explanation suggests that the down-dip limit is the boundary between overriding crust and serpentinized mantle wedge below, explained by aseismic layered serpentinite, brucite, and talc minerals within the mantle wedge [*Hyndman et al.*, 1997; *Peacock and Hyndman*, 1999; *Harris and Wang*, 2002; *Seno*, 2005]. This supposition

relies on laboratory experiments indicating that these materials show stable sliding behavior at seismogenic depths [*Reinen et al.*, 1991; *Moore et al.*, 1997; *Hilairet et al.*, 2007; *Moore and Lockner*, 2007]. Earthquake producing slip depends on which serpentinite polymorph is present at that depth; antigorite, brucite and talc were found in one study by *Moore and Lockner* [2007] to be velocity-strengthening, while lizardite and chrysotile were velocity-weakening at experimental temperatures. Thermal modeling suggests that lizardite may be the dominant phase at shallow depths in the Mariana mantle wedge [*Wada and Wang*, 2009].

2.3.3 Variability of the Plate Interface Seismogenic Zone

Some studies indicate variability in the sizes and characteristics of rupture with depth along the seismogenic width of subduction zones [e.g. *Hyndman et al.*, 1997; *Bilek and Lay*, 2000]. The subduction zones of Kermadec, Solomon, and Kamchatka exhibit a bimodal depth distribution of shallow thrust earthquakes [*Pacheco et al.*, 1993; *Hyndman et al.*, 1997], which has been explained by serpentinization at the shallowest mantle depths [*Hyndman et al.*, 1997]. In this model, the subducting plate slides aseismically while in contact with the serpentinized part of the mantle wedge but transitions back to stick-slip behavior deeper in the mantle wedge, where serpentinites are no longer stable and where the plate contact is in the ductile deformation regime. In the Mariana Islands, serpentinites were similarly used to explain the seemingly narrow seismogenic width, although no second, deep seismogenic zone was observed [*Hyndman et al.*, 1997]. Source-time durations for select circum-Pacific subduction zones, not including the

Mariana Islands, show a general trend of decreasing, normalized rupture time with increasing depth of plate interface earthquake [*Bilek and Lay*, 1999; 2000]. The results were interpreted to be indicative of an increase in rigidity due to compaction and de-watering of subducting sediments [*Bilek and Lay*, 1999; 2000].

Along-strike variability in interplate coupling as indicated by spatial distribution of shallow earthquakes [*Hasegawa et al.,* 2007] and earthquake rupture characteristics [*Ammon et al.,* 2005] has been noted to some extent in almost all subduction zones. Some subduction zones clearly show different degrees of locking versus stable sliding along strike [*Freymueller et al.*, 2008]. In the Mariana Islands, GPS data from the outer forearc are not available, so observations of creep and measures of interseismic locking cannot be obtained. The southern region may be more strongly coupled than the northern region [*Scholz and Campos*, 1995]; however this conclusion depends on the interpretation of large, shallow earthquakes in the historical records [*Pacheco et al.*, 1993] as well as the controversial 1993 Guam earthquake [*Tanioka et al.*, 1995; *Harada and Ishibashi*, 2008]. Observations of small earthquakes during a 2001 ocean bottom seismograph experiment in the Mariana Islands reveal distinct clusters of earthquakes - indicating that the plate interface may be slipping regularly in some regions, but may be either locked or slipping aseismically in other regions along the length of the subduction zone [*Shiobara et al.*, 2010].

Along-strike changes in shallow thrust seismicity have been explained due to effects of subducting oceanic seamounts or other bathymetric highs [*Tanioka et al.*, 1997; *Bilek et al.,* 2003; *DeShon et al.,* 2003; *Shinohara et al.*, 2005; *Bilek,* 2007]. To the north, the Magellan Seamount Cluster and Dutton Ridge within the East Mariana Basin

intersect the Mariana and Bonin trenches and are composed of Cretaceous volcanic seamounts (~100-120 Ma) [*Smith et al.,* 1989]. Intersecting the Mariana and Yap trenches in the south are the seamounts and islands of the Caroline Island chain, which is made up of young (less than ~12 Ma) volcanic seamounts and islands and atolls [*Keating et al.*, 1984]. At the trench east of Big Blue Seamount (~18.5°N) and the trench southeast of Celestial Seamount (~16°N), small, unnamed, ocean-floor seamounts in the vicinity of the larger Hussong and delCano Guyots are actively subducting, resulting in shallow depth of trench and disruption of the overriding Philippine plate (Figure 1) [*Gardner,* 2010; *Oakley et al.*, 2008]. *Oakley et al.* [2008] characterize the Mariana trench as four distinct sections, with the northern region near Big Blue as one section having increased seamount subduction, shallower trench, and displaced overriding plate toe.

3. Data Analysis

3.1 Datasets

During the 2003-2004 Mariana Subduction Factory Imaging Experiment we deployed 20 broadband seismometers and 58 ocean-bottom seismometers (OBS) from May/June 2003 until April/May 2004 (Figure 1). The 20 land seismometers were either Streckheisen STS-2 or Guralp CMG-40T sensors paired with REFTEK 72A-08 data-loggers, and were deployed along the arc from Guam to Agrihan. At least one Streckheisen STS-2 sensor was deployed on each of the islands. The Guralp CMG-40T were deployed in dense arrays on the more southerly islands of Guam, Tinian, and Saipan. The instrument on the island of Anatahan experienced intermittent power

failures due to ash cover on solar panels from the 2003 volcanic eruption [*Pozgay et al.*, 2005]. The rest of the land stations operated throughout the year. Of the 58 OBSs placed on the ocean floor, 50 used Mark Products L4 sensors [*Webb et al.*, 2001], with 15 using an older, 16-bit datalogger (MPL4o) and 35 using a newer, 24-bit datalogger (MPL4n). Due to an error in the firmware of the data-logger, the newer, 24-bit model stopped recording after 50 days. The remaining 8 OBS used a Precision Measuring Devices sensor (PMD-WB2023LP) and were operated by University of Tokyo [*Shiobara et al.*, 2010]. The majority of the OBSs spanned from Pagan west into the backarc, with fourteen of the 58 OBSs deployed in the forearc (Figure 1). Station coordinates and dates of deployment are listed by *Pozgay et al.* [2007].

In addition to data from the temporary Mariana deployment, we used phase arrival-time data from the *International Seismological Center (ISC)* [2010] for all Mariana forearc earthquakes located between 17.5-18.5°N during 1976-2008 for use in relative relocations. Depths and moment tensors of earthquakes from 1976-2008 in the same region were taken from the Global Centroid Moment Tensor (GCMT) database [*Dziewonski et al.*, 1981; *www.globalcmt.org*].

3.2 Earthquake Location

As a first step, we used the Antelope software package to automatically detect and associate arrival times [*www.brtt.com*]. The P and S wave arrival times were then manually picked and the earthquakes were located using the GENeric LOCation algorithm [*Pavlis et al.*, 2004]. Following this initial location, a relative location

program, the hypocentroidal decomposition method of *Jordan and Sverdrup* [1981], was used to obtain better relative locations for all earthquakes with 15 or more P and S arrivals. In addition to the original method outlined by *Jordan and Sverdrup* [1981], we included the ability to calculate travel times according to a local velocity model for nearby stations. Our local P-wave velocity model was obtained from the seismic refraction study of *Takahashi et al.* [2007], with S-wave velocities calculated from the P-wave velocities using Vp/Vs of 1.8. This ratio is the global average Vp/Vs in the uppermost mantle [*Dziewonski and Anderson*, 1981] and was found by *Rossi et al.* [2006] at shallow mantle wedge depths (< 80 km) in the Alaskan subduction zone.

We also determined the relative positions of larger 1976-2008 teleseismic earthquakes using the hypocentroidal decomposition method and arrival times obtained from the ISC. We used P and PKP phase arrival data from all stations in the ISC Bulletin and S phase arrivals from stations closer than Δ=20° to relocate all earthquakes in our study area for which a GCMT solution exists. The IASP91 velocity model was used to calculate teleseismic travel times [*Kennett and Engdahl*, 1991].

Subduction zone earthquakes located with only teleseismic data often show a significant hypocenter bias due to the velocity structure of the down-going slab [e.g. *Fujita et al.*, 1981], and teleseismic location accuracy is particularly poor in the Mariana arc due to the nearly complete absence of stations to the east. Teleseismic earthquakes recorded during 2003-2004 that were also recorded by the local array allow us to test and correct the teleseismic locations for bias due to unmodeled, large scale velocity structure of the earth. Comparison of the hypocenters for 2003-2004 earthquakes computed using only teleseismic arrivals with the hypocenters computed using only local array data

reveal a significant discrepancy between teleseismic and local array locations; those with local arrival data show a shift to shallower depths than those with only teleseismic arrivals. The uncertainty ellipsoids of the events computed with local arrivals are much smaller than uncertainties for the teleseismic datasets. We conclude that the locally-recorded earthquakes have inherently better location and depth resolution due to the presence of the array almost directly above the source region as well as the use of a local velocity model. Furthermore, the shallow locally-recorded earthquakes align with the deepest part of the plate interface determined from seismic reflection data [*Oakley et al.,* 2008].

In order to better constrain the absolute locations of the globally-recorded earthquakes, we simultaneously located them along with the locally-recorded earthquakes using the hypocentroidal decomposition method. The fact that larger earthquakes from 2003-2004 were recorded by both local and teleseismic station sets allowed the local data to provide constraints on the absolute position of all the earthquakes and resulted in reduced uncertainty for teleseismically recorded events (Figure 3).

3.3 Focal Mechanism Determination

We determined focal mechanisms for events in 2003-2004 using a grid-search waveform inversion method based on reflectivity synthetic seismograms [*Kennett*, 1983]. Synthetics were calculated for three fundamental double-couple source geometries [*Langston and Helmberger,* 1975], and then linearly combined to obtain synthetics for each focal mechanism in the grid search. Vertical and transverse component records

from the land Streckeisen STS-2 seismographs as well as the vertical components from Lamont-Doherty ocean-bottom seismometers were used in the inversion. The horizontal components from the ocean-bottom seismometers were not used due to the high level of long-period noise as well as some uncertainty in the orientations of the instruments. While the addition of the OBSs helped to increase the number of available signals for inversion, generally the low frequencies from the OBSs were noisier than those recorded on land due to their location on the seafloor. Furthermore, the 16-bit OBSs closest to the study region were sometimes omitted due to signal clipping.

For each station at which a clear and complete signal was recorded, the trace was filtered from 0.03-0.08 Hz and matched with synthetics computed for the same frequencies and the full range of possible fault solutions. We further refined event depths by varying our inversions over depths of +/- 20 km from the initial value. The solution misfit was defined as the squared difference between the observed and synthetic waveforms, and a cross correlation method was used to allow the synthetic times to vary by up to 2-3 seconds to minimize the effect of small changes in velocity structure. After finding the region of the parameter space for which the synthetics fit best, the grid search was narrowed in scope in order to further refine the solution. The results from the inversion were typically not reliable for earthquakes smaller than Ml 4.2, due to poor signal to noise ratios. Of the 188 earthquakes that we located in the shallow Big Blue region, only 4 of these were large enough to have clean low-frequency signal.

We tested our method on the only shallow earthquake to occur near the study region during the time of our deployment that was large enough to have a GCMT solution (Figure 4). The GCMT solution for this indicates a shallowly-dipping, slightly

oblique thrust faulting mechanism, but has a poorly constrained depth that was fixed at 15 km in the GCMT inversion. The GCMT solution contains a small CLVD component, but is predominantly double-couple with a strike of 7°, dip of 75°, and slip of 120° for the first fault plane and a strike of 124°, dip of 31°, and slip of 31° for the other fault plane of the mechanism. We assume that the north-south striking nodal plane is the plane of rupture; this is consistent with the north-south strike of the subduction zone. Our relocation and waveform modeling of this event indicated that the earthquake depth was slightly deeper (20-25 km). Grid-search results indicated two different mechanisms for which the synthetics had a small misfit to the data; this is likely due to the limited azimuthal coverage of the array, as most of stations were located to the southwest of the earthquake cluster. For the GCMT earthquake one of our best-fitting focal mechanisms was a slightly oblique N-S striking and west-dipping shallow thrust mechanism (fault plane 1: strike 0°, dip 70°, slip 125°; fault plane 2: strike 115°, dip 40°, slip 32°), and the other well-fitting mechanism was an E-W striking oblique normal faulting event (fault plane 1: strike 91°, dip 43°, slip 349°; fault plane 2: strike 189°, dip 83°, slip 226°). Although synthetics from both types of focal mechanisms fit the waveform data well, the N-S striking thrust mechanism had a slightly smaller misfit to the data than the other mechanism and was similar to the GCMT solution. After verifying our waveform inversion solution with the GCMT earthquake, we applied the technique to four other forearc earthquakes with Ml 4.2-4.7 occurring during June 2003-April 2004.

We also attempted to determine focal mechanism solutions for small, local earthquakes using first-motions of the P and S waves as well as SV/SH amplitude ratios inputted into the commonly used FOCMEC program [*Snoke et al.*, 1984]. Examination

revealed that the first motions for earthquakes in our region, specifically SV and SH phases, were often ambiguous, and that the station geometry was poor for focal mechanism determination with first motion data. The limited number of clear constraints resulted in non-unique solutions, so the first motion results are not used in this paper.

4. Results

4.1 Earthquake Locations

The year-long experiment recorded 3,452 earthquakes throughout the entire region of the Mariana Islands. Of these detected earthquakes, just over 1000 were located in the shallow forearc (16-19°N, 145.5-148°E, 0-120 km) with 10 or more P and S arrivals (Figure 5). We observed prominent clusters of earthquakes in the region directly west of Big Blue seamount (17.5-19°N), with significantly fewer events in the forearc south of Big Blue (16-17.5°N) (Figure 5). The proximity of event locations to the densest region of the 2003-2004 seismic array suggests at first that detection capability is dependent on array geometry; however locations for larger, easily-detectable, earthquakes recorded during this time reveal that the increased number of earthquakes near Big Blue Seamount is not dependent on array limitations (Figure 6). These larger earthquakes have $Ml \geq 3$; the estimated magnitude of completeness for our array is $Ml \sim$ 2-2.5. We also consider that the observed pattern of earthquakes may be temporally biased. Yet, the cluster of local events recorded during 2003-2004 coincides with noted patches of seismicity from an OBS deployment in 2001 [*Shiobara et al.*, 2010].

We calculated relative relocations for 188 shallow, locally-recorded earthquakes with 15+ arrivals within the vicinity of OBSs in the Big Blue Seamount region (17.5-18.5°N, 146-148°E, 0-80 km) (Figure 7 and Figure 8). These earthquakes have local magnitudes ranging from Ml 1.6 to 4.7. Of the 158 earthquakes recorded by the ISC during 1976-2008 in the Big Blue Seamount region, we relocated the 25 that have a GCMT solution. Twenty-two of these are thrust type earthquakes.

The locations and depths of the local and GCMT earthquakes cluster along a plane representing the Mariana shallow thrust zone extending from 20 km down to 60 km (Figure 8). This plane of seismicity shows continuance of the plate interface as determined by multi-channel seismic reflection along a survey line just south of Big Blue Seamount [*Oakley et al*., 2008]. The cluster of small earthquakes occurring immediately west of the Big Blue Seamount, elongated in a direction slightly west of north, is clearly delineated in the relative relocation results (Figure 7). Most of these shallow earthquakes occur 100-120 km west of the trench and have depths of 30-45 km (Figure 8). 95% uncertainties in the vertical direction are generally less than ~5-10 km and lateral uncertainties are generally less than 5 km. A few earthquakes have depths well beneath the thrust interface, and are likely related to the up-dip limit of the Mariana double seismic zone [*Barklage*, 2010; *Shiobara et al.,* 2010]. During the local deployment, no earthquakes shallower than 30 km occurred directly beneath the summit of the Big Blue serpentinite mud volcano, located just trench-ward of the majority of our recorded seismicity. The shallowest GCMT thrust earthquakes occur just west of Big Blue Seamount or in the forearc north of Big Blue. The deeper GCMT thrust earthquakes are

located ~30 km west of the shallow section of GCMT thrust earthquakes, with a noticeable gap separating the two groups.

4.2 Focal Mechanisms

All of the earthquakes for which we inverted waveforms to obtain the source had two best-fitting focal mechanisms: a N-S striking thrust mechanism and an E-W striking oblique normal mechanism. As was discussed in the previous section for the GCMT event, this non-uniqueness occurs because the predicted waveforms are similar for the two mechanism types within the limited azimuthal range of our recording stations. Because the thrust focal mechanism fit the well-recorded GCMT event better, despite having two separate mechanism with low misfit to the data, and because none of the GCMT earthquakes found in the region surrounding the Big Blue seamount show E-W striking oblique normal faulting, we select the N-S oriented thrust faulting mechanisms from our waveform inversions as the preferred sense of rupture (Figure 7; Table 3). This assumption, based on tectonic considerations is strengthened by the fact that many of the smaller magnitude earthquakes without focal mechanisms occur in the region immediately surrounding these thrust earthquakes; we presume that these also represent thrust faulting on a shallowly westward-dipping plane (Figure 8). The earthquakes occur along the top of the slab, and define the apparent location of the Mariana shallow megathrust fault.

5. Discussion

5.1 Depth Extent of the Interplate Seismogenic Zone

The seismogenic zone of the Northern Mariana plate interface, as defined by shallowly dipping thrust earthquakes, initiates about 60 km west of the trench at a depth of 20 km and ceases 160 km west of the trench at 60 km depth (Figure 8). This gives an average dip of 21° degrees and a seismogenic zone width of about 100 km. This is significantly larger than the width argued by *Hyndman et al.* [1997] and larger than the 74 km previously estimated by *Pacheco et al.* [1993]. Other island arc regions determined by *Pacheco et al.* [1993] have seismogenic widths ranging from 53 km in the Rat Islands and South Sandwich Islands up to 113 km in the Eastern Aleutians, making the Northern Mariana plate interface towards the wider end of this range.

The up-dip limit of thrust seismicity occurs approximately beneath Big Blue Seamount at the deepest part of the plate interface imaged in the seismic reflection study of *Oakley et al.* [2008]. The onset of seismicity also corresponds to the proposed 200°C isotherm beneath Big Blue Seamount [*Hulme et al.,* 2010] and the intersection between subducting slab and the forearc Moho [*Takahashi et al.,* 2007]. Plate interface thrust earthquakes continue for 40 km deeper than the Moho. Thus nearly all observed Mariana thrust zone seismicity occurs at the interface between the forearc mantle and the downgoing crust. Along with the observed 100 km width of the seismogenic zone, this contradicts the view that the aseismicity for large events along the Mariana subduction zone is a result of an anomalously narrow seismogenic width [*Hyndman et al.*, 1997; *Peacock and Hyndman*, 1999; *Hyndman*, 2007]. In northeast Japan, a setting with

similarly old Pacific oceanic crust, shallow thrust seismicity continues well below the Moho [*Igarashi et al.,* 2001; *Shinohara et al.,* 2005]. If down-dip limit corresponds to temperature, then the 550°C isotherm as determined by *Tichelaar and Ruff* [1993] for oceanic settings may be expected at depth of ~60 km and distance of ~160 km from the trench in Northern Mariana. We conclude that plate interface earthquakes are not limited by the shallow depth of the crust-mantle boundary in the Northern Mariana Subduction Zone.

Our observations of up-dip and down-dip limits may not fully identify the absolute boundaries of the seismogenic thrust, but rather identify a lower end estimate of seismogenic width. Geodetic results from Costa Rica show that the shallowest portion of the seismogenic zone is locked [*Norabuena et al*., 2004] and do not match with up-dip limit estimates from microseismicity [*DeShon et al., 2006*; *Schwartz and DeShon,* 2007]. If the Mariana plate interface is comparable to Costa Rica in this respect, then the shallowest section of the plate interface may be locked rather than sliding stably. Locking along this crust-crust contact would serve to increase the width of the seismogenic zone, which would further increase estimates of seismic slip deficits in this region. Futhermore, rupture along the shallow portion of the plate interface would increase the possibility of hazards associated with tsunamis. From recorded local seismicity, we cannot conclude whether this part of the contact is locked or sliding aseismically; rather we conclude only that underthrusting earthquakes were observed to begin at ~20 km depth.

Estimates of seismic coupling from Table 2 show that despite the addition of other $M \geq 7.0$ earthquakes, the percentage of slip occurring seismically is still very small.

Our estimate of a larger seismogenic plate interface affects calculation of seismic coupling even more. Row 3 of Table 2 illustrates that with more recent estimates of plate convergence rates [*Kato et al.,* 2003] and seismogenic width, the percentage of seismic slip decreases even further, causing the deficit in seismic moment to become unrealistically large (greater than the 1960 Chilean earthquake). Even if we consider only the Northern Mariana seismogenic zone, spanning from 15-19°N, and the events occurring within that region (Table 2, Row 4), the deficit in seismic slip requires that an earthquake greater than Mw 9 occur to compensate for the lack of large earthquakes. These simple calculations argue that because Mw > 9 earthquakes do not occur in this region every ~100 years as necessary to compensate for plate convergence rates, a significant amount of plate convergence must be accommodated through some mechanism allowing aseismic slip between plates.

5.2 Change in Seismogenesis with Depth

Seismogenic behavior continues along the entire depth range of the shallow plate interface in the Northern Mariana Subduction Zone but shows changes with depth. Larger magnitude earthquakes, represented by the 1976-2008 GCMT solutions with Mw 4.9-5.8 are located both up-dip and down-dip of the cluster of small, locally recorded earthquakes. The GCMT events occur mostly within a shallow region 70-100 km west of the trench and in a deeper region of the subduction zone 130-160 km west of the trench, with a prominent gap between them (Figure 8). If we consider only earthquakes that occur within +/-10 km in the vertical direction of our inferred seismogenic zone and

observe how many locally-recorded and GCMT earthquakes (as a percentage of the total number) occur at increasing distances from the trench, we note that many small, locally recorded earthquakes occur within the observed gap in GCMT earthquakes (Figure 9). Although our array recorded local events only during 2003-2004, *Shiobara et al.* [2010] recorded similar clusters of earthquakes during 2001. Therefore we infer that the clusters of small earthquakes are not a short-lived burst of seismicity, but rather a long-term feature.

The pattern of seismicity occurring during 2003-2004 is reminiscent of patterns observed at the Nicoya Peninsula of Costa Rica, where the majority of recorded earthquakes occurred at intermediate depths along the seismogenic zone, both down-dip and up-dip of stronger regions of partial locking as determined by geodesy [*Norabuena et al,*. 2004; *DeShon et al., 2006*]. A study of varying frequency-magnitude distributions (b-values) along-dip of the Costa Rica seismogenic zone indicated that shallow depths had lower b-values, presumably due to greater interplate locking as observed by geodesy [*Norabuena et al.,* 2004; *Ghosh et al.,* 2008]. As noted, our seismic results cannot determine whether the portion of the plate boundary up-dip from our observed seismicity is locked or slipping aseismically; however the frequency of small earthquakes at intermediate depths within the seismogenic zone indicates that the interface further up-dip from this may be more strongly coupled, and perhaps even locked at depths shallower than ~20 km.

The pattern of GCMT seismicity is also similar to the Kermadec, Solomon, and Kamchatka subduction zones, which show a gap in the depth distribution of shallow GCMT thrust earthquakes [*Pacheco et al.,* 1993; *Hyndman et al.*, 1997]. As mentioned

previously, *Hyndman et al.* [1997] hypothesized that gaps at shallow mantle depths along the plate interface in island arc subduction zones could be explained by aseismic mantle serpentinites, but suggested that the Mariana forearc was sufficiently serpentinized that the lower zone of unstable sliding was not reached, and that shallow thrust earthquakes were largely limited to the upper 20 km. Our results using more accurate relative locations of both locally and teleseismically recorded earthquakes contradict this view. The Northern Mariana plate interface seismogenic zone has a notable gap in GCMT events along the plate interface from 100-130 km west of the trench at depths of 30-45 km, which corresponds well with the location of the prominent cluster of smaller magnitude earthquakes. However, larger GCMT thrust faulting events clearly resume at deeper depths.

We propose that the relationship of small and large earthquakes as shown by locally recorded and GCMT events in Figure 8 is due to a change in the magnitudes of earthquakes occurring with depth in the seismogenic zone (Figure 9) that may result from variations in the degree of serpentinization or the presence of high pore fluid pressures. A higher degree of serpentinization could cause most of the seismogenic zone between depths of 30-45 km to show an increased amount of stable sliding and small earthquakes relative to regions up-dip or down-dip. In this case, only small patches of the fault contacting unserpentinized overriding mantle would exhibit stick-slip behavior, and the small size of these "asperities" would result in an absence of larger earthquakes and a predominance of smaller earthquakes within this region. Alternatively, the changing character of seismogenesis with depth could result from a greater abundance of fluids and higher pore pressures within the megathrust fault from 30-45 km. Expulsion of

fluids from pore water and loosely bound structural water within subducting igneous crust could be a potential source for additional fluids at these depths [*Jarrard*, 2003]. Increased pore pressures resulting from slab dehydration have been suggested to enable the occurrence of non-volcanic tremor and low frequency earthquakes in other subduction zones such as Cascadia and southwest Japan [*Shelly et al.,* 2006; *Audet et al.,* 2009]; similarly we expect this mechanism could prove to be a plausible explanation for increased occurrence of smaller magnitude earthquakes with depth. Non-volcanic tremor and low frequency earthquakes have not been detected at the Mariana subduction zone to date; attempts made to observe tremor using the 2003-2004 forearc OBS has been unsuccessful due to presence of other noise in the water column.

Another possibility is that variations in seismic characteristics with depth result from changes in the roughness of the surface of the subducted slab [*Tanioka et al.*, 1997; *Yamanaka and Kikuchi*, 2004; *Bilek*, 2007]. Physical structures of varying sizes, whether subducted seamounts, horst and graben structures, or ridges, would increase normal stress in some regions while decrease normal stress in others – thus producing a variation in size and frequency of earthquakes along the interface. This same mechanism has been invoked to explain patches of increased seismicity in other subduction zones such as Northeast Japan [*Tanioka et al.,* 1997; *Yamanaka and Kikuchi,* 2004] and Costa Rica [*Bilek et al.,* 2003; *DeShon et al.,* 2003; *Ghosh et al.,* 2008]. Large seamounts on the seafloor east of the Mariana Trench implies that the recently subducted seafloor is similarly rough and makes plate interface roughness a distinct possibility for the location and frequent occurrence of GCMT earthquakes beneath different portions of the Northern Mariana forearc. However, this possibility is difficult to test because the

positions of previously-subducted bathymetric features cannot be determined with confidence.

5.3 Along-Strike Plate Interface Heterogeneity

The distinct cluster of local earthquakes in the vicinity of Big Blue Seamount does not continue along the entire length of the Mariana Subduction Zone. Although sufficient seismic detection capabilities existed to the south, at latitudes of 16°-17.5°N, significantly fewer local earthquakes are found. This observation suggests significant lateral variability in plate interface and seismogenic characteristics.

Serpentinization of overriding forearc mantle need not be homogenous along the entire length of the subduction zone; along-strike changes in amount of mantle serpentinization could be created by variations in shallow water flux from the slab. In North and Central Mariana forearcs, results from Rayleigh wave phase velocities indicate lower shear velocities in the central portion of the forearc mantle than in the Northern forearc mantle near Big Blue [*Pyle et al.,* 2010]. If this heterogeneity is due to mantle serpentinization, then some regions of the forearc may be more highly serpentinized than others [*Pyle et al.,* 2010]. Similarly, heterogeneity in mantle serpentinization was proposed in the Northeast Japan mantle forearc [*Yamamoto et al.,* 2008]; regions of low Vp/Vs typical of unaltered mantle wedge material were found to correlate well with increased occurrence of large Mw > 7.0 earthquakes in the off-Miyagi region and regions of high Vp/Vs typical of serpentinized mantle wedge were found to correlate well with lack of large Mw < 7.0 earthquakes off-Fukushima.

Similar to serpentinization of forearc mantle, fluids present along the seismogenic plate interface can be heterogeneous along-strike. Expulsion of water from the subducting slab at shallow plate interface depths occurs due to dewatering of sediments and water trapped within the top of the crust [*Jarrard,* 2003; *Hacker*, 2008; *Oakley et al.,* 2008]. The Mariana subducting slab is generally lacking in sediment in comparison to other margins [*Oakley et al.,* 2008]. Yet recent multi-channel seismic reflection data from *Oakley et al.* [2008] reveals that the sediment layer thickness increases from 1 km in Northern Mariana, near our study area, to 2 km in Central Mariana, south of our study area. Sediments on the Pacific plate are composed of thin layers of cherts and more water-rich clays, with regions of thickened volcaniclastic sediment near seafloor seamounts [*Hacker,* 2008; *Oakley et al.,* 2008]. The change in amount of subducted sediment could provide an increase in water available for expulsion at the shallowest depths in the forearc south of Big Blue [*Jarrard,* 2003]. However, sediment may also act to insulate the incoming Pacific slab, allowing only conductive cooling of the slab in regions of thicker sediment cover rather than convective cooling through hydrothermal circulation [*Harris et al.,* 2010]. Altering the thermal state of the Pacific plate could delay or accelerate specific dehydration processes within the slab [*Spinelli and Wang*, 2009].

The present day Pacific slab subducting beneath the Mariana Islands is quite old, with many bathymetric highs and lows [*Stern and Smoot*, 1998; *Wessel,* 2001; *Stern et al.*, 2003; *Oakley et al.,* 2008]. Between ~16.5-17.75° N, the Mariana trench is deeper and the subducting Pacific plate has fewer seamounts; in the forearc west of this flat region and south of our observed earthquake clusters, thrust seismicity is notably scarce

(Figures 5, 6) [*Oakley et al.,* 2008]. The difference in the subducted seafloor along-strike is a compelling argument that the prominent seamounts subducted near 18°N is responsible for increased seismicity in the forearc of this region [*Tanioka et al.*, 1997; *Bilek,* 2007; *Oakley et al.,* 2008].

5.4 Mechanisms for Aseismic Slip in the Mariana Islands

The results of this study show a clear concentration of small earthquakes along the plate interface, connecting results from *Oakley et al.* [2008] and the locations of shallow thrust GCMT solutions. While this indicates that the seismogenic zone is in fact larger than previously discussed [*Pacheco et al.*, 1993; *Hyndman*, 2007], the results also show that there are changes in the interplate seismogenic zone both along-strike and with depth. Our results show heterogeneity in the size of earthquakes along dip of the seismogenic zone and indicate depth-dependent segmentation of the fault into strong and weak regions. Additionally, our observation of clusters of small earthquakes occurring within the same region as found in 2001 by *Shiobara et al.* [2010] indicates that coupling of the seismogenic zone changes in the along-strike direction as well.

Our observations that seismicity varies both with depth and along-strike of the Northern Mariana Subduction Zone imply a segmented and potentially less coupled seismogenic zone, but the exact cause of the observed variability remains uncertain. While recent tomographic results from the Mariana forearc suggest that partial serpentinization may contribute to our patterns of seismicity and quiescence [*Pozgay et al.,* 2009; *Barklage,* 2010; *Pyle et al.,* 2010], observations of seamounts subducting at the

trench suggest that the cause may be related to the roughness of the subducting seafloor [*Oakley et al.,* 2008].

We suggest that the observed variability is related to the mechanism responsible for presumed aseismic slip in Central and Northern Mariana. The variable seismogenic characteristics along-strike and with depth suggest that a single large locked region is not present along the Mariana subduction zone. Rather, the fault is likely creeping aseismically along portions of the interface, with stable sliding perhaps facilitated by the frictional characteristics of serpentine or by variable effective normal stresses at the plate interface. This heterogeneous character and prominence of stable sliding prohibits the formation of larger locked patches that could slip in great earthquakes, and leaves only disconnected small asperities capable of producing moderate-sized earthquakes.

6. Conclusions

The key conclusion which can be drawn from this study is that the apparent limits of seismogenesis as revealed by earthquake locations and focal mechanisms indicate a shallow thrust zone that is ~100 km wide, extending from 20 to 60 km depth in the Northern Mariana Islands at 18°N near Big Blue Seamount. While past studies have suggested that the lack of large earthquakes in Mariana results from a shallow down-dip limit of seismogenesis due to mantle serpentization, combined location inversions indicate that shallow thrust earthquakes found in the GCMT data set occur along with the locally recorded microearthquakes down to a depth of about 60 km. This result has a wide range of implications regarding seismogenesis along the plate interface in Northern

Mariana. Furthermore, we suggest that observed patterns of seismicity indicate changes in coupling both along strike of the margin and with depth along the plate interface. This can be explained by multiple factors, such as subducted slab topography, expulsion of water from the slab, and formation of serpentinites within the mantle wedge. These mechanisms likely disrupt the continuance of coupling along-strike and affect the potential for nucleation of great, shallow thrust earthquakes in the Northern Mariana Islands.

7. Acknowledgements

Many thanks to M. Barklage, H. Chou, G. Euler, D. Heeszel, S. Pozgay, M. Pyle, P. Shore, and S. Solomatov for their technical and scientific support. Special thanks to the scientists responsible for deployment and collection of the seismographs, including P. Shore, S. Webb, A. Sauter, H. Iwamoto, S. Pozgay, M. Barklage, B. Shiro, P. Jonke, J. Camacho, J. Kaipat, and R. Chong as well as the crew of the R/V Kaiyo, the R/V Wecoma, and the Super Emerald. Thanks to two anonymous reviewers and the associate editor whose attentive comments and suggestions improved this paper. Land seismometers were provided by the PASSCAL program of IRIS. Licensing for Antelope software was provided by IRIS. Research was funded by the MARGINS program of the National Science Foundation, under grants OCE-0001938 and EAR-0549056.

References

Abe, K. (1981), Magnitudes of Large Shallow Earthquakes from 1904 to 1980, *Physics of the Earth and Planetary Interiors*, *27*(1), 72-92, doi: 10.1016/0031-9201(81)90088-1.

Abe, K., and H. Kanamori (1979), Temporal Variation of the Activity of Intermediate and Deep Focus Earthquakes, *J. Geophys. Res., 84*(B7), 3589-3595, doi: 10.1029/JB084iB07p03589.

Abe, K., and S. Noguchi (1983), Revision of Magnitudes of Large Shallow Earthquakes, 1897-1912, *Physics of the Earth and Planetary Interiors*, *33*(1), 1-11, doi: 10.1016/0031-9201(83)90002-X.

Ammon, C. J., C. Ji, H.-K. Thio, D. Robinson, S. Ni, V. Hjorliefsdottir, H. Kanamori, T. Lay, S. Das, D. Helmberger, G. Ichinose, J. Polet, and D. Wald (2005), Rupture process of the 2004 Sumatra-Andaman earthquake, *Science*, *308*(5725), 1133-1139, doi: 10.1126/science.1112260.

Audet, P., M.G. Bostock, N.I. Christensen, and S.M. Peacock (2009), Seismic evidence for overpressured subducted oceanic crust and megathrust fault sealing, *Nature, 457*(7225), 76-78, doi: 10.1038/nature07650.

Barklage, M. (2010), Structure and Seismicity of the Upper Mantle using Deployments of Broadband Seismographs in Antarctica and the Mariana Islands, Ph.D. dissertation, 115 pp, Washington University in Saint Louis, Saint Louis.

Benton, L. D., J.G. Ryan, and I.P. Savov (2004), Lithium abundance and isotope systematics of forearc serpentinites, Conical Seamount, Mariana forearc: Insights

into the mechanics of slab-mantle exchange during subduction, *Geochemistry Geophysics Geosystems*, *5*, Q08J12, doi: 10.1029/2004GC000708.

Bilek, S. L. (2007), Influence of subducting topography on earthquake rupture, in *The Seismogenic Zone of Subduction Thrust Faults*, edited by T. H. Dixon and J. C. Moore, pp. 123-146, Columbia University Press, New York.

Bilek, S. L., and T. Lay (1999), Rigidity variations with depth along interplate megathrust faults in subduction zones, *Nature*, *400*(6743), 443-446, doi: 10.1038/22739.

Bilek, S. L., and T. Lay (2000), Depth dependent rupture properties in Circum-Pacific subduction zones, in *Geocomplexity and the physics of earthquakes*, edited by J. B. Rundle, et al., pp. 165-186, American Geophysical Union, Washington D.C.

Bilek, S.L., S.Y. Schwartz, and H.R. DeShon (2003), Controls on seafloor roughness on earthquake rupture behavior, *Geology, 31*(5), 455-458, doi: 10.1130/0091-7613(2003)031<0455:COSROE>2.0.CO;2.

Byrne, T., and D. Fisher (1990), Evidence for a Weak and Overpressured Decollement beneath Sediment-Dominated Accretionary Prisms, *Journal of Geophysical Research-Solid Earth and Planets*, *95*(B6), 9081-9097, doi: 10.1029/JB095iB06p09081.

Byrne, D. E., D.M. Davis, and L.R. Sykes (1988), Loci and Maximum Size of Thrust Earthquakes and the Mechanics of the Shallow Region of Subduction Zones, *Tectonics*, *7*(4), 833-857, doi: 10.1029/TC007i004p00833.

Campos, J., R. Madariaga, and C. Scholz (1996), Faulting process of the August 8, 1993, Guam earthquake: A thrust event in an otherwise weakly coupled subduction

zone, *Journal of Geophysical Research-Solid Earth*, *101*(B8), 17581-17596, doi: 10.1029/96JB00654.

DeShon, H.R., S.Y. Schwartz, S.L. Bilek, L.M. Dorman, V. Gonzalez, J.M. Protti, E.R. Flueh, and T.H. Dixon (2003), Seismogenic zone structure of the southern Middle America Trench, Costa Rica, *J. Geophys. Res., 108*(B10), doi: 10.1029/2002JB002294.

DeShon, H.R., S.Y. Schwartz, A.V. Newman, V. Gonzalez, M. Protti, L.M. Dorman, T.H. Dixon, D.E. Sampson, and E.R. Flueh (2006), Seismogenic zone structure beneath the Nicoya Peninsula, Costa Rica, from three-dimensional local earthquake P- and S-wave tomography, *Geophys. J. Int., 164*(1), 109-124, doi: 10.1111/j.1365-246X.2005.02809.x.

Dziewonski, A.M., and D.L. Anderson (1981), Preliminary reference Earth model, *Phys. Earth Planet. Inter., 25*(4), 297-356, doi: 10.1016/0031-9201(81)90046-7.

Dziewonski, A. M., T.A. Chou, and J.H. Woodhouse (1981), Determination of earthquake source parameters from waveform data for studies of global and regional seismicity, *J. Geophys. Res.*, *86*(NB4), 2825-2852, doi: 10.1029/JB086iB04p02825.

Freymueller, J. T., H. Woodard, S.C. Cohen, R. Cross, J. Elliott, C.F. Larsen, S. Hreinsdóttir, and C. Zweck (2008), Active deformation processes in Alaska, based on 15 years of GPS measurements, in *Active Tectonics and Seismic Potential of Alaska*, edited by J. T. Freymueller, et al., pp. 1-42, American Geophysical Union, Washington D.C.

Fryer, P. B., and M. H. Salisbury (2006), Leg 195 synthesis: Site 1200 - Serpentinite seamounts of the Izu-Bonin/Mariana convergent plate margin (ODP Leg 125 and 195 drilling results), in *Proc. ODP, Sci. Results,* vol. 195, edited by M. Shinohara et al., pp.1-30, Ocean Drilling Program, College Station, TX, doi: 10.2973/odp.proc.sr.195.112.2006.

Fryer, P., C.G. Wheat, and M.J. Mottl (1999), Mariana blueschist mud volcanism: Implications for conditions within the subduction zone, *Geology*, *27*(2), 103-106, doi: 10.1130/0091-7613(1999)027<0103:MBMVIF>2.3.CO;2.

Fujita, K., E.R. Engdahl, and N.H. Sleep (1981), Subduction zone calibration and teleseismic relocation of thrust zone events in the central Aleutian Islands, *Bull. Seism. Soc. Am.*, *71*(6), 1805-1828.

Gardner, J.V. (2010), US Law of the Sea cruises to map sections of the Mariana Trench and the eastern and southern insular margins of Guam and the Northern Mariana Islands, *Rep. UNH-CCOM/JHC Technical Report 10-003.*

Ghosh, A., A.V. Newman, A.M. Thomas, and G.T. Farmer (2008), Interface locking along the subduction megathrust from b-value mapping near Nicoya Peninsula, Costa Rica, *Geophysical Research Letters*, *35*(1), L01301, doi: 10.1029/2007GL031617.

Gutenberg, B. (1956), Great Earthquakes 1896-1903, *Trans. AGU., 37*(5), 608-614.

Gutenberg, B., and C.F. Richter (1954), *Seismicity of the Earth and Associated Phenomena* (2nd ed.), Hafner Publishing Co., New York.

Hacker, B.R. (2008), H2O subduction beyond arcs, *Geochemistry Geophysics Geosystems, 9*, Q03001, doi: 10.1029/2007GC001707.

Hacker, B. R., G.A. Abers, and S.M. Peacock (2003), Subduction factory - 1. Theoretical mineralogy, densities, seismic wave speeds, and H2O contents, *Journal of Geophysical Research-Solid Earth*, *108*(B1), doi: 10.1029/2001JB001127.

Hall, R. (2002), Cenozoic geological and plate tectonic evolution of SE Asia and the SW Pacific: computer-based reconstructions, model and animations, *J. Asian Earth Sci.*, *20*(4), 353-431, doi: 10.1016/S1367-9120(01)00069-4.

Hall, R., J.R. Ali, C.D. Anderson, and S.J. Baker (1995), Origin and motion history of the Philippine Sea Plate, *Tectonophysics*, *251*(1-4), 229-250, doi: 10.1016/0040-1951(95)00038-0.

Harada, T., and K. Ishibashi (2008), Interpretation of the 1993, 2001, and 2002 Guam earthquakes as intraslab events by a simultaneous relocation of the mainshocks, aftershocks, and background earthquakes, *Bulletin of the Seismological Society of America*, *98*(3), 1581-1587, doi: 10.1785/0120060227.

Harris, R. N., and K. Wang (2002), Thermal models of the middle America trench at the Nicoya Peninsula, Costa Rica, *Geophysical Research Letters*, *29*(21), 2010, doi: 10.1029/2002GL015406.

Harris, R.N., G. Spinelli, C.R. Ranero, I. Grevemeyer, H. Villinger, U. Barckhausen (2010), Thermal regime of the Costa Rican convergent margin: 2. Thermal models of the shallow Middle America subduction zone offshore Costa Rica, *Geochemistry Geophysics Geosystems, 11*(12), Q12S29, doi: 10.1029/2010GC003273.

Hasegawa, A., N. Uchida, T. Igarashi, T. Matsuzawa, T. Okada, S. Miura, and Y. Suwa (2007), Asperities and quasi-static slips on the subducting plate boundary east of

Tohoku, Northeast Japan, in *The Seismogenic Zone of Subduction Thrust Faults*, edited by T. H. Dixon and J. C. Moore, pp. 451-475, Columbia University Press, New York.

Hilairet, N., B. Reynard, Y.B. Wang, I. Daniel, S. Merkel, N. Nishiyama, and S. Petitgirard (2007), High-pressure creep of serpentine, interseismic deformation, and initiation of subduction, *Science*, *318*(5858), 1910-1913, doi: 10.1126/science.1148494.

Hulme, S.M., C.G. Wheat, P. Fryer, and M.J. Mottl (2010), Pore water chemistry of the Mariana serpentinite mud volcanoes: A window to the seismogenic zone, *Geochemistry Geophysics Geosystems, 11*, Q01X09, doi: 10.1029/2009GC002674.

Hyndman, R. D. (2007), What we know and don't know, in *The Seismogenic Zone of Subduction Thrust Faults*, edited by T. H. Dixon and J. C. Moore, pp. 15-40, Columbia University Press, New York

Hyndman, R. D., and K. Wang (1993), Thermal constraints on the zone of major thrust earthquake failure: The Cascadia Subduction Zone, *J. Geophys. Res.*, *98*(B2), 2039-2060, doi: 10.1029/92JB02279.

Hyndman, R. D., K. Wang, and M. Yamano (1995), Thermal constraints on the seismogenic portion of the southwestern Japan subduction thrust, *J. Geophys. Res.*, *100*(B8), 15,373-315,392, doi: 10.1029/95JB00153.

Hyndman, R. D., M. Yamano, and D.A. Oleskevich (1997), The seismogenic zone of subduction thrust faults, *Island Arc*, *6*(3), 244-260, doi: 10.1111/j.1440-1738.1997.tb00175.x.

Igarashi, T., T. Matsuzawa, N. Umino, and A. Hasegawa (2001), Spatial distribution of focal mechanisms for interplate and intraplate earthquakes associated with the subducting Pacific plate beneath the northeastern Japan arc: A triple-planed deep seismic zone, *J. Geophys. Res., 106*(B2), 2,177-2,191, doi: 10.1029/2000JB900386.

Int. Seismol. Cent (ISC) (2010), International Seismological Centre Bulletin, http://www.isc.ac.uk/search/index.html, Int. Seismol. Cent (ISC), Thatcham, U.K.

Jarrard, R.D. (2003), Subduction fluxes of water, carbon dioxide, chlorine, and potassium, *Geochemistry Geophysics Geosystems, 4*(5), 8905, doi: 10.1029/2002GC000392.

Jordan, T. H., and K. A. Sverdrup (1981), Teleseismic location techniques and their application to earthquake clusters in the South-Central Pacific, *Bull. Seism. Soc. Am.*, *71*(4), 1105-1130.

Kanamori, H. (1977), Seismic and aseismic slip along subduction zones and their tectonic implications, in *Island Arcs Deep Sea Trenches, and Back-Arc Basins,* edited by M. Talwani and W.C. Pitman, pp. 163-174, American Geophysical Union, Washington D.C.

Kato, T., J. Beavan, T. Matsushima, Y. Kotake, J.T. Camacho, and S. Nakao (2003), Geodetic evidence of back-arc spreading in the Mariana Trough, *Geophysical Research Letters*, *30*(12), doi: 10.1029/2002GL016757.

Keating, B.H., D.P. Mattey, C.E. Helsley, J.J. Naughton, D. Epp, A. Lazarewicz, and D. Schwank (1984), Evidence for a Hot Spot Origin of the Caroline Islands, *J. Geophys. Res., 89*(B12), 9,937-9,948, doi: 10.1029/JB089iB12p09937.

Kennett, B. L. N. (1983), *Seismic wave propagation in stratified media*, 339 pp., Cambridge University Press, Cambridge.

Kennett, B. L. N., and E. R. Engdahl (1991), Traveltimes for global earthquake location and phase identification, *Geophys J. Int.*, *105*(2), 429-465, doi: 10.1111/j.1365-246X.1991.tb06724.x.

Langston, C.A. and D.V. Helmberger (1975), A procedure for modeling shallow dislocation sources, *Geophysical Journal of the Royal Astronomical Society, 42*(1), 117-130.

Lay, T., H. Kanamori, C.J. Ammon, M. Nettles, S.N. Ward, R.C. Aster, S. L. Beck, S.L. Bilek, M.R. Brudzinski, R. Butler, H.R. DeShon, G. Ekström, K. Satake, and S. Sipkin (2005), The great Sumatra-Andaman earthquake of 26 December 2004, *Science*, *308*(5725), 1127-1133, doi: 10.1126/science.1112250.

Marone, C., and C. H. Scholz (1988), The depth of seismic faulting and the upper transition from stable to unstable slip regimes, *Geophysical Research Letters*, *15*(6), 621-624, doi: 10.1029/GL015i006p00621.

Maso, Rev. M.S. (1910), *Catalogue of Violent and Destructive Earthquakes in the Philippines, with an Appendix, Earthquakes in the Marianas Islands; 1599-1909*, Department of the Interior, Philippine Islands Weather Bureau, Manila Central Observatory.

Moore, D. E., and D. A. Lockner (2007), Comparative deformation behavior of minerals in serpentinized ultramafic rock: Application to the slab-mantle interface in subduction zones, *International Geology Review*, *49*(5), 401-415, doi: 10.2747/0020-6814.49.5.401.

Moore, D. E., D.A. Lockner, S.L. Ma, R. Summers, and J.D. Byerlee (1997), Strengths of serpentinite gouges at elevated temperatures, *J. Geophys. Res.*, *102*(B7), 14787-14801, doi: 10.1029/97JB00995.

Moore, J. C., and D. M. Saffer (2001), Updip limit of the seismogenic zone beneath the accretionary prism of southwest Japan: An effect of diagenetic to low-grade metamorphic processes and increasing effective stress, *Geology*, *29*(2), 183-186, doi: 10.1130/0091-7613(2001)029<0183:ULOTSZ>2.0CO;2.

Newman, A. V., S.Y. Schwartz, V. Gonzalez, H.R. DeShon, J.M. Protti, and L.M. Dorman (2002), Along-strike variability in the seismogenic zone below Nicoya Peninsula, Costa Rica, *Geophysical Research Letters*, *29*(20), doi: 10.1029/2002GL015409.

Norabuena, E., T.H. Dixon, S. Schwartz, H. DeShon, A. Newman, M. Protti, V. Gonzalez, L.R. Dorman, E.R. Flueh, P. Lundgren, F. Pollitz, and D. Sampson (2004), Geodetic and seismic constraints on some seismogenic zone processes in Costa Rica, *J. Geophys. Res. 109*, B11403, doi: 10.1029/2003JB002931.

Oakley, A. J., B. Taylor, P. Fryer, G.E. Moore, A.M. Goodliffe, and J.K. Morgan (2007), Emplacement, growth, and gravitational deformation of serpentinite seamounts on the Mariana forearc, *Geophysical Journal International*, *170*(2), 615-634, doi: 10.1111/j.1365-246X.2007.03451.x.

Oakley, A. J., B. Taylor, and G.F. Moore (2008), Pacific Plate subduction beneath the central Mariana and Izu-Bonin fore arcs: New insights from an old margin, *Geochemistry Geophysics Geosystems*, *9*(6), 28, doi: 10.1029/2007GC001820.

Oleskevich, D. A., R.D. Hyndman, and K. Wang (1999), The updip and downdip limits to great subduction earthquakes: Thermal and structural models of Cascadia, south Alaska, SW Japan, and Chile, *Journal of Geophysical Research-Solid Earth*, *104*(B7), 14965-14991, doi: 10.1029/1999JB900060.

Pacheco, J. F., and L. R. Sykes (1992), Seismic Moment Catalog of Large Shallow Earthquakes, 1900 to 1989, *Bulletin of the Seismological Society of America*, *82*(3), 1306-1349.

Pacheco, J. F., L.R. Sykes, and C.H. Scholz (1993), Nature of Seismic Coupling Along Simple Plate Boundaries of the Subduction Type, *Journal of Geophysical Research-Solid Earth*, *98*(B8), 14133-14159, doi: 10.1029/93JB00349.

Pavlis, G. L., F. Vernon, D. Harvey, and D. Quinlan (2004), The generalized earthquake-location (GENLOC) package: an earthquake-location library, *Computers and Geosciences*, *30*(9-10), 1079-1091, doi: 10.1016/j.cageo.2004.06.010.

Peacock, S. M., and R. D. Hyndman (1999), Hydrous minerals in the mantle wedge and the maximum depth of subduction thrust earthquakes, *Geophys. Res. Lett.*, *26*(16), 2517-2520, doi: 10.1029/1999GL900558.

Pozgay, S. H., R.A. White, D.A. Wiens, P.J. Shore, A.W. Sauter, and J.L. Kaipat (2005), Seismicity and tilt associated with the 2003 Anatahan eruption sequence, *J. Volcanol. Geotherm. Res.*, *146*(1-3), 60-76, doi: 10.1016/j.jvolgeores.2004.12.008.

Pozgay, S. H., D.A. Wiens, J.A. Conder, H. Shiobara, and H. Sugioka (2007), Complex mantle flow in the Mariana Subduction System: Evidence from shear wave

splitting, *Geophys. J. Int.*, *170*(1), 371-386, doi: 10.1111/j.1365-246X.2007.03433.x.

Pozgay, S., D.A. Wiens, J.A. Conder, H. Shiobara, and H. Sugioka (2009), Seismic attenuation tomography of the Mariana arc: Implications for thermal structure, volatile distribution, and dynamics, *Geochem. Geophys. Geosystems*, *10*, Q04X05, doi: 10.1029/2008GC002313.

Pyle, M., D.A. Wiens, D.S. Weeraratne, P.J. Shore, H. Shiobara, and H. Sugioka (2010), Shear velocity structure of the Mariana mantle wedge from Rayleigh wave phase velocities, *J Geophys. Res.*, *115*, B11304, doi: 10.1029/2009JB006976.

Reinen, L. A., J.D. Weeks, and T.E. Tullis (1991), The frictional behavior of serpentinite - Implications for aseismic creep on shallow crustal faults, *Geophysical Research Letters*, *18*(10), 1921-1924, doi: 10.1029/91GL02367.

Richter, C. F. (1958), *Elementary Seismology*, W.H. Freeman and Co., San Francisco, Calif.

Rossi, G., G.A. Abers, S. Rondenay, and D.H. Christensen (2006), Unusual mantle Poisson's ratio, subduction, and crustal structure in central Alaska, *J. Geophys. Res., 111*(B9), B09311, doi: 10.1029/2005JB003956.

Saffer, D. M., and C. Marone (2003), Comparison of smectite- and illite-rich gouge frictional properties: application to the updip limit of the seismogenic zone along subduction megathrusts, *Earth and Plan. Sci. Lett.*, *215*(1-2), 219-235, doi: 10.1016/S0012-821X(03)00424-2.

Satake, K., Y. Yoshida, and K. Abe (1992), Tsunami from the Mariana earthquake of April 5, 1990 – its abnormal propagation and implications for tsunami potential

from outer-rise earthquakes, *Geophys. Res. Lett., 19*(3), 301-304, doi: 10.1029/91GL02493.

Scholz, C. H., and J. Campos (1995), On the mechanism of seismic decoupling and back arc spreading at subduction zones, *J. Geophys. Res., 100*(B11), 22,103-22,115, doi: 10.1029/95JB01869.

Schwartz, S. Y., and H. R. DeShon (2007), Distinct updip limits to geodetic locking and microseismicity at the northern Costa Rica seismogenic zone: Evidence for two mechanical transitions, in *The Seismogenic Zone of Subduction Thrust Faults*, edited by T. H. Dixon and J. C. Moore, pp. 576-599, Columbia University Press, New York.

Seno, T. (2005), Variation of downdip limit of the seismogenic zone near the Japanese islands: Implications for the serpentinization mechanism of the forearc mantle wedge, *Earth and Plan. Sci. Lett.*, *231*(3-4), 249-262, doi: 10.1016/j.epsl.2004.12.027.

Shelly, D. R., G.C. Beroza, S. Ide, and S. Nakamula (2006), Low-frequency earthquakes in Shikoku, Japan, and their relationship to episodic tremor and slip, *Nature*, *442*(7099), 188-191, doi: 10.1038/nature04931.

Shinohara, M., R. Hino, T. Yoshizawa, M. Nishino, T. Sato, and K. Suyehiro (2005), Hypocenter distribution of plate boundary zone off Fukushima, Japan, derived from ocean bottom seismometer data, *Earth Planets and Space*, *57*(2), 93-105.

Shiobara, H., H. Sugioka, K. Mochizuki, S. Oki, T. Kanazawa, Y. Fukao, and K. Suyehiro (2010), Double seismic zone in the North Mariana region revealed by

long-term ocean bottom array observation, *Geophys. J. Int.*, *183*(3), 1455-1469, doi: 10.1111/j.1365-246X.2010.04799.x.

Smith, W.H.F., H. Staudigel, A.B. Watts, and M.S. Pringle (1989), The Magellan Seamounts: Early Cretaceous Record of the South Pacific Isotopic and Thermal Anomaly, *J. Geophys. Res., 94*(B8), 10,501-10,523, doi: 10.1029/JB094iB08p10501.

Snoke, J. A., J.W. Munsey, A.C. Teague, and G.A. Bollinger (1984), A program for focal mechanism determination by combined use of polarity and SV-P amplitude ratio data, *Earthquake Notes*, *55*, 15.

Soloviev, S. L., and Ch. N. Go (1974), *A catalogue of tsunamis on the western shore of the Pacific Ocean* [in Russian], Academy of Sciences of the USSR, Nauka Publishing House, Moscow. [English translation, 447 p., Canadian Translation In Fisheries and Aquatic Sciences, Ottawa, Ontario, Canada, 1984]

Spinelli, G. A., and D. M. Saffer (2004), Along-strike variations in underthrust sediment dewatering on the Nicoya margin, Costa Rica related to the updip limit of seismicity, *Geophysical Research Letters*, *31*(4), L04613, doi: 10.1029/2003GL018863.

Spinelli, G.A., and K. Wang (2009), Links between fluid circulation, temperature, and metamorphism in subducting slabs, *Geophysical Research Letters, 36,* L13302, doi: 10.1029/2009GL03876.

Stern, R. J., and N. C. Smoot (1998), A bathymetric overview of the Mariana forearc, *Island Arc*, *7*(3), 525-540, doi: 10.1046/j.1440-1738.1998.00208.x.

Stern, R. J., M.J. Fouch, and S.L. Klemperer (2003), An overview of the Izu-Bonin-Mariana subduction factory, in *Inside the Subduction Factory*, edited by J. M. Eiler, pp. 175-222, American Geophysical Union, Washington D.C.

Takahashi, N., S. Kodaira, S. L. Klemperer, Y. Tatsumi, Y. Kaneda, and K. Suyehiro (2007), Crustal structure and evolution of the Mariana intra-oceanic island arc, *Geology*, *35*(3), 203-206, doi: 10.1130/G23212A.1.

Tanioka, Y., K. Satake, and L. Ruff (1995), Analysis of Seismological and Tsunami Data from the 1993 Guam Earthquake, *Pure and Applied Geophysics*, *144*(3-4), 823-837, doi: 10.1007/BF00874396.

Tanioka, Y., L. Ruff, and K. Satake (1997), What controls the lateral variation of large earthquake occurrence along the Japan Trench?, *Island Arc*, *6*(3), 261-266, doi: 10.1111/j.1440-1738.1997.tb00176.x.

Tibi, R., D.A. Wiens, and X.H. Yuan (2008), Seismic evidence for widespread serpentinized forearc mantle along the Mariana convergent margin, *Geophys. Res. Lett.*, *35*(13), L13303, doi: 10.1029/2008GL034163.

Tichelaar, B. W., and L. J. Ruff (1993), Depth of seismic coupling along subduction zones, *J. Geophys. Res.*, *98*(B2), 2017-2037, doi: 10.1029/92JB02045.

Uyeda S., and H. Kanamori (1979), Back-arc opening and the mode of subduction, *J. Geophys. Res., 84*(B3), 1049-1061, doi: 10.1029/JB084iB03p01049.

Vrolijk, P. (1990), On the mechanical role of smectite in subduction zones, *Geology, 18*(8), 703-707, doi: 10.1130/0091-7613(1990)018<0703:OTMROS>2.3.CO;2

Wada, I., and K. L. Wang (2009), Common depth of slab-mantle decoupling: Reconciling diversity and uniformity of subduction zones, *Geochem. Geophys. Geosystems*, *10*, Q10009, doi: 10.1029/2009GC002570.

Webb, S. C., T.K. Deaton, and J.C. Lemire (2001), A broadband ocean-bottom seismometer system based on a 1-Hz natural period geophone, *Bulletin of the Seismological Society of America*, *91*(2), 304-312, doi: 10.1785/0120000110.

Wessel, P. (2001), Global distribution of seamounts inferred from gridded Geosat/ERS-1 altimetry, *J. Geophys. Res., 106*(B9), 19,431-19,441, doi: 10.1029/2000JB000083.

Yamamoto, Y., R. Hino, K. Suzuki, Y. Ito, T. Yamada, M. Shinohara, T. Kanazawa, G. Aoki, M. Tanaka, K. Uehira, G. Fujie, Y. Kaneda, T. Takanami, and T. Sato (2008), Spatial heterogeneity of the mantle wedge structure and interplate coupling in the NE Japan forearc region, *Geophys. Res. Lett., 35*(23), L23304, doi: 10.1029/2008GL036100.

Yamanaka Y. and M. Kikuchi (2004), Asperity map along the subduction zone in northeastern Japan inferred from regional seismic data, *J. Geophys. Res., 109*(B7), B07307, doi: 10.1029/2003JB002683.

Yoshida, Y., K. Satake, and K. Abe (1992), The large normal-faulting Mariana earthquake of April 5, 1990 in uncoupled subduction zone, *Geophys. Res. Lett., 19*(3), 297-300, doi: 10.1029/92GL00165.

Figure Captions

Figure 1:

Array geometry for the 2003-2004 Mariana Subduction Factory Imaging Experiment. Left image shows complete array of stations along with bathymetry. Top right image shows the stations that returned good data for the period before August 2003, prior to failure of the MPL4n OBS. Bottom right image shows station geometry following August 2003. Stations are indicated in both plots by colored triangles (dark blue: Guralp 40T; cyan: STS2; red: Japanese PMD OBS; dark gray: MPL4o OBS; and light gray: MPL4n OBS). Pacific plate convergence beneath the Mariana Forearc is shown by thick black arrows; rate of convergence as determined by Kato et al (2003) is noted above each arrow. Thick Red lines show the location of the back-arc spreading center. Inset map in lower left shows all subduction trenches (blue lines), spreading centers (red lines) and transform boundaries (green lines) in the vicinity of the Mariana subduction zone and the Philippine Sea.

Figure 2:

Locations for Events 5-16 listed in Table 1. All events are Mw or Ms $\geq$ 7.0, with depths less than 100 km, and are in or nearby the Mariana forearc. Epicenters of earthquakes occurring in 1902-1950 are indicated by yellow circles. Numbers within the yellow circles correspond to event numbers 5-13 listed in Table 1. Epicenters of thrust earthquakes occurring in 1951-2011 are indicated by red circles, and numbers within the red circles correspond to event numbers 14-16 in Table 1.

Figure 3:

Image shows the shift between GCMT earthquakes relocated only with other teleseismic events (yellow circles; average location yellow diamond) and GCMT earthquakes relocated along with local Mariana events (blue circles; average location blue diamond). Red squares show the trace of the plate interface just south of the Big Blue Seamount as determined by *Oakley et al.* (2008). Light blue squares show the location of forearc ocean-bottom seismometers during the 2003-2004 Mariana Subduction Factory Experiment. Black line shows the bathymetry of the forearc at 18° N. Thick black line shows the trace of the Moho in the region south of Celestrial Seamount, ~17° N, as determined by *Takahashi et al.* (2007).

Figure 4:

Example of data (solid line) and synthetics (dashed line) from the stations used in our waveform inversion for the 23 January 2004 event, for which a GCMT solution has been determined. Station azimuths range from 260º in the north on Agrihan island to 201º in the south at Rota island. The solid black lines of the focal mechanism show the fault planes from this study (P axis: solid black triangle; T axis: black outlined, inverted triangle), while the dashed gray lines show the best-fitting double couple from the GCMT solution (P axis: solid gray triangle; T axis: gray outlined, inverted triangle).

Figure 5:

Locations of earthquakes in the Mariana subduction zone from 15-20° N prior to relocation. Yellow circles indicate earthquakes at 0-50 km depth; orange circles are earthquakes at 50-100 km depth; red circles are earthquakes deeper than 100 km. Black squares show the locations of land and ocean-bottom seismographs. GCMT solutions from 1976-2008 are plotted on a lower-hemisphere projection and colored black (compressive quadrants) and white (extensional quadrants).

Figure 6:

Locations of earthquakes, with magnitude greater than or equal to Ml 3.0, in the Mariana subduction zone from 15-20° N prior to relocation. Yellow circles indicate earthquakes at 0-50 km depth; orange circles are earthquakes at 50-100 km depth; red circles are earthquakes deeper than 100 km. Black squares show the locations of land and ocean-bottom seismographs. GCMT solutions are plotted on a lower-hemisphere projection and colored black (compressive quadrants) and white (extensional quadrants).

Figure 7:

Top: Map view of study region showing locally-recorded seismicity during 2003-2004 in the vicinity of Big Blue Seamount. Yellow circles indicate earthquakes occurring at 0-30 km depth. Orange circles indicate earthquakes occurring at 30-60 km depth. Dark red circles indicate earthquakes occurring at 60-100 km depth. Relocated GCMT

earthquakes occurring between 17.5-18.5° N during 1976-2008 with double-couple focal mechanisms plotted on a lower-hemisphere projection and colored black (compressive quadrants) and white (extensional quadrants). Focal mechanisms determined in this study for the largest local earthquakes occurring during 2003-2004 are colored red (compressive quadrants) and white (extensional quadrants).

Bottom: Map view of study region, omitting bathymetry, showing the 2σ confidence ellipsoids projected onto the latitude-longitude plane. Ellipses with a thin, black outline show the confidence in horizontal location for locally-recorded earthquakes during 2003-2004. Ellipses with a thick, black outline show the confidence in horizontal location for GCMT earthquakes from 1976-2008. Focal mechanisms are shown for GCMT solutions and 2003-2004 earthquakes as described above.

Figure 8:

Top (a): Cross-section of all 1976-2008 relocated GCMT earthquakes along with 2003-2004 locally recorded earthquakes. Double-couple focal mechanisms for GCMT earthquakes (black) and this study (red) are shown in side-projection. Yellow circles show the locations of our locally-recorded earthquakes. Red squares show the trace of the plate interface just south of the Big Blue Seamount as determined by *Oakley et al.* (2008). Light blue squares show the location of forearc ocean-bottom seismometers during the 2003-2004 Mariana Subduction Factory Experiment. Black line shows the bathymetry of the forearc at 18° N. Thick black line shows the trace of the Moho in the region south of Celestrial Seamount, ~17° N, as determined by *Takahashi et al.* (2007).

Middle (b): Cross-sectional view showing the 2σ confidence ellipsoids for GCMT earthquakes projected onto the vertical plane. Large ellipses with a thick, black outline show the confidence in location and depth for GCMT earthquakes from 1976-2008. Focal mechanisms are shown for GCMT solutions as described above.

Bottom (c): Cross-sectional view showing the 2σ confidence ellipsoids for locally-recorded earthquakes projected onto the vertical plane. Small ellipses with a thin, black outline show the confidence in location and depth for locally-recorded earthquakes during 2003-2004. Focal mechanisms shown in side-projection determined for 2003-2004 earthquakes in this study are shown in red.

Figure 9:

The occurrence of 2003-2004 locally-recorded earthquakes (blue squares and blue line) and 1976-2008 GCMT thrust earthquakes (red squares and red line) within the seismogenic zone is plotted with increasing distance from the trench. Local and GCMT earthquakes are plotted as a percentage of the total amount of local and GCMT seismicity. All earthquakes shallower than 70 km and also within 10 km vertically of the observed seismogenic zone were culled from the entire region shown in Figure 8. For every 2.5 km of distance from the trench, the total number of earthquakes within a 5 km window (2.5 km to either side) was counted and represented as percentage of the total number of earthquakes of the same type (GCMT or local) occurring within the region inferred to be the seismogenic zone. Most of the locally-recorded earthquakes occur in a region where few GCMT earthquakes are located, suggesting some mechanism inhibiting

the occurrence of larger shallow thrust earthquakes in this middle region of the seismogenic zone.

Tables

Table 1. Large Shallow Earthquakes (M ≥ 7 or Guam MMI ≥ 8) in the Mariana Forearc 1825-2011

Event	Date	Time (UTC)	Latitude (°North)	Longitude (°East)	Depth (km)	Type of Slip	Magnitude &/or Intensity
1	Apr 1825	n/a	n/a[a]	n/a[a]	n/a	n/a	8 MMI[b]
2	May 1834	n/a	n/a[a]	n/a[a]	n/a	n/a	8 MMI[b]
3	25 Jan 1849	14:56[b,c]	n/a[a]	n/a[a]	n/a	n/a	M 7.5[d] 9 MMI[b]
4	16 May 1892	21:10[b,c]	n/a[a]	n/a[a]	n/a	n/a	M 7.5[d] 8 MMI[b]
5	22 Sept 1902	1:46:30[e]	18.0[e]	146.0[e]	n/a	n/a	Ms 7.4[f] 9 MMI[b]
6	23 Mar 1913	20:47.3	24[g]	142[g]	80[g]	n/a	mb 7.1[h]
7	24 Oct 1930	20:15:11	18.5[g]	147[g]	35[g]	n/a	Ms 7.0[h]
8	28 Jan 1931	21:24:03	11[g]	144.75[g]	35[g]	n/a	Ms 7.1[h]
9	24 Feb 1934	6:23:40	22.5[g]	144[g]	35[g]	n/a	Ms 7.1[f]
10	17 Jan 1940	01:15:00	17[g]	148[g]	80[g]	n/a	mb 7.3[i]
11	28 Dec 1940	16:37:44	18[e]	147.5[g]	80[g]	n/a	mb 7.3[i]
12	14 Jun 1942	03:09:45	15[g]	145[g]	80[g]	n/a	mb 7.0[h]
13	25 May 1950	18:35:07	13[g]	143.5[g]	90[g]	n/a	mb 7.0[h]
14	8 Aug 1993	8:34:49.3	13.06	145.31	59.3	Thrust	Mw 7.7
15	12 Oct 2001	15:02:23.3	12.88	145.08	42.0	Thrust	Mw 7.0
16	26 Apr 2002	16:06:13.9	13.15	144.67	69.1	Thrust	Mw 7.0

[a]Strong shaking felt on island of Guam, earthquake locations unknown.
[b]*Maso* [1910].
[c]Indicates Local Guam Time.
[d]*Soloviev and Go* [1974].
[e]*Gutenberg* [1956].
[f]*Pacheco and Sykes* [1992].

[g] *Gutenberg and Richter* [1954].
[h] *Abe* [1981].
[i] *Abe and Kanamori* [1979].
[j] Global CMT catalog, *Dziewonski et al* [1981].

Table 2. Parameters affecting seismic slip coefficient and maximum earthquake magnitude[a]

	Margin Length - L (km)	Seismogenic Width - W (km)	Time - T (yrs)	Convergence Rate - $\dot{u}_p$ (mm/yr)	Cumulative Moment - $\sum_i^N M_o^i$ (N-m)	Seismic slip coefficient – α	Moment deficit (N-m)	Magnitude deficit
1	1280	74	90	30	2.36 E20	0.0018	1.28 E23	9.34
2	1280	74	110	30	1.20 E21	0.0077	1.55 E23	9.39
3	1280	100	110	50	1.20 E21	0.0034	3.51 E23	9.63
4	560	100	110	40	4.62 E20	0.0037	1.23 E23	9.33

[a]Relationship used by *Pacheco et al.* (1993) for seismic slip coefficient: $\alpha = \frac{\dot{u}_s}{\dot{u}_p}$ where $\dot{u}_p$ is plate convergence rate and rate of seismic slip: $\dot{u}_s = \sum_i^N \frac{M_o^i}{\mu TWL}$. For all calculations, rigidity (μ) is 5.0E10 $\frac{N}{m^2}$. Parameters and results in Row 1 are those calculated by *Pacheco et al.* (1993) for the entire 1280 km length of the Mariana Subduction Zone. Row 2 incorporates a longer record and all shallow (depth <100), M ≥ 7.0 seismicity nearby the Mariana forearc. Row 3 assumes a 100 km seismogenic width and recent (averaged along the margin) plate convergence rate from *Kato et al.* (2003). Row 4 assumes the margin between 15-20°N and moment from all events in Table 1 at those latitudes. All calculations require that moment equivalent to a magnitude 9+ earthquake be released in order to compensate for the 110 years of Pacific plate convergence.

Table 3. Waveform Inversion Results: Earthquake Locations and Fault Orientations

Date	Time (UTC)	Latitude (°N)	Longitude (°E)	Depth (km)	Strike (°)	Dip (°)	Slip (°)	Mw
7 Jul 2003	17:29:41	18.37	147.23	26	0	89	110	4.3
8 Jul 2003	09:12:38	18.43	146.70	40	91	21	0	4.2
15 Jul 2003	14:51:32	18.08	146.85	40	20	89	123	5.1
23 Jan 2004	03:39:14	18.91	147.24	22.5	0	79	125	5.6
17 Apr 2004	21:56:30	18.38	146.92	29	5	89	112	4.5

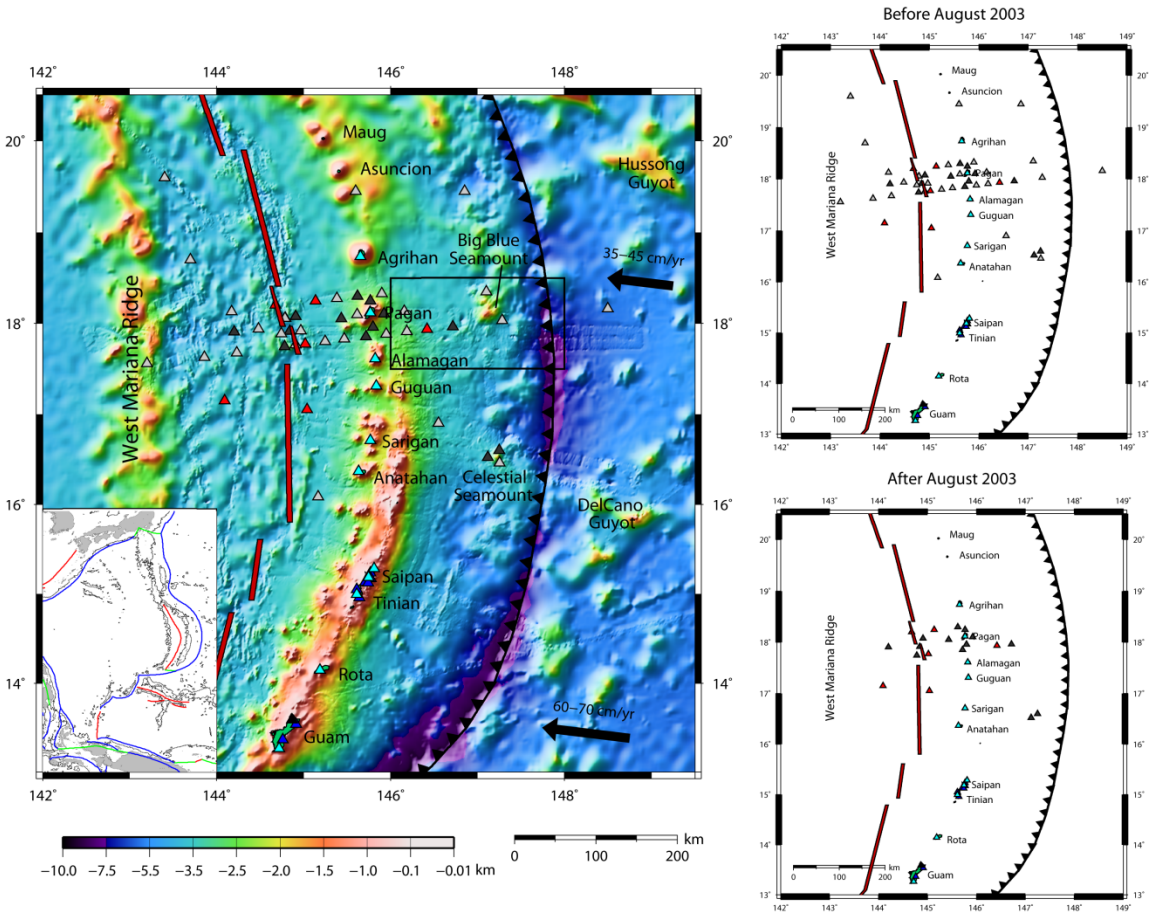

Figure 1 – 2003-2004 Mariana SubFac Deployment

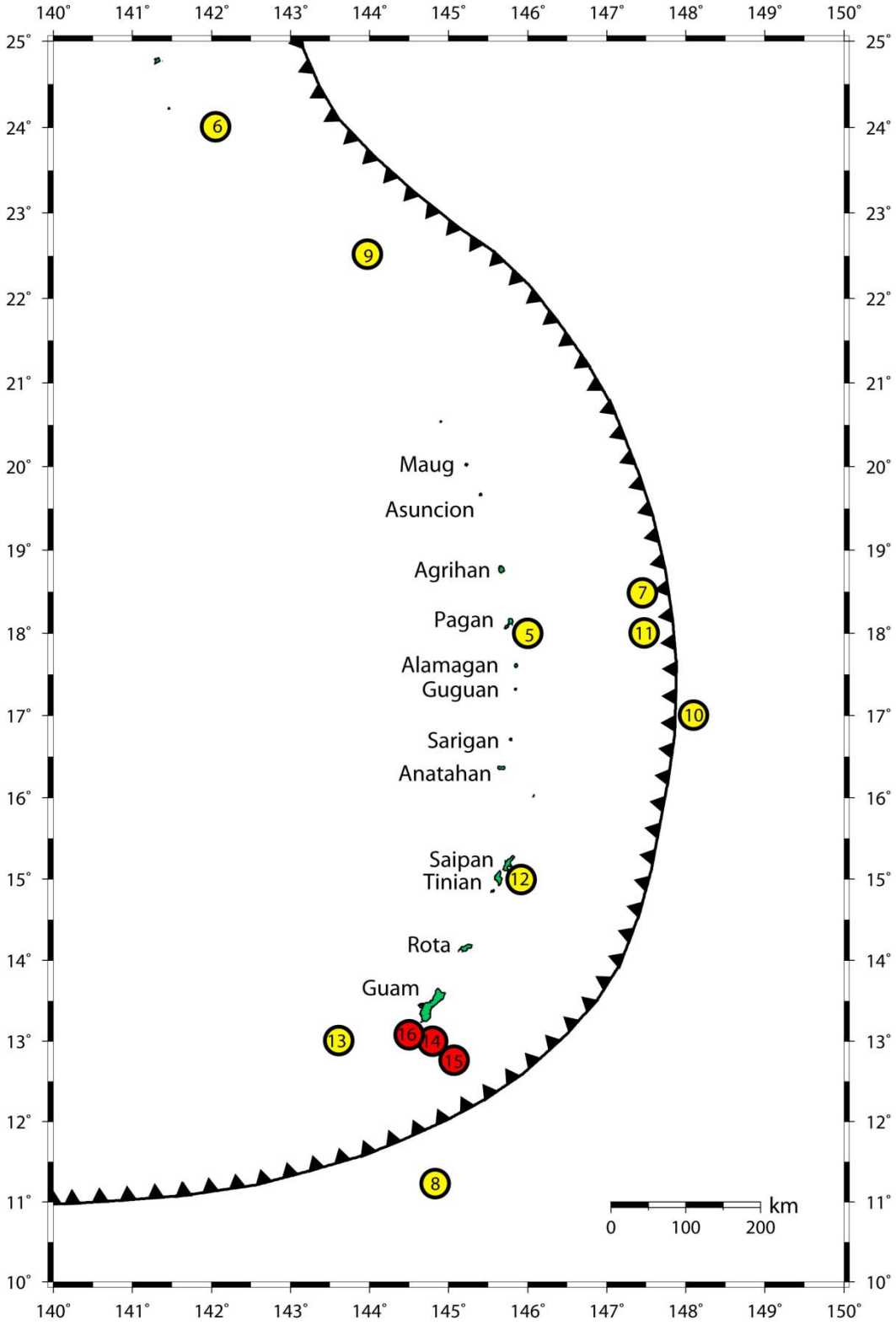

Figure 2 – Large Earthquakes at the Mariana Subduction Zone

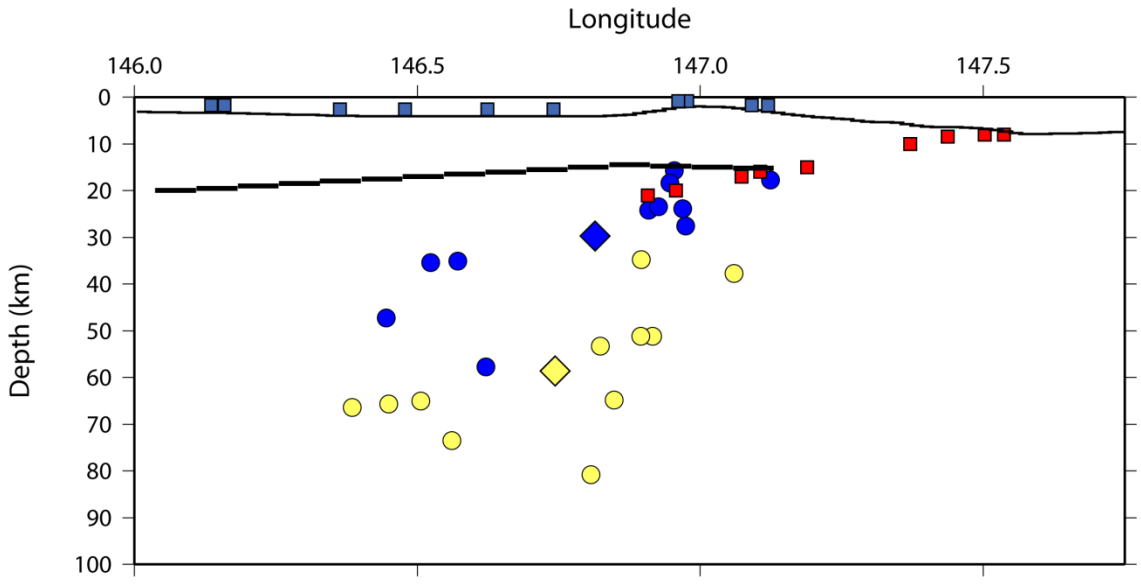

Figure 3 – Teleseismic Shift in Earthquake Locations

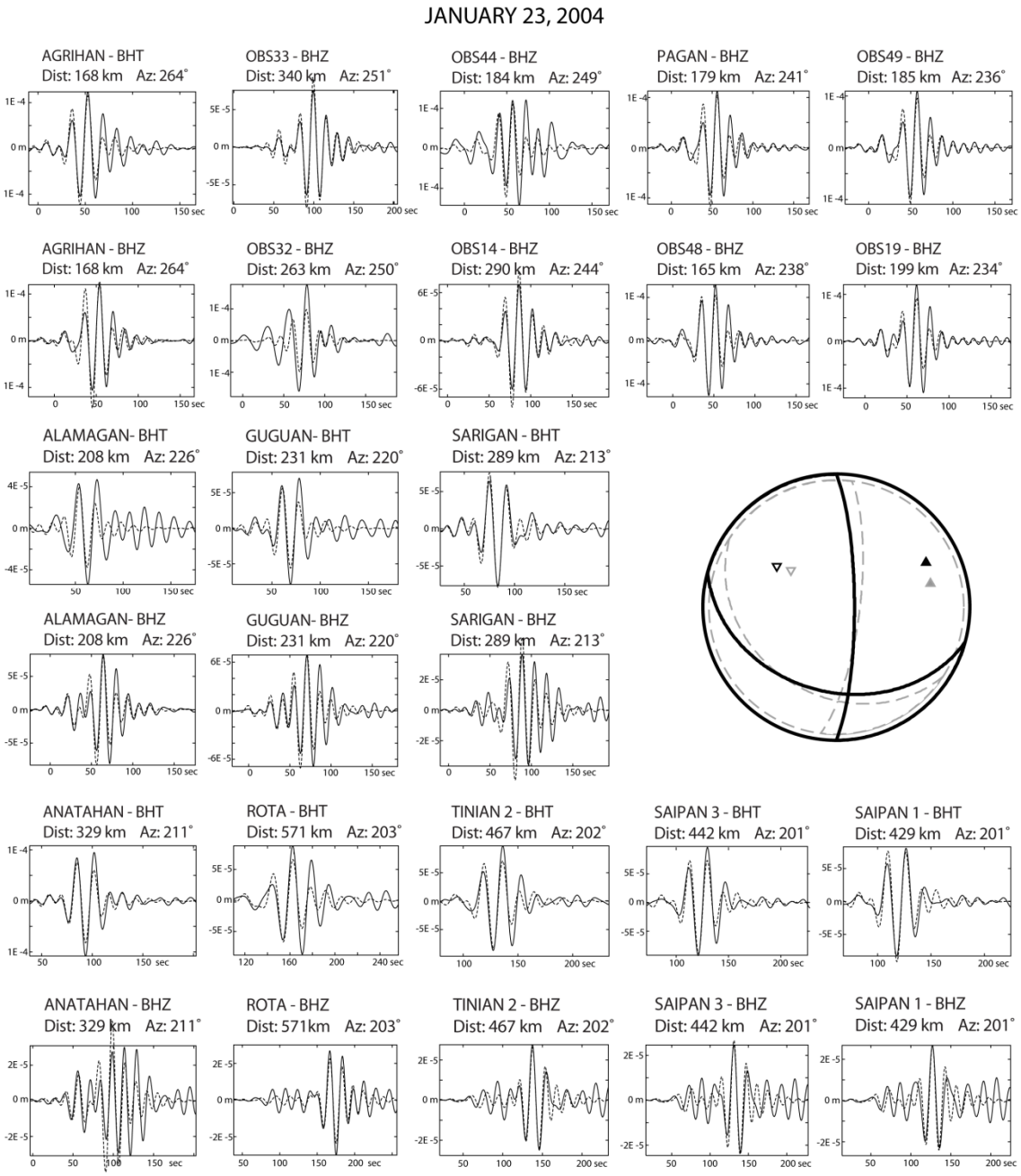

Figure 4 – Waveforms for 23 January 2004 Event

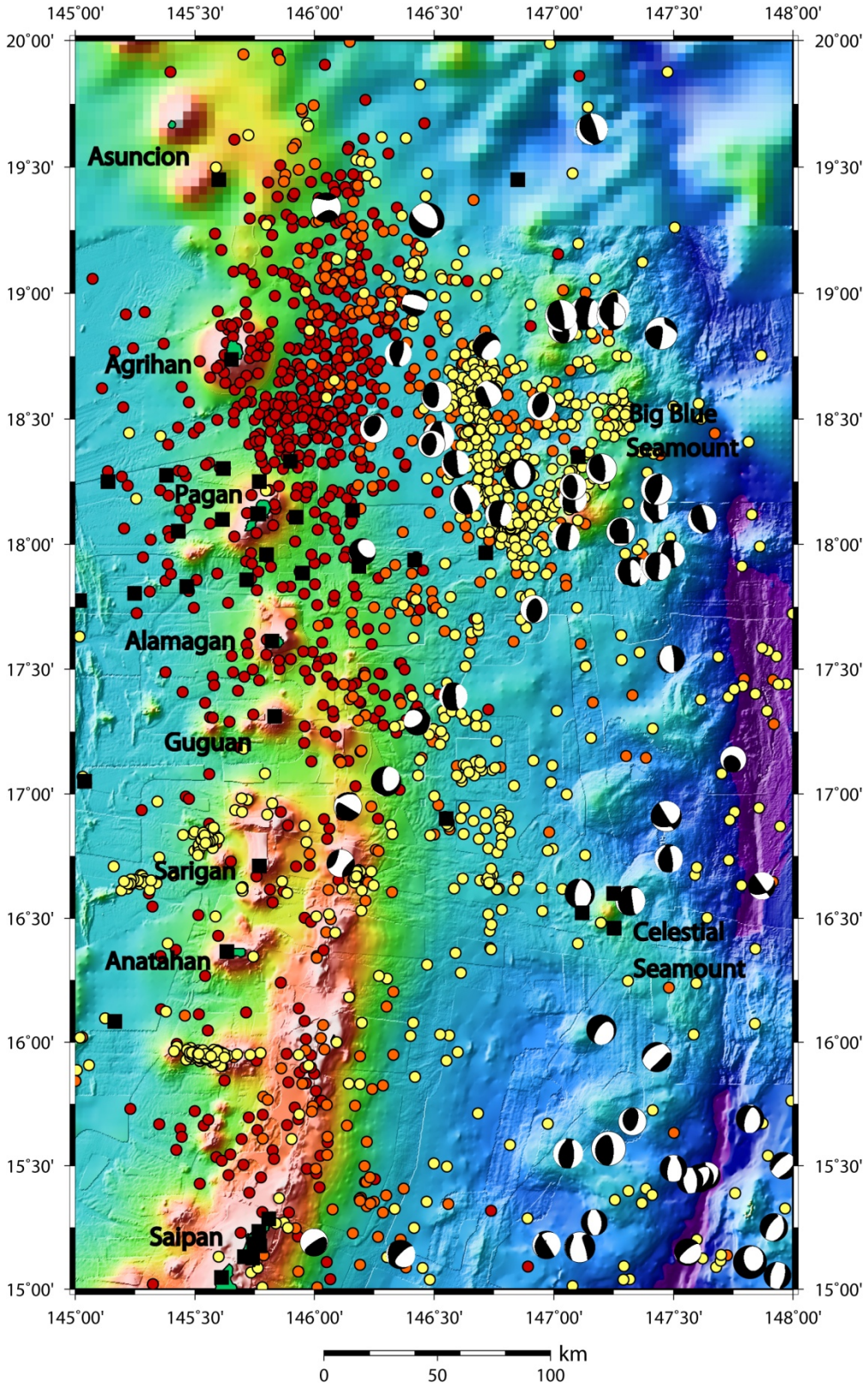

Figure 5 – Mariana Forearc Earthquakes

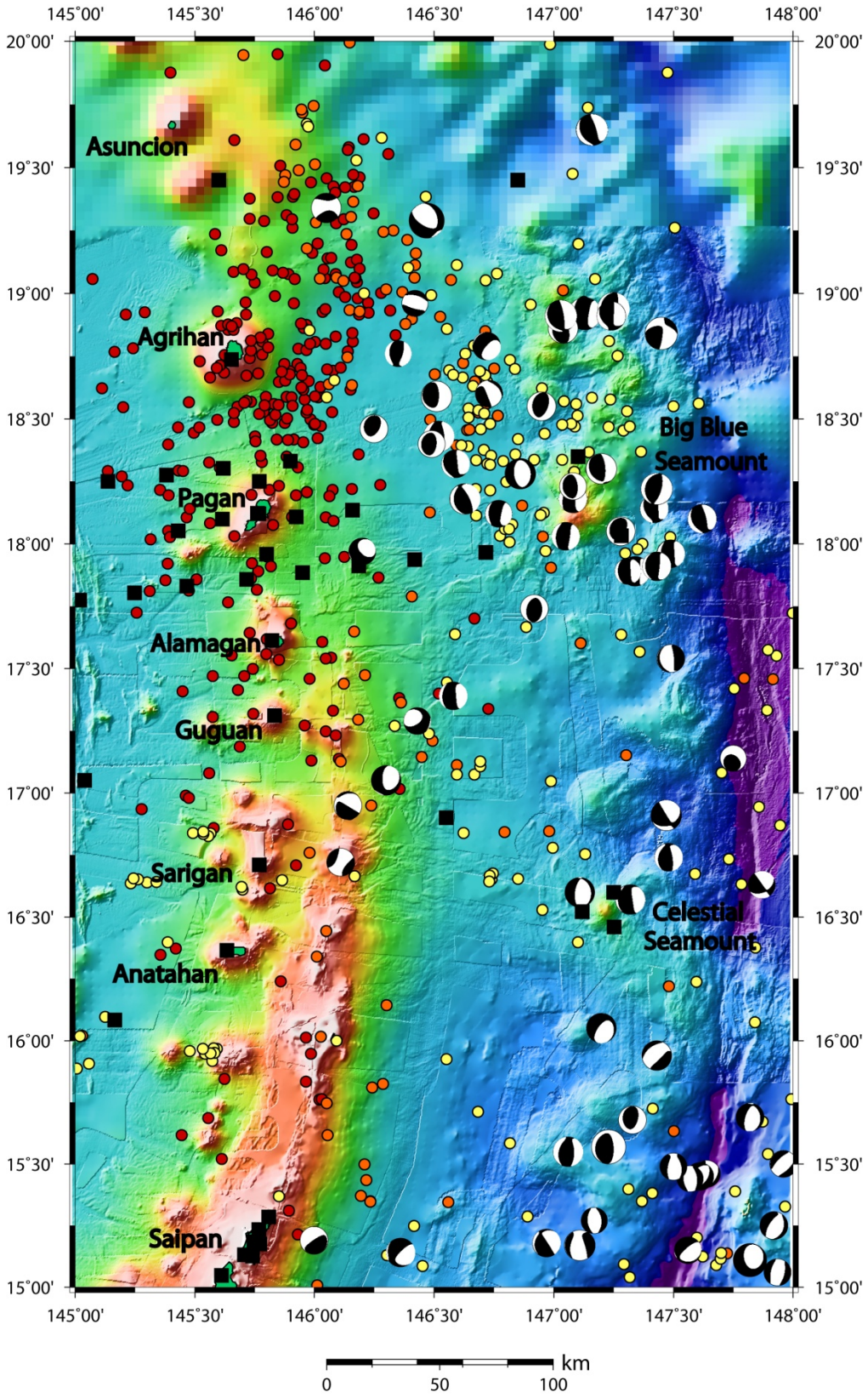

Figure 6 – Mariana Forearc Earthquakes (Ml > 3)

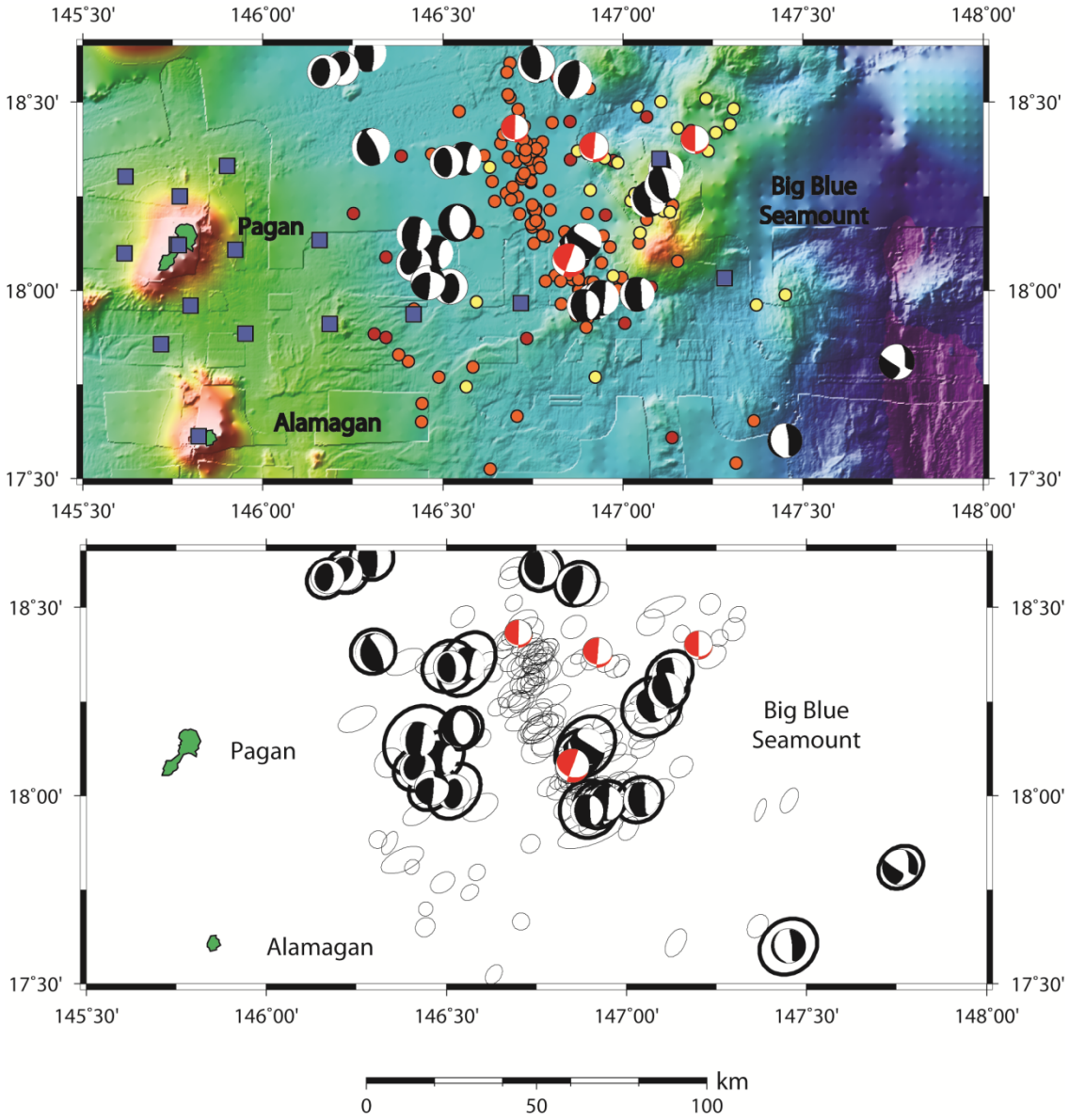

Figure 7 – Northern Mariana: Map and Error Ellipses

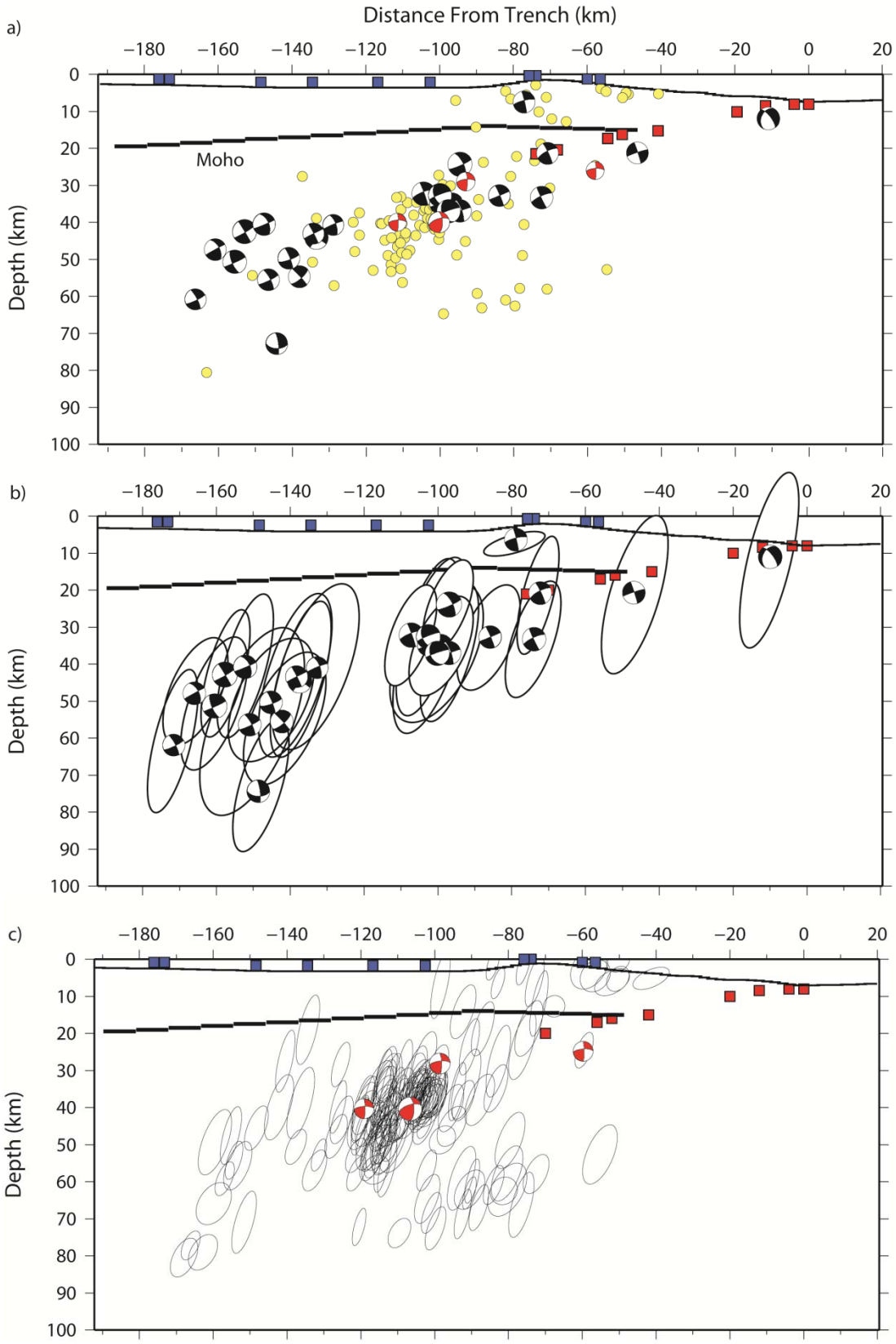

Figure 8 – Northern Mariana: Cross-Sections and Error Ellipses

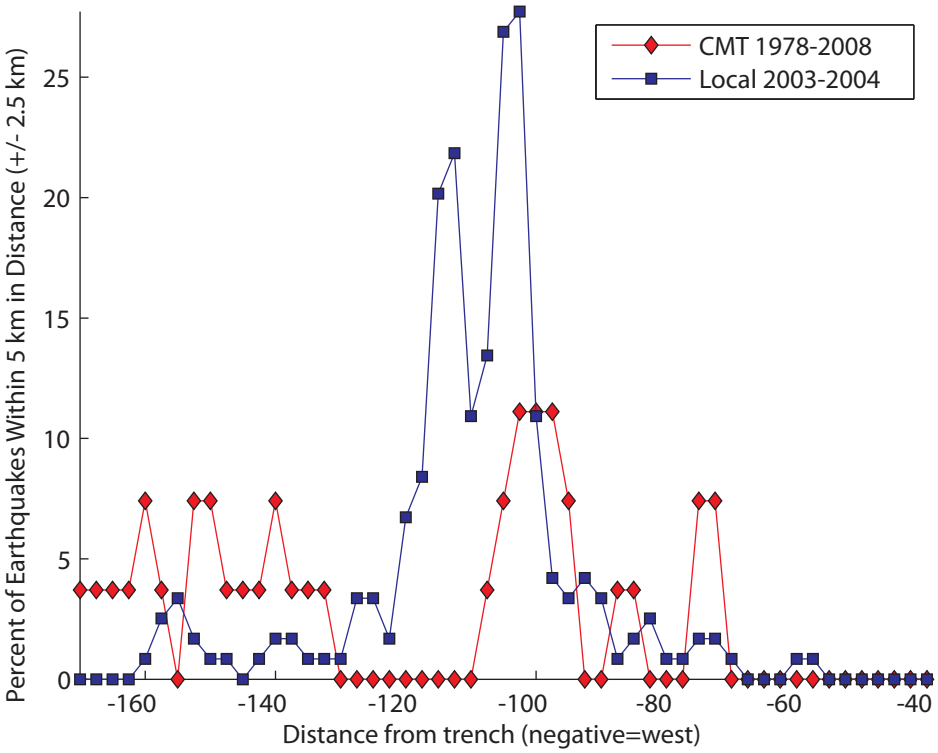

Figure 9 – Plate Interface Earthquakes vs. Distance From Trench

CHAPTER 3

FAULTING WITHIN THE PACIFIC PLATE AT THE MARIANA TRENCH: IMPLICATIONS TO PLATE INTERFACE COUPLING AND SUBDUCTION OF HYDROUS MINERALS

Abstract

We study the occurrence of extensional faulting in the outer rise of the Mariana subduction margin in an attempt to gain insight into the stresses within the bending Pacific plate, potential for Pacific plate mantle hydration, and the regional stress acting upon the plate interface. We determine accurate depths by inverting teleseismic P and SH waveforms from Global Centroid Moment Tensor (GCMT) earthquakes occurring from 1990 to present. For earthquakes with Mw 5.0+, we determine centroid depths and source time functions and further refine the fault parameters of the GCMT double-couple. For one smaller event with fewer clear waveforms, we invert only for the depth and source time function of the earthquake. Results from Central Mariana indicate that extensional earthquakes occur in the Pacific plate down to at least 18 km below the seafloor, or 11 km below the Moho. At the Southern Mariana trench, earthquakes with extensional mechanisms extend to a depth of 12 km below the seafloor, or 5 km below the Moho. The seismicity pattern in Southern Mariana is complicated by the presence of strike-slip and compressional earthquakes both near the trench and at distance. We model the flexurally-induced stress distribution within the Pacific lithosphere along two bathymetric profiles extending seaward from the Mariana Subduction Trench Axis to better understand whether observed earthquake depths match modeled scenarios of external forces and rheology. Results from our flexure models suggest that the Pacific plate at Central Mariana experiences a smaller bending moment in comparison to the Pacific

plate at Southern Mariana. In addition the Pacific plate at Central Mariana may be under great extension, possibly due to strong slab pull forces, whereas Southern Mariana may be undergoing compressional regional stress, possibly due to greater interplate coupling. We conclude that if the presence of extensional faulting promotes the infiltration of water into the subducting plate mantle, then we expect that at least the top 10 km of the Pacific plate mantle is serpentinized. Furthermore, the change between purely extensional to mixed extensional/compressional faulting styles in the Mariana outer rise may be an indication of increased plate interface coupling in Southern Mariana.

1. Introduction

The cycling of water into subduction zones is important for our understanding of a wide range of Earth processes, including subduction arc and back-arc volcanics [*Gill*, 1981; *Plank and Langmuir*, 1993; *Rüpke et al*, 2004], plate interface slip behavior [e.g. *Moore and Vrolijk*, 1992; *Audet et al*, 2009], intermediate depth earthquakes [*Raleigh and Paterson*, 1965; *Meade and Jeanloz*, 1991], water exchange between the Earth's surface and mantle [*Rüpke et al*, 2004], the composition of the deep mantle [*Thompson*, 1992; *Hirschmann, 2006*], and the initiation of plate tectonics [*O'Neill et al*, 2007]. The amount of water input at the trench is unconstrained for many subduction zones, due to unknown amounts of lower crustal and upper mantle hydration [*Jarrard,* 2003; *Hacker*, 2008]. The amount of hydrated (serpentinized) oceanic mantle is particularly important for water expulsion processes deep within subduction zones, at arc and at sub-arc depths [*Hacker*, 2008; *Van Keken et al*, 2011].

Faulting within the outer rise of subduction zones is an important pathway by which water can be transported into the Earth. These faults are the product of flexural stress resulting from ocean lithospheric bending [*Isacks et al*, 1968; *Chapple and Forsyth*, 1979]. The presence of an outer rise bulge is characteristic of elastic plate flexure [*Caldwell et al*, 1976]; however, the occurrence of earthquakes within the plate is an indication that it is not purely elastic, but is also experiencing permanent deformation in addition to elastic flexure [*Chapple and Forsyth*, 1979; *Goetze and Evans*, 1979]. Because mantle hydration is expected to be limited to the top of the oceanic plate where extensional brittle failure occurs [*Ranero et al*, 2003; *Lefeldt et al*, 2009], the distribution of stress within the bending oceanic plate may allow us to estimate water storage potential of the subducting lithosphere.

In addition to the stress resulting from elastic flexure [*Caldwell et al*, 1976; *Chapple and Forsyth*, 1979], interplate locking at strongly coupled subduction zones is thought to impact the stress distribution within the bending plate [*Christensen and Ruff*, 1988]. At strongly coupled margins, outer rise earthquakes are temporally linked to large plate interface earthquakes [*Christensen and Ruff*, 1988]. As first observed by *Stauder* [1968] in the Rat Islands, greater numbers of extensional outer rise earthquakes occur after large, megathrust earthquakes. This observation along with the occurrence of compressional outer rise earthquakes prior to megathrust rupture was suggested by *Christensen and Ruff* [1988] to be characteristic of strongly coupled subduction zones. However, at weakly coupled or uncoupled subduction zones, no compressional outer rise earthquakes occur and extensional outer rise events are not temporally related to the subduction plate interface [*Christensen and Ruff*, 1988]. These observations suggest that

the stress distribution within the bending oceanic plate at strongly coupled margins changes through time in response to the megathrust seismic cycle – in which case, the depth extent of water infiltration and mantle hydration also changes with time.

Because the maximum depth of mantle hydration is thought to be coincident with the location of the neutral plane, where plate bending stress switches from extension to compression, recent studies have determined the depth of the neutral plane as a means to infer depth of mantle hydration [*Lefeldt et al*, 2009]. At the Nicaragua outer rise, the depth of the neutral plane inferred from earthquake focal mechanisms [*Lefeldt et al* 2009] corresponds well with a region of low mantle P-wave velocities, suggestive of mantle serpentinization [*Van Avendonk et al*, 2011]. The Mariana subduction zone has long been cited as a water-rich system due to the prevalence of forearc serpentinite mud-volcanoes [*Fryer et al*, 1999], water-rich arc lavas [*Kelley et al*, 2010; *Parman et al*, 2011], and a serpentinized mantle wedge [*Tibi et al*, 2008; Pozgay *et al*, 2009; *Barklage*, 2010; *Pyle et al*, 2010], yet the initial amount of water stored within the Pacific plate mantle is unknown. Because the depth of the neutral plane estimated from earthquake focal mechanisms has been shown to coincide well with the depth of slow mantle P-wave velocities and presumably serpentinized mantle [*Lefeldt et al*, 2009; *Van Avendonk et al*, 2011], we explore faulting within the Pacific plate at the Mariana Subduction Zone by modeling the P- and SH-waves of outer rise earthquakes in order to obtain more accurate depths for these shallow events. We compare our new depths with two-dimensional finite-difference models of the stress distribution within the bending Pacific plate seaward of the Mariana trench and infer the depth extent to which the Pacific plate mantle is hydrated.

2. Background

2.1 Faulting and Hydration of Incoming Oceanic Plates

Bending-induced faulting of oceanic plates near the subduction zone trench axis is well established from bathymetric observations of horsts and grabens [*e.g. Ranero et al,* 2003; *Oakley et al*, 2008; *Gardner et al,* 2010]. In addition, multi-channel seismic reflection (MCS) studies of faulting within the bending oceanic plate have shown that faults exposed at the surface continue to depth [*Ranero et al,* 2003; *Nedimovic et al,* 2009]. At the Middle America trench axis offshore of Costa Rica and Nicaragua, faults continue from the surface down into the mantle [*Ranero et al,* 2003], however results from Cascadia reveal that faults do not continue deeper than the base of the crust [*Nedimovic et al* 2009]. This indicates that the state of stress within bending oceanic plates, the depth of outer rise faulting, and the possible extent to which mantle rocks may be exposed to water from the seafloor is not the same at all subduction zones.

Large-offset, outer rise faults may be newly created or reactivated by plate-bending stresses. In general, where existing faults (seafloor fabric) strike nearly parallel to the trench axis, plate bending is accommodated by fault reactivation, whereas new faults form more readily where seafloor fabric converges at a high angle with the trench axis [*Masson*, 1991; *Ranero et al*, 2005]. *Ranero et al* [2003] found that where seafloor fabric is sub-parallel to the trench axis, faults persist deeper within the bending oceanic plate than where new seafloor faults form – indicating that in addition to applied stress at the subduction trench, the depth of outer rise faults may also be dependent on the pre-existing structure of the oceanic plate.

Global and regional surveys of outer rise seismicity show that predominantly extensional earthquakes occur at the subduction zone outer rise, although compressional outer rise earthquakes occur at some regions [*Stauder,* 1968; *Chapple and Forsyth*, 1979; *Christensen and Ruff* 1983; 1988; *Kao and Chen*, 1996]. *Stauder* [1968] first observed that outer rise extensional earthquakes occurred in greater numbers following large megathrust earthquakes. This temporal relationship and the occurrence of compressional earthquakes at the Chilean subduction zone spurred *Christensen and Ruff* [1983; 1988] to propose that, in addition to plate-bending, stress along the megathrust during periods of interface locking affects the stress distribution within the bending plate seaward of the subduction trench. They suggest that the state of coupling along the plate interface is evidenced by patterns of seismicity in the outer rise [*Christensen and Ruff*, 1983; 1988]. The great earthquake doublet at the Kuril subduction zone [*Ammon et al,* 2008; *Lay et al,* 2009; *Raeesi and Atakan,* 2009], where a great extensional outer rise earthquake closely followed a great plate interface thrust earthquake, supports the hypothesis put forth by *Christensen and Ruff* [1983; 1988].

Outer rise earthquakes impact the hydration of oceanic plates prior to subduction. The observed pervasive faulting at the outer rise oceanic crust and mantle offshore from Nicaragua implies a clear pathway by which water can enter into the lower crust and uppermost mantle of the plate [*Ranero et al*, 2003]. However, the process by which water is pulled to depth despite high lithostatic pressure is uncertain; *Faccenda et al* [2009] postulate that tectonic pressure gradients within the upper oceanic lithosphere, created by plate bending, effectively pulls water deep into the plate mantle. They suggest that this process may be further enhanced by other mechanisms, such as seismic pumping

through faults [*Sibson,* 1994], thermal cracking [*Korenaga*, 2007], or migrating fluid-filled cracks (vug waves) [*Phipps Morgan and Holtzman*, 2005]. Despite the difficulties in constraining the mechanism by which water is pulled into the faulted plate, a number of recent seismic studies provide evidence that the oceanic mantle is significantly altered by serpentinization [*Contreras-Reyes et al*, 2007; *Ivandic et al,* 2010; Van *Avendonk et al,* 2011; *Savage,* 2012]. If serpentinization of dry mantle minerals occurs along all outer rise faults, then the amount of water within the oceanic plate mantle may equal the amount of water stored within the oceanic crust [*Ranero et al*, 2003] causing estimates of subduction zone water inputs to be significantly underestimated.

The amount of hydration stored within the different layers of the subducting oceanic plate has important effects on the progression of slab dehydration with depth [*Jarrard,* 2003; *Hacker,* 2008]. At shallowest depth, expelled water is sourced from pore and structurally-bound water in clay and opal sediments; the majority of this is expelled at depths shallower than ~10 km [*Jarrard*, 2003]. At slightly deeper depths, up to 50 km, pore water and structural water within upper crustal extrusives is removed from the slab [*Jarrard*, 2003]. This stage of water release may affect shallow subduction zone processes, such as plate interface slip [*Shelly et al*, 2006; *Audet et al,* 2009]. At intermediate depths, water is sourced from the lower crustal and, depending on the initial conditions of the subducting plate, possibly also from upper mantle serpentinites [*Jarrard*, 2003; *Van Keken et al*, 2011]. Water expulsion from the slab at intermediate depths is believed to impact volcanic arc outputs [*Gill*, 1981] as well as back arc basin outputs [*Kelley et al*, 2006]. Additionally, released water may travel to other parts of the slab and cause intermediate and deep earthquakes [*Raleigh and Paterson*, 1965; *Meade*

and Jeanloz, 1991] or recombine with other slab components to form high pressure hydrous phases, such as hydrous phase A, which are stable at great depths [*Ulmer and Trommsdorf*, 1995; *Schmidt and Poli*, 1998]. At deeper depths, depending on the conditions of the plate and the rate of subduction, mantle serpentinites, in particular antigorite, may carry water beyond the subduction zone and into the deep mantle [*Rüpke et al*, 2004; *Hacker*, 2008; *Van Keken et al*, 2011]. This deep transport of water is suspected to occur at subduction zones where the subducting slab is very old (cold) and converging rapidly [*Van Keken et al*, 2011].

2.2 The Mariana Trench and Outer Rise

The outer rise of the Mariana trench exhibits distinct faults, located closer than 100 km distance from the trench and coinciding with the ~6000 m bathymetric depth contour; some of these faults cut through prominent Pacific seafloor seamounts near the trench axis [*Oakley et al*, 2008; *Gardner*, 2010]. *Oakley et al* [2008] found that seafloor fabric is reactivated when it forms an angle less than ~25° with the Mariana trench axis. When the angle formed between the trench and the fabric is greater than ~25°, small offsets occur on existing faults, but the largest offsets occur on newly-created, trench-parallel faults [*Oakley et al*, 2008]. Results from MCS survey at the Marianas do not resolve the maximum depth extent of outer rise faults [*Oakley et al* 2008], however, near-surface offsets indicate that fault throws change significantly along strike and are impacted by the angle of the incoming seafloor fabric with the subduction trench, the depth of the subduction trench, and the presence of seafloor seamounts on the incoming

Pacific plate. Results from *Oakley et al* [2008] also indicate that the inclination of the Pacific plate changes abruptly at the subduction trench – from ~1-2° seaward of the trench to ~8-9° landward of the trench, beneath the forearc. They interpret this abrupt change as evidence that the Pacific plate fails completely, rather than bends, as it is subducted [*Oakley et al*, 2008].

At the Mariana Subduction Zone, few outer rise earthquakes have been studied to date; results for prior research of the Mariana outer rise earthquakes are compiled in Table 1. Very few of these events have had depths determined through waveform modeling techniques; rather most have been studied through earthquake relocation. Directly beneath the Mariana trench axis, a large, Mw 7.5 extensional earthquake occurred on 5 April 1990 and even created a minor tsunami [*Zhang and Lay*, 1992; *Satake et al*, 1992; *Yoshida et al*, 1992]. The source of this earthquake was studied extensively by both *Zhang and Lay* [1992] and *Yoshida et al* [1992] and the resultant tsunami was explored by *Satake et al* [1992]. Both *Zhang and Lay* [1992] and *Yoshida et al* [1992] found a best-fitting depth within the oceanic mantle. *Zhang and Lay* [1992] estimate a depth of 23± 5 km centroid depth and favor a steeply westward-dipping fault plane [*Zhang and Lay*, 1992], whereas *Yoshida et al* [1992] have a best-fitting depth of 16 km on a moderately westward-dipping fault plane. Analysis from *Zhang and Lay* [1992] shows very little horizontal directivity, suggesting that the rupture direction for the earthquake was predominantly downward. Based on relocation of aftershocks, *Yoshida et al* [1992] find that the fault was ~40 km wide. The occurrence of such a large, extensional outer rise earthquake suggests that the Pacific plate is experiencing large extensional forces; combined with the large-offset faulting observed by bathymetry, the

minerals within the oceanic plate mantle have the potential to be significantly hydrated, although the depth extent of hydration is yet unknown.

2.3 Mariana Volcanic Outputs and Water Budget

There are many signs of fluid flux occurring at shallow depths in the subduction zone. Results from the MARGINS Mariana SubFac Experiment have all indicated that the shallow mantle wedge beneath the Mariana forearc is serpentinized [*Tibi et al,* 2008; *Pozgay et al,* 2009; *Barklage*, 2010; *Pyle et al,* 2010]. In addition, the Mariana Subduction Zone has a number of well-exposed serpentinite seamounts along the length of the forearc, from which erupted muds indicate a source near the subducting plate boundary [*Fryer et al*, 1999]. The water contents of volcanic arc and back arc outputs vary along the length of the margin [*Kelley et al,* 2006; *Shaw et al,* 2008; *Kelley et al,* 2010; *Parman et al*, 2011]; back arc magmas at Mariana are generally ~0.5 wt% water, while the island arc magmas range from ~2-6 wt % water [*Kelley et al,* 2006; *Shaw et al,* 2008; *Kelley et al,* 2010; *Parman et al*, 2011]. At Southern Mariana, the back-arc is separated from island arc volcanoes by only 20-30 km, and the island arc volcanics in the region exhibit similarities to back arc outputs [*Fryer et al,* 1998; *Martinez et al*, 2000]. At the southernmost boundary, the upper Philippine Plate is rifting directly over the subducting slab, and *Martinez et al* [2012] propose that the setting promotes a weakened overriding oceanic lithosphere characterized by broad rifts and diffuse volcanism. Despite the numerous indications of large amounts of shallow and intermediate depth water flux, the amount of water subducted into Earth's deep mantle at Mariana based on

numerical models is estimated to be small [*Van Keken et al*, 2011]. However, the result from *Van Keken et al* [2011] is dependent upon the initial amount of slab mantle serpentinization, which is unconstrained for most subduction zones, including the Mariana Subduction Zone.

3. Data and Methods

3.1 Earthquake relocation

Prior to waveform inversion, earthquake relocation is needed to clearly delineate events within the subducting plate near the trench from those in the shallow thrust zone in the forearc. In general, shallow thrust earthquakes in the Mariana subduction zone do not occur within about 60 km of the trench axis [*Emry et al.,* 2011]. Earthquake arrival time data were collected from the International Seismic Center (ISC) Bulletin [2010] for all GCMT earthquakes occurring between 9-26° N and 138-154°E from 1 January 1976 to 1 October 2010. All GCMT earthquakes seaward of the trench axis plus all events within 80 km landward of the trench axis were then split into four regions for relocation. Four separate regions were used in the relative relocation to ensure that all earthquakes in the region are sampling similar global velocity heterogeneity. These regions were distinguished by latitude: the southern region near Guam extended from 10-14.5°N; the central region, near Celestial seamount extended from 14.5-17.5°N; the region near Big Blue seamount extended from 17.5-20.5°N; the northernmost region, north of Maug and almost into the Bonin subduction zone extended from 20.5-24°N.

The relative relocations were carried out using the hypocentroidal decomposition algorithm [*Jordan and Sverdrup*, 1981]. The initial locations were taken from the ISC bulletin [2010], and travel times for P, pP, PKP, and S phases from each event were calculated according to the IASP91 earth model [*Kennett and Engdahl*, 1991]. S phases were used only for stations closer than 20° to the earthquake hypocenter due to the large errors frequently found for teleseismic S waves reported to the ISC. The number of earthquakes relocated for each region varied greatly due to the difference in the number of GCMT events occurring since 1976. In the southern Mariana region, near Guam 151 events were relocated; 42 events were relocated in the central region east of the Celestial Seamount; 28 events were relocated in the central region east of the Big Blue Seamount; and 16 events were relocated in the northernmost region, north of the island of Maug.

3.2 Earthquake Source Inversion from P and SH waveforms

Following relocation, we requested waveform data from the IRIS Data Management Center (DMC) for all earthquakes greater than or equal to Mw 5.0 occurring seaward of the trench or in close proximity to the trench. For all earthquakes except one, only broadband data was used. For one earthquake occurring in 1990 (Event 11, Table 5), a combination of broadband and long period (1 sps) data was inverted due to a lack in clear broadband waveforms for that event. Events prior to 1990 had too few broadband waveforms to determine accurate depths and so they were not investigated further. Details regarding waveform data sources are listed in Appendix A.

We inverted teleseismic P- and SH- waveforms from stations at distances of 30-90° to determine the best fitting source parameters for earthquakes located on the incoming plate or near the trench axis. Rarely, for earthquakes with fewer clear arrivals, we searched through waveforms at 20-30° and 90-100° in order to collect more data. Waveforms were visually inspected for clear signals at frequencies of 0.02-0.5 Hz. For some events, low-frequency (0.02-0.18 Hz or 0.02-0.2 Hz) waveforms were sufficiently clear but the higher frequencies up to 0.5 Hz were not, due to the microseism peak around 0.2 Hz. For the one event in 1990 which utilizes long-period (1 sps) data, the upper frequency stop band was set at 0.18 Hz. The instrument responses provided by the IRIS DMC for each station were deconvolved from the data prior to comparison with the synthetics.

Waveform synthetics were computed using ray theory [e.g. *Langston & Helmberger* 1975] and utilized the ray parameter corresponding to teleseismic propagation in an IASP91 model. Synthetics were calculated for three fundamental double-couple source geometries and then linearly combined to obtain synthetics for each focal mechanism in the grid search. A ray expander routine was used to compute all the reflections and conversions in the near-source structure model above a cutoff amplitude. The source time function was modeled as a half sine wave with a best fitting duration determined by the inversion. We found our best-fitting source depth, time function, and focal mechanism strike, dip, and slip using a grid search. In the grid search, misfit was calculated at each station as the squared amplitude misfit between the data and synthetic normalized over the squared amplitude of the data, multiplied by the weight assigned to that station:

$$Misfit = \frac{\sum_{i=n_1}^{n_2}(d(i)-s(i)\times M)^2}{\sum_{i=n_1}^{n_2} d(i)^2} \quad (1)$$

where i spans the time window for which misfit is to be calculated, n_1 is the starting time for the window, n_2 is the end time for the window, d is each data point, s is each synthetic value, and M is the median seismic moment found for the whole set of stations. Total misfit for each mechanism, depth, and time function combination was the summation of individual station misfits (1) over the summation of weights assigned to each station:

$$SolutionMisfit = \frac{\sum_{i=1}^{n} Misfit(i)}{\sum_{i=1}^{n} Weight(i)} \quad (2)$$

where n is the number of stations used in the inversion.

Initially the search was performed over the entire model space with larger source parameter increments, and then searched again near the best fitting solutions with a smaller increment to obtain the optimal fit to the data within 1 km of depth, 1 second in source duration, and 1° of strike, dip, and slip respectively. The depth search extended throughout the oceanic crust and into the mantle to a depth 45 km below the seafloor.

The velocity models used in the waveform inversion differed along strike, based on the MCS reflection results from *Oakley et al* [2008]. Table 2 presents the latitude ranges and the velocities and thicknesses of the water, sedimentary layer (where applicable), upper crustal, lower crustal, and mantle layers. Although the thicknesses of the layers changed along strike, the seismic velocities and densities remained constant for each layer and are listed within Table 2.

One earthquake (Event 14, Table 3) showed clear P-wave arrivals at some stations but had insufficient good waveforms to provide a well-constrained focal mechanism. In

this instance, the best-fitting GCMT double couple focal mechanism was used and only the best fitting depth and time function were determined. Table 3 lists the differences in fault parameters, moment, and depth between our modeled results and the GCMT best-fitting double couple.

3.3 Flexure modeling

We compare our newly modeled earthquake centroid depths with a theoretical distribution of stress within the bending Pacific plate to determine whether our predictions for depth and location of compression, extension and the neutral plane match with that predicted by the bathymetric profile of the bending oceanic plate seaward of the trench axis. In order to accomplish this, we use the tAo two-dimensional finite difference flexure package of *Garcia-Castellanos et al* [1997]. This method was initially created to study rheologic properties beneath foreland basins by linking crustal shortening, erosion, sedimentation, and lithospheric flexure [*Garcia-Castellanos et al* 1997]. However the method can be applied to model other systems, such as oceanic plate flexure seaward of subduction thrust systems [*Garcia-Castellanos et al,* 2000].

Rather than modeling oceanic plate flexure as purely-elastic or as viscoelastic materials, which do not reflect strength profiles determined experimentally [*Goetze and Evans*, 1979], an elastic-plastic depth-dependent rheology is employed within the code in order to provide a more realistic stress distribution with depth in the lithosphere [*Garcia-Castellanos et al*, 1997]. This plate rheology allows for brittle failure to occur at shallow depths, limiting the amount of stress that the top of the plate can withstand [*Garcia-*

Castellanos et al, 1997]. The equations for frictional sliding are sensitive only to depth (pressure):

$$\sigma_E = \beta_{ext}\, z \tag{3}$$

$$\sigma_C = \beta_{comp}\, z \tag{4}$$

where σ_E and σ_C denote the yield stress for extension and compression respectively, β_{ext} and β_{comp} are the slopes of the brittle failure criteria, and z is depth. The bottom of the plate is limited by the temperature-sensitive flow laws governing ductile deformation of dry olivine. At low shear stress (< 200 MPa) the power law from *Goetze* [1978] and *Goetze and Evans* [1979] is assumed to control mantle deformation:

$$\dot{\varepsilon}_P = 70\sigma_s^3 exp\frac{-Q_p}{RT} \tag{5}$$

where $\dot{\varepsilon}_P$ represents the power law strain rate of deformation, σ_s is shear stress, Q_p is the power law activation energy for dry olivine, R is the universal gas constant, and T is the temperature (Table 4). At higher shear stress (> 200 MPa) the Dorn law is used to describe mantle flow [*Goetze,* 1978; *Goetze and Evans*, 1979]:

$$\dot{\varepsilon}_D = 5.7 \times 10^7 exp\left\{\frac{-Q_D}{RT}\left(1 - \frac{\sigma_s}{\sigma_p}\right)^2\right\} \tag{6}$$

where $\dot{\varepsilon}_D$ represents the strain rate of deformation, σ_s is shear stress, σ_p is the Peierl's stress, Q_D is the Dorn activation energy for dry olivine, R is the universal gas constant, and T is the temperature (Table 4).

In the tAo software, the moment and curvature is calculated iteratively following the methods of *McNutt* [1984] and *Waschbusch and Royden* [1992], and the depth dependent yield stress envelope then limits the stress within the bending plate [*Garcia-Castellanos et al,* 2000]. The yield stress envelope is determined from the temperature distribution for oceanic lithosphere given a certain age. We use the temperature profile for a 150 Myr plate using the GDH1 cooling plate model of *Stein and Stein* [1992], which defines the thickness of the lithosphere as the depth to the 1450°C isotherm. The model from *Stein and Stein* [1992] which predicts a thinner oceanic lithosphere (95 km) for older (> 75 Myr) plates, utilizes a larger heatflow dataset than the *Parsons and Sclater* [1977] model and better fits the trend of seafloor depth with age. Furthermore, *Garcia-Castellanos et al* [2000] find that flexure profiles computed for the Tongan trench using GDH1 [*Stein and Stein*, 1992] provides a better fit than the *Parsons and Sclater* [1977] model.

Bathymetry data was collected from global and local grids, obtained through the *National Geophysical Data Center* [2006] and recent Law of the Sea cruises [*Gardner*, 2010]. Unlike the approach used by *Garcia-Castellanos et al* [2000] for the Tonga subduction trench, profiles extending seaward of the subduction trench were not averaged along the entire length of the margin. Rather, input profiles for flexure models were specifically selected along corridors where few seafloor seamounts exist. This approach gives a better representation of the actual form of the bending plate, because the resultant profiles are not contaminated by the numerous, large, seafloor seamounts seaward of the Mariana trench [*Wessel*, 2001]. Furthermore, our approach takes into consideration that the slope of the outer trench changes significantly along the length of the Mariana trench

and allows us to explore how changes in the flexure of the plate along strike may be reflected in our earthquake locations and depths.

Using the trench-perpendicular bathymetry profiles (with seamounts avoided) as discussed above, we weight heavily the points closest to the trench (within 150 km from the trench) and the points furthest from the trench are weighted least (farther than 350 km from the trench). We run a grid-search using the distance-weighted bathymetric profiles to find an estimate for the best-fitting applied parameters (moment and external forces) and to approximate the distance of maximum plate bending moment and vertical stress profile and failure criteria which corresponds to that distance.

4. Results

4.1 Modeled Earthquakes

The relocated earthquake locations and accurate depths for 20 events within the Pacific plate were determined (Figure 2; Table 5). Of these, 10 were normal-faulting events or normal-faulting events with some component of strike-slip motion, with the remaining 10 showing strike-slip or compressional mechanisms. The earthquakes that we interpret to be related to Pacific plate bending were located within 70 km landward or 40 km seaward of the trench axis. Five events with depths determined by waveform models were located at 150-225 km seaward from the trench axis and are compressional or strike-slip earthquakes with tensional (T) axes which are not oriented perpendicular to the trench axis. The overall trend of the Pacific plate-bending earthquakes changes from strike-slip and slightly off-axis extensional earthquakes in the northernmost region to

purely extensional outer rise earthquakes with a maximum modeled depth of 13 km (6 km beneath the base of the crust) in the region at 17-18°N to purely extensional with a maximum depth of 18 km (11 km beneath the base of the oceanic crust) at 15-16°N to a combination of extensional, strike-slip, and compressional mechanisms at 10-13°N. The maximum depth of extension in Southern Marianas is 12 km beneath the top of the plate or 5 km below the base of the crust, and the minimum depth of compression is 34 km. This does not constrain the depth of the neutral plane well, due to the large distance between the deepest extensional and shallowest compressional earthquake. A similarly wide gap between extensional and compressional earthquakes was noted by *Bodine et al* [1981] in the global compilation of earthquake depths from *Chapple and Forsyth* [1979].

4.1.1 Northern and Central Mariana

In Central Mariana, ~15- 18°N, no compressional GCMT earthquakes exist in the trench or outer rise. However, many extensional earthquakes with strikes parallel to the trend of the trench axis occurred at these latitudes. A magnified view of the bathymetry and locations of modeled GCMT earthquakes in the vicinity (15°N-16°N) of the large 5 April 1990 outer rise earthquake is shown in Figure 3. The large extensional 5 April 1990 mainshock (Table 5, Event 10) had one of the deepest depths in our set of modeled events; we determined a centroid depth of 24 ± 2 km (18 km beneath the seafloor) and a magnitude (Mw) of 7.21. In comparison, results from *Zhang and Lay* [1992] and *Yoshida et al* [1992] for the same earthquake give a depth of 23 ± 5 km (Mw 7.5) and 16 km (Mw 7.5), respectively, by using the method of *Kikuchi and Kanamori* [1991]. Two

of the remaining three earthquakes in this region occurred during 1990 and are aftershocks of this large earthquake (Table 5, Events 13 and 11). Another small magnitude extensional earthquake occurred here during 2001 within the Pacific plate beneath the forearc (Table 5, Event 12). The events in this area, for which we have modeled new depths, are located between 25 km landward (west) of the trench axis and 30 km seaward (east) of the trench axis. Their depths range from 8-18 km beneath the top of the slab with a maximum depth of ~11 km below the Moho in this region.

A closer view of the bathymetry and locations of modeled earthquakes in the vicinity (16.4°N-18°N) of a recent active- and passive-source seismic experiment conducted by D. Wiens and D. Lizarralde is shown in Figure 4. The depths of the five modeled earthquakes in this region range from 9-13 km beneath the seafloor, and are located within the lower crust or within the top 6 km of the Pacific plate mantle. The earthquakes occurring seaward of the trench axis are in the proximity of several, long faults exposed at the surface of the seafloor. The locations for the modeled earthquakes span from 20 km landward of the trench axis to 40 km seaward of the trench axis. Here, unlike the region just to the south where the large Mw 7.5 earthquake occurred, the surface of the Pacific plate is relatively flat with few seamounts and the depths of extensional earthquakes are shallower, extending only a few kilometers beneath the base of the crust.

Fewer GCMT earthquakes occurred in the northernmost section of the subduction zone, and of the 16 relocated events, only two earthquakes were large enough to model their depths. One Mw 6.2 event was an extensional earthquake which occurred within the slab at 70 km landward of the trench axis, with a strike that was not oriented parallel

to the trench axis. The depth for this event was 49 km below the seafloor (Table 5, Event 20); however we do not have a good estimate for the depth of this event within the subducted Pacific plate, because the depth to the subducting plate in this region is poorly known. The other earthquake in this region was a compressional/strike-slip event occurring within the Pacific plate 30 km east of the trench axis at 25 km depth (Table 5, Event 19). Because the strikes of these earthquakes are not oriented parallel to the subduction trench, they may be related to a more complicated stress field than simple plate flexure at the subduction trench.

4.1.3 Southern Mariana

In comparison to Central and Northern Mariana, Southern Mariana has had few moderate to large extensional earthquakes (Figure 5). The extensional GCMT earthquakes large enough to be modeled are located near the southern Mariana trench axis at depths of 12 km or less within the Pacific plate (Table 5, Events 5, 6). Also in the vicinity of the southern Mariana trench is a moderate-sized compressional earthquake with a strike that is sub-parallel to the strike of the trench axis. The best-fitting depth for this event is 34 km beneath the top of the Pacific plate (Table 5, Event 9). The orientations for these extensional and compressional earthquakes are consistent with what is expected given bending of the Pacific plate at the subduction trench. The locations of the earthquakes range from 20 km landward of the trench to 20 km seaward of the trench. At greater distance from the trench axis (>150 km) are a number of compressional and strike-slip earthquakes oriented at angles that are not parallel to the strike of the trench

axis. The GCMT earthquakes for which we determine new depths in this location range in magnitude Mw (5.5-6.3) and in depth (5-34 km).

4.2 Flexure models

4.2.1 Central Mariana

At Central Mariana (17-18°N), the flexure model which fits the Pacific plate bathymetry best predicts small compressive regional stresses with a small region of extensional stresses extending outwards ~200 km from the trench axis (Figure 9a). The predicted maximum extensional stresses within this region for the model are notably small, with a neutral plane depth of ~25 km at the point of maximum plate bending (Figure 9b). This model predicts that brittle extensional faulting would cease at a depth of ~18 km. The modeled depth of the deepest and largest (Mw 7.5) extensional earthquake in our dataset was 18 km, and appears to directly contradict the best-fit flexure model that was generated using only bathymetric profiles extending seaward of the trench axis in this region.

Results from *Oakley et al* [2008] using MCS reflection in this region show that the surface of the Pacific plate changes abruptly at the trench from 1°-2° east of the trench to 7°-8° west of the trench. When the profile of the Central Mariana Pacific plate is extended to include the shallowest portion of the plate interface already subducted beneath the toe of the Mariana forearc, the best-fitting flexure model is significantly different and indicates a plate that is being acted upon by extensional forces throughout with a region of large extensional stresses beneath the trench and extending seaward ~50

km (Figure 9c). In addition, the predicted neutral plane for this model is ~38 km and brittle faulting is predicted to continue down to 30 km into the plate (Figure 9d). This model which fits the bathymetry seaward of the trench axis and the shallow, subducted plate interface west of the trench axis results in a plate stress distribution which is more likely, considering the depth and magnitude of our deepest extensional Central Mariana outer rise event.

4.2.2 Southern Mariana

At Southern Mariana, the trace of the plate interface landward of the trench is not known as at Central Mariana. For the bathymetric profile extending seaward of the trench axis in this region, the best-fitting flexure model indicates that the Pacific Plate is undergoing large amounts of plate flexure and is being acted on by regional compressive stresses (Figure 10c). According to this result, the greatest amount of compression occurs within ~100 km of the trench axis at ~30-40 km beneath the surface of the Pacific plate. In this region, extension is predicted within 150 km distance from the trench. At the point of maximum bending moment, the neutral plane is predicted to be ~25 km beneath the top of the plate, with brittle extensional faulting occurring down to ~20 km (Figure 10d). The stress distribution predicted by this model matches quite well with the seismic constraints given the 34 km modeled depth for the compressional outer rise event (Table 5, Event 9). Furthermore, an outer rise strike-slip event in this region with 24 km depth beneath the seafloor coincides well with the modeled neutral plane depth in Southern Mariana.

5. Discussion

5.1 Uncertainty associated with waveforms, misfit and velocity structure error estimates.

Waveform misfits to the data are provided for each earthquake in Table 5. Although estimates of misfit help us arrive at the best fitting solution for depth and fault orientation, they are not synonymous to depth error. There are inherently two separate components which contribute to error in our calculated depths: precision of waveform fits and uncertainty related to the velocity model. Often, the precision of waveform fits exhibits a codependency between modeled source and fault parameters, in particular the depth and source time function. Figure 6 shows a contour plot of the source depth/time function parameter space of the large 5 April 1990 earthquake. Contours of synthetic waveform misfits that are 2%, 5%, 10%, 20%, and 50% greater than the lowest misfit (best-fitting) solution are shown and correspond to Event 10 in Table 5. Misfit contour plots are provided for all remaining earthquakes in Appendix B. The depth uncertainty listed in Table 5 for each event is the difference in depth between the best-fitting solution and solutions that have misfits 5% greater than the best solution at the time-function listed in Table 5 for each event.

The second contributor to error in our depth estimates is uncertainties resulting from the seismic velocities and layer thicknesses assumed in our inversions. In our inversions we assumed the layer thicknesses determined by *Oakley et al* [2008] during a MCS reflection survey covering multiple trench-normal profiles throughout the Mariana and Izu-Bonin forearc and trench, ranging from ~14.5°N to ~32.5°N (Table 2). Because

no survey lines were located in Southern Mariana (~10-13°N) we assumed layer thicknesses of the southernmost Mariana MCS survey line 79-80 which has a 7 km thick oceanic crust [*Oakley et al*, 2008]. The model thicknesses determined by *Oakley et al* [2008] assumed seismic P-velocities found by *Takahashi et al* [2007] during their trench-normal seismic refraction survey – located in close proximity to *Oakley et al* [2008] line 53-54. The MCS results from *Oakley et al* [2008] at the Mariana trench reveal that crustal thicknesses vary from ~5 km with ~1 km of sediment at 18°N (line 22-23) to ~7 km with ~2 km of sediment at 16.5°N (line 53-54) to ~7 km with ~0.5 km of sediment at 14.5°N (line 79-80). In addition to the variations in the average thicknesses along strike, crustal layers exhibit local thickening due to the presence of seafloor seamounts, resulting in portions of the crust that are 9-10 km thick. The ranges of crustal layer velocities in the forearc are not stated by *Takahashi et al* [2007] however, the velocity range for arc and west Mariana ridge are given: upper crust (4.5-6.0 km/s), middle crust (6.0-6.5 km/s), and lower crust (6.8-7.3 km/s). Furthermore, mantle velocities are generally ~8.0-8.1 km/s, however a large amount of serpentinization has been found to alter bulk mantle velocities, making them as low as 6.9 km/s [*Van Avendonk et al*, 2011] offshore of Nicaragua.

Our method for determining depth, which is dependent upon the time delay between P or S arrivals and their respective depth phases, will have less uncertainty for shallower, crustal sources than for deeper mantle sources – given uncertainty in the assumed Moho depth and layer velocities. For earthquakes which occur within the crustal layers, any errors in the actual thickness of the crust will not contribute to errors in the calculated depth, although slight errors in the velocity of the layers above, such as the

sediment or upper crustal layer may. However for most of the Mariana trench, very little sediment is present on the Pacific plate [*Oakley et al*, 2008]. *Takahashi et al* [2007] found that the upper crustal layer of the Mariana backarc ranged by about ±0.75 km/s from the upper crustal velocity assumed in our model. If a vertically incident ray from an earthquake 2 km beneath the top of the crust traveled through material that was ±0.75 km/s, then the total time difference between the assumed velocity model P-pP time and the actual P-pP time is small (~0.1 sec) and translates to only ~0.5 km error in depth.

For events which occur within the top of the mantle, just below the Moho, the thickness of the crust and the assumed velocity will still have a small effect on event depth. Assuming that the Moho depth is inaccurate by ±2 km, and a vertically incident ray travels through material that is ±1.5 km/s, the resulting time difference between the two models would still be small (~0.1 sec) and would result in a depth error of ~1 km. At mantle depths, we assume an average upper mantle velocity of 8.0 km/s. Effects due to substantial mantle serpentinization could lower the velocity to ~7.5 km/sec at the top of the mantle. For an earthquake which occurs at depth 45 km, beneath a region with a velocity that is 0.5 km/sec slower than that assumed by our model, the difference in time between the P and pP would still only be ~0.75 sec, which would translate to a 5-6 km depth error. This is an overestimate assuming that the entire upper mantle (~45 km) above the earthquake is significantly serpentinized, which is unlikely. These estimates for depth error are inherently different than the estimates of precision of our waveform fits discussed above, and therefore cannot simply be combined. However, the main point to consider in our results is that given two events with equally clear and distributed

waveforms, the shallower event will be subject to less uncertainty in depth than the deeper event.

5.2 Uncertainties and Assumptions associated with flexure models

5.2.1 Non-uniqueness of model solutions

The stress distributions created from our flexure models appear to fit well with our extensional and compressional earthquake depths. We tested a range of model bending moments, horizontal forces, and vertical forces and find that our solution is non-unique; several solutions can fit the observed bathymetry reasonably well. The most trade-off exists between the bending moments and horizontal force. Figure 11 and 12 show three models with a low misfit at both Southern and Central Mariana. The left side of the figures shows the 2-d distribution of stress within the bending plate, and the right side shows how the modeled profile of the plate compares with the bathymetry. Despite the non-uniqueness of the models with respect to the bathymetry data, we can see that some of the models are not well fit by the seismic locations and depths, particularly at Southern Mariana (Figure 11).

5.2.2 Model parameter assumptions

The boundaries of the assumed yield stress envelope for the lithosphere is constructed based on the brittle failure criteria and the mantle flow laws for dry, single-crystal olivine. These rheological assumptions are based on results from laboratory

experiments, which are then extrapolated to real Earth conditions. Additionally, the mechanical thickness of the lithosphere in our models is calculated from the plate cooling model of Stein and Stein [1992] which represents the average seafloor depth and heat flow variations for 'normal' oceanic lithosphere. We will summarize the current knowledge on these matters and discuss in a qualitative manner how the uncertainty resulting from experimental assumptions and thermal models may impact our calculations of plate flexure.

The assumed slope for brittle failure within the upper portion of the bending plate is based on the laws for frictional sliding [*Goetze and Evans*, 1979], which, except for clays and other phyllosilicates, has been found experimentally to be independent of rock type [*Byerlee*, 1978]. Brittle failure is most sensitive to increasing pressure normal to the fault surface and is relatively insensitive to temperature [*Goetze and Evans,* 1979; *Kohlstedt et al*, 1995]. One key assumption made by the equation governing brittle failure is that effect of pore water within the rock is negligible. Pore water is known to weaken rocks through the physical effects of increased pore pressures and through chemomechanical effects due to water molecules adsorbed onto the rock surface [*Dieterich and Conrad,* 1984; *Kohlstedt et al*, 1995; *Scholz*, 2002]. If large amounts of pore fluid were present at the top of the oceanic lithosphere and if the pore pressure were hydrostatic, then the brittle strength would be ~1/3 less than the brittle strength assumed in our models [*Kohlstedt et al*, 1995].

The equations governing the bottom of the failure envelope are based on experimental observations of ductile deformation of dry, single-crystal olivines [*Goetze,* 1978; *Goetze and Evans,* 1979; *Bodine et al*, 1981]. However, the presence of water

within upper mantle rocks can significantly decrease the strength and viscosity of the materials [*Kohlstedt, et al,* 1995; *Hirth and Kohlstedt,* 1996]. Experimental results from *Post* [1977] showed a difference between the strength of wet and dry dunite and concluded that water in wet dunite facilitated the movement of dislocations by lowering the activation energy (Q). *Post* [1977] also found that hydrated dunite at 900°C had the same creep strength as dry dunite at 1300°C, which demonstrates a trade-off between assumed water content and assumed temperature profiles of our flexure models. *Hirth and Kohlstedt* [1996] estimate the concentration of water in mid-ocean ridge basalts to be ~1000 H/10^6 Si, which is significantly larger than the solubility of water in olivine; they conclude that this water concentration would significantly decrease mantle viscosities in comparison to dry olivine.

The depth-dependent strength envelope assumed in our flexure models separates the mechanical part of the lithosphere into three regimes – brittle failure, an elastic core, and ductile deformation. However, the nature of the transition between brittle failure and ductile deformation is a gradual boundary, not sharp as is assumed by our models and shown in Figure 8 [*Scholz,* 2002; *Karato*, 2008]. More realistically, with increased depth and temperatures, rocks enter a region of semi-brittle deformation, a zone in which different minerals transition from brittle to plastic behavior [*Scholz,* 2002]. Within this semi-brittle region, a mixture of both cataclastic flow and ductile faulting can occur; the ductile faulting mechanism has been proposed to explain earthquakes which occur well below the depth expected for brittle failure [*Post,* 1977; *Chapple and Forsyth*, 1979; *Karato,* 2008]. The presence of a deep compressional earthquake beneath the Southern Mariana outer rise and the large amount of compressional stress at depth predicted by our

flexure models for this region suggests that a ductile faulting mechanism may explain the occurrence of this event.

Garcia-Castellanos et al [2000] found that the warmer and thinner GDH1 temperature model from *Stein and Stein* [1992] fit the observed trace of the bending Pacific plate at the Tonga subduction zone best in comparison to the temperature profile of *Parsons and Sclater* [1977]. Similarly, *McNutt* [1984] found that the thick thermal plate from the *Parsons and Sclater* [1977] model did not accurately fit the determined mechanical thickness of the old oceanic plates at the Bonin and Mariana trench. As discussed by *Garcia-Castellanos et al* [2000], although the flexure profile produced by the *Stein and Stein* [1992] model better fits the bathymetry at the Tongan trench, trade-offs between thermal and rheological parameters, in particular as discussed above for wet and dry dunite, does not allow the "right" thermal model from being identified.

5.3 Stresses within the Pacific Oceanic Plate

The Pacific Plate at Central Mariana (15-18°N) has had many, recent, normal faulting earthquakes. In this region, a large Mw 7.5 extensional outer rise earthquake occurred within the Pacific plate almost directly beneath the trench [*Zhang and Lay*, 1992; *Yoshida et al*, 1992] suggesting that large extensional forces must be present in this region of the Pacific plate. Similar to the results found by *Garcia-Castellanos et al* [2000] at the Tonga-Kermadec subduction zone, the best-fitting boundary forces acting on the subducting slab determined by our plate flexure inversion require both extensional regional horizontal forces and downward vertical forces. The interpretation presented by

Garcia-Castellanos et al [2000] for the stress distribution within the Pacific plate at the Tonga-Kermadec subduction zone was that tension within the Pacific plate outer rise was created by strong slab pull forces. At Central and Northern Mariana, the subducting slab is dipping almost vertically [*Stern et al*, 2003] and this steep dip and the associated strong slab pull forces have been suggested by *Uyeda and Kanamori* [1979] to contribute to a decoupled plate interface in the Mariana subduction zone. Strong coupling along the subduction plate interface is the cause for compressional regional forces, and so the lack of horizontal compressive forces in the resultant flexure models in this region appears consistent with the interpretation that the Mariana plate interface is decoupled [*Uyeda and Kanamori*, 1979].

In southern Mariana, both extensional and compressional earthquakes are located within the outer rise. The existence of compressional outer rise earthquakes was suggested by *Christensen and Ruff* [1983; 1988] to be indicative of strong coupling along the shallow subduction plate interface. The island of Guam has a history of strong shaking, although the cause for shaking may not be due only to large plate interface earthquakes [*Maso*, 1910; *Soloviev and Go*, 1974; *Emry et al*, 2011; *Okal et al*, submitted]. Three Mw > 7.0 earthquakes occurring near Guam in 1993, 2001, and 2002 [*Global CMT catalog; Dziewonski et al*, 1981] were initially thought to have occurred along the subduction plate interface [*Scholz and Campos*, 1995; *Campos et al*, 1996]; however others have proposed a source within the subducting slab [*Tanioka et al*, 1995; *Harada and Ishibashi*, 2008]. In addition, the Southern Mariana plate interface has been suggested to be more strongly coupled than the Central and Northern plate interface based on the simple geometry of the subduction system [*Scholz and Campos*, 1995].

The viability of the mechanism proposed by *Christensen and Ruff* [1983; 1988] to predict regions of strong interplate coupling is not certain. Although the Northern Kuril subduction zone has exhibited the relationship described by *Christensen and Ruff* [1983; 1988] prior to and following the 2006-2007 great earthquake doublet [*Ammon et al,* 2008*; Raeesi and Atakan,* 2009*; Lay et al,* 2009], the Tongan subduction zone also has several compressional outer rise earthquakes – and this subduction zone although potentially capable of having large megathrust ruptures does not exhibit the temporal relationship that *Christensen and Ruff* [1983; 1988] describe [*Lay et al,* 2010]. In southern Mariana, new results from historic waveform data suggest that an Mw 7.0 deep, compressional outer rise event occurred in 1940 within the outer rise ~200 km north of the compressional outer rise earthquake examined in this study [*Okal et al,* submitted]. Although limited historic data generally makes location and earthquake focal mechanism determination difficult, similarly large compressional outer rise earthquakes have occurred at other subduction zones [*Ammon et al,* 2008; *Lay et al,* 2009; *Raeesi and Atakan*, 2009]. Over the past 70 years since the occurrence of this apparent large, compressional outer rise earthquake [*Okal et al*, submitted], no great megathrust earthquake has occurred within this region as would be predicted by *Christensen and Ruff* [1983; 1988]. At this point, it is not clear whether the compressional earthquakes occurring at the Southern Mariana outer rise are indicative of plate interface locking as at the Kuril Subduction Zone [*Ammon et al*, 2008] or if they exhibit the characteristics of the plate interface at the Tongan Subduction Zone [*Lay et al*, 2010]. Given the compressional outer rise earthquakes and the results from flexure models predicting a strongly-bending Pacific plate that is undergoing regional compression, we argue for a

strongly coupled Southern Mariana plate interface with greater seismic potential– in agreement with *Scholz and Campos* [1995].

The question of whether Southern Mariana has compressional outer rise earthquakes because it is strongly coupled or whether they are linked to other factors is important to the discussion of outer rise mantle serpentinization. If the Southern Mariana plate interface is strongly coupled, similar to the Kuril Subduction Zone, then slip along the megathrust could invoke an increase in extensional faulting beneath the outer rise. This would impact the long-term estimate of outer rise mantle hydration spanning multiple seismic cycles, meaning that our short-term survey of extensional outer rise earthquakes would underestimate the actual depth extent of serpentinization. However if Southern Mariana is not strongly coupled, then our depth estimates of outer rise extension would not be dependent upon the megathrust seismic cycle. Regardless of the state of the plate interface, the pattern of seismicity since 1990 represents a short window of time and should be kept in consideration.

5.4 Water cycle of the Mariana Subduction Zone

Our modeled earthquake depths and plate flexure models suggest that the maximum depth of extension in the outer rise may vary along length of the Mariana subduction zone. If we assume that depth of brittle extensional stresses marks the lower depth at which water can percolate into the bending plate as was assumed by *Ranero et al* [2003] and *Lefeldt et al* [2009], then we expect that some regions of the Pacific plate may have more serpentinized mantle than others, in particular the site of the 5 April 1990 Mw

7.5 outer rise earthquake. However, the shallow forearc and wedge east of the volcanic arc should not be impacted by the amount of slab mantle hydration, as it requires greater temperatures and pressures to cause dehydration reactions in serpentinite [e.g. *Ulmer and Trommsdorf*, 1995]. If as suggested by *Van Keken et al* [2011], the Mariana Subduction Zone does not have significant potential for deep mantle water subduction, then the majority of water stored within the slab mantle should have the greatest effects on the subduction mantle wedge and the arc and back arc volcanic outputs. At Mariana, the water content as measured by olivine fluid inclusions and liquid lines of descent suggest no clear patterns for the amount of water output from the arc and is notably variable along the length of the subduction zone [*Kelley et al,* 2006; *Shaw et al,* 2008; *Kelley et al,* 2010; *Parman et al*, 2011]. Although the water content of Mariana backarc volcanics is generally small [*Kelley et al,* 2006], the southernmost Mariana back-arc exhibits higher water content as the arc and the back arc are separated by smaller distances [*Fryer et al,* 1998; *Martinez et al*, 2000].

Current subduction water flux models are dependent upon many factors: the initial extent of slab mantle hydration [e.g. *Rüpke et al*, 2004; *Van Keken et al*, 2011], the controls on fluid expulsion due to interactions between slab mineral assemblages as they metamorphose with increasing depth [*Ulmer and Trommsdorf*, 1995; *Rüpke et al*, 2004; *Hacker*, 2008], and the physical conditions of the slab, such as faults, which may enable a faster rate of fluid expulsion [*Wada et al,* submitted]. The most current estimate of the amount of water subducted into the deep Earth at the Mariana Subduction Zone is small [*Van Keken et al*, 2011]; however, the initial amount of slab mantle serpentinization was

necessarily assumed to be the same at all subduction zones, an assumption which our results, as well as other studies, suggests is not realistic.

Assuming that the depth of extension in the outer rise reflects the depth of mantle serpentinization, our results suggest that at Central Mariana the top 11 km of the slab mantle is hydrated (Figure 13). For their partially serpentinized scenario (2 wt % H_2O for the upper 2 km of the mantle), *Van Keken et al* [2011] estimate the mantle contribution of input water at the Mariana subduction zone at 18°N to be 6.5 Tg/Myr/m, or 3.3 E6 Tg/Myr for the full 500 km length of the Southern-Central Mariana subduction zone. According to *Carlson and Miller* [2003], 2 wt % H_2O corresponds to a mantle that is ~15% serpentinized. However, *Van Avendonk et al* [2011] find evidence at Nicaragua for mantle that is ~20-30% serpentinized corresponding to 3-4 wt % H_2O down to ~5-10 km depth. If we assume the 2 wt % H_2O from *Van Keken et al* [2011] down to the depth of our deepest extensional earthquake (11 km below the crust), then the amount of water input into the Mariana subduction zone would be 36.3 Tg/Myr/m, which is 5.5 times greater than *Van Keken et al* [2011]. However, if as observed by *Van Avendonk et al* [2011] at Nicaragua, the percentage of mantle hydration is really ~3.5 wt % H_2O, then the amount of water input at Central Mariana (assuming 11 km depth of mantle hydration) would be 63.5 Tg/Myr/m, or almost 10 times larger than assumed by *Van Keken et al* [2011]. Although we cannot definitively assign any certainty on the amount of mantle hydration based on our earthquake centroid depths, it does appear very likely that the Mariana Subduction zone inputs significantly more water than the global average assumed by recent models.

5.5 Intermediate depth earthquakes – reactivating plate bending fault planes?

Intermediate and deep earthquakes have been hypothesized to reactivate faults created at the outer rise and outer trench wall of the subduction zones [e.g. *Savage,* 1969]. Observations that focal mechanisms of outer rise earthquakes correlate with the pre-subduction orientations of intermediate depth earthquake focal mechanisms reinforce this hypothesis [e.g. *Silver et al,* 1995; *Jiao et al*, 2000]. Intermediate and deep-focus earthquakes occur within the subducting Mariana slab down to 600 km in distinct patches along the length of the subduction zone [*Burbach and Frohlich*, 1986]. All intermediate and deep earthquake fault planes identified by *Myhill and Warren* [2012] in the Izu-Bonin-Mariana subducting slab are sub-horizontal. Predominantly sub-horizontal faults have been found at intermediate depths within subduction zones [*Warren et al,* 2007; *Warren*, 2010; *Kiser et al*, 2011]; at many of these subduction zones, the dominant dip of outer rise faults is toward the trench (or landward-dipping). However, if intermediate depth earthquakes were caused by reactivation of outer rise faults, then the subhorizontal fault planes at depth would correspond to the seaward-dipping (away from the trench) faults at the outer rise [*Myhill and Warren*, 2012].

The location, depths and dips of the majority of the outer rise earthquakes in this study do not definitively identify which of the focal mechanism planes was the actual plane of rupture (Appendix C). The one exception to this is the large 5 April 1990 Mw ~7.5 earthquake and one of its larger aftershocks occurring on 6 April 1990. Although both *Zhang and Lay* [1992] and *Yoshida et al* [1992] favor a west-ward dipping rupture plane for the mainshock, our relative locations and depths for the two nearby events are more suggestive of an east-ward dipping rupture plane – assuming that the large

aftershock occurred along the same fault plane as the mainshock (Figure 7). Given the close temporal and spatial proximity of the two events, the assumption that they both occurred along the same fault plane is not unreasonable. Furthermore, high resolution bathymetry and MCS results indicate both trenchward- and seaward-dipping faults in the central Mariana outer rise [*Oakley et al*, 2008; *Gardner*, 2010]. In particular, the seafloor directly above the site of the large 5 April 1990 earthquake, as imaged by a recent Law of the Sea cruise [*Gardner,* 2010] shows the largest throws on the seaward-dipping, not landward-dipping, fault planes.

The bathymetry profile shown in Figure 7 is oriented perpendicular to the strike of the seafloor fault planes and shows a dip angle of ~20° for the faults with the largest offsets, after correction for the vertical exaggeration of the cross-sections. Given this, the horizontal location and the apparent dip of the faults do not immediately seem to correlate, as the faults are too shallow and the earthquakes are located too far west. However for this region, *Emry et al* [2011] found that earthquake locations determined using only teleseismic data are biased by ~10 km to the west in comparison to locations for the same events using data from a local ocean-bottom seismic array. This could mean that the relocations of events in the Central and Northern Mariana outer rise should be shifted ~10 km towards the east (or away from the trench axis). In addition to this potential lateral shift in the earthquake locations, the faults exposed at the surface of the seafloor are not newly formed. Over time, we can assume that the exposed fault erodes and becomes shallower as sediment collects within the depression created by the fault. If this is true, then the only constraint we have from bathymetry for the fault is that it must be steeper than the apparent 20° dip. In Figure 7, alternate faults are drawn to illustrate

that with an increase in the observed dip to ~35°, observed seismicity at mantle depths appears to be more closely related to the exposed faults on the seafloor.

6. Conclusion

Our relative relocations and refined depths of outer rise and outer trench wall earthquakes of moderate to large magnitude occurring during the last 22 years at the Mariana Subduction trench indicate that the Pacific plate undergoes more extensional faulting in the central section of the subduction zone. The observed maximum centroid depth of extensional earthquakes in Central Mariana is 18 km below the seafloor, or 11 km below the base of the crust. The best-fitting models to the bathymetry profiles in this section of the subduction zone indicate that the Central Mariana is acted upon by large extensional horizontal forces and that brittle failure can be expected to depths greater than 30 km; this prediction for depth of extensional stresses coincides well with our modeled earthquake depths. We interpret these results to suggest large amounts of regional tension in Central Mariana, possibly due to previously suggested lack of plate coupling and strong slab pull forces. In Southern Mariana, fewer moderate to large magnitude extensional earthquakes occurred in the past 22 years. The maximum depth for extensional earthquakes near the Southern Mariana trench was 12 km, or 5 km below the base of the crust in this region. The modeled depth of the moderately sized compressional earthquake in this region was 34 km. The best-fitting models corresponding to the bathymetric profile in Southern Mariana suggest a plate that is undergoing a strong bending moment as well as significant regional compression, which

coincides well with our modeled extensional and compressional earthquake depths. We interpret these observations to be indicative of a more strongly coupled plate interface in Southern Mariana. Based on the differences between the two regions, we suggest that the Pacific plate is hydrated to greater depth in the Central section of the margin than in Southern Mariana.

7. Acknowledgements – Many thanks to H.Chou, J.Conder, D. Garcia-Castellanos, K. Kelley, D. Lizarralde, F. Martinez, B. Myhill, B. Savage, B. Shiro, P. Shore, P. Skemer, S. Solomatov, S. Stein, P. Van Keken, I. Wada, and L. Warren for scientific and technical assistance. Thank you to the IRIS Data Management Center, which provided access to the waveform data used in this study. Support for this research was provided under grants OCE-0426408, OCE-0752476, and OCE-0841074. Additional funding to present this research was provided by the NSF Earthscope and GeoPRISMs programs as well as the NSF/FESD CIDER program. Maps and cross-section were created using the GMT software [Wessel and Smith, 1991].

References

Ammon, C.J., H. Kanamori, and T. Lay (2008), A great earthquake doublet and seismic stress transfer cycle in the central Kuril islands, *Nature, 451*(7178), 561-566, doi:10.1038/nature06521.

Audet, P., M.G. Bostock, N.I. Christensen, and S.M. Peacock (2009), Seismic evidence for overpressured subducted oceanic crust and megathrust fault sealing, *Nature, 457*(7225), 76-78, doi: 10.1038/nature07650.

Barklage, M. (2010), Structure and Seismicity of the Upper Mantle using Deployments of Broadband Seismographs in Antarctica and the Mariana Islands, Ph.D. dissertation, 115 pp, Washington University in Saint Louis, Saint Louis.

Bodine, J. H., M. S. Steckler, and A. B. Watts (1981), Observations of flexure and rheology of the oceanic lithosphere, *J. Geophys. Res., 86*(B5), 3695-3707.

Burbach, G.V. and C. Frohlich (1986) Intermediate and deep seismicity and lateral structure of subducted lithosphere in the Circum-Pacific region, *Rev.Geophys., 24*(4), 833-874, 10.1029/RG024i004p00833.

Byerlee, J. (1978), Friction of rocks, *Pure App. Geophys., 116*(4-5), 615-626.

Caldwell, J. G., W. F. Haxby, D. E. Karig, and D. L. Turcotte (1976), On the applicability of a universal elastic trench profile, *Earth Planet. Sci. Lett., 31*, 239-246.

Campos, J., R. Madariaga, and C. Scholz (1996), Faulting processes of the August 8, 1993, Guam earthquake: A thrust event in an otherwise weakly coupled subduction zone, *J. Geophys. Res., 101*(B8), 17,581-17,596, doi:10.1029/96JB00654.

Carlson, R. L. and D. J. Miller (2003), Mantle wedge water contents estimated from seismic velocities in partially serpentinized peridotites, *Geophys. Res. Lett., 30*(5), 1250, doi:10.1029/2002GL016600.

Chapple, W.M. and D.W. Forsyth (1979), Earthquakes and bending of plates at trenches, *J. Geophys.l Res., 84*(B12), 6729-6749.

Christensen, D.H. and L.J. Ruff (1983) Outer-rise earthquakes and seismic coupling, *Geophys. Res. Lett., 10*(8), 697-700, 10.1029/GL010i008p00697.

Christensen, D.H. and L.J. Ruff (1988) Seismic coupling and outer rise earthquakes, *J. Geophys.Res., 93*(B11), 13,421-13,444, 10.1029/JB093iB11p13421.

Contreras-Reyes, E., I. Grevemeyer, E.R. Flueh, M. Scherwath, and M. Heesemann (2007) Alteration of the subducting oceanic lithosphere at the southern central Chile trench-outer rise, *Geochem. Geophys. Geosyst., 8*(7), Q07003, doi:10.1029/2007GC001632.

Dieterich, J. H. and G. Conrad (1984), Effect of humidity on time- and velocity-dependent friction in rocks, *J. Geophys. Res., 89*(B6), 4196-4202.

Emry, E.L., D.A. Wiens, H. Shiobara, and H. Sugioka (2011) Seismogenic characteristics of the Northern Mariana shallow thrust zone from local array data, *Geochem. Geophys. Geosyst., 12*(12), Q12008, doi:10.1029/2011GC003853.

Faccenda, M., T.V. Gerya, and L. Burlini (2009) Deep slab hydration induced by bending-related variations in tectonic pressure, *Nature Geoscience, 2,* 790-793, doi: 10.1038/NGEO656.

Fryer, P., H. Fujimoto, M. Sekine, L.E. Johnson, J. Kasahara, H. Masuda, T. Gamo, T. Ishii, M. Ariyoshi, and K. Fujioka (1998) Volcanoes of the southwestern

extension of the active Mariana island arc: New swath-mapping and geochemical studies, *The Island Arc, 7,* 596-607, doi: 10.1111/j.1440-1738.1998.00212.x

Fryer, P., C.G. Wheat, and M.J. Mottl (1999), Mariana blueschist mud volcanism: Implications for conditions within the subduction zone, *Geology*, *27*(2), 103-106, doi: 10.1130/0091-7613(1999)027<0103:MBMVIF>2.3.CO;2.

Garcia-Castellanos, D., M. Fernàndez, and M. Torne (1997) Numerical modeling of foreland basin formation: A program relating thrusting, flexure, sediment geometry and lithosphere rheology, *Computers & Geosciences, 23*(9), 993-1003, doi: 10.1016/S0098-3004(97)00057-5.

Garcia-Castellanos, D., M. Torne, and M. Fernàndez (2000) Slab pull effects from a flexural analysis of the Tonga and Kermadec trenches (Pacific Plate), *Geophys. J. Int., 141*(2), 479-484, doi: 10.1046/j.1365-246x.2000.00096.x

Gardner, J.V. (2010), US Law of the Sea cruises to map sections of the Mariana Trench and the eastern and southern insular margins of Guam and the Northern Mariana Islands, *Rep. UNH-CCOM/JHC Technical Report 10-003.*

Gill, J. B. (1981), *Orogenic Andesites and Plate Tectonics*, 390 pp., Springer, New York.

Goetze, C. (1978), The mechanisms of creep in olivine, *Phil. Trans. R. Soc. Lond., 288*, 99-119.

Goetze, C. and B. Evans (1979), Stress and temperature in the bending lithosphere as constrained by experimental rock mechanics, *Geophys. J. R. Astr. Soc., 59*(3).

Hacker, B.R. (2008), H2O subduction beyond arcs, *Geochem. Geophys. Geosyst., 9*, Q03001, doi: 10.1029/2007GC001707.

Harada, T. and K. Ishibashi (2008), Interpretation of the 1993, 2001, and 2002 Guam earthquakes as intraslab events by a simultaneous relocation of the mainshocks, aftershocks, and background earthquakes, *Bull. Seismol. Soc. Am., 98*(3), 1581-1587, doi:10.1785/0120060227.

Hirschmann, M.M. (2006) Water, melting, and the deep Earth H_2O cycle, *Annu. Rev. Earth Planet. Sci., 34*, 629-653, doi: 10.1146/annurev.earth.34.031405.125211.

Hirth, G. and D. L. Kohlstedt (1996), Water in the oceanic upper mantle: implications for rheology, melt extraction and the evolution of the lithosphere, *Earth Planet. Sci. Lett., 144*, 93-108.

International Seismological Centre, *On-line Bulletin*, http://www.isc.ac.uk, Internatl. Seis. Cent., Thatcham, United Kingdom, 2010.

Isacks, B., J. Oliver, and L.R. Sykes (1968) Seismology and the new global tectonics, *J. Geophys. Res. 73*(18), 5855-5899.

Ivandic, M., I. Grevemeyer, J. Bialas, and C. J. Petersen (2010), Serpentinization in the trench-outer rise region offshore of Nicaragua: constraints from seismic refraction and wide-angle data, *Geophys. J. Int. 180*, 1253-1264, doi:10.1111/j.1365-246X.2009.04474.x.

Jarrard, R.D. (2003), Subduction fluxes of water, carbon dioxide, chlorine, and potassium, *Geochem. Geophys. Geosyst., 4*(5), 8905, doi: 10.1029/2002GC000392.

Jiao, W., P.G. Silver, Y. Fei, and C.T. Prewitt (2000) Do intermediate- and deep-focus earthquakes occur on preexisting weak zones? An examination of the Tonga

subduction zone, *J. Geophys. Res., 105*(B12), 28,125-28,138, doi: 10.1029/2000JB900314.

Jordan, T. H., and K. A. Sverdrup (1981), Teleseismic location techniques and their application to earthquake clusters in the South-Central Pacific, *Bull. Seism. Soc. Am.*, *71*(4), 1105-1130.

Kao, H. and W.-P. Chen (1996) Seismicity in the outer rise-forearc region and configuration of the subducting lithosphere with special reference to the Japan Trench, *J. Geophys. Res., 101*(B12), 27,811-27,831, doi: 10.1029/96JB01760.

Karato, S. (2008), *Deformation of Earth Materials: An Introduction to the Rheology of Solid Earth*, 463 pp., University Press, Cambridge.

Kelley, K.A., T. Plank, T.L. Grove, E.M. Stolper, S. Newman, and E. Hauri (2006) Mantle melting as a function of water content beneath back-arc basins, *J. Geophys. Res., 111*, B09208, doi:10.1029/2005JB003732.

Kelley, K.A., T. Plank, S. Newman, E.M. Stolper, T.L. Grove, S. Parman, and E.H. Hauri (2010) Mantle melting as a function of water content beneath the Mariana Arc, *J. Petrology, 51*(8), 1711-1738, doi:10.1093/petrology/egq036.

Kennett, B. L. N., and E. R. Engdahl (1991), Traveltimes for global earthquake location and phase identification, *Geophys J. Int.*, *105*(2), 429-465, doi: 10.1111/j.1365-246X.1991.tb06724.x.

Kikuchi, M. and H. Kanamori (1991) Inversion of complex body waves – III, *Bull. Seismological Soc. Am., 81*(6), 2335-2350,

Kiser, E., M. Ishii, C. H. Langmuir, P. M. Shearer, and H. Hirose (2011), Insights into the mechanism of intermediate-depth earthquakes from source properties as imaged

by back projection of multiple seismic phases, *J. Geophys. Res., 116*, B06310, doi:10.1029/2010JB007831.

Kohlstedt, D.L., B. Evans, and S.J. Mackwell (1995), Strength of the lithosphere: Constraints imposed by laboratory experiments, *J. Geophys. Res., 100*(B9), 17,587-17,602.

Korenaga, J. (2007), Thermal cracking and the deep hydration of oceanic lithosphere: A key to the generation of plate tectonics?, *J. Geophys. Res., 112,* B05408, doi:10.1029/2006JB004502.

Langston, C.A. and D.V. Helmberger (1975), A procedure for modeling shallow dislocation sources, *Geophysical Journal of the Royal Astronomical Society, 42*(1), 117-130.

Lay, T., H. Kanamori, C.J. Ammon, A.R. Hutko, K. Furlong, and L. Rivera (2009), The 2006-2007 Kuril Islands great earthquake sequence, *J. Geophys. Res., 114*, B11308, doi:10.1029/2008JB006280.

Lay, T., C. J. Ammon, H. Kanamori, L. Rivera, K. D. Koper, and A. R. Hutko (2010), The 2009 Samoa-Tonga great earthquake triggered doublet, *Nature, 466,* 964-968, doi:10.1038/nature09214.

Lefeldt, M., I. Grevemeyer, J. Goßler, and J. Bialas (2009), Intraplate seismicity and related mantle hydration at the Nicaraguan trench outer rise, *Geophys. J. Int., 178*(2), 742-752, doi: 10.1111/j.1365-246X.2009.04167.x.

Martinez, F., P. Fryer, and N. Becker (2000), Geophysical characteristics of the southern Mariana Trough, 11°50’N-13°40’N, *J. Geophys. Res., 105*(B7), 16,591-16,607, doi: 10.1029/2000JB900117.

Martinez, F., K. A. Kelley, and R. J. Stern (2012), Creation and deformation of hydrous lithosphere at the So uthern Mariana margin, *Geophys. Res. Abs. 14*.

Maso, M. S. (1910), *Catalogue of Violent and Destructive Earthquakes in the Philippines, with an Appendix, Earthquakes in the Marianas Islands; 1599-1909*, Philipp. Isl. Weather Bur., Manilla.

Masson, D. G. (1991), Fault patterns at outer trench walls, *Mar. Geophys. Res., 13*(3), 209-225, doi:10.1007/BF00369150.

McNutt, M. K. (1984), Lithospheric flexure and thermal anomalies, *J. Geophys. Res., 89*(B13), 11180-11194.

Meade, C. and R. Jeanloz (1991), Deep-focus earthquakes and recycling of water into the Earth's mantle, *Science, 252*(5002), 68-72, doi: 10.1126/science.252.5002.68.

Moore, J. C. and P. Vrolijk (1992), Fluids in accretionary prisms, *Rev. Geophys., 30*(2), 113-135.

Myhill, R. and L.M. Warren (2012), Fault plane orientations of deep earthquakes in the Izu-Bonin-Marianas subduction zone, *J. Geophys. Res,117,* B06307, doi:10.1029/2011JB009047.

Nedimovic, M.R., D.R. Bohnenstiehl, S.M. Carbotte, J.P. Canales, and R.P. Dziak (2009), Faulting and hydration of the Juan de Fuca plate system, *Earth Planet. Sci. Lett., 284*(1-2), 94-102, doi:10.1016/j.epsl.2009.04.013.

Oakley, A. J., B. Taylor, and G.F. Moore (2008), Pacific Plate subduction beneath the central Mariana and Izu-Bonin fore arcs: New insights from an old margin, *Geochem. Geophys. Geosyst.*, *9*(6), 28, doi: 10.1029/2007GC001820.

Okal, E. A., D. Reymond, and S. Hongsresawat (submitted), Large, pre-digital earthquakes of the Bonin-Mariana Subduction Zone, *Tectonophysics*.

O'Neill, C., A. M. Jellinek, and A. Lenardic (2007), Conditions for the onset of plate tectonics on terrestrial planets and moons, *Earth Planet. Sci. Lett., 261*, 20-32, doi:10.1016/j.epsl.2007.05.038.

Parman, S.W., T.L. Grove, K.A. Kelley, and T. Plank (2011), Along-arc variations in the pre-eruptive H_2O contents of Mariana arc magmas inferred from fractionation paths, *J. Petrology, 52*(2), 257-278, doi:10.1093/petrology/egq079.

Parsons, B. and J. G. Sclater (1977), An analysis of the variation of ocean floor bathymetry and heat flow with age, *J. Geophys. Res., 82*(5), 803-827.

Phipps Morgan, J., and B. K. Holtzman (2005), Vug waves: A mechanism for coupled rock deformation and fluid migration, *Geochem. Geophys. Geosyst., 6*(8), Q08002, doi:10.1029/2004GC000818.

Plank, T. and C. H. Langmuir (1993), Tracing trace elements from sediment input to volcanic output at subduction zones, *Nature, 362*, 739-743.

Post, R. L. (1977), High-temperature creep of Mt. Burnet dunite, *Tectonophys., 42*, 75-110.

Pozgay, S., D.A. Wiens, J.A. Conder, H. Shiobara, and H. Sugioka (2009), Seismic attenuation tomography of the Mariana arc: Implications for thermal structure, volatile distribution, and dynamics, *Geochem. Geophys. Geosyst.*, *10*, Q04X05, doi: 10.1029/2008GC002313.

Pyle, M., D.A. Wiens, D.S. Weeraratne, P.J. Shore, H. Shiobara, and H. Sugioka (2010), Shear velocity structure of the Mariana mantle wedge from Rayleigh wave phase velocities, *J Geophys. Res.*, *115*, B11304, doi: 10.1029/2009JB006976.

Raeesi, M. and K. Atakan (2009), On the deformation cycle of a strongly coupled plate interface: The triple earthquakes of 16 March 1963, 15 November 2006, and 13 January 2007 along the Kurile subduction zone, *J. Geophys. Res., 114*, B10301, doi:10.1029/2008JB006184.

Raleigh, C.B. and M.S. Paterson (1965), Experimental deformation of serpentinite and its tectonic implications, *J. Geophys. Res., 70*(16), 3965-3985.

Ranero, C.R., J. Phipps Morgan, K. McIntosh, and C. Reichert (2003), Bending-related faulting and mantle serpentinization at the Middle America trench, *Nature, 425*(6956), 367-373, doi:10.1038/nature01961.

Ranero, C. R., A. Villasenor, J. P. Morgan, W. Weinrebe (2005), Relationship between bend-faulting at trenches and intermediate-depth seismicity, *Geochem. Geophys. Geosyst., 6*(12), Q12002, doi:10.1029/2005GC000997.

Rüpke, L.H., J. Phipps Morgan, M. Hort, and J.A.D. Connolly (2004), Serpentine and the subduction zone water cycle, *Earth Planet. Sci. Lett., 223*(1-2), 17-34, doi:10.1016/j.epsl.2004.04.018.

Satake, K., Y. Yoshida, and K. Abe (1992), Tsunami from the Mariana earthquake of April 5, 1990 – its abnormal propagation and implications for tsunami potential from outer-rise earthquakes, *Geophys. Res. Lett., 19*(3), 301-304, doi: 10.1029/91GL02493.

Savage, J.C. (1969), The mechanics of deep-focus faulting, *Tectonophys., 8*(2), 115-127.

Savage, B. (2012), Seismic constraints on the water flux delivered to the deep Earth by subduction, *Geology, 40*(3), 235-238, doi:10.1130/G32499.1.

Schmidt, M.W. and S. Poli (1998), Experimentally based water budgets for dehydrating slabs and consequences for arc magma generation, *Earth Planet. Sci. Lett., 163*(1-4), 361-379, doi:10.1016/S0012-821X(98)00142-3.

Scholz, C. H. (2002), *The Mechanics of Earthquakes and Faulting* 2nd ed., University Press, Cambridge.

Scholz, C. H. and J. Campos (1995), On the mechanism of seismic decoupling and back arc spreading at subduction zones, *J. Geophys. Res., 100*(B11), 22103-22115.

Shaw, A.M, E.H. Hauri, T.P. Fischer, D.R. Hilton, and K.A. Kelley (2008), Hydrogen isotopes in Mariana arc melt inclusions: Implications for subduction dehydration and the deep-Earth water cycle, *Earth Planet. Sci. Lett., 275*(1-2), 138-145, doi:10.1016/j.epsl.2008.08.015.

Shelly, D. R., G.C. Beroza, S. Ide, and S. Nakamula (2006), Low-frequency earthquakes in Shikoku, Japan, and their relationship to episodic tremor and slip, *Nature*, *442*(7099), 188-191, doi: 10.1038/nature04931.

Sibson, R.H. (1994), Crustal stress, faulting and fluid flow, in *Geofluids: Origin, Migration and Evolution of Fluids in Sedimentary Basins, Geo. Society. Spec. Pub. 78*, edited by J. Parnell, pp. 69-84, Geological Society, London.

Silver, P.G., S.L. Beck, T.C. Wallace, C. Meade, S.C. Myers, D.E. James, and R. Kuehnel (1995), Rupture characteristics of the deep Bolivian earthquake of 9 June 1994 and the mechanism of deep-focus earthquakes, *Science, 268*(5207), 69-73, doi:10.1126/science.268.5207.69.

Stauder, W. (1968), Mechanism of the Rat Island earthquake sequence of February 4, 1965, with relation to island arcs and sea-floor spreading, *J. Geophys. Res., 73*(12), 3847-3858

Stein, C.A. and S. Stein (1992), A model for the global variation in oceanic depth and heat flow with lithospheric age, *Nature, 359*(6391), 123-129, doi: 10.1038/359123a0.

Takahashi, N., S. Kodaira, S. L. Klemperer, Y. Tatsumi, Y. Kaneda, and K. Suyehiro (2007), Crustal structure and evolution of the Mariana intra-oceanic island arc, *Geology*, *35*(3), 203-206, doi: 10.1130/G23212A.1.

Tanioka ,Y., K. Satake, and L. Ruff (1995), Analysis of seismological and tsunami data from the 1993 Guam Earthquake, *Pure Appl. Geophys., 144*(3-4), 823-837, doi:10.1007/BF00874396.

Thompson, A.B. (1992), Water in the Earth's upper mantle, *Nature, 358*(6384), 295-302, doi:10.1038/358295a0.

Tibi, R., D. A. Wiens, and X. Yuan (2008), Seismic evidence for widespread serpentinized forearc mantle along the Mariana convergence margin, *Geophys. Res. Lett., 35*, L13303, doi:10.1029/2008GL034163.

Ulmer, P., and V. Trommsdorf (1995), Serpentine stability to mantle depths and subduction-related magmatism, *Science, 268*(5212), 858-861.

U.S. Department of Commerce, National Oceanic and Atmospheric Administration, National Geophysical Data Center, 2006. *2-minute Gridded Global Relief Data (ETOPO2v2)* http://www.ngdc.noaa.gov/mgg/fliers/06mgg01.html

Uyeda, S., and H. Kanamori (1979), Back-arc opening and the mode of subduction, *J. Geophys. Res., 84*(B3), 1049-1061, doi: 10.1029/JB084iB03p01049.

Van Avendonk, H.J.A., W.S. Holbrook, D. Lizarralde, and P. Denyer (2011), Structure and serpentinization of the subducting Cocos plate offshore Nicaragua and Costa Rica, *Geochem. Geophys. Geosyst., 12*, Q06009, doi:10.1029/2011GC003592.

Van Keken, P.E., B.R. Hacker, E.M. Syracuse, G.A. Abers (2011), Subduction factory: 4. Depth-dependent flux of H_2O from subducting slabs worldwide, *J. Geophys. Res., 116*, B01401, doi:10.1029/2010JB007922.

Wada, I., M. D. Behn, and A. M. Shaw (submitted), Effects of localized hydration in the incoming plate, slab rehydration, and mantle wedge hydration on slab-derived fluid flux in subduction zones, submitted to *Earth Planet. Sci. Lett*.

Warren, L. M., A. N. Hughes, and P. G. Silver (2007), Earthquake mechanics and deformation in the Tonga-Kermadec subduction zone from fault plane orientations of intermediate- and deep-focus earthquakes, *J. Geophys. Res., 112*, B05314, doi:10.1029/2006JB004677.

Warren, L. M. (2010), Measurement of differential rupture duration as constraints on the source finiteness of deep-focus earthquakes: 2. Synthetic tests to estimate errors in rupture vectors and their effect on fault plane identification, *J. Geophys. Res. 115*, B09307, doi:10.1029/2009JB007071.

Wessel, P. and W. H. F. Smith (1991), Free software helps map and display data, *EOS Trans. AGU, 72*, 441.

Wessel, P. (2001), Global distribution of seamounts inferred from gridded Geosat/ERS-1 altimetry, *J. Geophys. Res., 106*(B9), 19,431-19,441, doi: 10.1029/2000JB000083.

Yoshida, Y., K. Satake, and K. Abe (1992), The large normal-faulting Mariana earthquake of April 5, 1990 in uncoupled subduction zone, *Geophys. Res. Lett., 19*(3), 297-300, doi: 10.1029/92GL00165.

Zhang, J.J. and T. Lay (1992), The April 5, 1990 Mariana Islands earthquake and subduction zone stresses, *Phys. Earth Planet. Int., 72*(1-2), 99-121, doi:10.1016/0031-9201(92)90052-W.

Figure Captions

Figure 1: The best fitting focal mechanism for the 5 April 1990 earthquake at 18 km depth in the Pacific plate. First-motion polarities for P-wave arrivals at each station are indicated by open circles (dilatation) and closed circles (compression). Waveform data (BHZ) for select stations are shown in thick black lines and modeled synthetic waveforms are shown in a dashed black line. The x-axis (time) is given in seconds and the y-axis (displacement amplitude) is in meters.

Figure 2: Relocated and modeled GCMT earthquakes at 10°-22°N in map view. Lower hemisphere stereographic projections for modeled earthquakes are shown with T-axes (in black) and P-axes (in white). The event numbers next to each focal mechanism correspond to Table 5. The red arrow shows the angle and rate of convergence of the Pacific plate relative to the Mariana forearc as determined by *Kato et al* [2003]. High resolution bathymetry data in Northern and Central Mariana are from 2010 Mariana Law of the Sea Cruise [*Gardner*, 2010] courtesy of *D. Lizarralde* and high resolution bathymetry in Southern Mariana are courtesy of *F.Martinez*. Inset: Tectonic setting of the Philippine Sea. Bathymetry contours are shown by thin black lines. Subduction trenches are shown in blue; spreading centers are shown in red; transforms are shown in green.

Figure 3: Top: Relocated and modeled GCMT earthquake locations at 15°-16°N in map view. Lower hemisphere stereographic projections are shown with T-axes (in black) and P-axes (in white). Event numbers next to each focal mechanism correspond to Table 5.

The red arrow shows the angle and rate of convergence of the Pacific plate relative to the Mariana forearc as determined by *Kato et al* [2003]. High resolution bathymetry data are from 2010 Mariana Law of the Sea Cruise [*Gardner*, 2010] courtesy of *D. Lizarralde*. Inset: Bathymetry contours are shown by thin black lines. The subduction trench is shown in blue; back-arc spreading is in red; transform is in green.

Bottom: Trench perpendicular cross-section with the location of the subduction trench at 0 km; negative distances indicate the distance landward (or west of the trench) and positive distances indicate seaward distances (or east of the trench). Thick black lines indicate the bathymetry along the transect (15.2236°N, 147.0582°E) to (14.9072°N, 148.5767°E). The thick red line shows the depth to the Moho used in our waveform modeling technique. Black squares show the depth to the plate interface at ~17°N as determined by *Oakley et al* [2008] and red squares show the continuation of the Moho landward of the trench. Focal mechanisms for the region are rotated 90° into cross-section. P-axes are indicated by white while T-axes are indicated by red shading. The event numbers next to each focal mechanism correspond to Table 5. Vertical Exaggeration (V.E.) is 1.5.

Figure 4: Top: Relocated and modeled GCMT earthquake locations at 16.4°-18°N in mapview. Lower hemisphere stereographic projections for modeled earthquakes are shown with T-axes (in black) and P-axes (in white). Event numbers next to each focal mechanism correspond to Table 5. The red arrow shows the angle and rate of Pacific plate convergence relative to the forearc as determined by *Kato et al* [2003]. High

resolution bathymetry data are from 2010 Mariana Law of the Sea Cruise [*Gardner*, 2010] courtesy of *D. Lizarralde*. Inset shows the tectonic setting of the Mariana Islands. Bathymetry contours are shown by thin black lines. The subduction trench is shown in blue; back-arc spreading center is in red; transform is in green.

Bottom: Trench perpendicular cross-section with the location of the subduction trench at 0 km; negative distances indicate the distance landward (or west of the trench) and positive distances indicate seaward distances (or east of the trench). Thick black lines indicate the bathymetry along the transect (17.25°N, 147.3577°E) to (17.2752°N, 148.9311°E). Thick red line shows the depth to the Moho used in our waveform modeling technique. Black squares show the depth to the plate interface at ~17°N as determined by *Oakley et al* [2008] and red squares show the continuation of the Moho landward of the trench. Focal mechanisms for the region are rotated 90° into cross-section. P-axes are indicated by white while T-axes are indicated by red shading. The event numbers next to each focal mechanism correspond to Table 5. Vertical Exaggeration (V.E.) is 1.5.

Figure 5: Top: Relocated and modeled GCMT earthquake locations at 11.25°-12.75°N in map view. Lower hemisphere stereographic projections for modeled earthquakes are shown with T-axes (in black) and P-axes (in white). The event numbers next to each focal mechanism correspond to Table 5. The red arrow shows the angle and rate of Pacific plate convergence relative to the forearc from *Kato et al* [2003]. High resolution bathymetry data are courtesy of *F. Martinez*. Inset shows the tectonic setting of the

Mariana Islands. Bathymetry contours are shown by thin black lines. The subduction trench is shown in blue; back-arc spreading center is in red; transform is in green.

Bottom: Trench perpendicular cross-section with the location of the subduction trench at 0 km; negative distances indicate the distance landward (or northwest of the trench) and positive distances indicate seaward distances (or southeast of the trench). Thick black lines indicate the bathymetry along the transect (12.4708°N, 144.7513°E) to (11.1262°N, 145.4304°E). Thick red line shows the depth to the Moho used in our waveform modeling technique. Focal mechanisms for the region are rotated 90° into cross-section. P-axes are indicated by white while T-axes are indicated by red shading. The event numbers next to each focal mechanism correspond to Table 5. Vertical Exaggeration (V.E.) is 1.5.

Figure 6: Misfit contours in depth vs. source time function parameter space for the 5 April 1990 large extensional outer rise earthquake (Event 10, Table 5). Misfit is calculated according to equations (1) and (2). Contours for the solutions at 2%, 5%, 10%, 20%, and 50% greater than the best-fitting solution are given. The y-axis shows depth (km) below sea-level. The x-axis represents the source time function (seconds). The solution shows a simple relationship with one global minimum misfit solution for the entire depth-time parameter space.

Figure 7: Top: Cross-sectional profile in the vicinity of the 5 April 1990 outer rise earthquake with vertical exaggeration (V.E.) = 4 along the transect (15.4°N, 147.4°E) to

(15.2°N, 148°E). Bathymetry is shown in thick black lines, estimated continuation of surface faults for the dip apparent from bathymetry (~15-20°) neglecting effects of sediment deposition (gray dashed line) and for a steeper dipping fault (~35°) in consideration of possible sediment deposition and slumping (black dashed line). The apparent fault traces in this region are dipping in the seaward (east) direction. Bottom: Same cross-section as above with vertical exaggeration (V.E.) = 0.25. Thick black lines indicate the bathymetry, and thick red line shows the depth to the Moho assumed in our waveform modeling technique. Black squares show the depth to the plate interface ~17°N as determined by *Oakley et al* [2008] and red squares show the continuation of the Moho landward of the trench. Focal mechanisms for the 5 April 1990 and 6 April 1990 earthquakes (Events 10 and 14, Table 5) are rotated 90° into cross-section. Focal mechanisms at the original relocation position are further left on the diagram, and P-axes are indicated by white and T-axes are indicated by maroon shading. Shifted focal mechanisms for the same events following the observations of *Emry et al* [2011], are further right on the diagram, and P-axes are indicated by white and T-axes are indicated by red. Shallow-dipping faults are shown as dashed gray lines and steeper-dipping faults are shown as black dashed lines.

Figure 8: Yield Stress Envelope (YSE) corresponding to the distance of maximum bending moment for the best-fitting flexure model in Southern Mariana. X-axis gives stress values (MPa) with compression (negative) to the left of the origin and tension (positive) to the right or the origin. Y-axis gives the depth (km) beneath the top of the plate. Black lines outline the failure envelope. Coulomb (cataclastic) failure criteria in

compression (left) and tension (right) extends from the origin point to depths of ~40-45 km before ductile deformation intersects and controls deformation to the depth of the mechanical thickness ~50 km. Thin grey line shows the 0 MPa trend line and the thick grey line shows the stress profile of the bending plate with depth. Dashed grey lines show the depths at which the stress profile switches from the brittle failure regime to elastic, the transition from extensional to compressional stress (the neutral plane), the point at which the stress profile switches from elastic to ductile/plastic deformation, and the mechanical thickness depth.

Figure 9: Stress distribution within the bending plate with distance (km) and depth (km) for the best-fitting Northern Mariana profile using only the bathymetry seaward of the trench (top) and the best-fitting northern profile using the bathymetry seaward of the trench and the landward continuation of the slab as determined by *Oakley et al* [2008]. Positive (extensional) stress values are indicated by blue and negative (compressional) stress values are indicated by red. White circles indicate locations of extensional earthquakes as determined in this study, gray circles indicate locations of strike-slip events, and black circles indicate locations of compressional earthquakes. Thick black lines show the top of the Pacific plate and the depth of the mechanical thickness. The failure envelopes to the right (similar to the enlarged plot in Figure 8) of each 2-d profile shows the stress with depth at the point of maximum bending moment, with the neutral surface marked.

Figure 10: Stress distribution within the bending plate with distance (km) and depth (km) for the best-fitting Northern Mariana profile using the bathymetry seaward of the trench and the landward continuation of the slab as determined by *Oakley et al* [2008] and the best-fitting Southern Mariana profile using the bathymetry seaward of the trench (no landward profiles for this region are available). Positive (extensional) stress values are indicated by blue and negative (compressional) stress values are indicated by red. White circles indicate locations of extensional earthquakes as determined in this study, gray circles indicate locations of strike-slip events, and black circles indicate locations of compressional earthquakes. Thick black lines show the top of the Pacific plate and the depth of the mechanical thickness. The failure envelopes to the right (similar to the enlarged plot in Figure 8) of each 2-d profile shows the stress with depth at the point of maximum bending moment, with the neutral surface marked.

Figure 11: Plot shows three distinct low misfit solutions for plate flexure at Southern Mariana. The left three profiles show the stress distribution within the plate, with blue indicating regions of extensional stress and red indicating regions of compressional stress. On each profile, the distribution of extensional, strike-slip, and compressional earthquakes is shown by white diamonds, black crosses, and gray circles, respectively. The model parameters and misfits are noted on each stress distribution. The right two profiles shows the comparison between the profiles of the three models and the bathymetry data, with royal blue showing the best-fitting model, red showing a distinctly different solution with low misfit, and cyan showing another distinctly different solution with low misfit. The lower plot shows the whole modeled profile (0-600 km from the

trench), and the upper plot shows a close-up view of the profiles in the vicinity of the outer rise bulge.

Figure 12: Plot shows three distinct low misfit solutions for plate flexure at Central Mariana. The left three profiles show the stress distribution within the plate, with blue indicating regions of extensional stress and red indicating regions of compressional stress. On each profile, the distribution of extensional earthquakes is shown by white diamonds. The model parameters and misfits are noted on each stress distribution. The right two profiles shows the comparison between the profiles of the three models and the bathymetry data, with royal blue showing the best-fitting model, red showing a distinctly different solution with low misfit, and cyan showing another distinctly different solution with low misfit. The lower plot shows the whole modeled profile (0-600 km from the trench), and the upper plot shows a close-up view of the profiles in the vicinity of the outer rise bulge.

Figure 13: Histograms showing distribution of earthquakes at Central/Northern Mariana with depth. Left plot (red) indicates the number of events which occurred in the 0-4, 5-9, and 10-14 km depth range. Depths are given below the base of the crust (below the Moho). Right plot (blue) shows the cumulative seismic moment which occurred within the 0-4, 5-9, and 10-14 km depth ranges.

Table 1 – Previously studied Mariana outer rise Earthquakes

Date	Latitude	Longitude	Depth[a]	Type of Event	Magnitude	Reference
17 Jan 1940	17.24	148.12	n/a	Strike-slip	M 7.3	Okal et al, 2012
14 Jun 1942	14.53	147.92	n/a	Compression	M 7.0	Okal et al, 2012
4 July 1964	11.72	144.63	n/a	Tension	Mb 6.0	Katsumata and Sykes, 1969
27 Oct 1966	22.15	145.94	n/a	Tension	Mb 6.0	Katsumata and Sykes, 1969; Okal et al, 2012
5 Apr 1967	20.00	147.35	n/a	Tension	Mb 5.9	Katsumata and Sykes, 1969
1 Sept 1970	17.7	147.6	n/a	Tension	Mb 6.3	Chapple and Forsyth, 1979; Okal et al, 2012
11 May 1974	19.7	147.3	n/a	Tension	Mb 6.4	Chapple and Forsyth, 1979; Okal et al, 2012
5 Apr 1990	15.288	147.397	16	Tension	Ms 7.5	Yoshida et al, 1992
5 Apr 1990	15.125	147.596	23 ± 5	Tension	Mw 7.5	Zhang and Lay, 1992

[a]depth determined through waveform modeling

Table 2 – Velocity models used during inversion

Velocity Models					
Layer	Properties	Northern Mariana (20-21°N)	Central Mariana (17.5-18°N)	Central Mariana (15-17°N)	Southern Mariana (10-13°N)
Water	α = 1.5 km/s β = 0 km/s ρ = 1.0 g/cm^3	Thickness: 5-6 km	Thickness: 6-8 km	Thickness: 4-6 km	Thickness: 4-8 km
Sediment	α = 2.0 km/s β = 1.1 km/s ρ = 2.0 g/cm^3	Thickness: 0 km	Thickness: 0-1 km	Thickness: 0 km	Thickness: 0 km
Upper Crust	α = 5.2 km/s β = 3.0 km/s ρ = 2.6 g/cm^3	Thickness: 2 km	Thickness: 2 km	Thickness: 3 km	Thickness: 3 km
Lower Crust	α = 6.8 km/s β = 4.0 km/s ρ = 3.0 g/cm^3	Thickness: 3 km	Thickness: 3 km	Thickness: 4 km	Thickness: 4 km
Mantle	α = 8.0 km/s β = 4.5 km/s ρ = 3.3 g/cm^3	N/A	N/A	N/A	N/A

Table 3 –Best-fitting modeled focal mechanism vs. GCMT solution

Event #	Model Strike (°)	Model Dip (°)	Model Slip (°)	Model Moment (dyn-cm)	Model Depth (km)	GCMT Strike (°)	GCMT Dip (°)	GCMT Slip (°)	GCMT Moment (dyn-cm)	GCMT Depth (km)
1	8	66	154	4.99 E 24	5	12	60	146	4.74 E 24	12
2	142	24	76	2.49 E 24	7	140	33	68	1.96 E 24	12
3	111	58	61	2.56 E 24	34	116	64	67	2.21 E 24	31
4	277	86	1	3.75 E 25	12	99	77	8	3.17 E 25	13.7
5	319	43	-29	1.77 E 24	11	309	50	-25	1.34 E 24	12
6	68	41	-76	2.76 E 25	12	72	34	-80	1.93 E 25	15
7	22	72	164	3.55 E 24	24	27	83	178	4.95 E 24	28.2
8	197	32	156	2.19 E 24	31	180	24	138	2.43 E 24	40.5
9	20	37	97	1.79 E 24	34	4	27	82	1.83 E 24	42.9
10	189	45	-98	8.18 E 26	18	185	31	-108	1.63 E 27	15
11	18	49	-94	2.08 E 25	13	35	32	-50	2.33 E 25	15
12	185	52	-109	7.81 E 23	18	195	55	-67	4.74 E 23	41
13	36	42	-77	8.71 E 24	8	30	24	-85	7.52 E 24	15
14[a]	172	32	-123	7.25 E 23	13	172	32	-123	6.29 E 23	17.1
15	18	40	-57	4.52 E 23	9	11	42	-82	4.17 E 23	17.1
16	26	48	-67	3.70 E 25	10	8	39	-80	3.41 E 25	16
17	350	32	-83	2.41 E 24	11	347	19	-116	2.26 E 24	15
18	12	54	-30	1.46 E 24	9	16	55	-17	1.76 E 24	15
19	177	57	7	7.82 E 23	25	168	83	0	6.14 E 23	53.7
20	113	80	-75	2.27 E 25	49	124	80	-64	3.03 E 25	41.2

[a]GCMT double couple parameters were assumed due to lack in clear S phases in data.

Table 4 - Parameters assumed in flexure models

Initial depth – Southern Mariana (m)	5800
Initial depth – Northern Mariana (m)	5500
Model horizontal limit (km)	600
Model vertical limit (km)	100
Horizontal grid spacing (km)	0.856
Vertical grid spacing (km)	0.99
Water density (kg/m^3)	1013
Mantle density (kg/m^3)	3300
Time (Ma)	1.0
Time increment (Ma)	0.5
Thickness of the lithosphere - SS[a] (km)	95
Temperature at bottom of lithosphere – SS[a] (°C)	1450
Brittle failure slope - extension (β_{ext}) (MPa/km)	16
Brittle failure slope - compression (β_{comp}) (MPa/km)	-40
Power law Q_p (kJ/mol-K)	520
Power law ref. strain rate (s^{-1})	7.0×10^{-14}
Power law exponent	3
Dorn law Q_D (kJ/mol-K)	545
Dorn reference strain rate (s^{-1})	5.7×10^{11}
Peierls' stress (Pa)	8.5×10^9
Gas constant R (J/K·mol)	8.314
Strain rate (s^{-1})	1×10^{-16}

[a]reference Stein and Stein [1992]

Table 5 – Modeled Mariana Earthquakes (ordered by increasing latitude)

Event	Date	Time (UTC)	Latitude (°North)	Longitude (°East)	Depth[ab] (km)	Time Func. (sec)	Mw	Type of Event[c]	# P-data	# SH-data	Top freq. (Hz)	Misfit[d]
1	12 Nov 2007	00:25:45.76	10.4706	145.8160	5 ± 1	1	5.73	SS	23	19	0.5	0.4649
2	30 Sept 2007	15:02:18.09	10.5057	145.6567	7 ± 1	3	5.53	C	21	13	0.5	0.4019
3	31 Aug 2003	09:01:32.43	10.5619	146.5327	34 ± 2	1	5.54	C – SS	23	11	0.5	0.3149
4	10 July 2010	11:43:35.44	11.1146	146.1478	12 ± 1	2	6.32	SS	24	21	0.5	0.4707
5	4 May 2005	04:38:09.54	11.7264	143.8479	11 ± 1	1	5.43	SS	12	7	0.5	0.3620
6	19 Dec 2000	13:11:49.37	11.7616	144.8650	12 ± 2	7	6.23	T	25	11	0.5	0.4438
7	13 May 2004	17:34:36.88	11.7851	144.3199	24 ± 1	2	5.63	SS	19	16	0.2	0.3117
8	2 Apr 2001	06:50:04.93	11.9032	147.4938	31 ± 2	3	5.49	SS	12	22	0.5	0.2585
9	10 Nov 1997	19:04:23.69	12.3763	145.7198	34 ± 3	1	5.43	C	28	22	0.2	0.4963
10	5 Apr 1990	21:12:37.95	15.2195	147.6103	18 ± 2	5	7.21	T	9	11	0.5	0.2486
11	6 Apr 1990	14:57:21.23	15.2550	147.5977	13 ± 1	6	6.15	T	11	11	0.18	0.2799
12	4 Aug 2001	18:55:11.22	15.7843	147.4597	18 ± 1	3	5.20	T	6	8	0.18	0.3832
13	13 Oct 1990	00:20:22.19	15.7884	147.9803	8 ± 4	4	5.89	T	9	6	0.5	0.5212
14	10 Nov 1995	22:30:59.80	16.5791	148.1561	13 ± 3	1	5.17	T	12	2	0.2	0.3479
15	16 July 2008	17:23:44.20	16.8317	148.1483	9 ± 3	1	5.04	T -SS	7	8	0.18	0.4267
16	30 Aug 1998	01:48:09.84	17.0937	148.2210	10 ± 1	5	6.31	T	23	17	0.5	0.2796
17	4 May 2000	23:24:41.34	17.5084	147.6909	11 ± 2	1	5.52	T	11	14	0.5	0.2894
18	1 May 2003	00:14:09.47	17.7258	147.8452	9 ± 1	1	5.38	SS	17	9	0.2	0.3186
19	19 July 2000	14:28:38.97	20.5277	147.4411	25 ± 1	2	5.20	SS	4	5	0.2	0.3700
20	14 Feb 2006	15:27:24.95	20.8419	146.2316	49 ± 2	4	6.17	T	32	18	0.5	0.5338

[a]Denotes depth beneath seafloor (depth within plate)

[b]Depth error calculated as depth which misfit is 5% more than the best-fitting solution –not including errors in velocity model.

[c]SS – strike-slip; C –compression; T –extension

[d]Misfit is calculated according to equations (1) and (2)

Figures

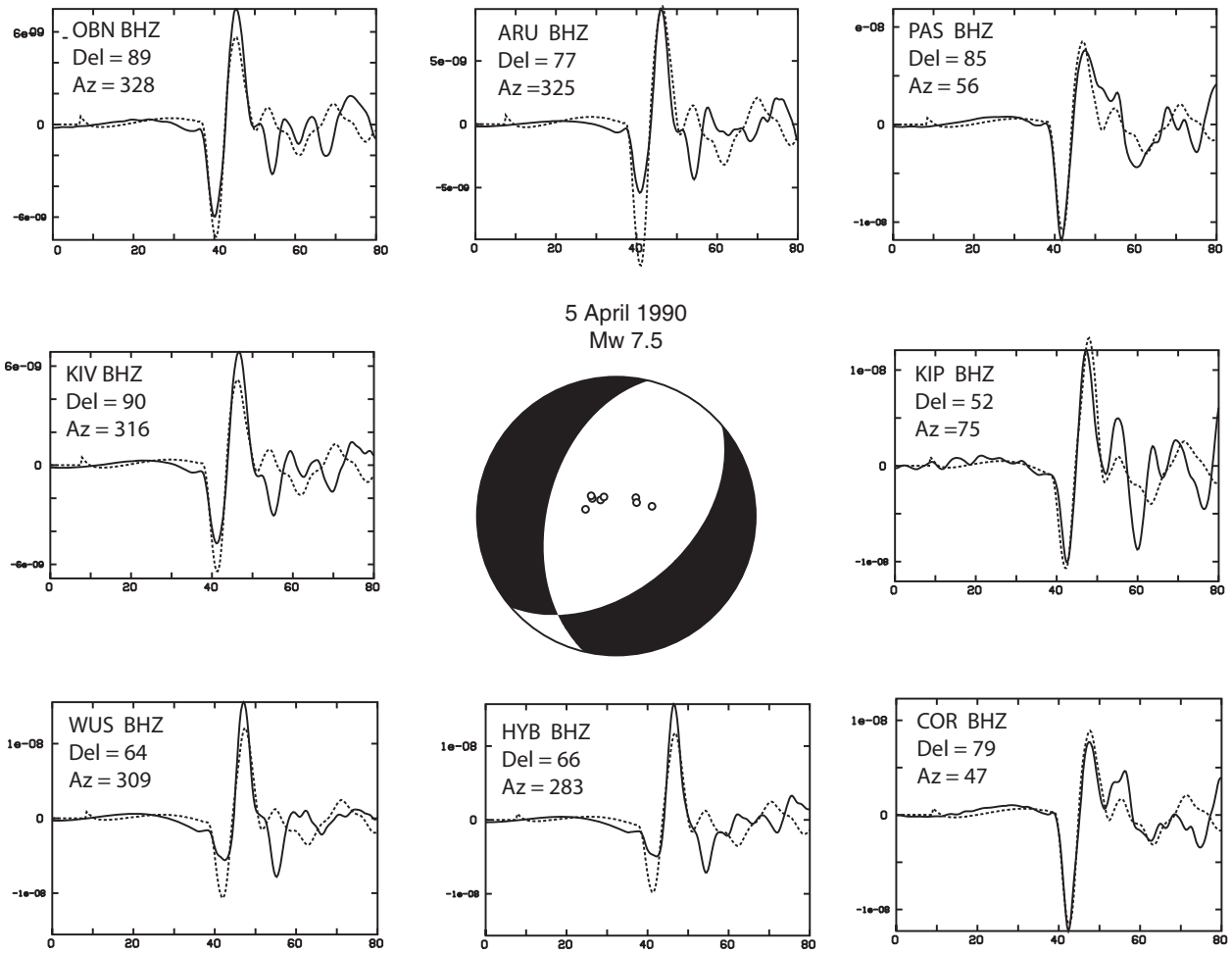

Figure 1 -

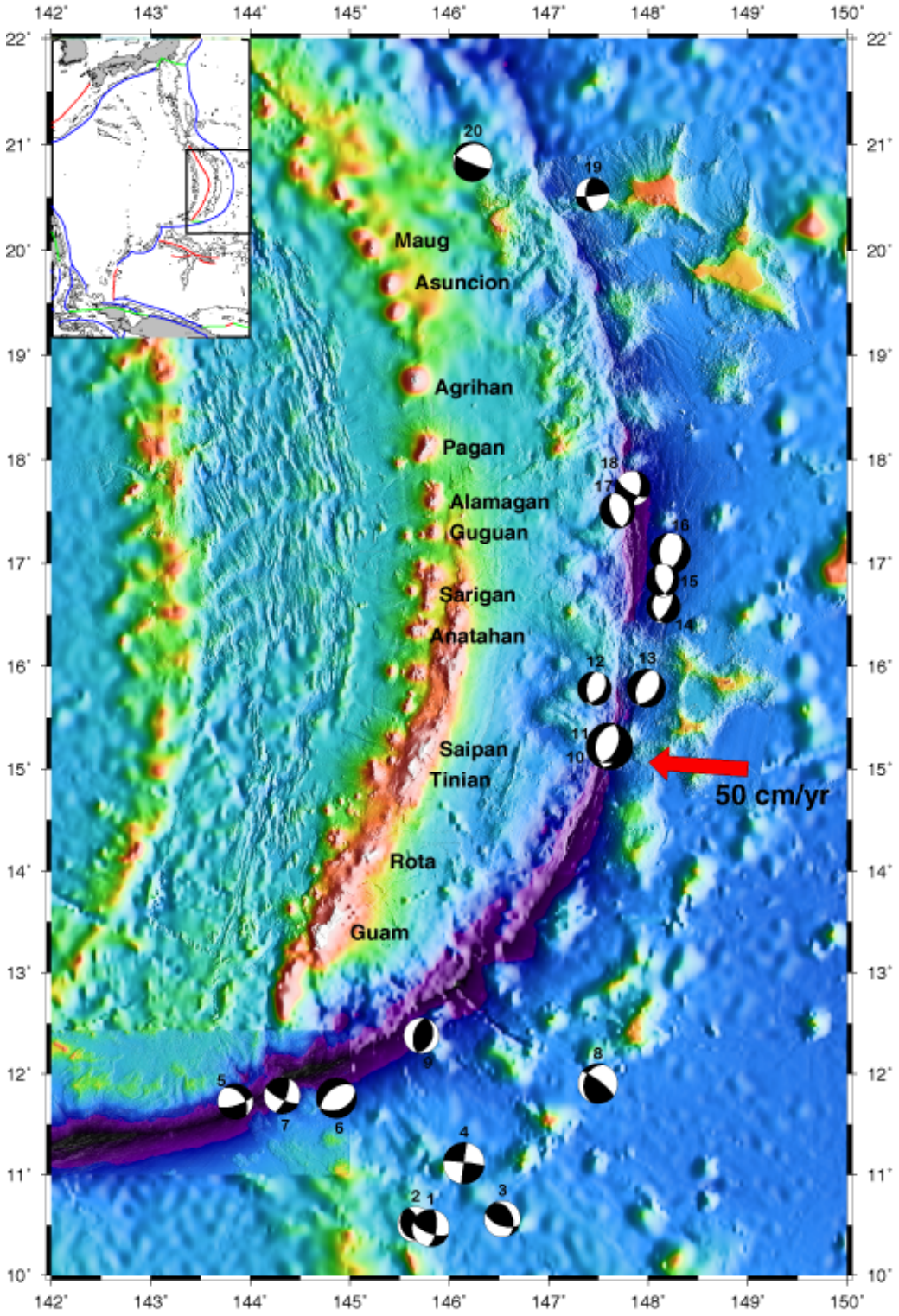

Figure 2 – Map of Modeled Mariana Trench Seismicity

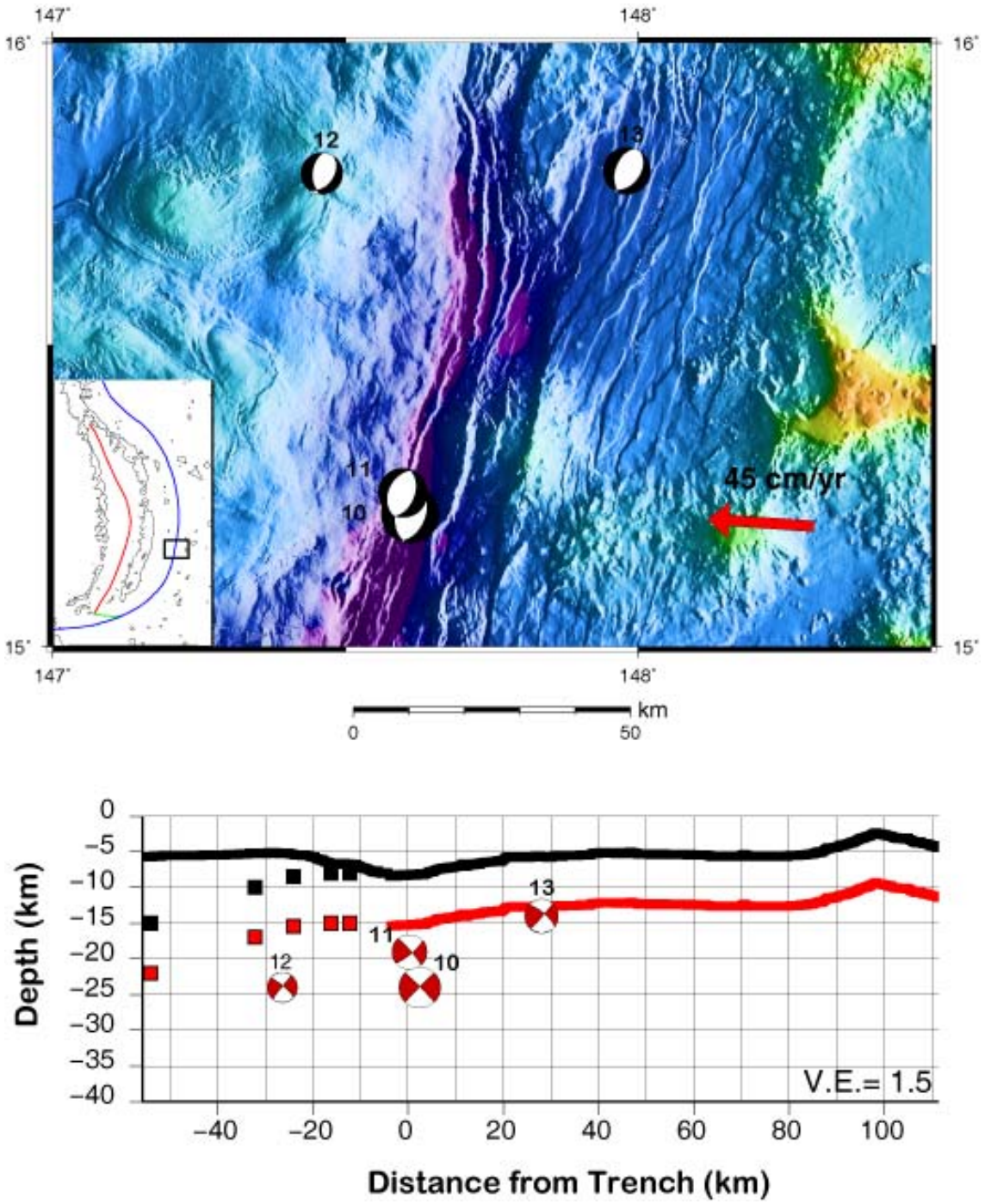

Figure 3: Central Mariana near 15°N: Map and Cross-Section

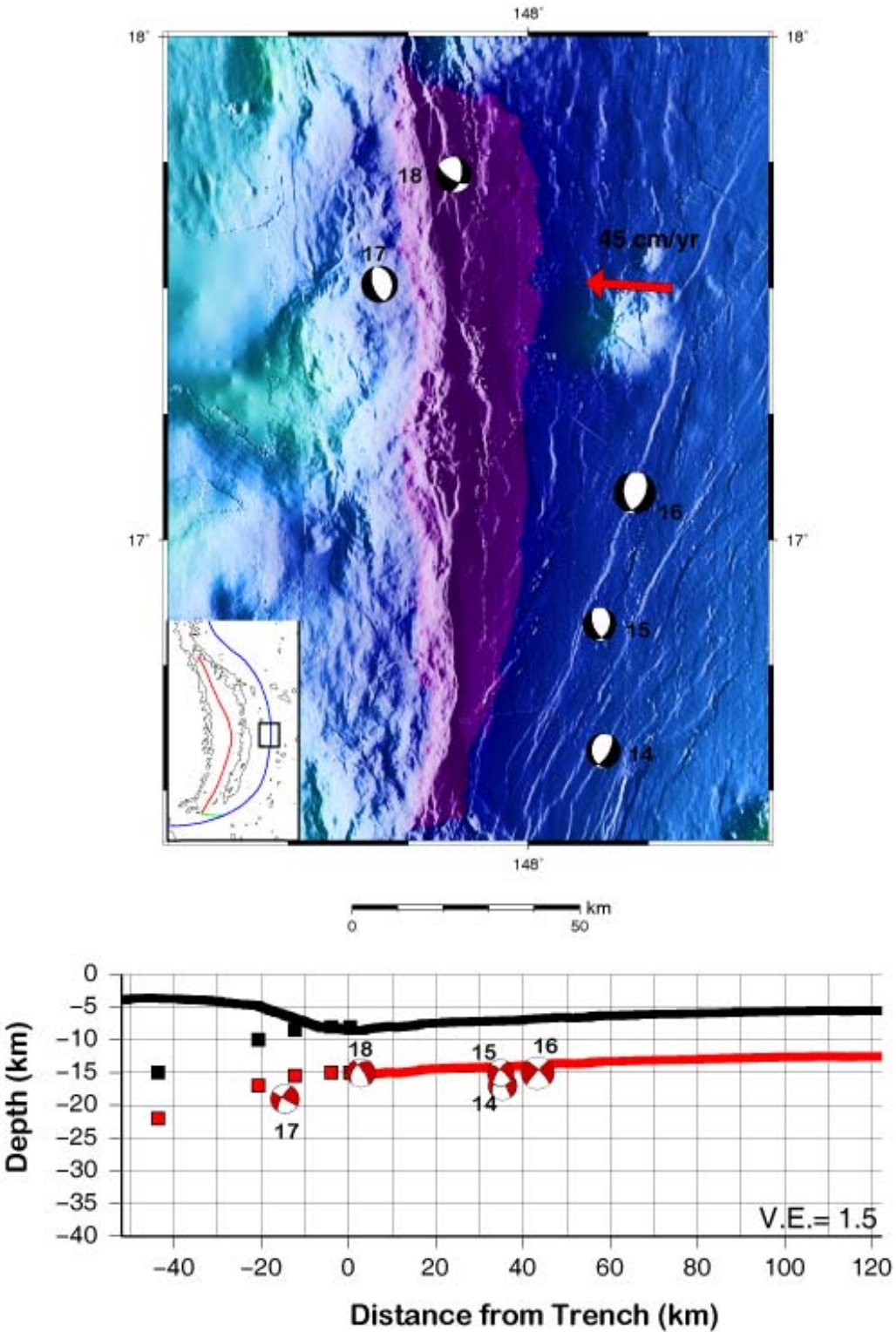

Figure 4 – Central Mariana near 17°N: Map and Cross-Section

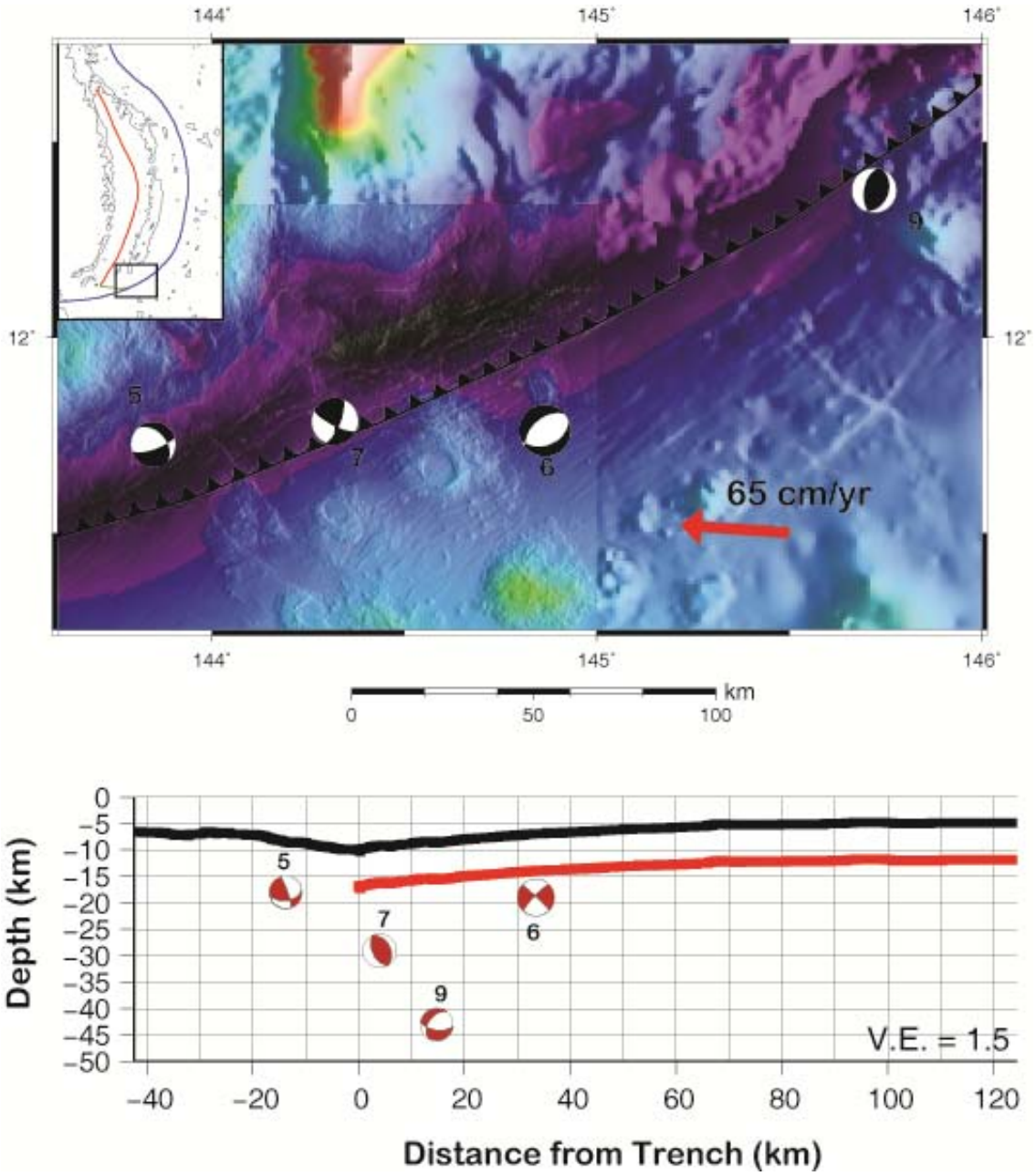

Figure 5 – Southern Mariana: Map and Cross-Section

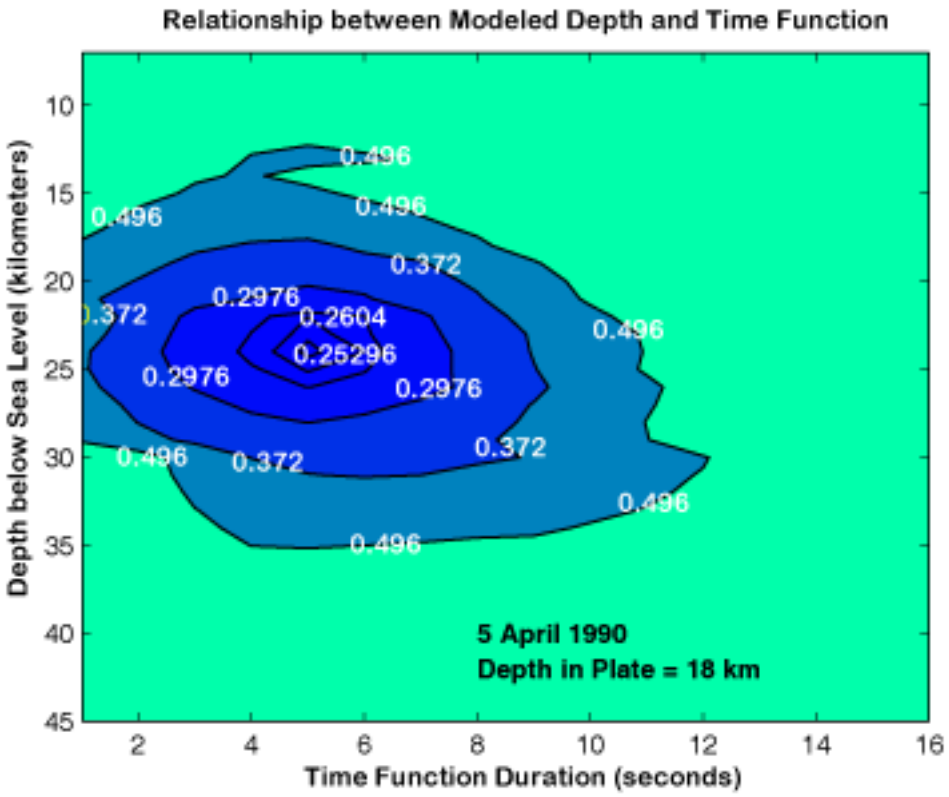

Figure 6 – Error Contours of the 5 April 1990 Mariana Earthquake

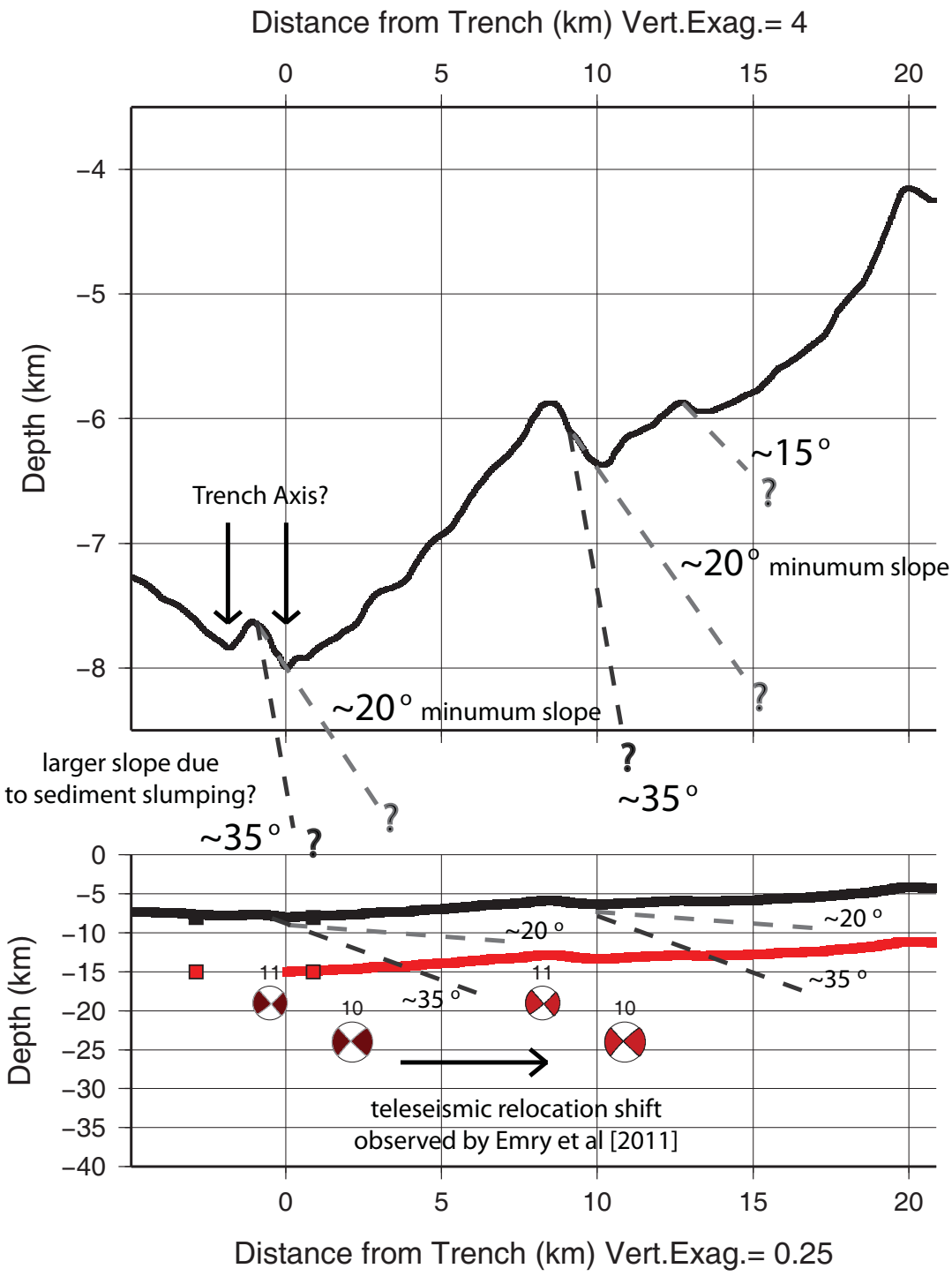

Figure 7 – Magnified Cross-Section and Modeled Earthquakes near 15°N

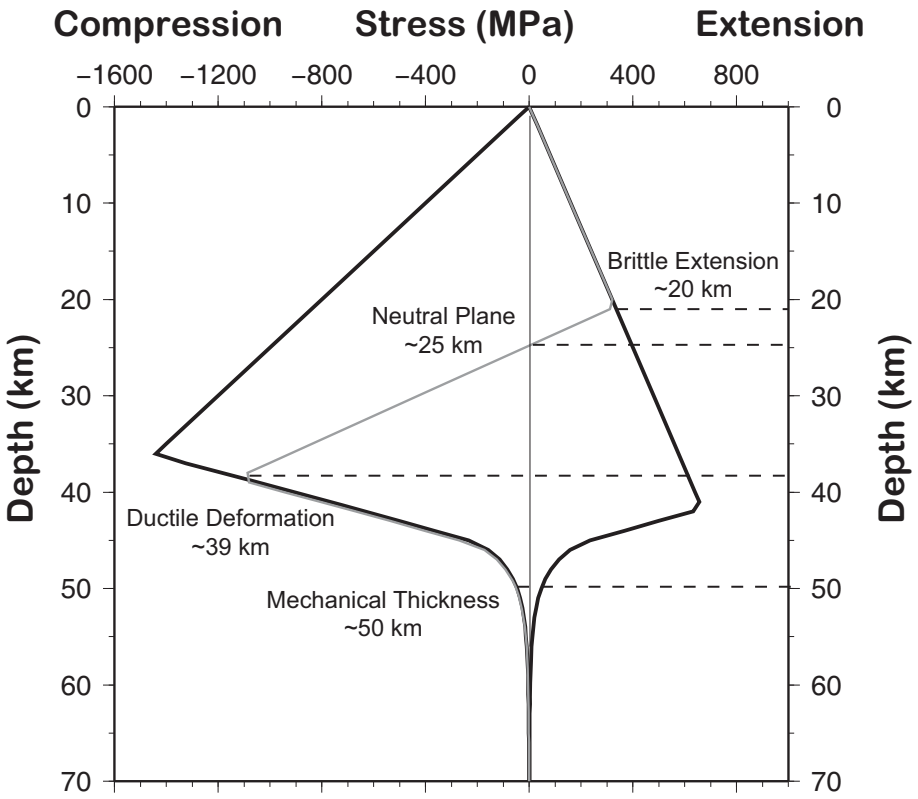

Figure 8 – Example Yield Stress Envelope: Southern Mariana

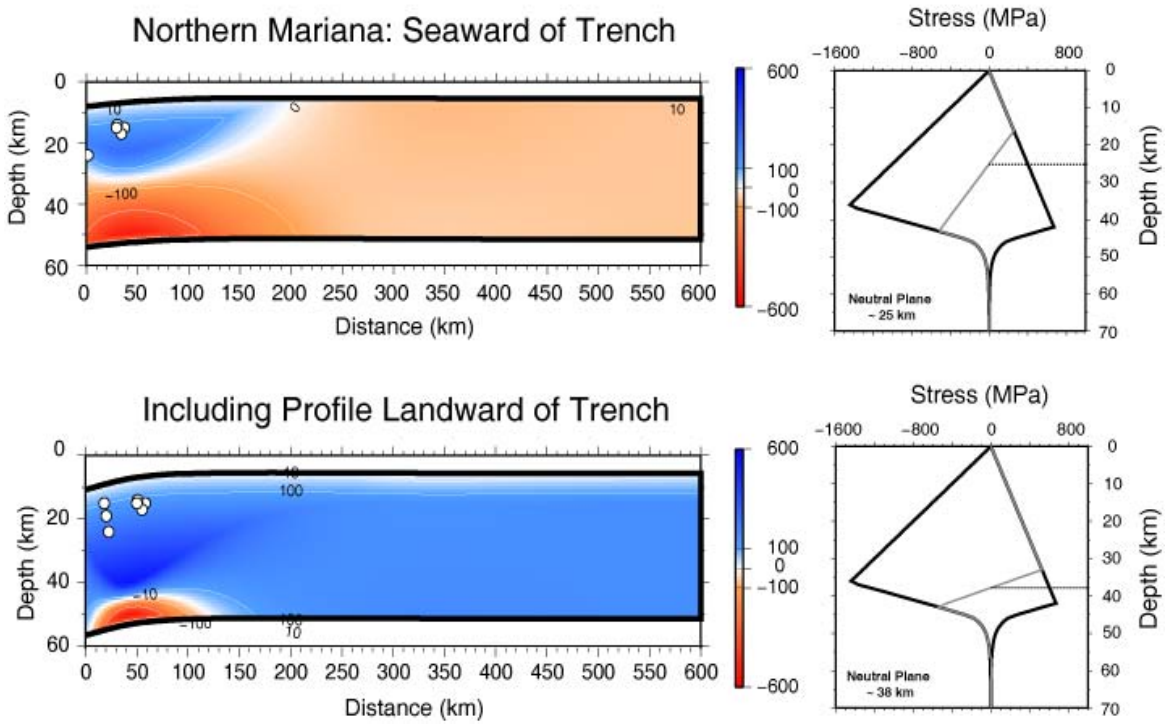

Figure 9 – Stress Distribution at Northern Mariana

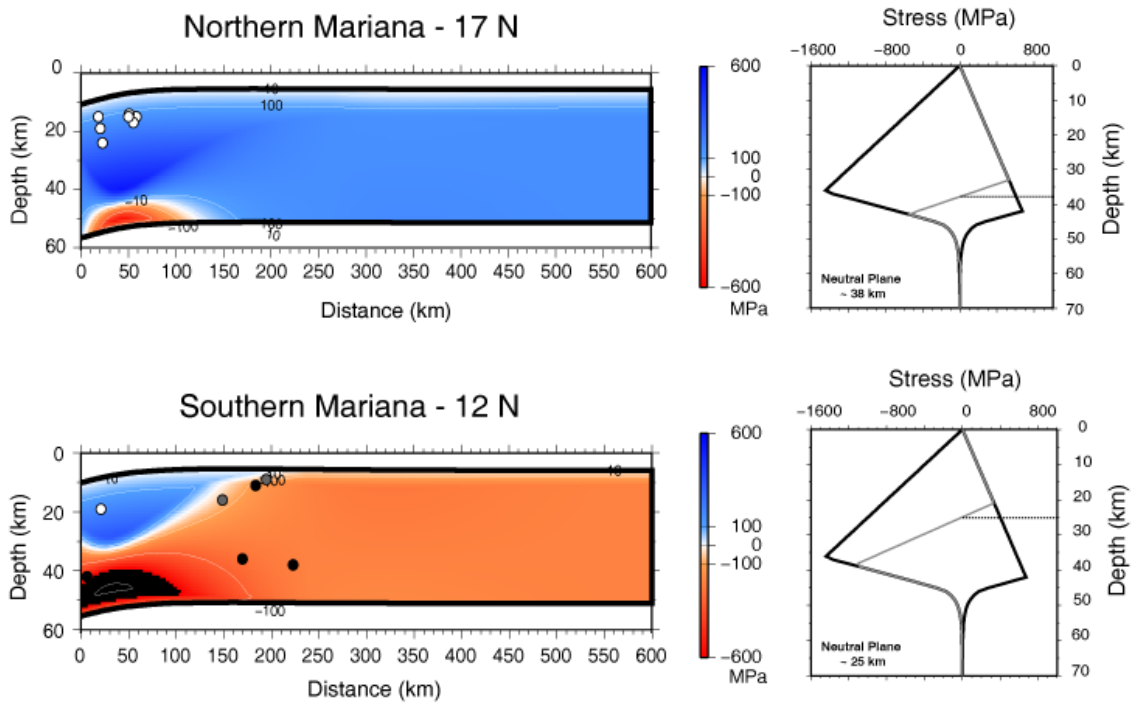

Figure 10 – Stress Distribution at Southern Mariana

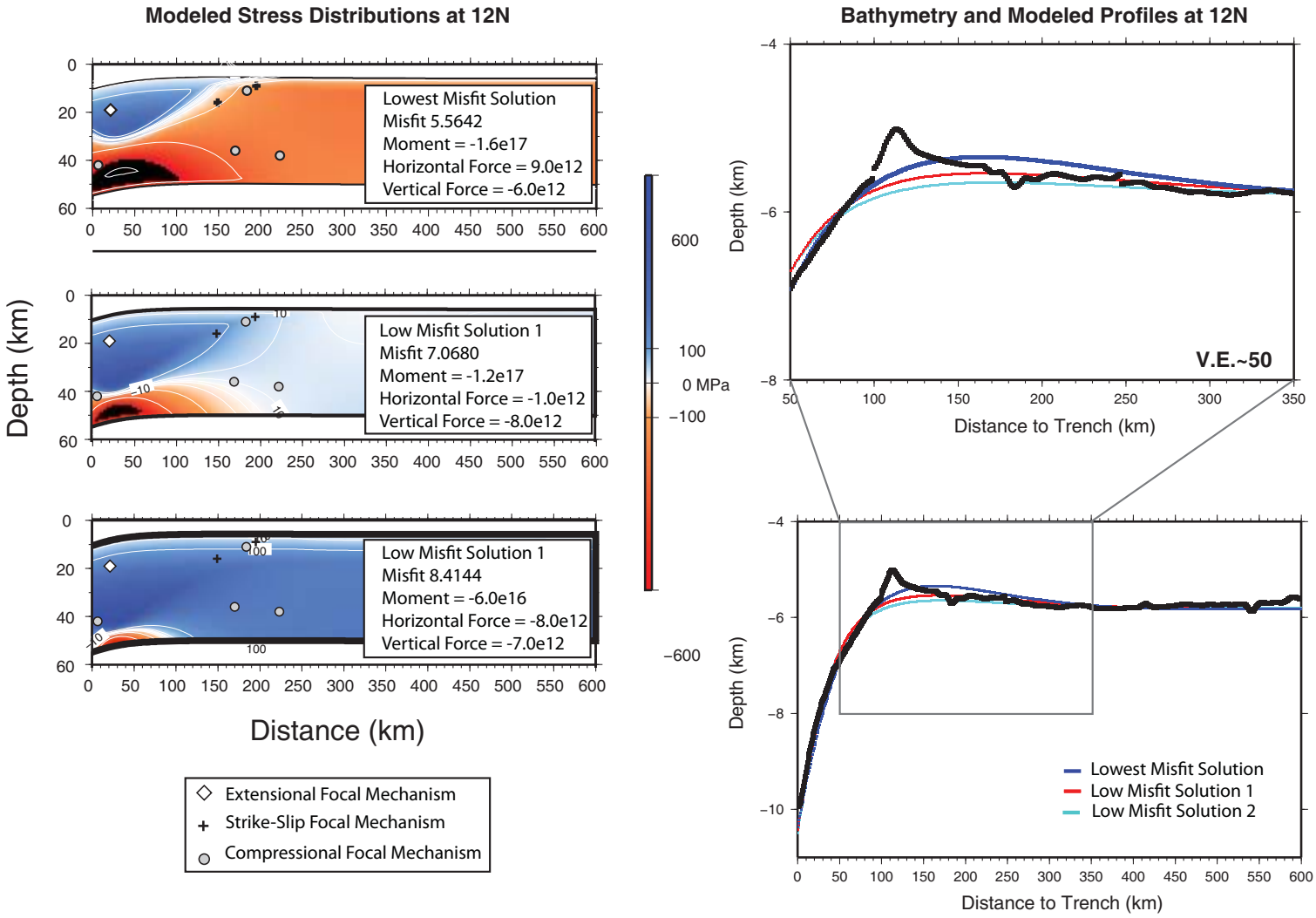

Figure 11 - Low misfit flexure model solutions at Southern Mariana

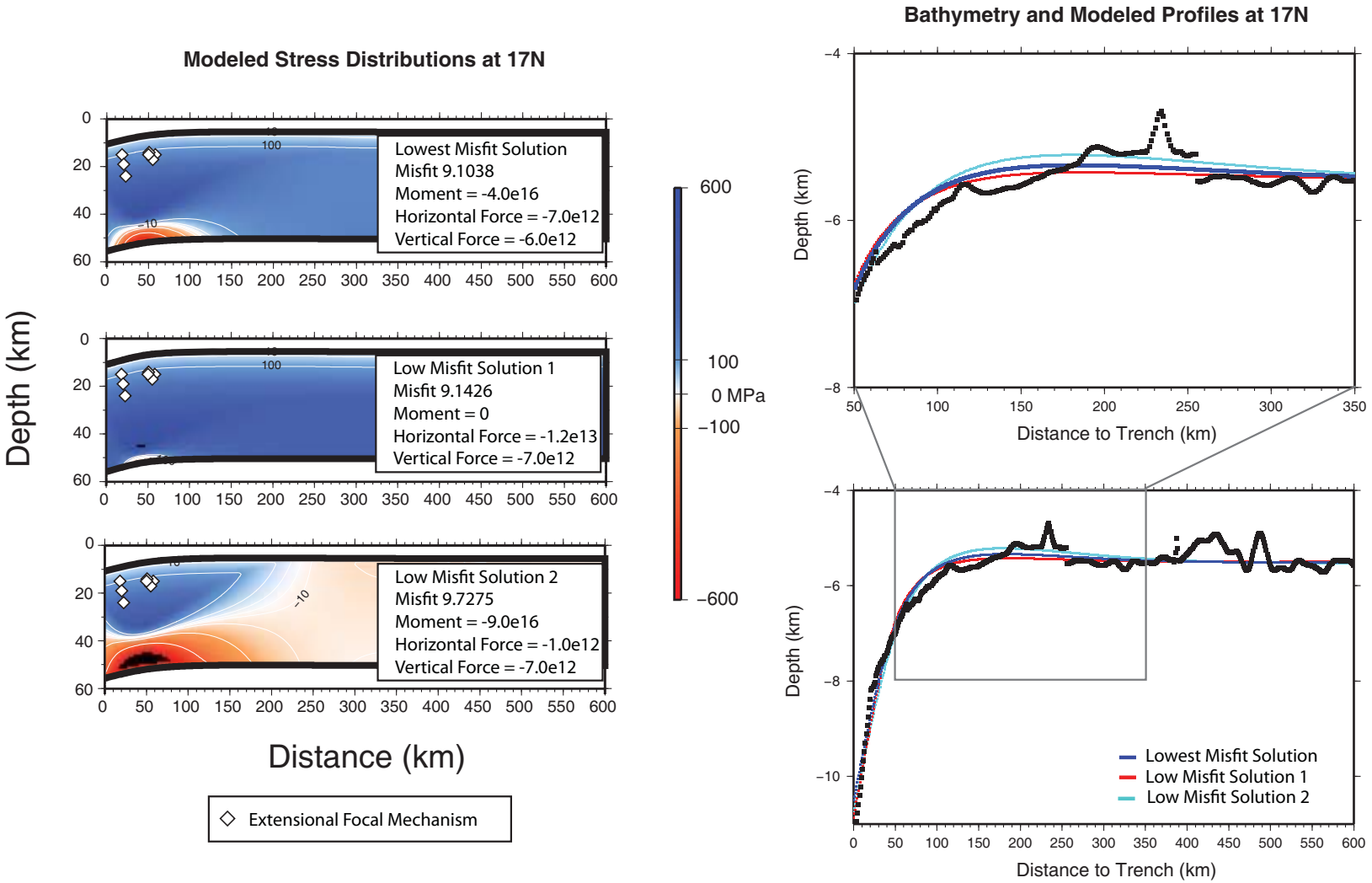

Figure 12 - Low misfit flexure model solutions at Northern Mariana

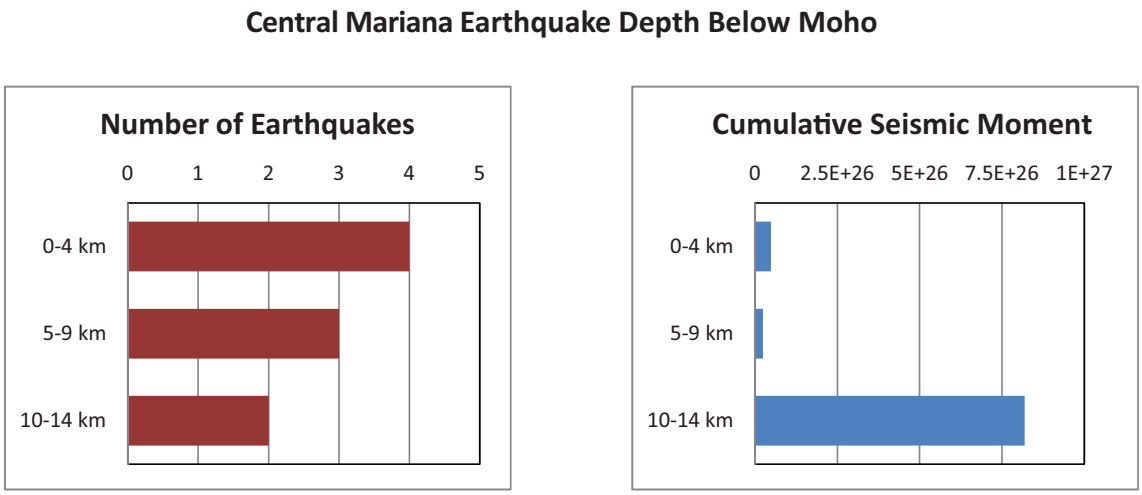

Figure 13 - Depth of Extensional Earthquakes in Mantle: Histogram

Appendix A – Data sources

Table A1 – Seismic Networks Used

Network Code	Network Name	Number of Stations Used
BK	Berkeley Digital Seismograph Network	1
CD	China Digital Seismograph Network	2
CI	Southern California Seismic Network (SCSN) Caltech/USGS	1
G	GEOSCOPE (IPGP)	2
HK	Hong Kong Seismograph Network	1
IC	New China Digital Seismograph Network	10
II	Global Seismograph Network (GSN)	22
IU	Global Seismograph Network (GSN)	32
TS	TERRAscope (SCSN)	2

Table A2 – Seismic Stations Used

Station Code	**Network Code**	**Location**	**Event Numbers**
AAK	II	Ala Archa, Kyrgyzstan	1,6, 7, 8, 9, 14, 16, 17, 18
ABKT	II	Alibek, Turkmenistan	2, 3, 6, 7, 8, 14, 20
ADK	IU	Adak, Aleutian Islands, Alaska	16
ALE	II	Alert, Northwest Territories, Canada	3, 4, 5, 6, 7
ARU	II	Arti, Russia	2, 3, 4, 6, 7, 9, 10, 11, 16, 17, 18, 20
BILL	IU	Bilibino, Russia	1, 2, 3, 6, 7, 9, 12, 16, 17, 20
BJI	CD	Baijiatuan, Beijing, China	10
BJT	IC	Baijiatuan, Beijing, China	1, 2, 3, 4, 6, 7, 8, 9, 14, 15, 16, 17, 18, 20
BRVK	II	Borovoye, Kazakhstan	1, 2, 3, 4, 6, 7, 9, 12, 14, 16, 17, 18, 19, 20
CASY	IU	Casey, Antarctica	1, 2, 4, 9
CHTO	IU	Chiang Mai, Thailand	1, 2, 3, 4, 6, 8, 9, 14, 16, 17, 18, 19
CMB	BK	Columbia College, California, USA	4, 9, 16
COCO	II	West Island, Cocos (Keeling) Islands	6, 20

COL	IU	College Outpost, Alaska, USA	11
COLA	IU	College Outpost, Alaska, USA	1, 3, 4, 5, 16, 18, 20
COR	IU	Corvallis, Oregon, USA	4, 7, 10, 11, 16, 20
CTAO	IU	Charters Towers, Australia	4, 6, 9, 11, 18, 20
ENH	IC	Enshi, Hubei Province, China	3, 5, 7, 8, 9, 15, 16, 20
ERM	II	Erimo, Hokkaido Island, Japan	3, 4, 13, 15
FFC	II	Flin Flon, Canada	16, 18, 20
GAR	II	Garm, Tajikistan	10, 11, 13,
GNI	IU	Garni, Armenia	20
GSC	TS	Goldstone, California, USA	13
HIA	IC	Hailar, Neimenggu Province, China	1, 2, 3, 4, 7, 9, 10, 11, 14, 15, 16, 17, 18, 19, 20
HKPS	HK	Hong Kong Island	4
HNR	IU	Honiara, Solomon Islands	20
HYB	G	Hyderabad, India	10, 11, 13
INCN	IU	Inchon, Korea	2, 3, 4, 6, 9, 15
KAPI	II	Kappang, Sulawesi, Indonesia	2, 6, 8
KBL	IU	Kabul, Afghanistan	4
KBS	IU	Ny-Alesund, Spitzbergen, Norway	7, 9, 16
KDAK	II	Kodiak Island, Alaska, USA	4, 5, 7, 16, 18, 20
KEV	IU	Kevo, Finland	7, 9, 10, 11, 15
KIP	IU	Kipapa, Hawaii, USA	10
KIV	II	Kislovodsk, Russia	10, 11, 17
KMI	IC	Kunming, Yunnan Province, China	1, 2, 3, 4, 5, 7, 8, 9, 13, 15, 16, 18, 20
KURK	II	Kurchatov, Kazakhstan	1, 2, 4, 6, 7, 9, 12, 14, 15, 18, 19, 20
LSA	IC	Lhasa, Tibet Province, China	1, 2, 3, 4, 5, 7, 8, 9, 14, 16, 18, 19, 20
LVZ	II	Lovozero, Russia	1, 4, 9, 17, 20
LZH	CD	Lanzhou, Gansu Province, China	10, 11
MA2	IU	Magadan, Russian	6, 8, 9, 12, 16, 17, 20
MAJO	IU	Matsushiro, Japan	13
MAKZ	IU	Makanchi, Kazakhstan	6, 8, 9, 17
MBWA	IU	Marble Bar, Western Australia	2, 20
MDJ	IC	Mudanjiang, Heilongjiang Province, China	1, 2, 3, 4, 5, 8, 9, 12, 15, 16, 17
MSVF	II	Monasavu, Fiji	4
NIL	II	Nilore, Pakistan	5, 6, 8, 9, 14, 16, 18, 20
NRIL	II	Norilsk, Russia	9
NWAO	IU	Narrogin, Australia	20
OBN	II	Obninsk, Russia	10, 11, 17, 20
PALK	II	Pallekele, Sri Lanka	5, 6, 8, 20

PAS	TS	Pasadena, California, USA	10, 13
PASC	CI	Pasadena, California, USA	4
PET	IU	Petropavlovsk, Russia	4, 17, 20
PFO	II	Pinon Flat, California, USA	4, 16, 20
PMG	IU	Port Moresby, Papua New Guinea	20
POHA	IU	Pohakaloa, Hawaii, USA	4
QIZ	IC	Qeongzhong, Guangduong Province, China	1, 3, 4, 5, 7, 8, 18, 20
RSSD	IU	Black Hills, South Dakota, USA	20
SEY	G	Seymchan, Russia	13
SSE	IC	Sheshan, Shanghai, China	1, 3, 4, 8
SNZO	IU	South Karori, New Zealand	6, 20
TATO	IU	Taipei, Taiwan	15
TIXI	IU	Tiksi, Russia	1, 3, 6, 7, 8, 18
TLY	II	Talaya, Russia	1, 2, 3, 4, 6, 7, 8, 14, 15, 17, 18, 19
TUC	IU	Tucson, Arizona, USA	20
ULN	IU	Ulaanbaatar, Mongolia	1, 2, 6, 7, 8, 9, 15, 16, 17, 18, 19, 20
WMQ	IC	Urumqi, Xinjiang, China	1, 2, 3, 5, 6, 7, 8, 9, 10, 11, 12, 14, 16, 18, 20
WRAB	II	Tennant Creek, NT, Australia	2, 4, 8, 9, 16, 20
WUS	G	Wushi, Xinjiang Uygur, China	10, 11, 13
XAN	IC	Xi’an, China	1, 2, 3, 5, 6, 7, 8, 9, 14, 16, 18, 20
XMAS	IU	Kiritimati Island, Republic of Kiribati	4
YAK	IU	Yakutsk, Russia	1, 2, 3, 4, 6, 7, 8, 9, 12, 15, 16, 17, 20
YSS	IU	Yuzhno Sakhalinsk, Russia	2, 3, 4, 6, 7, 8, 9, 12

Appendix B – Misfit Contours of Earthquake Source and Fault Parameters

The following plots (Figures B1-B19) show contours of synthetic-to-data misfits. The plotted contours represent misfit-to-data that are 2%, 5%, 10%, 20%, and 50% greater than the best-fitting depth and source time function value assuming a constant strike, dip, and slip corresponding to the best-fitting parameters determined in the inversion. Values for the best-fitting strike, dip, and slip as well as the event moment magnitude are denoted beneath each error contour. The depth errors listed in Table 2 in the main text of Chapter 2 correspond the greatest difference between the best-fitting solution and the +5% contour at the best-fitting source time function. Error contours generally reflect the quality of the waveform data as well as the azimuthal coverage of the station distribution.

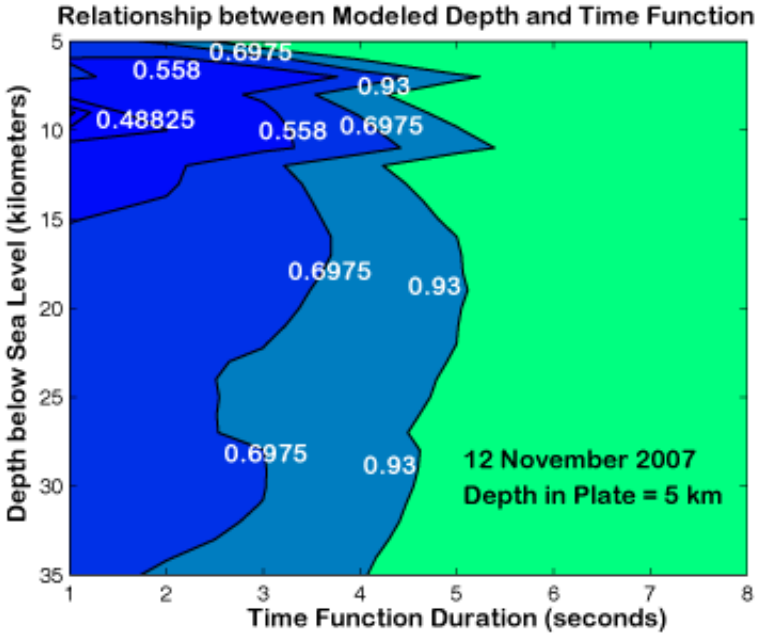

Figure B1 – Event 1, 12 November 2007
Strike: 8° Dip:66° Slip:154° Magnitude: 5.73 Mw

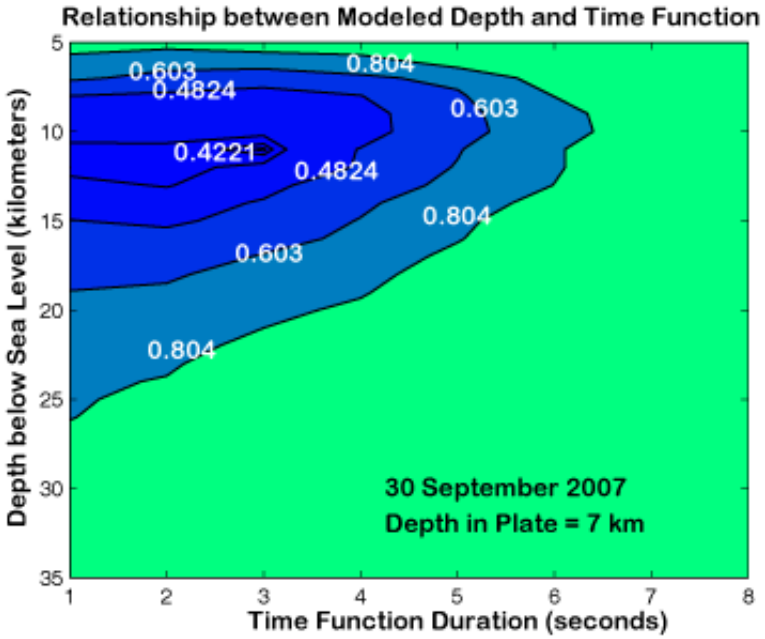

Figure B2 – Event 2, 30 September 2007
Strike:142° Dip:24° Slip:76° Magnitude: 5.53 Mw

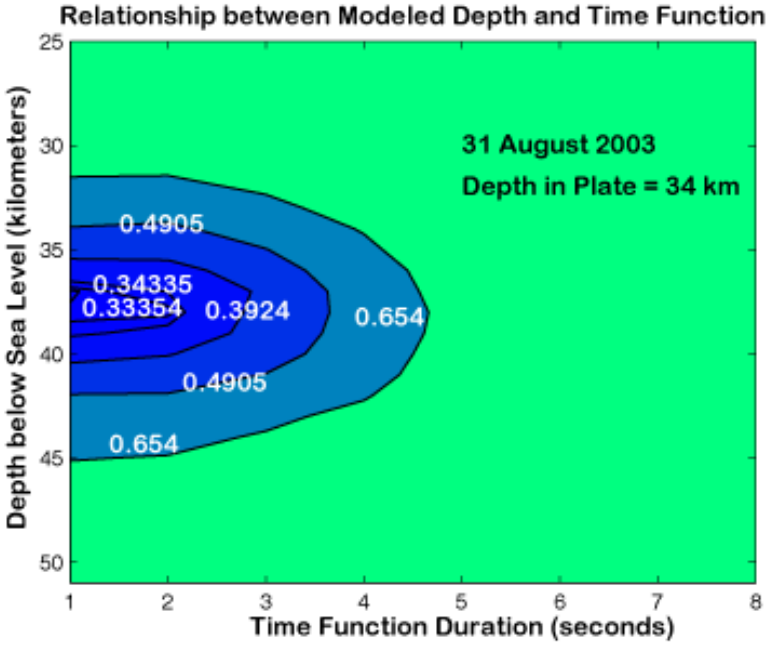

Figure B3 – Event 3, 31 August 2003
Strike: 111° Dip: 58° Slip: 61° Magnitude: 5.54 Mw

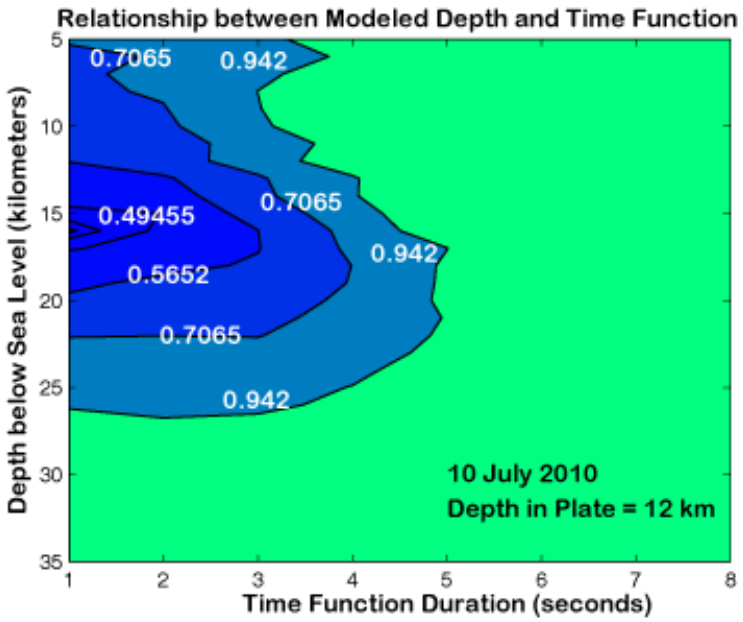

Event B4 – Event 4, 10 July 2010
Strike: 277° Dip: 86° Slip: 1° Magnitude: 6.32

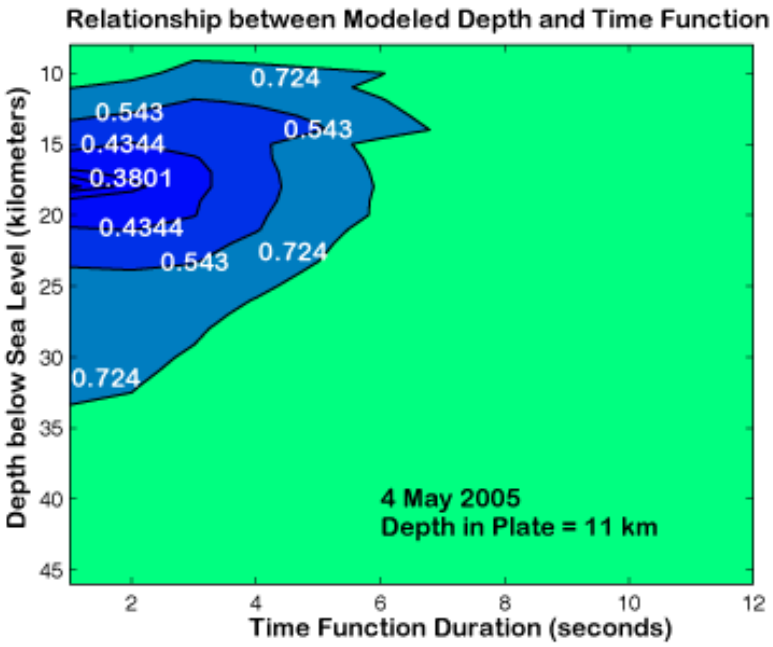

Figure B5 – Event 5, 4 May 2005
Strike: 319° Dip: 43° Slip: -29° Magnitude: 5.43

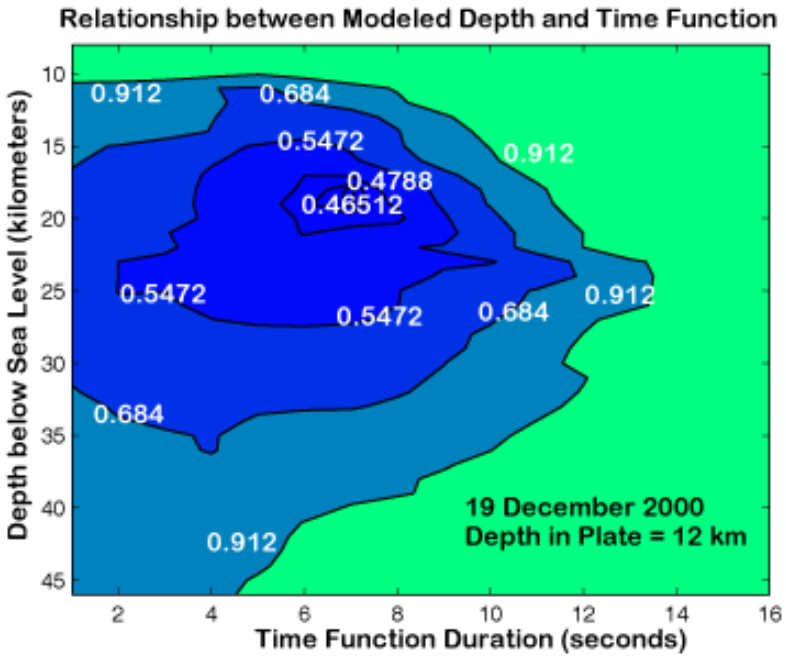

Figure B6 – Event 6, 19 December 2000
Strike: 68° Dip: 41° Slip: -76° Magnitude: 6.23 Mw

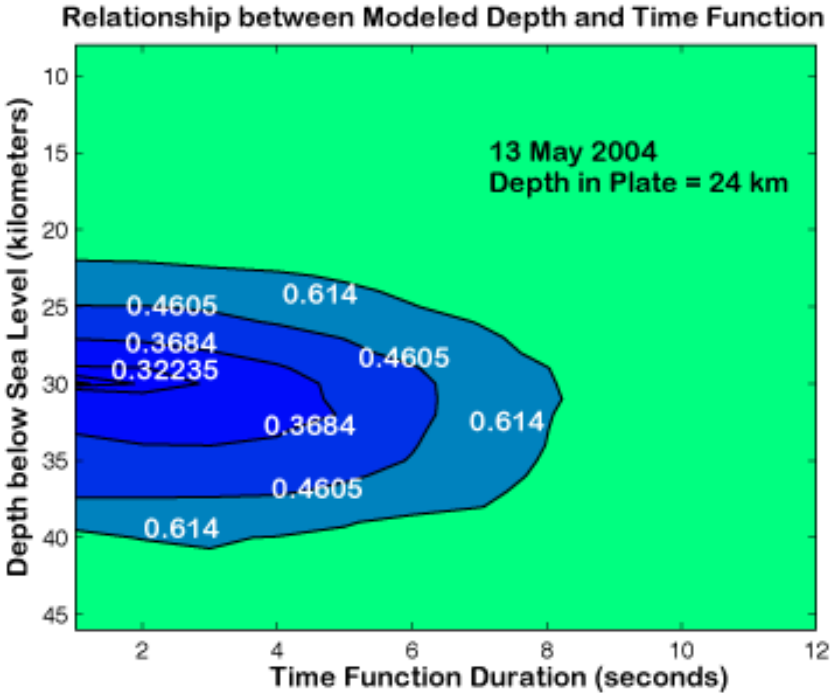

Figure B7 – Event 7, 13 May 2004
Strike: 22° Dip: 72° Slip: 164° Magnitude: 5.63 Mw

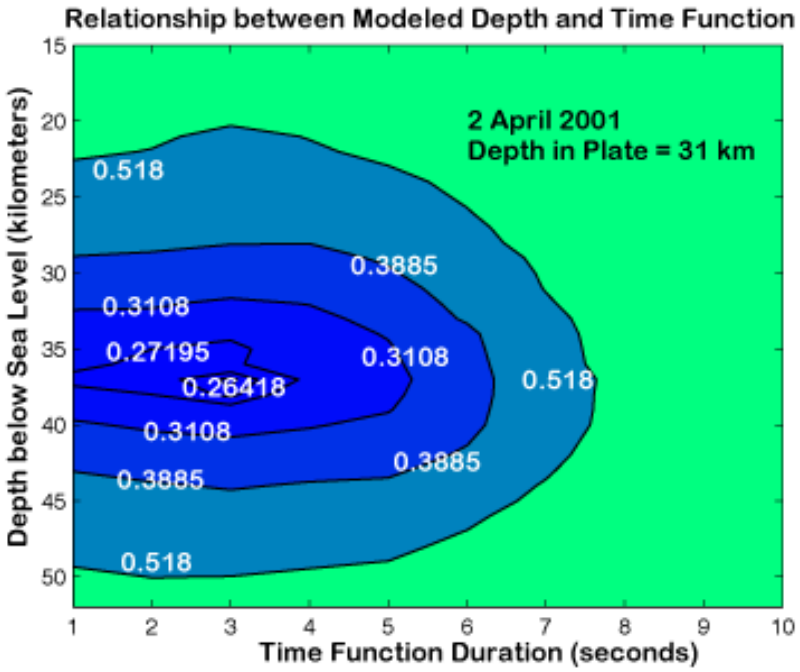

Figure B8 – Event 8, 2 April 2001
Strike: 197° Dip: 32° Slip: 156° Magnitude: 6.16 Mw

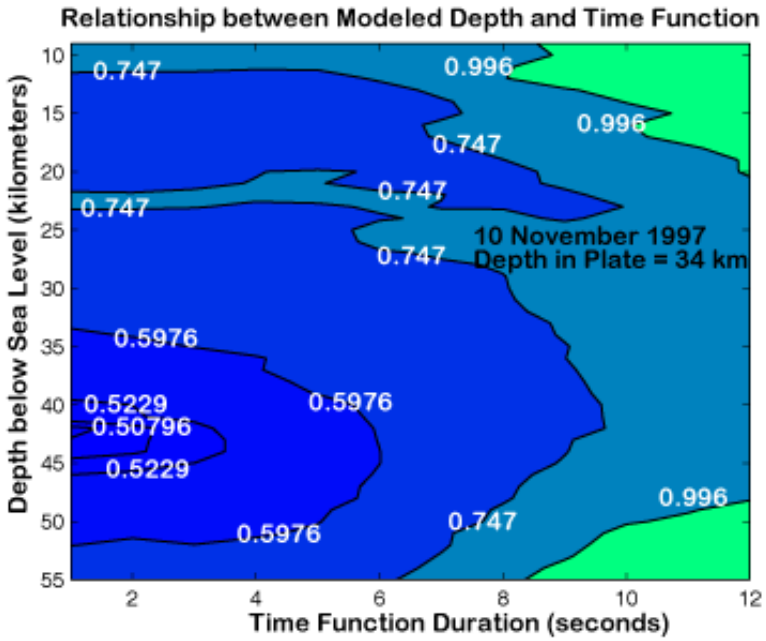

Figure B9 – Event 9, 10 November 1997
Strike: 20° Dip: 37° Slip: 97° Magnitude: 5.43 Mw

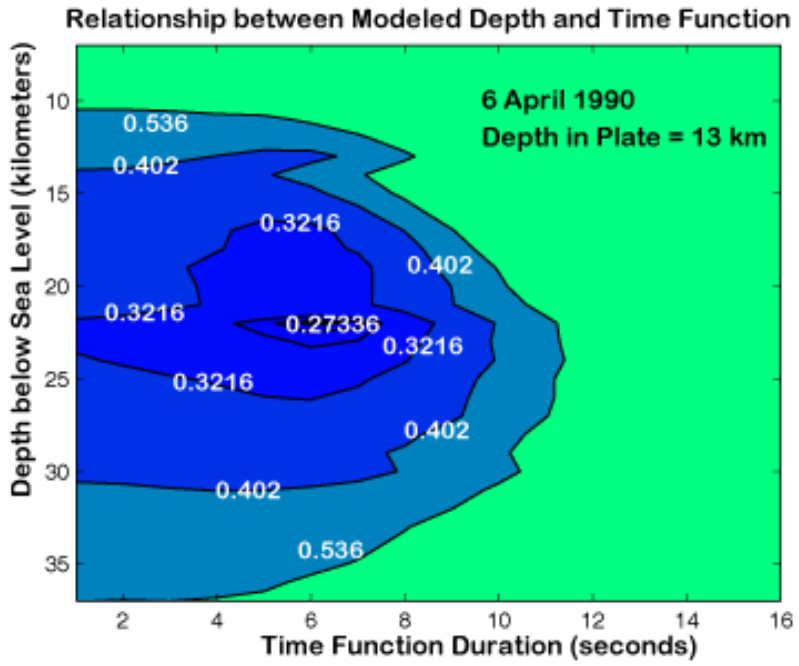

Figure B10 – Event 11, 6 April 1990
Strike: 18° Dip: 49° Slip: -94° Magnitude: 6.15 Mw

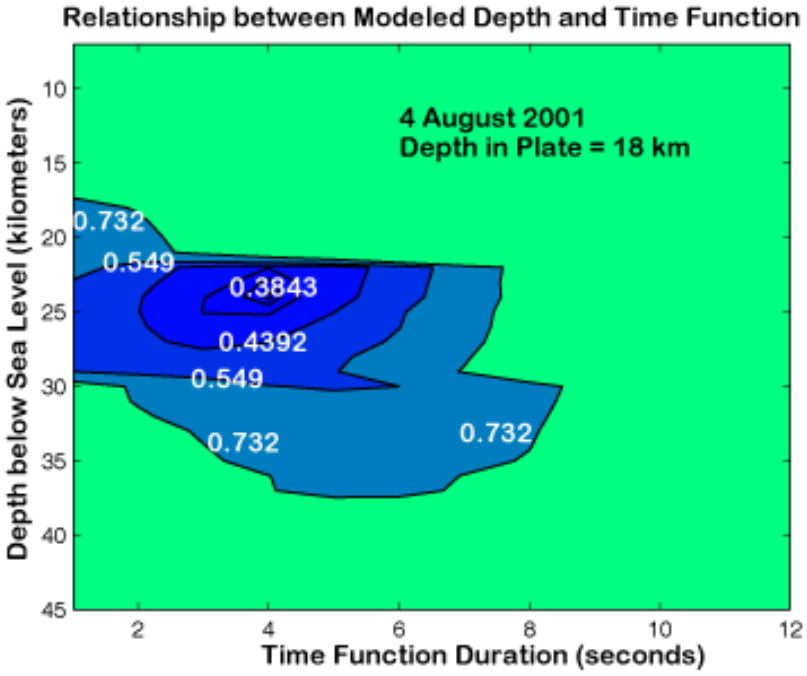

Figure B11 – Event 12, 4 August 1990
Strike: 185° Dip: 52° Slip: -109° Magnitude: 5.20 Mw

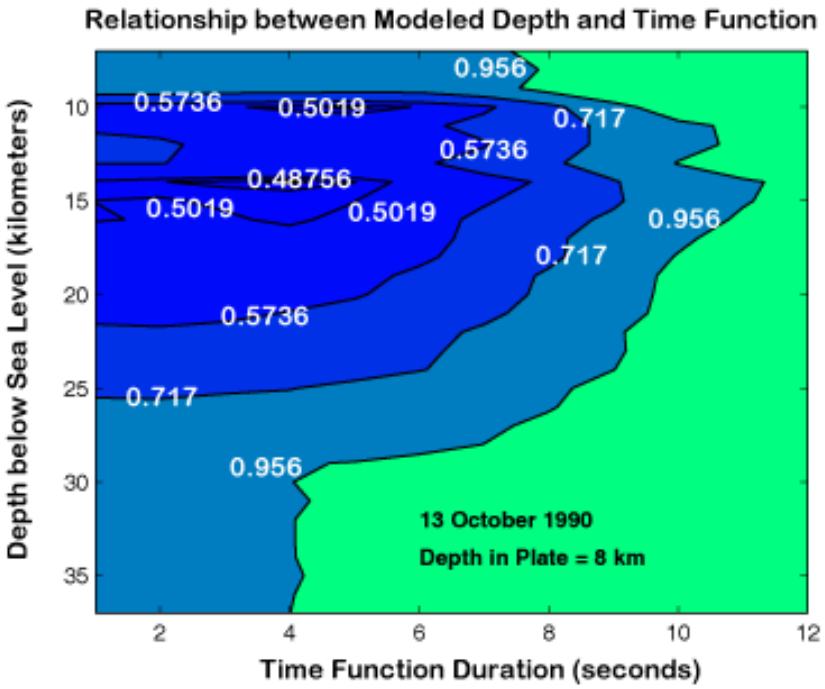

Figure B12 – Event 13, 13 October 1990
Strike: 36° Dip: 42° Slip: -77° Magnitude: 5.89 Mw

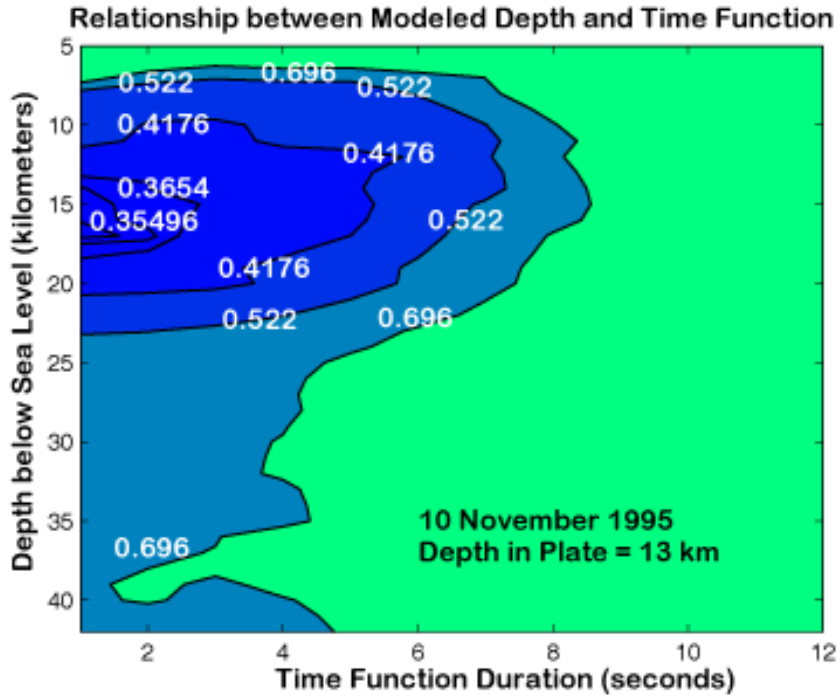

Figure B13 – Event 14, 10 November 1995
Strike: 172° Dip: 32° Slip: -123° Magnitude: 5.17 Mw

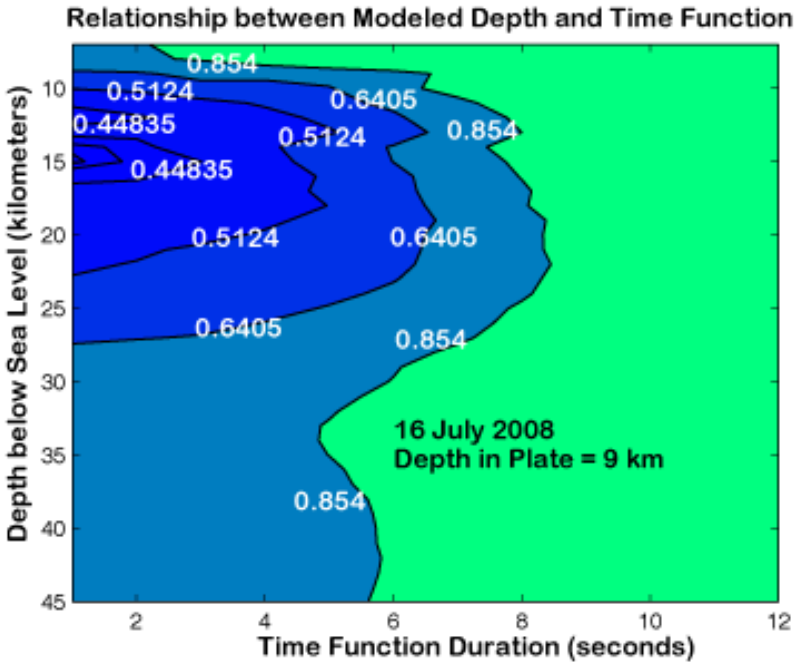

Figure B14 – Event 15, 16 July 2008
Strike: 18° Dip: 40° Slip: -57° Magnitude: 5.04 Mw

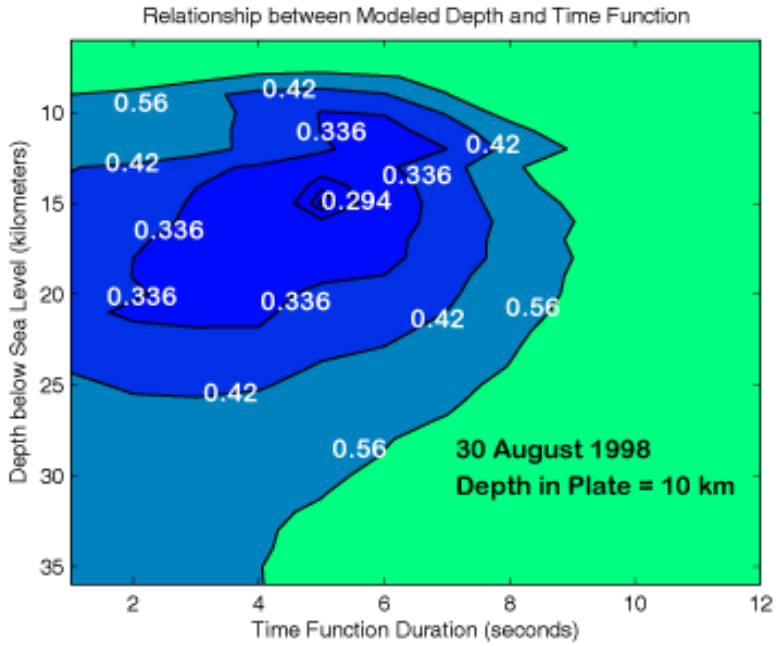

Figure B15– Event 16, 30 August 1998
Strike: 26° Dip: 48° Slip: -67° Magnitude: 6.31 Mw

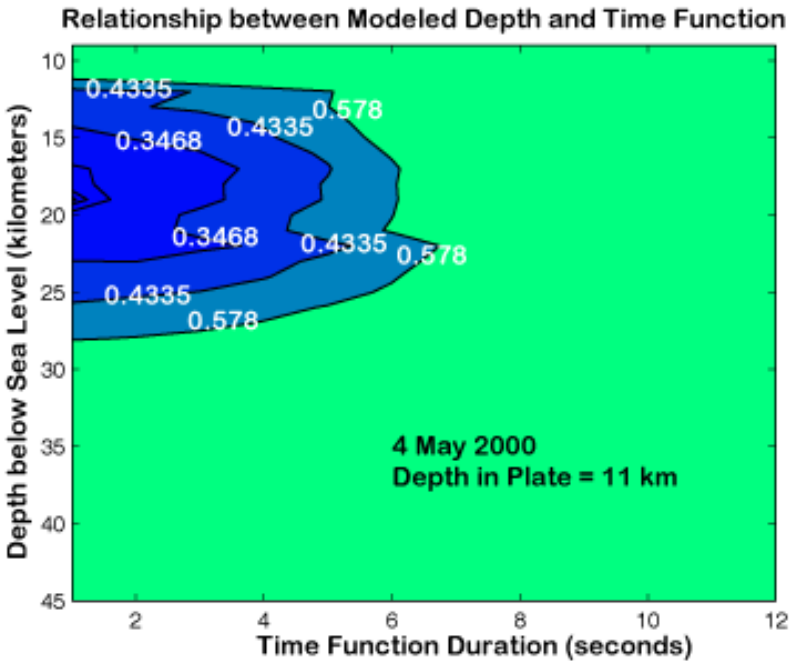

Figure B16 – Event 17, 4 May 2000
Strike: -10° Dip: 32° Slip: -83° Magnitude: 5.52 Mw

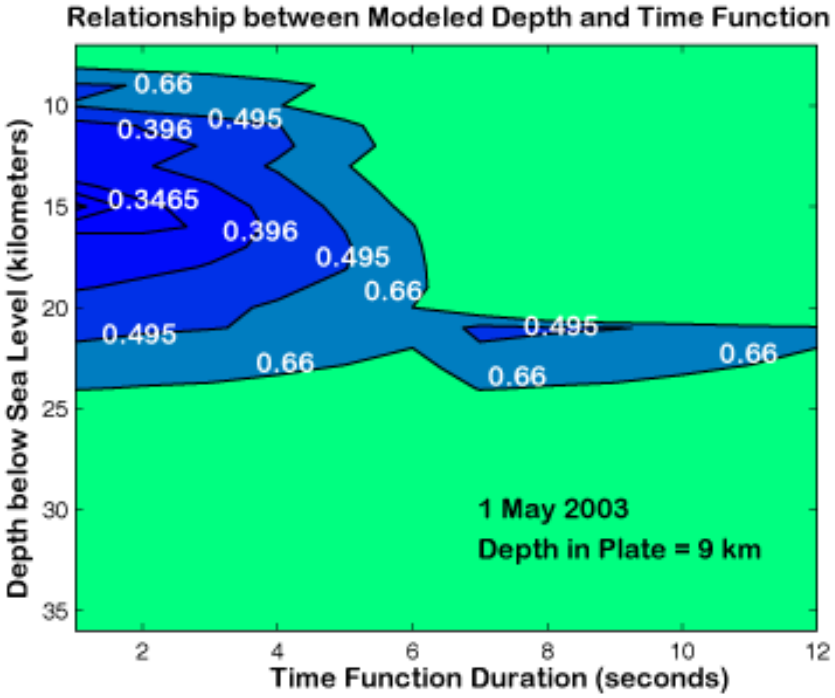

Figure B17 – Event 18, 1 May 2003
Strike: 12° Dip: 54° Slip: -30° Magnitude: 5.38 Mw

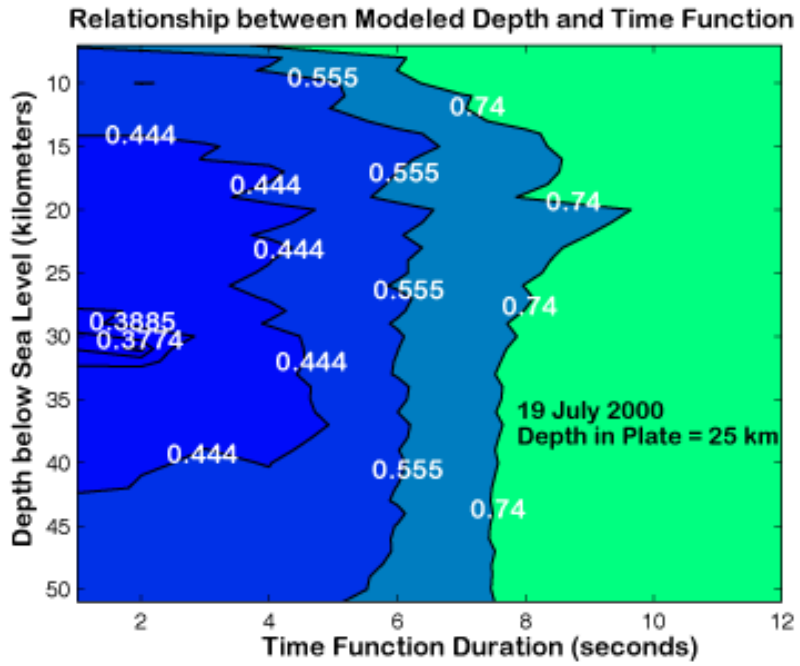

Figure B18 – Event 19, 19 July 2000
Strike: 177° Dip: 57° Slip: 7° Magnitude: 5.52 Mw

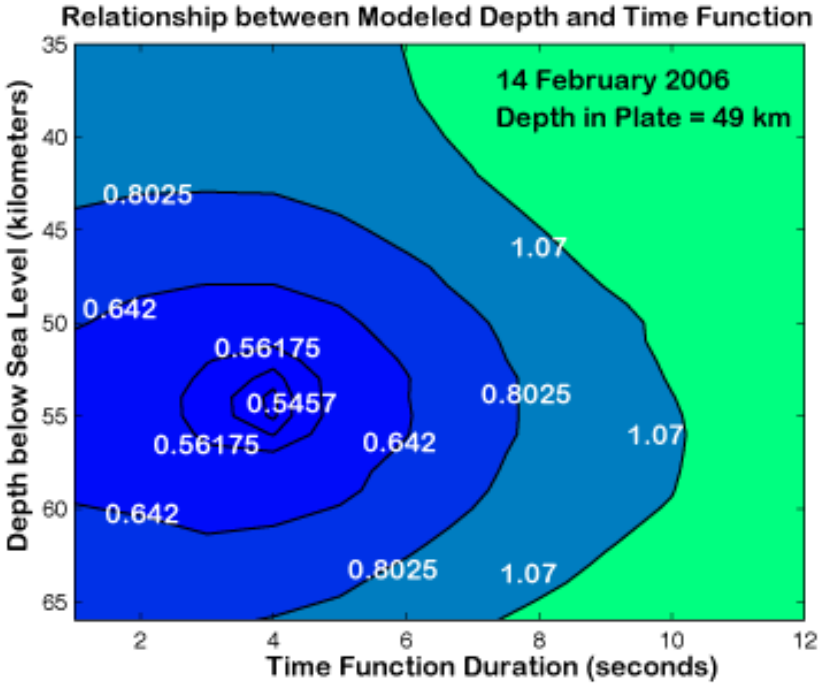

Figure B19 – Event 20, 14 February 2006
Strike: 113° Dip: 80° Slip: -75° Magnitude: 6.17 Mw

Appendix C – Magnified cross-sections of the Mariana outer rise

In order to explore whether a our focal mechanisms might correspond with any of the faults exposed at the seafloor, we map the vertically exaggerated bathymetric profile perpendicular to the exposed trace of the fault and attempt to connect to the locations and mechanisms of our events at depth. In general, the apparent dip of the fault at the seafloor does not match the dip of our focal mechanisms; the dip angles of our focal mechanisms tend to be larger in comparison to the apparent dip of the surface faults (corrected to account for the vertical exaggeration in the cross-section).

However, some geologic and geophysical considerations should be made before concluding whether the earthquakes at depth are connected to the faults exposed at the surface. First, the apparent dip of the fault at the surface is likely shallower than the dip of the actual fault at depth due to erosion and infilling from sediment over time – particularly if the fault is long-lived and has slipped in several separate seismic events. If this is true than the apparent dip at the surface is likely a lower bound for the actual dip of the fault. Secondly, it may not be reasonable to assume a planar fault with the same dip near the surface as at depth, although without any seismic reflection data for the region, the trace of the fault at depth is uncertain. Thirdly, relative relocations using global arrival time data are susceptible to lateral shifts resulting from large-scale heterogeneities within the interior of the Earth. From the comparison between relocations done with only teleseismic arrival time data and with local plus teleseismic arrival time data, a slight westward (~10 km) shift in the teleseismic-only arrival data has been observed at Northern Mariana [*Emry et al*, 2011]. If we assume that our teleseismic relocations

should similarly be shifted towards the east in this part of the Mariana Subduction zone, then some events begin to appear as if they may be correlated to some of the surface faults (Figure 7, main text). Finally, for many of the cross-sections shown below, surface ruptures appear to dip in both the landward and seaward direction. Except for Figure 7 in the main text, no dominant dip directions can be inferred from the bathymetry above our earthquakes.

All of the following figures show two cross-sections. The top cross-sections show the vertically exaggerated bathymetric profile oriented at 90° to the trace of the outer rise faults exposed at the surface of the seafloor. Bathymetry is shown in thick black lines and the estimated subsurface dip angles and fault planes of exposed faults are shown as dashed black line. The bottom cross-sections shows the same region with a smaller vertical exaggeration and the location and focal mechanism of nearby GCMT events for which we have modeled depth with compressional axes indicated by white and tensional axes indicated by red shading. Thick black lines indicate the bathymetry and the thick red line shows the depth to the Moho used in our waveform modeling technique.

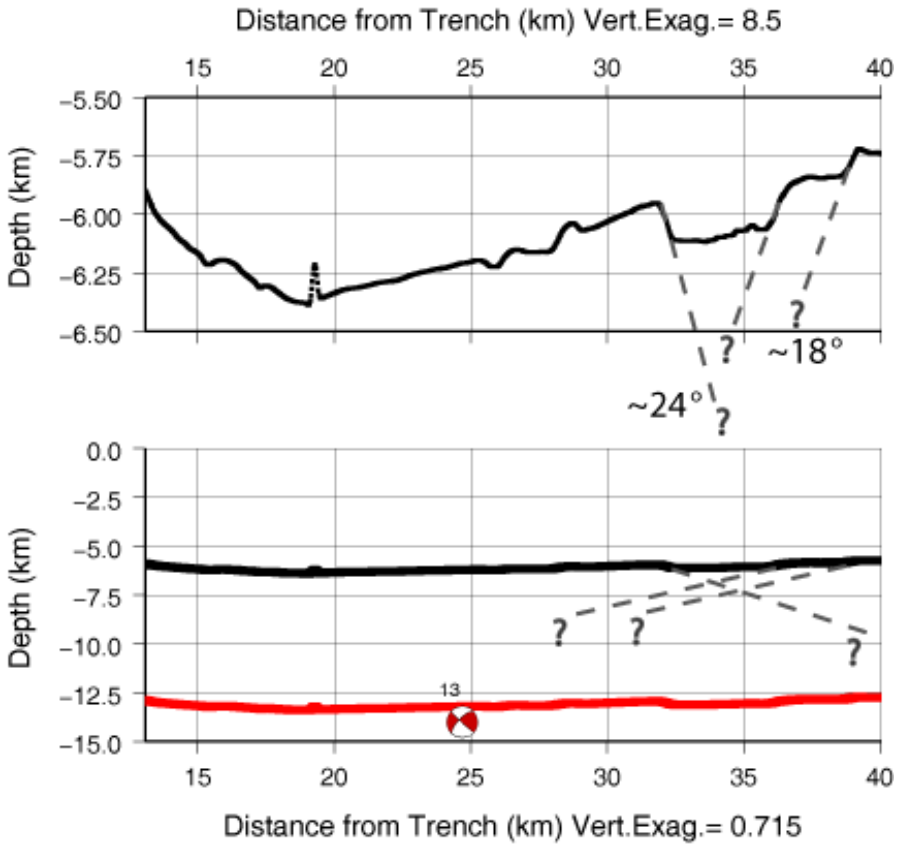

Figure C1: Top figure shows cross-sectional profile line B-B' from mapview in Figure 3 with vertical exaggeration (V.E.) = 8.5. The dips of the proposed fault traces appear to range ~18-24° both in the seaward dipping (east) direction and the trenchward dipping (west) direction. Bottom figure shows the same cross-section at vertical exaggeration (V.E.) = 0.715. Focal mechanism for the 13 October 1990 earthquake (Event 13, Table 2) is rotated 90° into cross-section.

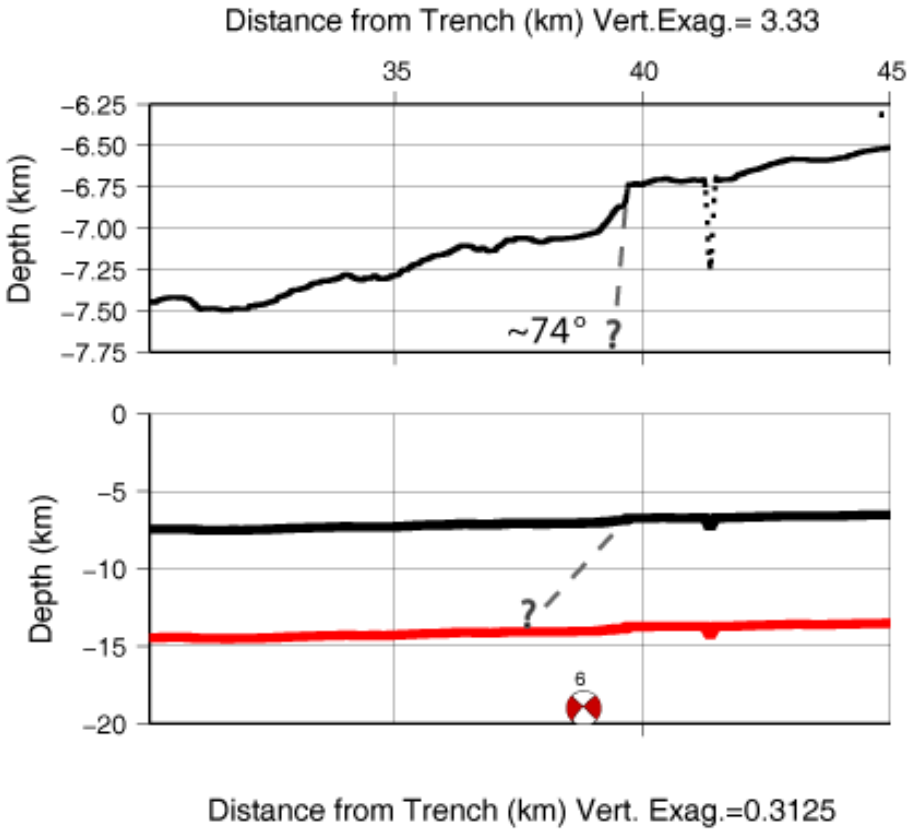

Figure C2: Top figure shows cross-sectional profile line C-C' from mapview in Figure 3 with vertical exaggeration (V.E.) = 3.33. The dip of the proposed fault trace appears to ~74° in the trenchward dipping (north) direction. Bottom figure shows the same cross-section at vertical exaggeration (V.E.) = 0.3125. Focal mechanism for the 19 December 2000 earthquake (Event 6, Table 2) is rotated 90° into cross-section.

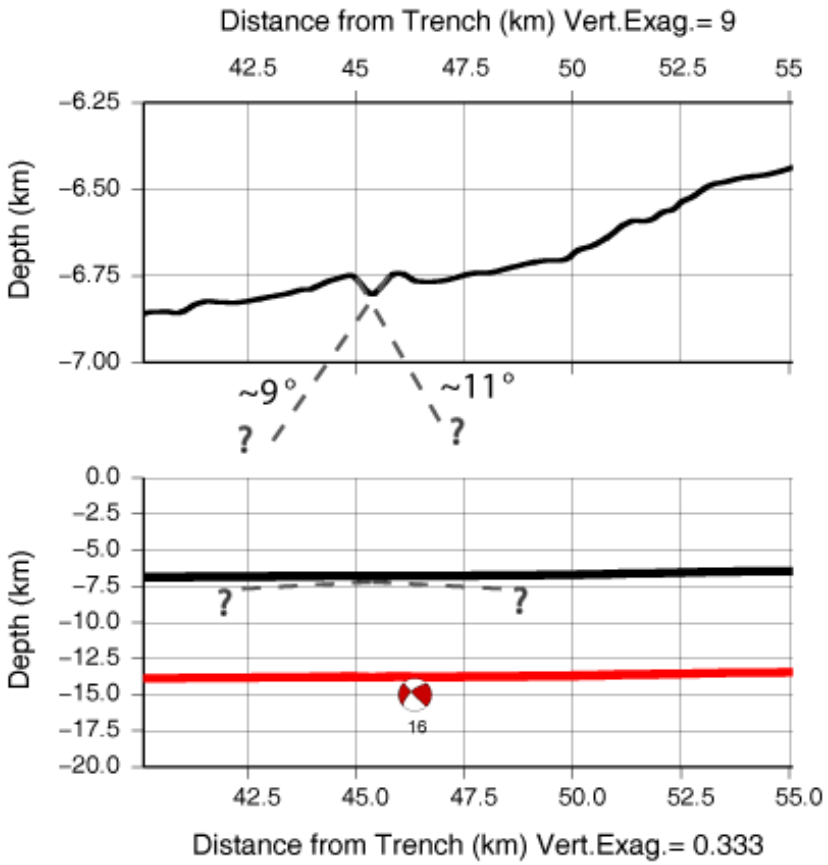

Figure C3: Top figure shows cross-sectional profile line D-D' from mapview in Figure 3 with vertical exaggeration (V.E.) = 9. Very small surface offsets do not reveal any obvious faults; however two potential fault lines are included. The dip of the proposed fault traces are ~10° either in the seaward dipping (east) direction or trenchward dipping (west) direction. Bottom figure shows the same cross-section at vertical exaggeration (V.E.) = 0.333. Focal mechanism for the 30 August 1998 earthquake (Event 16, Table 2) is rotated 90° into cross-section.

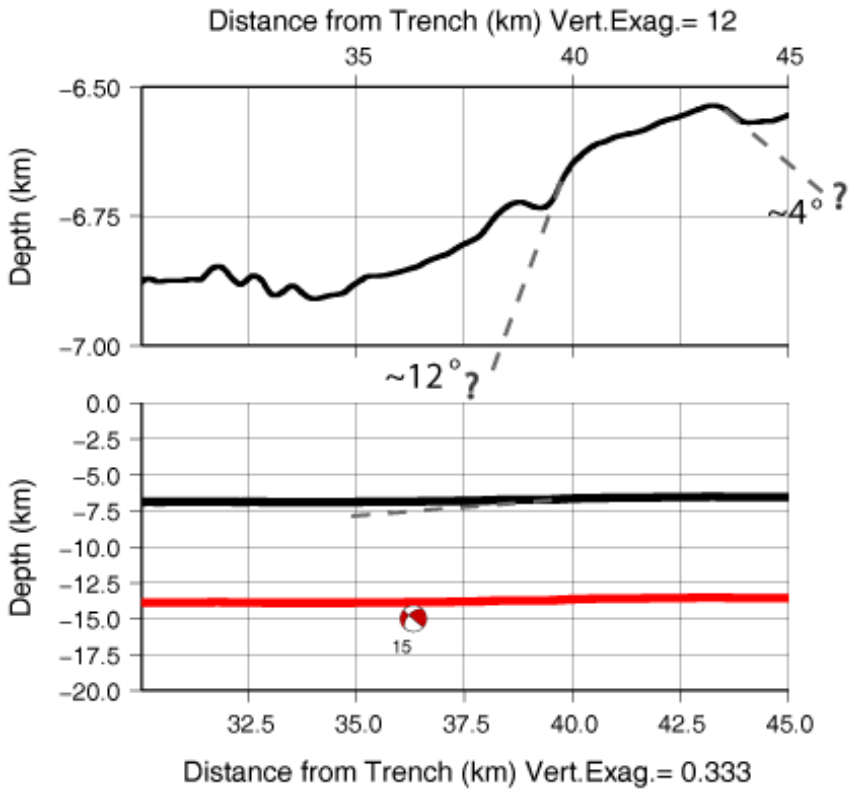

Figure C4: Top figure shows cross-sectional profile line E-E' from mapview in Figure 3 with vertical exaggeration (V.E.) = 12. The dips of the proposed fault traces are ~4-12° either in the seaward dipping (east) direction or trenchward dipping (west) direction. Bottom figure shows the same cross-section at vertical exaggeration (V.E.) = 0.333. Focal mechanism for the 16 July 2008 earthquake (Event 15, Table 2) is rotated 90° into cross-section.

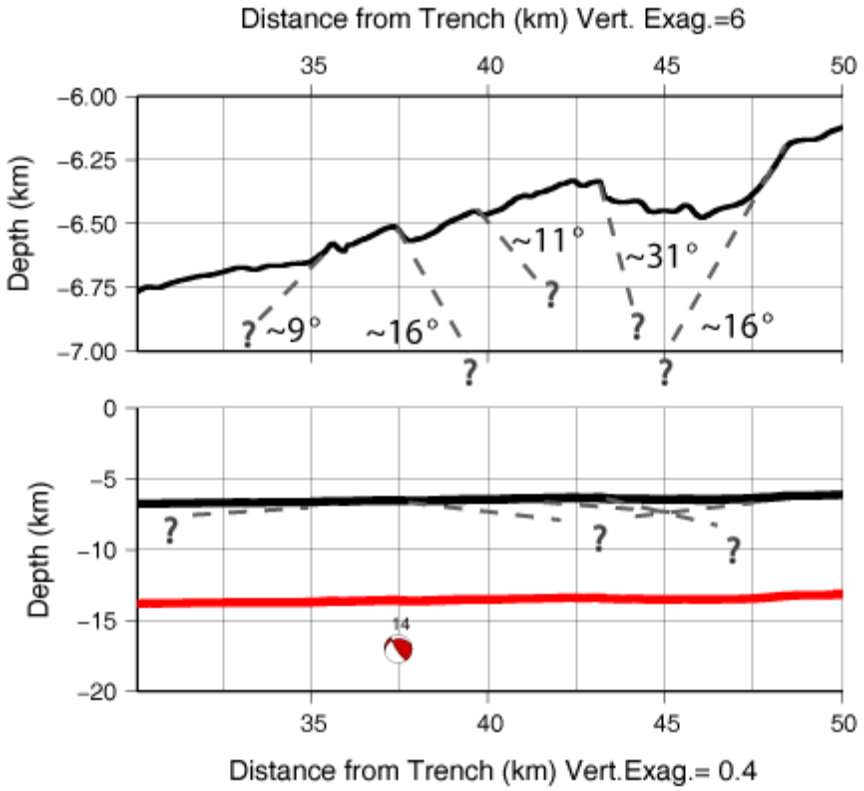

Figure C5: Top figure shows cross-sectional profile line F-F' from mapview in Figure 3 with vertical exaggeration (V.E.) = 6. The dips of the proposed fault traces are ~9-31° either in the seaward dipping (east) direction or trenchward dipping (west) direction. Bottom figure shows the same cross-section at vertical exaggeration (V.E.) = 0.4. Focal mechanism for the 10 November 1995 earthquake (Event 14, Table 2) is rotated 90° into cross-section.

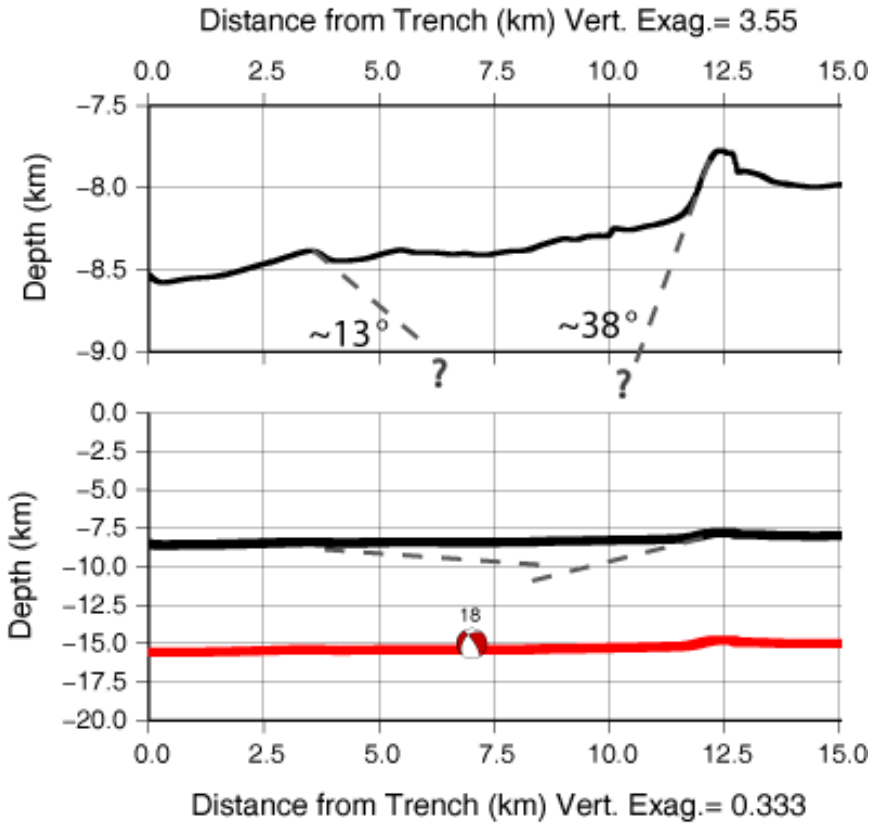

Figure C6: Top figure shows cross-sectional profile line G-G' from mapview in Figure 3 with vertical exaggeration (V.E.) = 3.55. The dips of the proposed fault traces are ~13-38° either in the seaward dipping (east) direction or trenchward dipping (west) direction. Bottom figure shows the same cross-section at vertical exaggeration (V.E.) = 0.333. Focal mechanism for the 1 May 2003 earthquake (Event 18, Table 2) is rotated 90° into cross-section.

CHAPTER 4

FAULTING IN NORTHERN AND WESTERN PACIFIC SUBDUCTION ZONE TRENCHES AND IMPLICATIONS FOR SUBDUCTION ZONE WATER BUDGETS

Abstract

The greatest uncertainty in the amount of water input into the Earth at subduction zones results from poor constraints on the degree and depth extent of mantle serpentinization in the incoming plate. The depth of serpentinization in the incoming plate mantle may be controlled by the maximum depth of extensional faulting which arises from lithospheric bending at the outer rise and trench, and as suggested by active-source seismic refraction experiments at several subduction zones. We explore the maximum depth of extension within the incoming plate at Northern and Western Pacific Subduction Zones in order to estimate the possible limits on extension and serpentinization and to identify variations between subduction zones. We relocate trench earthquakes to identify which events occurred within the incoming plate and determine accurate depths for 61 incoming plate earthquakes occurring during 1988-2011 by inverting teleseismic P and SH waveforms. We observe that the top 10-15 km of the outer rise mantle experiences extensional faulting at all of the subduction zones with a reasonable sample of earthquakes; 60% of the total number of extensional earthquakes occur within the top 5 km of the mantle, 80% occur within the top 10 km of the mantle, and 95% occur within to top 15 km. There is some evidence for variations throughout the different regions of study, for example extensional earthquakes occur down to 20 km below the crust in the western Aleutians; however, we are limited to a ~20 year record of

outer rise events for our analysis, which prevents any firm conclusions of this nature. We observe a limited number of compressional outer rise earthquakes, which may be an indication of increased plate interface coupling, at two of the five Northwestern Pacific Basin subduction zones. We propose that the greater number of extensional faulting events in the top 5 km of the incoming plate mantle results in greater concentrations of mantle hydration (3 wt% H_2O) and that the incoming plate mantle is partly serpentinized to a depth of ~15 km (1 wt% H_2O). Given these assumptions for water content, $\sim 8 \times 10^9$ Tg/Myr of water would be input into subduction zones at the Northern and Western Pacific. However, because the distribution of mantle hydration in the incoming plate is likely heterogeneous along the length of these subduction zones, we expect smaller actual concentrations of H_2O.

1. Introduction

Prominent extensional faulting within the incoming plates at subduction zone trenches may provide a pathway by which seawater can infiltrate down to mantle depths and hydrate dry mantle rocks prior to subduction. This has led some to postulate that large amounts of slab mantle serpentinites within the incoming plate may significantly impact subduction zone and upper mantle water budgets [e.g. *Ranero et al*, 2003]. Mantle serpentinites within the subducting slab would remain stable to greater depths and would therefore have a more significant contribution to water flux from the slab at intermediate and deep depths [*Jarrard*, 2003; *Hacker*, 2008; *Van Keken et al*, 2011]. Depending on the subduction zone, this could impact island arc and back arc basin

volcanism [*Kelley et al*, 2006] or the amount of water released into the Earth's upper mantle [*Rüpke et al*, 2004; *Hirschmann*, 2006].

Overlapping surveys of faults, seismicity and seismic tomography at the same region of the Nicaragua outer rise, have shown that deep extensional faults are continuous from the surface to mantle depths [*Ranero et al*, 2003], that extensional earthquakes occur down to ~6-9 km within the outer rise mantle [*Lefeldt et al*, 2009], and that regions of slow mantle P-wave velocities extend down to 12 km within the mantle [*Van Avendonk et al*, 2011]. The estimates of mantle hydration from *Van Avendonk et al* [2011] from seismic tomography extend slightly deeper than the depth estimate for the neutral plane (maximum depth of extensional earthquakes) from *Lefeldt et al* [2009]; however this difference may be explained by the effects of seismic anisotropy on observed P-wave velocities or the effect of plate interface locking on the short-term stress distribution within the outer rise [*Van Avendonk et al*, 2011]. Despite the differences, it is clear that the region of the slowest observed mantle P-wave velocities (and the greatest amount of mantle hydration) extends to depths that are generally consistent with the observed neutral plane [*Lefeldt et al,* 2009]. Therefore, by inferring the location of the neutral plane from outer rise seismicity we can estimate the depth of mantle serpentinization at places where active source seismic tomography is not yet available.

As *Hacker* [2008] and *Van Keken et al* [2011] suggest from their thermomechanical numerical models, flux of water from the subducting slab is dependent on a number of variables including the hydration state, temperature and convergence rate of the subducting slab. The Northern and Western Pacific oceanic plate is converging at a moderate rate, yet it also is subducting some of the oldest oceanic lithosphere on Earth.

In addition, most of the Northern and Western Pacific subduction zones have experienced large extensional outer rise earthquakes during instrumental and historic records [*Kanamori,* 1971; *Abe,* 1972; *Lay et al*, 2009]. Similar to results from *Van Avendonk et al* [2011] which show regions of slow seismic velocities varying in depth between the Nicaragua and Costa Rica outer rises, we expect that varying amounts of faulting and subsequent hydration of the Northern and Western Pacific subduction zones may contribute to regional differences in volcanic arc water contents, occurrence of intermediate depth earthquakes, and possibly even mantle transition zone water concentrations.

In this paper, we focus on the Northern and Western Pacific subduction zone outer rises spanning from the Alaska-Aleutian system to the Izu-Bonin subduction zone. Although earthquake depths are determined systematically by the International Seismic Centre (ISC), teleseismic depths determined from phase arrival picks are subject to large uncertainties due to misidentification of depth phases. Additionally, depths determined by the Global Centroid Moment Tensor (GCMT) catalog for their moment tensor inversion are often fixed at ~15 km for shallow events. Many of these subduction zone outer rises have been evaluated separately in event-specific studies; however we present a systematic analysis spanning many time periods at regions with varying tectonic characteristics and compare and contrast our observations throughout the entire Northern and Western Pacific region, in order to infer the extent of serpentinization within the incoming oceanic plate and how that may vary throughout these subduction zones.

2. Background

The occurrence of earthquakes within the subduction zone outer rise was first connected to oceanic plate flexure by *Isacks et al* [1968] and was noted to closely follow large plate interface earthquakes by *Stauder* [1968]. The realization that the distribution of stresses within the outer rise may be dependent upon the strength of coupling along the plate interface was explored by *Christensen and Ruff* [1988] and *Dmoska et al*. [1988]. Many prior studies have explored the locations of outer rise earthquakes or have determined focal mechanisms using first-motion techniques. In Table 1, we list all Northern and Western Pacific outer rise earthquakes which have been studied using body-wave modeling techniques to obtain source depth estimates.

2.1 Aleutian Islands and Alaska

The Alaska-Aleutian subduction zone margin changes significantly along its 4000 km length, from continental subduction beneath mainland Alaska and the Alaskan peninsula, to island arc subduction beneath the Aleutian Islands – west of Unimak Island and the Beringian margin, and then to oblique subduction and transform faulting beneath the western Aleutian-Kommandorski Islands [*Nishenko and Jacobs*, 1990; *Fliedner et al,* 2000]. The age of the subducting oceanic lithosphere changes along the length of the margin from ~30 Ma at mainland Alaska to 63 Ma in the eastern Aleutians to 43 Ma in the Western Aleutians at the Kula Rift fossil spreading center and then becoming older further to the west; this complicated pattern of ages is thought to be related to the change in Pacific plate motion around 55 Ma [*Lonsdale*, 1988; *Muller et al,* 2007; *Ruppert et al*,

2007]. The overriding plate of the Aleutian Islands is comprised of a number of small, rotating microplates [*Ruppert et al*, 2012]. In the mid-20th century, the majority of the Alaska-Aleutian plate interface ruptured during several sizeable plate interface earthquakes. The largest of these earthquakes was the 1964 Mw9.2 earthquake beneath mainland Alaska, although both the Andreanof and Rat Islands regions ruptured as well in great earthquakes during M8.6 1957 and Ms8.2 1965 [*Ruppert et al*, 2007; Carver *and Pflaker,* 2008]. Much of the megathrust which did not rupture during the mid 1900's is suspected to have ruptured during the preceeding 200 years, as historical accounts in the region indicate great shaking and tsunamis [*Carver and Pflaker*, 2008].

The Central and Western Aleutians have a history of large extensional outer rise earthquakes. At the Central Aleutians, a large Ms 7.6 outer rise earthquake occurred in 1929. Based on limited available waveform data, *Kanamori,* [1972] proposed that this event was a great outer rise earthquake, similar to the 1933 Sanriku event which ruptured through most of the lithosphere. At the Western Aleutians, several extensional outer rise earthquakes followed the 1965 Rat Islands megathrust earthquake, one of which was a large mb 7 event [*Stauder,* 1968]. Based on aftershock locations, *Abe* [1972] proposed that the rupture for this event extended 60 km into the Aleutian outer rise, fracturing most of the oceanic lithosphere. However more recent analysis modeling long-period P-waves, *Beck and Christensen* [1991] determined a maximum depth extent of 30-35 km for the large aftershock.

In addition to the large outer rise events at the Aleutians, a number of Alaska-Aleutian outer rise earthquakes were including in the global compilations from *Forsyth* [1982], *House and Jacob* [1983], *Ward* [1983], and *Christensen and Ruff* [1988] with

depths determined using waveform modeling techniques (Table 1). Many of these extensional outer rise events where noted to follow large megathrust earthquakes by *Stauder* [1968], and later work by *Christensen and Ruff* [1988] proposed that this temporal pattern observed at the Alaska-Aleutian margin was indicative of strongly coupled shallow thrust zones.

2.2 Kamchatka

The Kamchatka subduction zone connects to the oblique/transform margin of the Kommandorski Islands. The age of the oceanic plate at this margin is older than 100 Ma [*Lonsdale*, 1988]. In the northern part of the Kamchatka trench, near the intersection with the Aleutian trench, anomalously high heat flow has been observed [*Smirnov and Sugrobov*, 1982] and is apparently coincident with a plume imaged by seismic tomography [*Gorbatov et al*, 2001]. Observations of shallowing slab seismicity in Northern Kamchatka, near the junction of the Kamchatka and Aleutian trenches was interpreted as a tear in the subducting Pacific plate [*Davaille and Lees*, 2004]; however with more recent tomographic results, the gap in seismicity has been explained as a gap or window in the subducted slab beneath the Kamchatka and Aleutian trench junction [*Lees et* al, 2007; *Jiang et al,* 2009]. In Southern Kamchatka, results from a seismic P-wave tomography images the subducting slab extending down to and beyond the 660 km discontinuity [*Jiang et al*, 2009].

The Kamchatka subduction zone has produced a number of great earthquakes; including 1904 (Ms 8.3), 1917 (Ms 8.1), 1923 (Mw 8.3), 1952 (Mw 9.0), 1959 (Mw 8.2),

and 1997 (Mw 7.8) [*Ruppert et al*, 2007]. The largest of these, the 1952 Mw 9.0 event, occurred in southern Kamchatka near the northern edge of the Kuril subduction zone [*Christensen and Ruff*, 1988]. A few tensional outer rise earthquakes at Kamchatka were compiled by *Christensen and Ruff* [1988], although none had depths determined using their waveform modeling techniques. Perhaps due to the limited number of events which have occurred since good global seismic coverage has been available, few outer rise earthquakes along the Kamchatka subduction zone have had accurate depths determined using waveform modeling (Table 1). Two shallow, tensional outer rise events were reanalyzed by *Ward* [1983] and are listed in Table 1.

2.3 Kuril

The Kuril subduction zone has also experienced a large number of great earthquakes in 1915 (Ms 8.3), 1918 (Mw 8.3), 1958 (Ms 8.7), 1963 (Ms 8.3), 1969 (Ms 8.2), 1994 (Mw 8.3), 2006 (Mw 8.3), and 2007 (Mw 8.1) [*Ruppert et al*, 2007]. Preceeding the great 2006 Kuril megathrust event, a number of compressional earthquakes were observed at the outer rise, including an Ms 7.2 in 1963 [*Christensen and Ruff*, 1988; *Raeesi and Atakan*, 2009; *Lay et al*, 2009]. According to slip models from *Raeesi and Atakan* [2009], the compressional event nucleated at ~35 km depth but then ruptured two larger asperities updip, in the shallowest region of the bending plate where extension is expected to occur. The occurrence of compressional earthquakes at the Kuril subduction zone prompted *Christensen and Ruff* [1988] to propose a seismic

gap along that section of plate interface, which was located between the great 1952 Mw 9.0 Kamchatka and 1963 Mw 8.5 Kuril megathrust ruptures.

As predicted by *Christensen and Ruff* [1988], a great Mw 8.3 shallow megathrust earthquake occurred in November 2006 and was followed by several extensional earthquakes within the outer rise; one of these aftershocks was a great Mw 8.1 extensional event in January 2007 [*Ruppert et al*, 2007; Ammon *et al,* 2008; Raeesi *and Atakan*, 2009; *Lay et al,* 2009]. These two great events were identified as a 'doublet' and exhibited the temporal pattern observed by *Christenson and Ruff* [1988] of a megathrust earthquake accompanied by a transition from compression to extension within the outer rise [*Ammon et al*, 2008; *Lay et al*, 2009]. *Raeesi and Atakan* [2009] propose that the large 1963 compressional outer rise earthquake occurred at the same depths as the 2007 extensional outer rise earthquake, suggesting that this region switched from compression to extension following the 2006 megathrust event.

Both *Raeesi and Atakan* [2009] and *Lay et al* [2009] model the majority of the slip for the great 2007 outer rise earthquake at shallow depth within the top 20 km of the plate; however, *Lay et al* [2009] models small amounts of slip down to 33 km. They interpret this rupture extent to mean that the neutral surface of the bending plate is located deeper than 33 km [*Lay et al*, 2009] following the 2006 megathrust event. Both *Raeesi and Atakan* [2009] and *Lay et al* [2009] found that the 2007 outer rise earthquake rupture was longer than 200 km. In 2009, only two years after the great 2007 outer rise earthquake, another deep, large compressional earthquake occurred at the Kuril outer rise near the location of the 1963 compressional outer rise earthquake. This earthquake was found to occur at 45 km depth, with a rupture plane that extended from~35 km to ~55 km

in depth [*Lay et al*, 2009]. As discussed by *Lay et al* [2009], the presence of extensional slip at depths that almost overlap with the region of compressional slip may mean that the Kuril outer rise is lacking a strong elastic core. If the depth distribution of the 1963 compressional earthquake from *Raeesi and Atakan* [2009] is accurate, compressional slip occurs in the same regions and possibly along the same faults as extensional slip, which would also indicate that the Kuril outer rise is lacking a strong elastic core.

2.4 Northern Japan

The recent Mw 9.1 Tohoku megathrust earthquake occurred along the megathrust of the Japan subduction zone [e.g. *Nettles et al*, 2011]. Prior to this event, the subduction zone was not expected to be capable of producing earthquakes with Mw greater than about 8.5. Following this event, a large extensional Mw 7.6 outer rise earthquake occurred after only 40 minutes [*Nettles et al*, 2011; *Lay et al*, 2011], and a large number of outer rise earthquakes have occurred since that time [*Obana et al*, 2012]. To the north of the region affected by the 2011 Tohoku earthquake, the outer rise was ruptured by a great event in 1933 [*Kanamori*, 1971]. *Kanamori* [1971] suggested on the basis of surface wave analysis and aftershock locations that this event ruptured through the entire thickness of the oceanic lithosphere.

Seaward of the 2011 Tohoku rupture, outer rise seismicity prior to the great megathrust earthquake indicated that the neutral surface of the bending Pacific plate was at ~20-30 km [*Seno and Gonzalez*, 1987; *Gamage et al*, 2009]. *Seno and Gonzalez* [1987] showed that teleseismically recorded shallow extensional earthquakes were

located at depths of 16 km or less beneath the seafloor and one deeper compressional event was located at 41 km. More recently, *Gamage et al* [2009] used sP arrivals at nearby land stations to estimate earthquake depth, and detected an upper plane of extensional earthquakes and a lower plane of compressional earthquakes; they suggested that the neutral surface was located at ~20-25 km beneath the Japan trench. In 2005, a large Mw 7.0 normal-faulting earthquake occurred in the Japan outer rise; the location of the 2005 extensional earthquake is nearly coincident with the location of the largest outer rise aftershock of the 2011 Tohoku earthquake [*Nettles et al*, 2011]. The tensional aftershocks of the 2005 outer rise earthquake were located by an array of ocean-bottom seismometers and were found to be shallower than 20 km; additionally, compressional earthquakes were located at ~40 km [*Hino et al*, 2009]. After the great 2011 Tohoku earthquake, the patterns of seismicity in this region changed, with extensional earthquakes continuing as deep as ~40 km [*Obana et al*, 2012].

2.5 Izu-Bonin-Mariana

The Izu-Bonin-Mariana (IBM) subduction zone is an island arc stretching southward from the triple junction between the North American, Pacific, and Philippine Sea Plates at 35°N terminating at the Challenger cusp at 11°N [*Stern et al*, 2003]. The subduction zone developed at about 43 Ma, although it has split twice since then, due to the extensional nature of the subduction zone [*Stern et al*, 2003]. There is little definitive evidence for great plate interface earthquakes at this subduction zone due to limited historical records [*Emry et al*, 2011; *Okal et al*, submitted]. *Uyeda and Kanamori* [1979]

considered the Mariana segment to be the aseismic endmember of global subduction zones, incapable of producing large megathrust earthquakes, and many hypotheses have been put forward to explain the lack of great megathrust earthquakes here [*Scholz and Campos,* 1995; *Hyndman et al*, 1997].

Two large extensional outer rise earthquakes have occurred at the IBM trench. In 1990, an Mw 7.5 extensional earthquake and a series of extensional aftershocks occurred in the Pacific plate just seaward of the Mariana trench near ~15°N [*Satake et al*, 1992; *Yoshida et al*, 1992; *Zhang and Lay*, 1992]. A recent Mw 7.4 extensional outer rise earthquake occurred in 2010 east of the Bonin Islands [*Obana et al*, 2011; *Global CMT Catalog*]. Only a small number of moderate-sized outer rise earthquakes at the IBM trench, outside of the two large events occurring in 1990 and 2010, have been researched beyond the standard GCMT analysis. Moderate events within the IBM outer rise were explored by *Katsumata and Sykes* [1969] and *Forsyth* [1982]. Results for more accurate earthquake depths from their waveform inversions are presented in Table 1. Recent results from *Okal et al* [submitted] who analyze historic seismograms from 1930-1974 identify 4 earthquakes in the Mariana outer rise, two normal-faulting, one large compressional, and one strike-slip event. The recent work described in Chapter 3 explores Mariana outer rise seismicity from 1990-2010 in more detail and determines accurate depths for 20 earthquakes, 15 of which occur within 100 km of the trench and are likely associated with Pacific plate flexure; they also identify one deep compressional outer rise event not far from the 1940 compressional earthquake from *Okal et al* [submitted].

3. Data Sets and Methods

3.1 Earthquake Relocation

We first relocated all GCMT earthquakes which occur near the subduction zone trench; we do this in order to separate earthquakes which occur along the subduction shallow plate interface from the events which occur within the incoming plate outer rise. Arrival time data for all GCMT earthquakes occurring at the Alaska-Aleutian, Kamchatka, Kuril, Japan and Izu-Bonin subduction zones during January 1976-July 2011 were collected from the International Seismic Center (ISC) Bulletin [2010]. All GCMT earthquakes occurring within 60 km landward of the subduction trench axis or occurring at any distance seaward of the trench were split into separate regions for relocation. We divide earthquakes by region in order to ensure that the travel times of all the events are similarly affected by the large scale structure of the earth, as required for the relative relocation method. The divisions used to separate events were determined based on the spatial distributions of event locations prior to relocation; the latitudes or longitudes used to separate groups are listed in Table 2.

We used the hypocentroidal decomposition relative relocation algorithm of *Jordan and Sverdrup* [1981] to relocate all of the earthquakes within each region to obtain a more accurate lateral distribution. The initial earthquake locations used in the inversion were taken from the ISC bulletin [2010]. Travel times for P, pP, PKP, and S phases from each event were calculated according to the IASP91 earth model [Kennett and Engdahl, 1991]. S phases for all stations farther than 20° to the earthquake hypocenter were omitted due to large errors reported at these distances. The total number of earthquakes

relocated within each region varied due to differences in the occurrence of GCMT events since 1976; the total size of each relocation group is listed as well in Table 2.

3.2 Waveform Models

Following relocation, we use teleseismic P- and SH- waveform inversion to determine the best fitting source parameters for moderate-sized earthquakes located on the incoming plate or near the trench axis. We requested waveform data from the IRIS DMC (*www.iris.edu*) for all normal-faulting earthquakes greater than Mw 5.5 occurring after 1990 seaward of the trench or in close proximity to the trench. Additionally, we requested data for all compressional earthquakes greater than Mw 5.0 that were located seaward or near the trench, which were not obviously shallow thrust events, and which had a good signal to noise ratio (SNR) as discussed below. We distinguish shallow thrust events as those earthquakes with shallow dip (<~25°) oriented in the direction of plate convergence with a slip angle near 90°. Of the 8 events we identified as potential outer rise compressional earthquakes, after waveform analysis, 5 events were recognized to be shallow thrust earthquakes and 3 were found to be compressional outer rise events at the Alaskan and Northern Kurils/Southern Kamchatka subduction trenches.

Additionally, waveforms for all extensional Mw 5.0-5.4 incoming plate earthquakes were tested to find events with a sufficient signal to noise ratio (SNR) at the frequency range used in this study to permit P and SH waveform inversion. For each of these events, GSN broadband data were collected, the instrument response was removed, and the SNR was determined for three separate pass bands: 0.02-0.5 Hz, 0.02-0.2 Hz, and

0.02-0.18 Hz. For each pass band, the SNR was computed using three separate methods with the SEIZMO MATLAB software package [*Euler, pers. comm.*]: peak-to-peak amplitude SNR, root-mean-square (RMS) SNR, and the ratio of the peak-to-peak amplitude of the signal vs. RMS of the noise. The time window used to determine the noise was 50-10 seconds prior to the P- and S-arrival times calculated for the event according to the TAUP travel time calculator [*Crotwell et al*, 1999], and the window for the signal was 10 seconds prior to the estimated arrival time to 40 seconds following the arrival time. The SNR for P-wave arrivals were determined from the vertical components and the SNR for S-wave arrivals were determined from the horizontal components. Events showing at least 10 P or S traces with a SNR of greater than 5 were selected for waveform inversion. Our criteria requiring 10 data traces with peak-to-peak SNR 5+ is based on the results of the peak-to-peak signal vs. peak-to-peak noise of the 0.02-0.5 Hz pass band, which was the target frequency range used in this study. We use the more stringent peak-to-peak SNR criteria, because waveform modeling analyses for Mw 5.5+ events in this study and in Chapter 3 were visually inspected for clear SNR – a process which would be akin to the peak-to-peak SNR criteria.

For most of the earthquakes analyzed in this study, broadband data were used; for two events occurring before 1990, a mixture of broadband and long-period data was used. Although most Mw 5.5+ earthquakes occurring after 1990 have great enough SNR to be analyzed, a few were omitted, either because the signal was too small within the 0.02-0.5 Hz passband or because long period signal from prior large earthquakes overwhelmed the signal of the earthquakes of interest. One event at the Kuril-Kamchatka trench occurring in 1989 and one event at the Aleutian trench in 1988 were also analyzed, because of the

large size (Mw ~6.7 and Mw~6.4) and the availability of clear waveform data. Many larger events (Mw 5.6+) had enough clear data to invert using only GSN-broadband stations; however for some of the smaller events (~Mw 5.0-5.6) additional waveforms were requested from the DMC. All waveform data used for our modeled earthquake depths were 30-90° from the GCMT earthquake source. Waveforms were visually checked for clear signals at frequencies at 0.02-0.5 Hz, and instrument responses given by the IRIS DMC were deconvolved from the data prior to fitting the synthetics.

The method used to model synthetic data was the same as used for the analysis done in Chapter 3. We use the ray theory method [e.g. Langston & Helmberger 1975] and the ray parameter that corresponds to teleseismic propagation through an IASP91 model to compute our synthetic waveforms. Synthetics were first calculated for three fundamental double-couple source geometries and then combined to obtain synthetics for each focal mechanism tested within the grid search. A ray expander routine was used to compute all the reflections and conversions in the near-source structure model above a cutoff amplitude, and the duration of the source time function, which was modeled as a half sine, was determined within the grid search. The 1-d average shallow velocity structures used to compute synthetics were estimated from active source refraction experiments and are listed in Table 3. Figure 1 shows an example of several waveforms and matching synthetics for an example outer rise earthquake at the Aleutian trench.

4. Results and Relationship to Regional Tectonics

In total, we relocated 759 GCMT earthquakes and we inverted the waveforms of 66 earthquakes with Mw 5.2 – 7.4 (Table 4; Figure 2). The results of the modeled depths using our waveform inversion are plotted against the original GCMT event depths (Figure 3). We consider the depths modeled in our inversions to be more accurate than the depth computed during the GCMT inversions because 1) the passband of our analysis extends to 0.5 Hz whereas the general GCMT analysis uses longer period waves, and higher frequencies are inherently better able to resolve depth, 2) the depth of GCMT inversions are often necessarily fixed at 12 or 15 km for shallow events, and 3) we compute our depths as the depth below the seafloor using 1-d local velocity models which provides additional information by modeling the pwP water reflection. A summary of the waveform inversion results are provided in Table 4.

4.1 Alaska and Aleutian Subduction Zone

The modeled events at the Alaskan and Aleutian Subduction Zone are plotted on top of the regional bathymetry in Figure 4. In general, most modeled extensional trench earthquakes occurred at the Aleutian trench; only one extensional earthquake large enough to be modeled occurred at the outer rise seaward of Alaska. Between these regions, the subduction zone changes from an intraoceanic subduction zone in the west to subduction of an oceanic plate beneath a continental plate. East of this transition, one compressional earthquake was modeled deep within the slab – although the strike of this event was not parallel to the trench axis. West of this transition, only extensional

earthquakes occurred within the outer rise seaward of the Aleutian Islands – the maximum observed depth of these extensional earthquakes is ~10-15 km deeper in the western Aleutians than in the eastern Aleutians.

Very few outer rise earthquakes occurred seaward of the mainland Alaska or the Alaskan peninsula megathrust. Of the events in this region, one tensional and one compressional earthquake was large enough to be analyzed by our method. The compressional earthquake was found to have occurred at significant depth within the bending Pacific plate lithosphere (Table 4). However, the compressional event in this region has a strike orientation which forms a high angle with the strike of the trench axis – therefore it is uncertain whether it was produced through a simple plate flexure mechanism or whether it is a result of strong regional compressive forces related to coupling along the Alaskan megathrust. The compressional earthquake in this region occurs near the western boundary of the 1964 Mw 9.2 plate interface rupture.

Extensional outer rise earthquakes were more abundant slightly farther west, at the eastern region of the Aleutian Islands, in the vicinity of the Fox Islands. All of the modeled events here are located at shallow mantle depths, shallower than 5 km below the crust, and distributed laterally from the trench axis to ~60 km seaward of the trench (Figure 5). This is in contrast to the observed pattern of much deeper extensional earthquakes within the outer rise towards the west. In this region, west of the Fox Islands at the Andreanof and Delarof Islands, most of the normal-faulting earthquakes are ~ 5 km or less beneath the base of the crust; however, one extensional event occurred at a depth of ~15 km within the outer rise mantle (Figure 6). The example in Figure 1 shows the polarities of the modeled P-waves plotted atop the focal mechanism for the event and a

subset of waveforms that are representative of the total azimuthal range. All of the recorded P-waveforms show a dilatation first-motion and a significantly distinct P and pP arrival, which is indicative of a deeper event depth. As indicated by the misfit contours in Figure 7, this particular event has a well-constrained depth and source time function – reliably located at ~30-35 km. All of the extensional earthquakes beneath the Andreanof and Delarof outer rise occurred ~20 km seaward of the trench axis to ~40 km landward of the trench axis. Both the Fox Islands further to the east and the Andreanof Islands are located seaward of the great 1957 Mw 8.6 plate interface rupture. It is unclear whether the difference in the patterns of seismicity between these two regions is due to the limited temporal resolution of our study (20-25 years) or whether this pattern is persistent through time. However, if it were representative of the long-term seismicity, the pattern could indicate a gradual transition of highly compressional subduction tectonics (mainland Alaska and the Alaskan peninsula) grading through a region of shallow extension (Fox Islands) to a highly extensional region (Andreanof Islands).

Like the outer rise seaward of the Andreanof Islands, the westernmost region explored in this study, in the vicinity of the Near and Rat Islands, shows a pattern of both shallow and deep extensional events; the deepest event occurred 20 km below the base of the crust (Figure 8). However, unlike the Andreanof region, the lateral distribution of the earthquakes ranged from almost directly beneath the trench axis out to a distance of ~70 km seaward of the trench axis, and the deepest earthquake has a small strike-slip component in addition to the extensional mechanism. The Rat Islands is the site of the large Ms 7.5 outer rise earthquake which occurred following the 1965 megathrust earthquake [*Beck and* Christensen, 1991]. If this earthquake in fact ruptured down to 30-

35 km as suggested, then the presence of significantly deep extensional recent outer rise earthquakes in this region may be related.

As discussed, it is unclear whether the differences between the western Aleutians, the eastern Aleutians, and continental Alaska can be explained by limited sampling through time or whether they are persistent characteristics of the region. It does appear that the Central and Western Aleutians may have persistently deep outer rise extension, as two large outer rise earthquakes have occurred in the there in 1929 at the Central Aleutians and in 1965 at the Rat Islands [*Abe,* 1972; *Kanamori,*1972; *Beck and Christensen*, 1991]. We find that in the western Aleutians there is clear evidence that extensional outer rise earthquakes continue as far as 15-20 km below the base of the crust.

4.2 Kamchatka

Very few events occurred in the outer rise seaward of Kamchatka since 1990; most occurred during the period between 1976-1990, prior to the widespread availability of broadband digital seismometers. Of the six events studied, four are located in the northernmost corner of the subduction zone, near the intersection of the Kuril-Kamchatka trench with the Aleutian trench. At the northernmost region, the combination or high observed heat flows [*Cormier*¸1975; *Smirnov and Sugrobov*, 1982], seismicity [*Devaille and Lees*, 2004] and seismic tomography [*Gorbatov et al,* 2001; *Jiang et al*, 2009] indicate that the observed seismicity may be more indicative of the complicated tectonics

of the area, suggesting that the northernmost events at Kamchatka may not be good indicators of pure lithospheric bending stresses.

The southernmost Kamchatka events are located near the boundary between southern Kamchatka and the northernmost Kuril Islands. The extensional event occurred in 1989, and therefore does not have the same azimuthal coverage of seismic stations expected for more recent events. However, because of the earthquake's large size (Mw 6.7), the available broadband and long period data are excellent; still we are limited to analyzing the waveforms at a more limited frequency pass band (0.02-0.18 Hz). As a result the depth determination is not as well constrained as with higher frequency data. The depth is 9.5 km, which is only 2 km below the base of the crust. However, the shallow depth of this extensional earthquake is consistent with the shallow distribution of extensional outer rise earthquakes at the Kuril Subduction zone just to the south. The compressional earthquake in this region was located near the boundary between the Southern Kamchatka and Northern Kuril subduction zones. The event is quite small, and as a result has relatively large misfit; however, the waveforms indicate that it is clearly a deep event at ~40-45 km within the plate.

4.3 Kurils

Results from the Kuril subduction zone indicate that most extensional earthquakes depths are located near the Moho, although both the northern and southern regions have at least one earthquake located ~10 km below the base of the crust (Figure 9). These deeper extensional Kuril events are still 5-10 km shallower than the deep extensional

earthquakes within the Aleutian outer rise (Figures 6, 8). All of the analyzed extensional outer rise earthquakes occur between the time of the great 2006 Kuril megathrust and the great Kuril outer rise earthquake. The 2007 great outer rise earthquake which followed the great 2006 megathrust event may have ruptured to a maximum depth of ~ 33 km beneath the seafloor; however most of the slip was actually concentrated within the top 20 km of the mantle [*Raeesi and Atakan*, 2009; *Lay et al*, 2009]. Following this great outer rise earthquake, few moderate-sized extensional earthquakes occurred within the outer rise; however in 2009 a large Mw 7.4 deep compressional earthquake occurred in the same region as the 1963 Ms 7.2 compressional earthquake [*Lay et al*, 2009]. The slip for this event is thought to range from ~35 km to ~55 km in depth. For this event, we obtained a centroid depth of ~37 km. As discussed above, another deep compressional event occurred near the southern boundary of the Kamchatka outer rise; this event is also plotted in Figure 9. The somewhat shallow depths (< ~20 km below the seafloor) of the Kuril extensional earthquakes including the great 2007 extensional event appear to fit, given the recent large, compressional outer rise event rupturing as shallow as ~ 35 km.

4.6 Northern Japan

We determined depths for 13 normal-faulting or strike-slip events within the Japan outer rise (Figure 10). Ten of these events occurred following the great 2011 Tohoku megathrust event, and they show show large amounts of tensional outer rise seismicity directly east of the rupture location of the 2011 Tohoku earthquake. The outer rise events in this region have been studied by many sources. *Nettles et al* [2011]

determined the centroid moment tensors for many of the Tohoku aftershocks including events within the outer rise. *Lay et al* [2011] explored the expected stress distribution within the outer rise resulting from the great megathrust event and significant aftershocks. *Obana et al* [2012] located many smaller aftershocks using data from a rapid-response outer rise ocean-bottom seismic array deployed from 1 May to 30 June 2011. The extensional outer rise earthquakes which we analyze were located from ~40 km landward of the trench axis to as much as ~85 km seaward of the trench. Our determined depths range from shallow mantle to depths of 10 km below the base of the crust. Furthermore, results from locally-detected seismicity indicate that the plate is in extension down to ~40 km depth [*Obana et al*, 2012], although the number of extensional events at this depth was only 5% of their total recorded earthquakes.

4.7 Izu-Bonin-Marianas

The extensional outer rise earthquakes modeled at the Izu-Bonin subduction zone (Figure 11) were located at shallow depth beneath the Izu and Northern Bonin segments and extend significantly deeper within the Southern Bonin segment of the outer rise (Figures 12, 13, 14). Along the Izu segment of the outer rise (Figure 12), noticeable faults exposed at the seafloor occur within ~30-40 km distance seaward of the trench axis. The moderate-sized earthquakes in our study occur within the Pacific plate crust at ~25 km distance from the trench and extend down to the top few kilometers of the Pacific plate mantle within ~10 km of the trench axis. Further south, at the outer rise seaward of the Northern Bonin segment, faults are exposed on the seafloor within ~40 km from the

trench axis (Figure 13). Modeled depths for the moderate-sized earthquakes in this region all occur within the lower crust or the top ~5 km of the Pacific plate mantle. Unlike the pattern exhibited further to the north at the Izu segment of the outer rise, the deepest extensional events are not directly beneath the trench axis.

The southern segment of the Bonin outer rise, however, is quite distinct from the segments further north (Figure 14). In this region, a large, extensional Mw 7.4 earthquake occurred on December 21, 2010, followed by a number of aftershocks. We modeled the centroid depths of this mainshock and three extensional or strike-slip aftershocks occurring during late December 2010 or early January 2011. Two of the modeled earthquakes were not associated with the December 2010 event. However, like the normal-faulting earthquakes associated with the large 2010 mainshock, the strike of the focal mechanism is oriented at a large angle to the trench axis, in the northwest to southeast direction. This section of the Izu-Bonin subduction zone is distinct in its proximity to the Ogasawara Plateau; this large region within the Pacific plate that is currently at the subduction trench shallows the depth of the trench to less than 5 km [*Stern et al*, 2003; *Nakanishi*, 1993] In the same region, a long, northwest-southeast linear feature appears on the bathymetric maps (Figure 13); however it is unclear whether this linear feature which appears to cut across the edge of the Ogasawara Plateau is due to artifacts in the bathymetry or is a real feature on the seafloor.

If we combine the results from the Izu-Bonin segments with observations of the Mariana segment from Chapter 3, we find that the maximum modeled depth for extensional GCMT events varies along the entire 2800 km length of the Izu-Bonin-Mariana outer rise. The deepest normal-faulting events were found in the Southern

Bonin segment, near the subduction of the Ogasawara plateau, and extended down to 25-26 km below the top of the seafloor, or 15-20 km below the base of the crust. The other region of deep extension was at the Central Mariana segment, where a large Mw 7.5 extensional outer rise earthquake occurred on April 5, 1990 [*Satake et al,* 1992; *Yoshida et al*, 1992; Zhang *and Lay*, 1992]. The centroid depth for the large Mw 7.5 event was 18 km below the seafloor (11 km beneath the base of the crust), however, the actual rupture plane certainly extends at least a few kilometers below that centroid depth (Chapter 3).

Other similarities between the Izu-Bonin segments and the Mariana outer rise segments was the occurrence of strike-slip earthquakes located at depths that were consistently below the extensional earthquakes and above any compressional earthquakes (Chapter 3). These outer rise strike-slip events occurred at the Southern Bonin segment (Figure 13), the Northern Mariana segment, and the Southern Mariana segment (Chapter 3); all of these regions of strike-slip outer rise events are located at segments of the trench axis where it deviates from the general north-south trend. It is unclear what the implications of these outer rise extensional earthquakes are; however if these events perhaps mark a transition between the extensional and compressional flexure regimes, then they may be useful predictors of approximate neutral plane depth in regions where compressional earthquakes are not present or where the depth separation between observed extensional and compressional earthquakes is too large to identify the neutral plane.

5. Discussion

5.1 Depth Extent of Faulting and Strength of the Bending Lithosphere

The depth and distribution of the studied Pacific basin extensional earthquakes are somewhat variable between subduction zones and within each subduction zone; we note that extension occurs in every outer rise region down to at least the top few kilometers of the mantle (Figure 15). In addition, almost all of the studied Pacific subduction zones have extensional earthquakes in the outer rise down to 10-15 km below the Moho. At two subduction zone outer rises, the Western Aleutians and Southern Bonin, extensional earthquakes occur even deeper, down to ~20 km (Figure 15). Based, on these observations, we suspect that the most pervasive faulting extends down to the top 5 km of the incoming plate mantle and that sparser faulting extends to significantly deeper depths, down to 10-20 km within the bending plate mantle.

It has been proposed that many subduction zones (Izu-Bonin, Kermadec, Philippines, Aleutians, Sumatra, etc) are susceptible to outer rise earthquakes which rupture through the lithosphere [*Kao and Chen,* 1996]. *Kao and Chen* [1996] suggest that great outer rise earthquakes occur due to moment saturation of the outer rise plate curvature, at which point additional increases in curvature does so without significant increase in the bending moment. If the plate were represented simply as three regions of brittle faulting, a strong elastic core, and ductile deformation, in a moment saturation scenario, the stress distribution within the plate would transition over a very short vertical distance between brittle extensional faulting to the brittle compressional regime, diminishing its strong elastic core. *Kao and Chen* [1996] suggest that following this

point, the plate would no longer be coupled to the overriding plate at the megathrust, that the incoming plate would then only be susceptible to slab pull forces, and that future great megathrust events would not occur until the damaged plate had subducted.

The Kurile outer rise is an interesting case study in this respect. The prevalence of deep outer rise compressional events and large extensional earthquakes at the Kuril trench prompted *Christensen and Ruff* [1988] to classify this margin as strongly coupled. However, *Raeesi and Atakan* [2009] propose that the Ms 7.2 compressional earthquake of 1963 nucleated deep (~35 km) but that most of the slip from the event occurred at shallow depths, almost up to the surface of the incoming plate. If this is true, then the subsequent 2007 Mw 8.1 extensional outer rise event had to have ruptured the same depths as the 1963 compressional event, and according to *Raeesi and Atakan* [2009], perhaps along the same fault plane. However, it should be noted that the slip distribution from *Raeesi and Atakan* [2009] necessarily relies upon only 18 available digitized WWSSN seismograms of good quality.

Slip distributions from both *Raeesi and Atakan* [2009] and *Lay et al* [2009] for the more recent 2007 Mw 8.1 outer rise earthquake indicate that the majority of slip occurred at shallow depths along a fault that was ~200 km long. The models from *Lay et al* [2009] suggests that small amounts of slip occurs as deep as ~30-35 km, nearly overlapping with the updip slip extent (~30-35 km) modeled by them for the 2009 Mw 7.4 compressional event. Both the results from *Lay et al* [2009] and from *Raeesi and Atakan* [2009] suggest a diminished or absent strong core for the incoming oceanic lithosphere. Yet, unlike the moment saturation scenario proposed by *Kao and Chen* [1996], the Kuril megathrust is clearly strongly coupled. At the Kuril outer rise, most of the centroid depths for the

extensional earthquakes occur at shallow crustal and upper mantle depths with only a one extensional earthquake in the northern section of the Kurils and one extensional event in the southern section occurring a depth of ~10 km below the crust (Figure 9). Our best-fitting centroid depth for the 2009 Mw 7.4 compressional outer rise earthquake was 37 km, which is relatively shallow in comparison to where *Lay et al* (2009) model the majority of the slip. This difference may be caused by modeling the large and complicated rupture of the 2009 event as a point-source with a simple source time function.

The western and central Aleutian outer rise is also a region that does not clearly fit the model proposed by *Christensen and Ruff* [1988], where currently only extensional outer rise earthquakes occur, some of which are relatively deep and/or quite large [*Abe,* 1972; *Kanamori,* 1972; *Beck and Christensen*, 1991]. Although initial estimates for the depth extent determined for these events were not well constrained, reanalysis of the 1965 Rat Island outer rise event from *Beck and Christensen* [1991], suggest that the events did rupture down to ~30-35 km into the lithosphere, which is similar to the modeled depth extent of the 2007 Mw 8.1 Kuril outer rise event [*Lay et al*, 2009]. In these same regions near the Andreanof and Rat Islands, we observed some of the deepest extensional earthquakes in our dataset, extending to 20-25 km below the base of the crust. At this point, it is not clear if the prevalence of extensional earthquakes currently in this region is due to the great 1965 Rat Islands and 1957 Andreanof megathrust events or whether this region does not follow the pattern proposed by *Christensen and Ruff* [1988] for strongly coupled subduction zones. The true dimensions of many of the large outer rise events occurring prior to ~1990 are not well constrained; however these outer rise

earthquakes indicate that extension occasionally occurs as deep as 20-30 km into the incoming oceanic plate. If these events allow water into the deeper parts of the mantle, then many of the Pacific plate outer rises may be partially serpentinized at these depths.

5.2 Seismic Cycles and Stress 'Reversals'

The occurrence of large and great extensional outer rise earthquakes at some subduction zones implies that the depth extent of outer rise faulting may at least temporarily extend deeper than the average observed by this study. Many of these large, deep extensional outer rise events follow great megathrust ruptures. It has been proposed that great megathrust earthquakes can perturb the stress distribution within the incoming oceanic plates; this effect is also evidenced by the change from compressional outer rise seismicity to extensional seismicity following the rupture [*Christensen and Ruff*, 1988; *Dmowska et al*, 1988]. These possible temporary stress reversals are important to understanding the amount of incoming plate hydration, because it could contribute to a heterogeneous distribution of extensional events with depth along the length of the incoming plate outer rise.

The recent large Kuril outer rise earthquakes, as discussed above may be evidence for stress 'reversals' within the outer rise following a great megathrust earthquake. Prior to the great 2006 megathrust event only compressional earthquakes occurred within the incoming plate located seaward of this seismic gap [*Christensen and Ruff*, 1988; *Lay et al*, 2009]. *Raeesi and Atakan* [2009] argue that the 1963 compressional outer rise earthquake ruptured well into the top of the incoming plate, in a region where extensional

plate bending stresses are generally expected. They also argue that the 2006 megathrust event ruptured in this same region where the 1963 compressional earthquake ruptured [*Raeesi and Atakan*, 2009]. Whether or not their slip distribution for the 1963 event is accurate, considering the lack of clear data available to them, it is interesting to note the relative lack of outer rise extensional earthquakes in this region prior to the 2006 megathrust event (Table 1; Table 4) [*Forsyth,* 1982; *Ward,* 1983; *Christensen and Ruff*, 1988].

The Japan outer rise is another region where a change of stress from compression to extension has been observed. Recent results from *Obana et al* [2012] using an outer rise ocean-bottom seismic array show small, tensional earthquakes within the deep (~40 km) lower plane of the Japan outer rise, where a only few years earlier compression existed [*Seno and Gonzalez*, 1987; *Hino et al*, 2009; Gamage *et al*, 2009]. Only 5% of the earthquakes recorded by *Obana et al* [2012] occurred at depths greater than 30 km, and 4 of these deep earthquakes have first-motion polarities which suggest extension in this lower plane. They propose that the great 2011 Tohoku megathrust event changed the sense of stress within the deeper plane of the incoming plate from compression to extension.

Although great megathrust earthquakes and great outer rise earthquakes occur infrequently, their occurrence may be significant in regards to mantle hydration. If the stress distribution within the outer rise changes from compression to extension, and if water is able to penetrate the plate to these depths during these times, then over many seismic cycles, the deeper region of the outer rise mantle may become at least partly serpentinized. It is impossible to separate our observations of maximum earthquake

depth from the limited temporal range of our datasets (~20 years) as this length of time does not cover even the shortest estimates of the seismic cycle at subduction zones (~100 years). It is therefore important to remember that the overall long-term stress distribution within the different regions of the incoming Pacific plate may not be well represented by our short-term study of seismicity. However, this study is valuable, because we determine more accurate depths for the incoming plate earthquakes which have occurred; therefore illuminating the maximum observed depth of extensional outer rise faulting at several subduction zones.

5.3 Water storage in Pacific Oceanic Mantle

Regardless of the complications resulting from the subduction zone seismic cycle, great outer rise ruptures, and the possibility of stress changes or "reversals" within the bending plate, we have observed that extensional outer rise faulting generally occurs to ~10-15 km at most of the studied Pacific subduction zones, with 60% of these extensional outer rise events occurring within the crust or the top 5 km of the incoming plate mantle. The deepest extensional outer rise events were found at the Central and Western Aleutian Islands and at the Southern Bonin segment of the Izu-Bonin-Mariana subduction zone. *Ranero et al* [2003] and *Lefeldt et al* [2009] have suggested that the extensional outer rise earthquakes within the top of bending oceanic plates are the pathway by which water travels into the slab to mantle depths and hydrates dry ultramafic mantle materials. These serpentinites, which are stable to greater than 600°C at 5 GPa are thought to carry water to significant depth in the subduction zone and following

serpentinite dehydration, other phases such as the hydrous phase A may then carry water even deeper into the Earth [*Ulmer and Trommsdorf*, 1995].

However, large amounts of uncertainty exist regarding the mechanism by which water permeates into the plate. With increasing lithostatic pressure at depth, buoyant water should be prevented from traveling deeper into the plate. *Faccenda et al* [2009] proposed that the tectonic underpressure created within the extensional regime of the top of the bending plate should focus along the faults and effectively pull water deeper into the plate to mantle depths. They suggest that this mechanism of tectonic underpressure is responsible for the majority of water transport, but that other previously proposed mechanisms could further contribute to this process [*Sibson*, 1994; *Phipps Morgan and Holtzman*, 2005; *Korenaga,* 2007; *Faccenda et al*, 2009]. Resolution of potential impediments to water transport into the incoming plate mantle is necessary; however, it is clear from active-source seismic refraction experiments that water transport into the incoming plate does occur by some mechanism [*Contreras-Reyes et al*, 2007; *Ivandic et al,* 2010; *Van Avendonk et al*, 2011]..

The estimates of mantle serpentinization incorporated into numerical models of slab dehydration and water flux vary widely between authors. *Van Keken et al* [2011] conservatively estimate the slab mantle as either unserpentinized, partially serpentinized (2 wt % H_2O) down to 2 km, or fully saturated to 2 km. *Hacker* [2008] estimated the mantle to have 2 wt % H_2O down to 4 km; *Schmidt and Poli* [1998] assumes 5 km of mantle hydration with 10% average serpentinization; and *Rüpke et al* [2004] assume 10 km of upper mantle hydration. In our observations of extensional earthquake depths, it appears that no subduction zones have extensional faulting only at crustal depths. A few

small regions of some subduction zones have normal-faulting earthquakes only down to the top ~2 km of the mantle over the short time period explored by our study (~20 years); however in consideration of the subduction zone seismic cycle and its effects on outer rise stresses, it is likely that the longer-term average is larger than this. From our compilation of Northern and Western Pacific subduction zones, we make a conservative estimate of 5 km of extensional faulting and hydration, which we consider to be the lower bound depth estimate of slab hydration. It appears more likely however, given the large number of normal-faulting events occurring at 10-15 km depths and the occurrence of occasional large and great outer rise earthquakes which rupture to 20-30 km depths, that the mantle is faulted and partially hydrated to as deep as ~15 km.

If we use the estimates and assumptions of *Van Keken et al* [2011] for convergence rate, subduction zone length, and mantle density, and we assume the mantle is partially serpentinized (~2 wt % H_2O) to a depth of 5 km or 15 km, then the Northern and Western Pacific Subduction Zones subduct ~4×10^9 Tg/Myr or 9×10^9 Tg/Myr, respectively (Table 5). Combined with the crustal hydration contribution from *Van Keken et al* [2011], these values are ~1-3 times larger than those of *Van Keken et al* [2011]. Estimates for subduction zone water input are given for a range of water concentrations (Table 5). *Van Keken et al* [2011] assumed 2 wt % H_2O for their partially serpentinized case; however *Van Avendonk et al* [2011] observed water contents which range from 2-5 wt% H_2O in the hydrated region at the Nicaragua outer rise. If we assume an average water concentration of 3.5 wt % H_2O, then as much as ~10^{10} Tg of H_2O would be subducted every Myr at the Northern and Western Pacific subduction zones. This amount of mantle hydration is almost certainly too large; 10^{10} Tg/Myr would be greater

than 10 times the estimate for the subduction zone inputs for the whole Earth from *Van Keken et al* [2011] or 2-5 times more than *Hacker* (2008) or *Jarrard* (2003) and would also result in Earth's oceans being input into the subduction zone once every 100 Myr.

It is likely that the hydration within the incoming oceanic plate is not homogenous with depth or along the length of a subduction zone. This result was shown by *Van Avendonk et al* [2011] for the entire length of the Nicaragua-Costa Rica outer rise. At this subduction zone, *Van Avendonk et al* [2011] found evidence for deep mantle serpentinization at the northwestern region near Nicaragua, where *Ranero et al* [2005] also observed large off-set faulting parallel to the subduction trench axis, and identified very little mantle serpentinization at the southeastern region near Costa Rica, where *Ranero et al* [2005] found very little outer rise faulting. It is problematic to attempt to identify lateral heterogeneities along the length of the Northern and Western Pacific subduction zones, as the temporal coverage for our record is obviously incomplete; however, as shown in Figure 15, it appears that while most subduction zones have at least a few extensional earthquakes at ~10-15 km below the crust, 60% of the extensional earthquakes occur within the crust and top 5 km of the mantle. If we approximate incoming plate hydration as a shallow region of greater mantle serpentinization (~3 wt % H_2O down to 5 km) overlying a region of less mantle serpentinization (~1 wt % H_2O down to 15 km), then we estimate still that ~8×10^9 Tg/Myr of water is input into subduction zones.

Although seismic refraction results from *Van Avendonk et al* [2011] show heterogeneous patches of slow mantle velocities, the actual pattern of serpentinization is most likely even more localized within the mantle rocks adjacent to faults. This

heterogeneous distribution of serpentinites along fault planes could have an important effect on the dehydration rate of subducted slabs. *Wada et al* [in press] demonstrate through numerical models of the dehydrating slab that localized hydration would be expelled from the slab faster and at shallower depths than a uniformly hydrated slab. If this is true, then we might expect that the amount of water that is carried beyond subduction zones and into the upper mantle would be significantly less, and an increase in the amount of hydration within the incoming oceanic plate as suggested by our results may imply a greater flux of water from the slab at shallower depths than proposed by *Hacker* [2008] and *Van Keken et al* [2011].

6. Conclusion

We explored extensional and compressional outer rise earthquakes at Northern and Western Pacific subduction zones in order to estimate the depth at which extensional faulting may allow water to infiltrate into and serpentinize dry mantle rocks prior to subduction. We relocated and analyzed teleseismic P- and SH- waveforms of 66 subduction zone outer rise and trench earthquakes ranging from Mw 5.2-7.4, and we find that the mantle at most Northern and Western Pacific subduction zone outer rises exhibits extensional faulting to depths of ~15 km, with the highest concentration of extensional events extending down to ~5 km below the crust. We observe some regional variation between the different subduction zones, and we observe some variation along the length of individual subduction zones; however the length of the seismic record is short (~20 years), and regional variations may not be consistent through time. If the top ~5 km of

mantle is pervasively faulted & hydrated (~3 wt% H_2O) and if the mantle down to ~15 km is partially faulted and hydrated, then the amount of water input into the Northern and Western Pacific subduction zones would be quite large (~8×10^9 Tg/Myr). We expect that this is an upper limit, and actual concentrations of faulting and hydration would be limited by lateral heterogeneity along the length of subduction zone trenches.

7. Acknowledgements – Many thanks to H.Chou, G. Euler, P. Shore for scientific and technical assistance. Thank you to the IRIS Data Management Center, which provided access to the waveform data used in this study. Support for this research was provided under grants OCE-0426408, OCE-0752476, and OCE-0841074. Additional funding to present this research was provided by the NSF Earthscope and GeoPRISMs programs as well as the NSF/FESD CIDER program. Maps and cross-section were created using the GMT software [Wessel and Smith, 1991].

References

Abe, K. (1972), Lithospheric normal faulting beneath the Aleutian trench, *Phys. Earth Planet Interiors, 5*, 190-198.

Ammon, C. J., H. Kanamori, and T. Lay (2008), A great earthquake doublet and seismic stress transfer cycle in the central Kuril islands, *Nature, 451*, 561-566, doi: 10.1038/nature06521.

Beck, S.L. and D.H. Christensen (1991), Rupture process of the February 4, 1965, Rat Islands Earthquake, *J. Geophys. Res., 98*(B2), 2205-2221.

Carver, G., and G. Pflaker (2008), Paleoseismicity and neotectonics of the Aleutian Subduction Zone – An overview, in *Active Tectonics and Seismic Potential of Alaska*, edited by J. T. Freymueller, P. J. Haeussler, R. L. Wesson, and G. Ekström, pp. 43-63, American Geophysical Union, Washington D.C.

Christensen, D. H., and L. J. Ruff (1988), Seismic coupling and outer rise earthquakes, *J. Geophys. Res., 93*(B11), 13421-13444.

Contreras-Reyes, E., I. Grevemeyer, E.R. Flueh, M. Scherwath, and M. Heesemann (2007) Alteration of the subducting oceanic lithosphere at the southern central Chile trench-outer rise, *Geochem. Geophys. Geosyst., 8*(7), Q07003, doi:10.1029/2007GC001632.

Cormier, V. (1975), Tectonics near the junction of the Aleutian and Kuril-Kamchatka arcs and a mechanism for middle Tertiary magmatism in the Kamchatka Basin, *Geol. Soc. Am. Bull., 86*(4), 443-453.

Crotwell, H. P., T. J. Owens, and J. Ritsema (1999), The TauP Toolkit: Flexible seismic travel-time and ray-path utilities, *Seism. Res. Lett., 70*, 154-160.

Davaille, A., and J. M. Lees (2004), Thermal modeling of subducted plates: tear and hotspot at the Kamchatka corner, *Earth Planet. Sci. Lett., 226*, 293-304.

Dmowska, R., J.R. Rice, L.C. Lovison, and D. Josell (1988), Stress transfer and seismic phenomena in coupled subduction zones during the earthquake cycle, *J. Geophys. Res., 93*(B7), 7869-7884.

Emry, E.L., D.A. Wiens, H. Shiobara, and H. Sugioka (2011), Seismogenic characteristics of the Northern Mariana shallow thrust zone from local array data, *Geochem. Geophys. Geosystems, 12*(12), Q12008, doi: 10.1029/2011GC003853.

Faccenda, M., T.V. Gerya, and L. Burlini (2009) Deep slab hydration induced by bending-related variations in tectonic pressure, *Nature Geoscience, 2,* 790-793, doi: 10.1038/NGEO656.

Fliedner, M. M. and S. L. Klemperer (2000), Crustal structure transition from oceanic arc to continental arc, eastern Aleutian Islands and Alaska Peninsula, *Earth and Planet. Sci. 179*, 567-579.

Forsyth, D.W. (1982), Determinations of focal depths of earthquakes associated with the bending of oceanic plates at trenches, *Phys. Earth Planet. Interiors, 28*, 141-160.

Gamage, S.S.N., N. Umino, A. Hasegawa, and S.H. Kirby (2009), Offshore double-planed shallow seismic zone in the NE Japan forearc region revealed by sP depth phases recorded by regional networks, *Geophys. J. Int., 178*, 195-214, doi: 10.1111/j.1365-246X.2009.04048.x.

Gorbatov, A., Y. Fukao, S. Widiyantoro, and E. Gordeev (2001), Seismic evidence for a mantle plume oceanwards of the Kamchatka-Aleutian trench junction, *Geophys. J. Int., 146*, 282-288.

Hacker, B.R. (2008), H2O subduction beyond arcs, *Geochem. Geophys. Geosyst., 9*, Q03001, doi: 10.1029/2007GC001707.

Hino, R., R. Azuma, Y. Ito, Y. Yamamoto, K. Suzuki, H. Tsushima, S. Suzuki, M. Miyashita, T. Tomori, M. Arizono, and G. Tange (2009), Insight into complex rupturing of the immature bending normal fault in the outer slope of the Japan Trench from aftershocks of the 2005 Sanriku earthquakes (Mw = 7.0) located by ocean bottom seismometry, *Geochem. Geophys. Geosystems, 10*(7), Q07O18, doi: 10.1029/2009GC002415.

Hirschmann, M.M. (2006) Water, melting, and the deep Earth H_2O cycle, *Annu. Rev. Earth Planet. Sci., 34*, 629-653, doi: 10.1146/annurev.earth.34.031405.125211.

Holbrook, W. S., D. Lizarralde, S. McGeary, N. Bangs, and J. Diebold (1999), Structure and composition of the Aleutian island arc and implications for continental crustal growth, *Geology, 27*(1), 31-34.

House, L.S. and K.H. Jacob (1983), Earthquakes, plate subduction, and stress reversals in the eastern Aleutian arc, *J. Geophys. Res., 88* (B11), 9347-9373.

Hyndman, R. D., M. Yamano, and D.A. Oleskevich (1997), The seismogenic zone of subduction thrust faults, *Island Arc*, *6*(3), 244-260, doi: 10.1111/j.1440-1738.1997.tb00175.x.

Isacks, B., J. Oliver, and L. R. Sykes (1968), Seismology and the New Global Tectonics, *J. Geophys. Res. 73*(18), 5855-5899.

Int. Seismol. Cent (ISC) (2010), International Seismological Centre Bulletin, http://www.isc.ac.uk/search/index.html, Int. Seismol. Cent (ISC), Thatcham, U.K.

Ivandic, M., I. Grevemeyer, J. Bialas, and C. J. Petersen (2010), Serpentinization in the trench-outer rise region offshore of Nicaragua: constraints from seismic refraction and wide-angle data, *Geophys. J. Int. 180*, 1253-1264, doi:10.1111/j.1365-246X.2009.04474.x.

Iwasaki, T., H. Shiobara, A. Nishizawa, T. Kanazawa, K. Suyehiro, N. Hirata, T. Urabe, and H. Shimamura (1989), A detailed subduction structure in the Kuril trench deduced from ocean bottom seismographic refraction studies, *Tectonophysics, 165*(1-4), 315-336.

Jarrard, R.D. (2003), Subduction fluxes of water, carbon dioxide, chlorine, and potassium, *Geochem. Geophys. Geosyst., 4*(5), 8905, doi: 10.1029/2002GC000392.

Jiang, G., D. Zhao, and G. Zhang (2009), Seismic tomography of the Pacific slab edge under Kamchatka, *Tectonophysics, 465*, 190-203.

Jordan, T. H., and K. A. Sverdrup (1981), Teleseismic location techniques and their application to earthquake clusters in the South-Central Pacific, Bull. Seismol. Soc. Am., 71(4), 1105–1130.

Kanamori, H. (1971), Seismological evidence for a lithospheric normal faulting- the Sanriku earthquake of 1933, *Phys. Earth Planet. Interiors, 4*, 289-300.

Kanamori, H. (1972), Mechanism of tsunami earthquakes, *Phys. Earth Planet. Interiors, 6*, 346-359.

Kao, H. and W.-P. Chen (1996), Seismicity in the outer rise-forearc region and configuration of the subducting lithosphere with special reference to the Japan Trench, *J. Geophys. Res., 101*(B12), 27,811-27,831.

Katsumata, M. and L.R. Sykes (1969), Seismicity and tectonics of the Western Pacific: Izu-Mariana-Caroline and Ryuku-Taiwan regions, *J. Geophys. Res., 74*(25), 5923-5948.

Kelley, K.A., T. Plank, T.L. Grove, E.M. Stolper, S. Newman, and E. Hauri (2006) Mantle melting as a function of water content beneath back-arc basins, *J. Geophys. Res., 111*, B09208, doi:10.1029/2005JB003732.

Kennett, B. L. N., and E. R. Engdahl (1991), Traveltimes for global earthquake location and phase identification, *Geophys. J. Int., 105*(2), 429-465, doi:10.1111/j.1365-246X.1991.tb06724.x.

Korenaga, J. (2007), Thermal cracking and the deep hydration of oceanic lithosphere: A key to the generation of plate tectonics?, *J. Geophys. Res., 112,* B05408, doi:10.1029/2006JB004502.

Langston, C. A., and D. V. Helmberger (1975), A procedure for modeling shallow dislocation sources, *Geophys. J. R. Astron. Soc., 42*(1), 117-130, doi:10.1111/j.1365-246X.1975.tb05854.x.

Lay, T., H. Kanamori, C. J. Ammon, A. R. Hutko, K. Furlong, and L. Rivera (2009), The 2006-2007 Kuril Islands great earthquake sequence, *J. Geophys. Res., 114,* B11308, doi:10.1029/2008JB006280.

Lay, T., C.J. Ammon, H. Kanamori, M.J. Kim, and L. Xue (2011), Outer trench-slope faulting and the 2011 Mw 9.0 off the Pacific coast of Tohoku Earthquake, *Earth Planets Space, 63*, 713-718.

Lees, J.M., J. VanDecar, E. Gordeev, A. Ozerov, M. Brandon, J. Park, and V. Levin (2007), Three Dimensional Images of the Kamchatka-Pacific Plate Cusp, in *Volcanism and Subduction: The Kamchatka Region*, edited by J. Eichelberger, E. Gordeev, P. Izbekov, M. Kasahara, and J. Lees, pp. 65-75, American Geophysical Union, Washington D.C.

Lefeldt, M., I. Grevemeyer, J. Goßler, and J. Bialas (2009), Intraplate seismicity and related mantle hydration at the Nicaraguan trench outer rise*, Geophys. J. Int., 178*(2), 742-752, doi: 10.1111/j.1365-246X.2009.04167.x.

Lonsdale, P. (1988), Paleogene history of the Kula plate: Offshore evidence and onshore implications, *Geol. Soc. Am. Bull.,* 733-754.

Müller, R. D., M. Sdrolias, C. Gaina, and W. R. Roest (2007), Age, spreading rates, and spreading asymmetry of the world's ocean crust, *Geochem. Geophys. Geosystems, 9*(4), Q04006, doi:10.1029/2007GC001743.

Nakanishi, M. (1993), Topographic expression of five fracture zones in the Northwestern Pacific Ocean, in *The Mesozoic Pacific: Geology, Tectonics, and Volcanism,* edited by M. S. Pringle, W. W. Sager, W. V. Sliter, and S. Stein, pp. 121-136, American Geophysical Union, Washington D.C.

Nettles, M., G. Ekström, and H.C. Koss (2011), Centroid-moment-tensor analysis of the 2011 off the Pacific coast of Tohoku Earthquake and its larger foreshocks and aftershocks, *Earth Planets Space, 63*, 519-523.

Nishenko, S. P., and K. H. Jacob (1990), Seismic potential of the Queen Charlotte-Alaska-Aleutian seismic zone, *J. Geophys. Res., 95* (B3), 2511-2532.

Oakley, A. J., B. Taylor, and G.F. Moore (2008), Pacific Plate subduction beneath the central Mariana and Izu-Bonin fore arcs: New insights from an old margin, *Geochemistry Geophysics Geosystems*, *9*(6), 28, doi: 10.1029/2007GC001820.

Obana, K., T. Takahashi, T. No, Y. Kaiho, S. Kodaira, M. Yamashita, T. Sato, N. Noguchi, and T. Nakamura (2011), *Eos Trans. AGU ,* Fall Meet. Suppl., Abstract T31A-2320

Obana, K., G. Fujie, T. Takahashi, Y. Yamamoto, Y. Nakamura, S. Kodaira, N. Takahashi, Y. Kaneda, and M. Shinohara (2012), Normal-faulting earthquakes beneath the outer slope of the Japan Trench after the 2011 Tohoku earthquake: Implications for the stress regime in the incoming Pacific plate, *Geophys. Res. Lett., 39*, L00G24, doi: 10.1029/2011GL050399.

Okal, E.A., D. Reymond, and S. Hongsresawat (submitted), Large, pre-digital earthquakes of the Bonin-Mariana Subduction Zone, *Tectonophysics*.

Phipps Morgan, J., and B. K. Holtzman (2005), Vug waves: A mechanism for coupled rock deformation and fluid migration, *Geochem. Geophys. Geosyst., 6*(8), Q08002, doi:10.1029/2004GC000818.

Raeesi, M. and K. Atakan (2009), On the deformation cycle of a strongly coupled plate interface: The triple earthquakes of 16 March 1963, 15 November 2006, and 13 January 2007 along the Kurile subduction zone, *J. Geophys. Res., 114,* B10301, doi:10.1029/2008JB006184.

Ranero, C.R., J. Phipps Morgan, K. McIntosh, and C. Reichert (2003), Bending-related faulting and mantle serpentinization at the Middle America trench, *Nature, 425*(6956), 367-373, doi:10.1038/nature01961.

Ranero, C. R., A. Villasenor, J. P. Morgan, W. Weinrebe (2005), Relationship between bend-faulting at trenches and intermediate-depth seismicity, *Geochem. Geophys. Geosyst., 6*(12), Q12002, doi:10.1029/2005GC000997.

Rüpke, L.H., J. Phipps Morgan, M. Hort, and J.A.D. Connolly (2004), Serpentine and the subduction zone water cycle, *Earth Planet. Sci. Lett., 223*(1-2), 17-34, doi:10.1016/j.epsl.2004.04.018.

Ruppert, N.A., J.M. Lees, and N.P. Kozyreva (2007), Seismicity, earthquakes and structure along the Alaska-Aleutian and Kamchatka-Kurile subduction zones: A review, in *Volcanism and Subduction: The Kamchatka Region*, edited by J. Eichelberger, E. Gordeev, P. Izbekov, M. Kasahara, and J. Lees, pp. 129-144, American Geophysical Union, Washington D.C.

Ruppert, N.A., N.P. Kozyreva, and R.A. Hansen (2012), Review of crustal seismicity in the Aleutian Arc and implications for arc deformation, *Tectonophys. 522-523*, 150-157.

Satake, K., Y. Yoshida, and K. Abe (1992), Tsunami from the Mariana earthquake of April 5, 1990 – its abnormal propagation and implications for tsunami potential from outer-rise earthquakes, *Geophys. Res. Lett., 19*(3), 301-304, doi: 10.1029/91GL02493.

Schmidt, M.W., and S. Poli (1998), Experimentally based water budgets for dehydrating slabs and consequences for arc magma generation, *Earth Planet. Sci. Lett., 163*(1-4), 361-379, doi: 10.1016/S0012-821X(98)00142-3.

Scholz, C. H. and J. Campos (1995), On the mechanism of seismic decoupling and back arc spreading at subduction zones, *J. Geophys. Res., 100*(B11), 22103-22115.

Seno, T., and D. G. Gonzalez (1987), Faulting caused by earthquakes beneath the outer slope of the Japan trench, *J. Phys. Earth, 35*, 381-407.

Sibson, R.H. (1994), Crustal stress, faulting and fluid flow, in *Geofluids: Origin, Migration and Evolution of Fluids in Sedimentary Basins, Geo. Society. Spec. Pub. 78*, edited by J. Parnell, pp. 69-84, Geological Society, London.

Smirnov, Ya.B., and Sugrobov, V.M. (1982), Terrestrial heat flow in the northwestern Pacific, *Tectonophys., 83* (1982).

Stauder, W. (1968) Tensional character of earthquake foci beneath the Aleutian Trench with relation to sea-floor spreading, *J. Geophys. Res. 73*(24), 7693-7701.

Stern, R. J., M.J. Fouch, and S.L. Klemperer (2003), An overview of the Izu-Bonin-Mariana subduction factory, in *Inside the Subduction Factory*, edited by J. M. Eiler, pp. 175-222, American Geophysical Union, Washington D.C.

Ulmer, P., and V. Trommsdorf (1995), Serpentine stability to mantle depths and subduction-related magmatism, *Science, 268*(5212), 858-861.

Uyeda, S., and H. Kanamori (1979), Back-arc opening and the mode of subduction, *J. Geophys. Res., 84*(B3), 1049-1061, doi: 10.1029/JB084iB03p01049.

Van Avendonk, H.J.A., W.S. Holbrook, D. Lizarralde, and P. Denyer (2011), Structure and serpentinization of the subducting Cocos plate offshore Nicaragua and Costa Rica, *Geochem. Geophys. Geosyst., 12*, Q06009, doi:10.1029/2011GC003592.

Van Keken, P.E., B.R. Hacker, E.M. Syracuse, G.A. Abers (2011), Subduction factory: 4. Depth-dependent flux of H_2O from subducting slabs worldwide, *J. Geophys. Res., 116,* B01401, doi:10.1029/2010JB007922.

Wada, I., M. D. Behn, A. M. Shaw (in press), Effects of heterogeneous hydration in the incoming plate, slab rehydration, and mantle wedge hydration on slab-derived H_2O flux in subduction zones, *Earth Planet. Sci. Lett.*

Ward, S.N. (1983) Body Wave Inversion: Moment Tensors and Depths of Oceanic Intraplate Bending Earthquakes, *J. Geophys. Res. 88*(B11), 9315-9330.

Yoshida, Y., K. Satake, and K. Abe (1992), The large normal-faulting Mariana earthquake of April 5, 1990 in uncoupled subduction zone, *Geophys. Res. Lett., 19*(3), 297-300, doi: 10.1029/92GL00165.

Zhang, J.J. and T. Lay (1992), The April 5, 1990 Mariana Islands earthquake and subduction zone stresses, *Phys. Earth Planet. Int., 72*(1-2), 99-121, doi:10.1016/0031-9201(92)90052-W.

9. Figure Captions

Figure 1: The best-fitting focal mechanism for a deep extensional Aleutian trench event plotted with tensional axes in black and compressional axes in white. P-wave polarities are plotted on top of the focal mechanism showing all dilatational first-arrivals (open circles). The match between synthetic (black dashed lines) and data (thick gray lines) are shown in the waveforms surrounding the focal mechanism.

Figure 2: Focal mechanisms of modeled trench earthquakes around the Northern and Western Pacific Basin are shown in mapview. Red focal mechanisms correspond to events on Table 4 and are relocated GCMT earthquakes for which new depths and refined fault planes have been modeled. Focal mechanisms are lower-hemisphere projections with tensional quadrants shown in red and compressional quadrants are shown in white.

Figure 3: The best-fitting depths for the whole set of earthquakes modeled through our waveform inversions are plotted against the depths for the same earthquakes determined during the GCMT moment tensor inversion. The diagonal black line shows a 1:1 relationship, where the depth of our waveform modeling matches the GCMT depth.

Figure 4: Focal mechanisms of modeled trench earthquakes in the Aleutian Islands and Alaskan Peninsula are shown in mapview. Red focal mechanisms correspond to Events 1-17 on Table 4 and are relocated GCMT earthquakes for which new depths and refined fault planes have been modeled. Focal mechanisms are lower-hemisphere projections with tensional quadrants shown in red and compressional quadrants are shown in white. The cross-sectional profile lines corresponding to Figures 4, 5, and 7 are shown as solid black lines.

Figure 5: Top: Map view of the Fox Islands in the Eastern Aleutians showing relocated and newly modeled GCMT earthquakes. Focal mechanisms are lower-hemisphere projections with tensional quadrants shown in red and compressional quadrants shown in white. Solid black lines show the locations of the cross-sectional profiles below. **Bottom:** Cross-sectional view near the Fox Islands showing the distance and depth of modeled GCMT earthquakes. Red shading indicates tensional quadrants and white shading indicates compressional quadrants. The thick black line shows bathymetry; the thick red line shows the boundary between the crust and mantle (Moho) as input into our waveform inversion.

Figure 6: Top: Map view of the Delarof and Andreanof Islands in the Central Aleutians showing relocated, newly modeled GCMT earthquakes. Focal mechanisms are lower-hemisphere projections with tensional quadrants shown in red and compressional quadrants shown in white. Solid black lines show the locations of the cross-sectional profiles below. **Bottom:** Cross-sectional view near the Andreanof and Delarof Islands showing the distance and depth of modeled GCMT earthquakes. Red shading indicates tensional quadrants and white shading indicates compressional quadrants. The thick black line shows bathymetry; the thick red line shows the boundary between the crust and mantle (Moho) as input into our waveform inversion.

Figure 7: Average misfit countours in the depth vs. source time function parameter space for the 11 November 1993 Andreanof deep extensional outer rise earthquake corresponding to the waveforms shown in Figure 1. Contours for the solutions at 2%, 5%, 10%, 20%, and 50% greater than the best-fitting solution are given. The y-axis

shows depth below sealevel, and the depth of the Moho is marked in a solid black line at a depth of 14 km.

Figure 8: Top: Map view of the Rat and Near Islands in the Western Aleutians showing relocated, newly modeled GCMT earthquakes. Focal mechanisms are lower-hemisphere projections with tensional quadrants shown in red and compressional quadrants shown in white. Thick black lines show the locations of the cross-sectional profiles below. **Bottom:** Cross-sectional view near the Rat and Near Islands in the Western Aleutians showing the distance and depth of modeled GCMT earthquakes. Red shading indicates tensional quadrants and white shading indicates compressional quadrants. The thick black line shows bathymetry; the thick red line shows the boundary between the crust and mantle (Moho) as input into our waveform inversion.

Figure 9: Top: Map view of the Kuril Islands showing relocated, newly modeled GCMT earthquakes. Focal mechanisms are lower-hemisphere projections with tensional quadrants shown in red and compressional quadrants shown in white. Two large GCMT mechanisms from 2007 and 2009 are also plotted with dashed tie lines pointing to their locations. The slip distribution from these events were modeled by *Lay et al* [2009]. They are lower-hemisphere projections with tensional quadrants in black and compressional quadrants in white. Solid black lines show the locations of the cross-sectional profiles below. **Middle:** Cross-sectional view near the Northern Kuril Islands showing the distance and depth of modeled GCMT earthquakes. Red shading indicates tensional quadrants and white shading indicates compressional quadrants. Black shading indicates tensional quadrants and white shading indicates compressional quadrants for the two large 2007 and 2009 outer rise events. The dashed gray lines show the fault plane

dimensions as modeled by *Lay et al* [2009]. The thick black line shows bathymetry; the thick red line shows the boundary between the crust and mantle (Moho) as input into our waveform inversion. **Bottom:** Cross-sectional view near the Southern Kuril Islands showing the distance and depth of modeled GCMT earthquakes. Red shading indicates tensional quadrants and white shading indicates compressional quadrants. The thick black line shows bathymetry; the thick red line shows the boundary between the crust and mantle (Moho) as input into our waveform inversion.

Figure 10: Top: Map view of Northern Japan showing relocated, newly modeled GCMT earthquakes. Focal mechanisms are lower-hemisphere projections with tensional quadrants shown in red and compressional quadrants shown in white. Solid black lines show the locations of the cross-sectional profiles below. **Middle:** Cross-sectional view along the northernmost Japan profile line showing the distance and depth of modeled GCMT earthquakes. Red shading indicates tensional quadrants and white shading indicates compressional quadrants. The thick black line shows bathymetry; the thick red line shows the boundary between the crust and mantle (Moho) as input into our waveform inversion. **Bottom:** Cross-sectional view along the southernmost Japan profile line showing the distance and depth of modeled GCMT earthquakes. Red shading indicates tensional quadrants and white shading indicates compressional quadrants. The thick black line shows bathymetry; the thick red line shows the boundary between the crust and mantle (Moho) as input into our waveform inversion.

Figure 11: Top: Map view of the Izu-Bonin subduction trench showing relocated, newly modeled GCMT earthquakes. Focal mechanisms are lower-hemisphere projections with

tensional quadrants shown in red and compressional quadrants shown in white. Solid black lines show the locations of cross-sectional profiles in Figures 11, 12, and 13.

Figure 12: Top: Map view of at the Izu subduction zone showing relocated, newly modeled GCMT earthquakes. Focal mechanisms are lower-hemisphere projections with tensional quadrants shown in red and compressional quadrants shown in white. Solid black lines show the locations of the cross-sectional profiles below. **Bottom:** Cross-sectional view along the Izu profile line showing the distance and depth of modeled GCMT earthquakes. Red shading indicates tensional quadrants and white shading indicates compressional quadrants. The thick black line shows bathymetry; the thick red line shows the boundary between the crust and mantle (Moho) as input into our waveform inversion.

Figure 13: Top: Map view of Northern Bonin showing relocated, newly modeled GCMT earthquakes. Focal mechanisms are lower-hemisphere projections with tensional quadrants shown in red and compressional quadrants shown in white. Solid black lines show the locations of the cross-sectional profiles below. **Bottom:** Cross-sectional view along the Northern Bonin profile line showing the distance and depth of modeled GCMT earthquakes. Red shading indicates tensional quadrants and white shading indicates compressional quadrants. The thick black line shows bathymetry; the thick red line shows the boundary between the crust and mantle (Moho) as input into our waveform inversion.

Figure 14: Top: Map view of Southern Bonin showing relocated, newly modeled GCMT earthquakes. Focal mechanisms are lower-hemisphere projections with tensional

quadrants shown in red and compressional quadrants shown in white. Solid black lines show the locations of the cross-sectional profiles below. **Bottom:** Cross-sectional view along the Southern Bonin profile line showing the distance and depth of modeled GCMT earthquakes. Red shading indicates tensional quadrants and white shading indicates compressional quadrants. The thick black line shows bathymetry; the thick red line shows the boundary between the crust and mantle (Moho) as input into our waveform inversion.

Figure 15: Top: Histogram showing the number of extensional outer rise earthquakes occurring at each depth range: Crustal, 0-4 km below the crust, 5-9 km below the crust, 10-14 km below the crust, 15-19 km, and 20-24 km below the crust. Alaska and the Aleutians are shown in royal blue, Kamchatka is red, Kurils are shown in olive green, Japan is shown in purple, Izu-Bonin is light-blue, and Mariana is orange. **Bottom:** Histogram showing the total cumulative seismic moment for extensional outer rise earthquakes occurring at each depth range: Crustal, 0-4 km below the crust, 5-9 km below the crust, 10-14 km below the crust, 15-19 km, and 20-24 km below the crust. Alaska and the Aleutians are shown in royal blue, Kamchatka is red, Kurils are shown in olive green, Japan is shown in purple, Izu-Bonin is light-blue, and Mariana is orange.

10. Tables

Table 1: Prior research on Northern and Western Pacific Outer Rise Earthquakes

Date	Time	Type	Lat. (° N)	Lon. (° E)	Depth (km)	Reference
Alaska-Aleutian						
30 Mar 1965	2:27:03.4	T	50.32	177.93	18	Beck and Christensen, 1991
2 June 1966	3:27:53.0	T	51.1	176	13[a]	Forsyth, 1982
1 July 1967	23:10:08.6	SS	54.44	147.94	12	House and Jacob, 1983
20 June 1969	2:37:15.0	T	53.31	-162.41	14	Christensen & Ruff, 1988
27 Feb 1970	7:07:57.1	T	50.1	-179.6	6[a]	Forsyth, 1982
19 Mar 1970	23:33:29.0	T	51.3	173.8	20[a]	Forsyth, 1982
13 Oct 1972	4:46	T	52.89	162.98	10	Christensen & Ruff, 1988
2 Aug 1975	10:18	T	53.48	161.39	15	Christensen & Ruff, 1988
5 June 1981	7:09:18.1	T	51.74	-165.85	8	Ward, 1983
Kamchatka						
1 Feb 1981	22:43:30.8	T	53.03	162.41	14	Ward, 1983
1 Oct 1981	17:04:44.3	T	50.31	160.75	10	Ward, 1983
Kuril						
16 Mar 1963	8:45	C	46.5	154.7	10-50	Christensen & Ruff, 1988
5 Apr 1965	13:52:13.4	T	44.6	151.1	25[a]	Forsyth, 1982;
9 Sept 1971	23:01:06.8	T	44.4	150.9	15[a]	Forsyth, 1982
30 Apr 1981	14:41:40.6	T	43.15	150.14	8	Ward, 1983
23 Aug 1981	12:00:28.5	C	48.46	157.99	38	Ward, 1983
13 Jan 2007	4:23:21.16	T	46.243	154.524	0-33	Raeesi & Atatkan, 2009; Lay et al, 2009
15 Jan 2009	17:49:39.0	C	46.857	155.154	33-53	Lay et al, 2009
Northern Japan						
8 July 1967	19	C	37.74	143.88	41[a]	Seno & Gonzalez, 1987
23 Aug 1969	2	T	39.7	144.38	2[a]	Seno & Gonzalez, 1987
24 Aug 1969	22	T	39.8	144.3	4[a]	Seno & Gonzalez, 1987

23 Aug 1969	6	T	39.72	144.29	5[a]	Seno & Gonzalez, 1987
4 Dec 1969	8	T-SS	40.74	144.69	14[a]	Seno & Gonzalez, 1987
14 June 1975	23	T	36.31	143.3	16[a]	Seno & Gonzalez, 1987
5 Apr 1978	7	T-SS	39.64	144.46	31[a]	Seno & Gonzalez, 1987
30 Apr 1981	14:41:40.6	T	43.15	150.14	8	Ward, 1983
Izu-Bonin-Mariana						
4 July 1964	n/a	T	11.72	144.63	10	Katsumata & Sykes, 1969
10 Feb 1966	n/a	SS	20.77	146.38	38	Katsumata & Sykes, 1969
27 Oct 1966	n/a	T	22.15	145.94	21	Katsumata & Sykes, 1969
5 Apr 1967	n/a	T	20.00	147.35	34	Katsumata & Sykes, 1969
25 Aug 1974	23:245:09.3	T	32.1	142.3	7[a]	Forsyth, 1982

[a] Depth is given as depth below seafloor

Table 2: Regional divisions for relative relocation

Subduction Zone	Region	Latitude (°North)	Longitude (°East)	# Events Relocated
Aleutian	Alaskan Peninsula and Fox Islands	51 – 62	-145 – -165	23
Aleutian	Andreanof/Delarof Islands	48 – 54	-180 – -165	51
Aleutian	Near/Rat Islands	48 – 54	170 – 180	37
Kamchatka	North Kamchatka	52.5 – 57	161 – 167	78
Kamchatka	South Kamchatka / North Kurils	48 – 52.5	154 – 164	24
Kuril	North Kuril	45 – 48	151 – 158	154
Kuril	South Kuril	42 – 48	146 – 154	71
Japan	Hokkaido / Honshu	38.5 – 42	141 – 150	39
Japan	Honshu	35 – 38.5	141 – 146	107
Izu-Bonin	Izu Islands	31 – 35	141 – 145	84
Izu-Bonin	Izu Islands/ Bonin Islands	28 – 31	141 – 147	29
Izu-Bonin	Bonin Islands	25 – 28	141 – 147	62

Table 3: Local velocity models used in waveform inversions

Velocity Models						
Layer	Properties	Alaska/Aleutian (170°E - 145°W)[a]	Kamchatka (48°N – 57°N)[a]	Kurils (42°N - 48°N)[b]	Japan (35°N - 42°N)[c]	Izu-Bonin (25°N - 35°N)[d]
Water	α = 1.5 km/s β = 0 km/s ρ = 1.0 g/cm^3	Thickness: 6.5 km	Thickness: 5.5-6.5 km	Thickness: 6-7 km	Thickness: 4-8 km	Thickness: 6 km
Upper Crust	α = 5.2 km/s β = 3.0 km/s ρ = 2.6 g/cm^3	Thickness: 2 km	Thickness: 2 km	Thickness: 2.5 km	Thickness: 2.5 km	Thickness: 2.5 km
Lower Crust	α = 6.8 km/s β = 4.0 km/s ρ = 3.0 g/cm^3	Thickness: 5.5 km	Thickness: 4-5.5 km	Thickness: 6.5 km	Thickness: 5 km	Thickness: 3.5 km
Mantle	α = 8.0 km/s β = 4.5 km/s ρ = 3.3 g/cm^3	N/A	N/A	N/A	N/A	N/A

[a]Holbrook et al (1997)
[b]Iwasaki et al (1989)
[c]Seno & Gonzalez (1987) and references therein
[d]Oakley et al (2008)

Table 4: New locations and modeled depths

Event	Date	Time (UTC)	Latitude (° North)	Longitude (° East)	Depth[ab] (km)	Time Func. (sec)	Mw	Type of Event	Top freq. (Hz)	Misfit[c]
Alaska-Aleutian										
1	16 Jan 1999	10:44:42.90	56.3538	-147.2899	26.5	2	5.93	C	0.5	0.2858
2	27 Sept 1992	17:48:12.96	53.7911	-157.4670	9.5	1	5.84	N	0.5	0.5824
3	3 May 2010	14:04:23.70	52.5430	-163.6016	9.5	1	5.46	N	0.5	0.4886
4	7 Aug 2004	09:30:17.98	51.7127	-166.3158	8.5	4	6.00	N	0.5	0.3191
5	28 Dec 2002	09:36:12.73	51.5603	-168.5633	10.5	2	5.49	N	0.5	0.6413
6	14 Apr 1993	05:58:34.24	51.1857	-168.8008	10.5	3	5.95	N	0.5	0.4936
7	19 Aug 1992	00:57:41.81	50.5824	-174.9484	12.5	3	6.11	N	0.5	0.4090
8	15 Apr 1992	05:35:04.50	50.3010	-176.0652	10.5	1	5.53	N-SS	0.5	0.5141
9	26 June 2006	01:59:17.20	50.3040	-176.1655	9.5	2	5.41	N	0.5	0.4056
10	11 Nov 1993	00:28:36.38	50.3164	-177.4839	24.5	2	5.89	N	0.5	0.5010
11	15 Aug 2007	20:22:13.32	50.3687	-177.5885	9.5	3	6.41	N	0.5	0.4110
12	2 Sept 1999	02:33:37.56	50.7070	-177.6827	8.5	2	5.34	SS	0.4	0.5077
13	6 July 2009	14:53:12.71	50.4593	177.0526	30.5	1	6.05	N-SS	0.5	0.4674
14	7 Feb 1988	18:15:07.40	50.8566	173.4344	9.5	6	6.38	N	0.18	0.3632
15	12 Feb 1997	05:19:04.70	52.1393	171.2434	6.5	1	5.36	N	0.5	0.6449
16	4 Aug 2006	07:45:49.69	52.1743	171.0589	12.5	1	5.53	N	0.5	0.4665
Kamchatka										
17	18 May 2011	17:42:36.55	55.4763	163.8497	16.5	1	5.50	N	0.5	0.5691
18	26 Nov 1999	00:29:01.84	55.2337	165.3382	21	2	6.06	SS	0.5	0.4301
19	27 Jan 1998	19:07:59.95	55.1801	164.5708	16.5	1	5.53	SS	0.5	0.5510
20	27 Nov 1999	23:12:31.27	55.0789	165.6125	4.5	5	5.95	SS-N	0.5	0.4155
21	11 Apr 1989	03:56:37.29	49.5404	159.0874	9.5	8	6.71	N	0.18	0.2338

22	10 Aug 2005	12:47:39.77	48.6982	158.0978	42	1	5.38	C	0.5	0.5105
Kuril										
23	28 May 1992	21:24:51.36	47.6389	155.3989	7	2	5.58	N	0.5	0.6191
24	17 Nov 2006	04:09:55.38	47.0563	155.4486	4	2	5.53	N	0.5	0.5628
25	17 Nov 2006	06:33:50.32	47.0434	155.5093	4	1	5.43	N	0.5	0.6512
26	15 Nov 2006	19:25:26.56	47.0323	154.9654	3	1	5.65	N	0.5	0.5688
27	13 Jan 2007	04:23:22.65	46.9157	156.2620	17	3	6.37	N-SS	0.5	0.3017
28	15 Jan 2009	17:49:39.41	46.8595	155.1822	30	15	7.41	C	0.5	0.5937
29	5 Sept 1994	22:13:48.95	46.8178	155.1344	9	1	5.55	N-SS	0.5	0.4620
30	24 Nov 2006	15:34:11.04	46.7845	153.7519	10	1	5.61	N	0.5	0.4755
31	20 Sept 1999	09:32:42.62	46.3778	153.4320	10	2	5.59	ST	0.5	0.4851
32	16 Nov 2006	06:20:21.76	46.3528	154.4874	10	2	6.00	N	0.5	0.4774
33	16 Sept 1999	17:34:54.53	46.3433	153.4260	15	1	5.54	ST	0.5	0.6176
34	7 Dec 2006	19:10:21.77	46.1696	154.3725	10	4	6.37	N	0.5	0.3940
35	13 Sept 2004	03:00:14.75	43.8884	151.3214	4	3	5.97	N	0.5	0.3634
36	6 Feb 2003	18:48:40.02	43.1867	147.9108	23	4	5.57	N-SS	0.5	0.5450
Northern Japan										
37	7 May 1991	13:09:31.72	39.4835	144.6595	20	1	5.99	N	0.5	0.2614
38	5 May 2011	14:58:20.68	38.2463	144.0672	18	3	5.96	N	0.5	0.5610
39	14 Nov 2005	21:38:51.86	38.1550	144.9285	9	8	7.00	N	0.5	0.2261
40	17 Jan 2010	06:04:37.92	37.9833	143.5729	24	3	5.58	SS	0.5	0.4105
41	18 Mar 2011	03:23:55.61	37.8227	143.5179	15	1	5.62	N	0.5	0.5685
42	9 May 2011	20:15:55.89	37.8124	143.5359	13	1	5.70	N	0.5	0.5852
43	14 June 2011	13:06:54.78	37.7940	143.5197	16	1	5.80	N-SS	0.5	0.6431
44	12 Mar 2011	12:53:50.52	37.7827	143.5197	16	3	5.96	N	0.5	0.6171
45	3 June 2011	00:05:05.29	37.3472	143.9234	14	3	6.15	N-SS	0.5	0.3819
46	22 Mar 2011	07:18:47.55	37.2562	144.1037	10	5	6.45	N	0.5	0.239
47	22 Mar 2011	12:01:21.94	36.8978	143.2142	22	2	5.76	N	0.5	0.7258

48	17 Aug 2011	11:44:09.36	36.8189	143.7666	8	3	6.22	N	0.5	0.3291
49	14 Mar 2011	03:15:53.22	36.3166	142.0871	13	2	5.47	ST	0.5	0.5575
50	13 Mar 2011	01:26:06.28	35.7527	141.6793	19	4	6.26	N	0.5	0.4761
Izu-Bonin										
51	15 June 1993	04:42:54.37	34.8798	141.7431	16	3	5.59	ST	0.5	0.3334
52	29 July 2005	20:25:03.96	33.4587	142.3966	4	4	5.55	N	0.5	0.4072
53	27 July 2005	02:39:22.51	33.4050	142.3880	3	1	5.41	N	0.5	0.5988
54	25 Oct 1999	07:29:58.65	32.1033	142.2747	11	2	5.87	N	0.5	0.5820
55	5 Jan 2011	00:57:31.69	31.6720	142.2905	10	1	5.63	N	0.5	0.5919
56	8 May 1998	04:48:36.86	30.9836	141.8681	10	2	5.39	ST	0.5	0.6602
57	2 Nov 2004	08:46:00.58	28.8189	143.2545	10	2	5.74	N-SS	0.5	0.4334
58	4 Mar 2002	20:21:23.42	28.5644	143.3213	7	3	5.62	N	0.5	0.5664
59	1 June 2003	17:50:26.96	28.2978	142.8072	9	2	5.62	N	0.5	0.4803
60	6 Nov 1996	20:01:02.53	28.1193	143.5693	12	4	6.46	N-SS	0.5	0.2557
61	21 Dec 2010	17:19:41.19	26.9231	143.7696	18	6	7.18	N-SS	0.5	0.2533
62	15 June 2011	04:40:59.72	26.8284	144.1564	7	3	5.66	N	0.5	0.3428
63	22 Dec 2010	21:49:41.05	26.8056	143.6767	28	2	6.40	SS	0.5	0.5870
64	22 Dec 2010	01:31:20.03	26.7521	143.5144	8	3	5.62	N-SS	0.5	0.4356
65	6 Aug 2006	18:16:40.48	26.1467	144.0780	24	1	5.89	N	0.5	0.2439
66	9 Feb 2005	18:46:10.91	26.1019	144.1007	25	6	6.35	N	0.5	0.2126

[a]Denotes depth beneath seafloor (depth within plate)

[b]Depth error is calculated as depth at which misfit to data is 5% more than the misfit of the best-fitting solution – not including uncertainty resulting from variations in the shallow velocity model.

[c]SS – strike-slip; C –compression; N – extensional; ST – shallow thrust

[d]Misfit is measured as the squared amplitude error.

Table 5: Estimates for mantle hydration and subducted water

Region	Concentration of water in mantle (wt %)	Depth of mantle serpentinization (km)	Rate of water subducted per length of margin (Tg/Myr/m)	Total rate subducted water per subduction zone (Tg/Myr)
NW Pacific	2	5	557	4.3×10^{9}
NW Pacific	2	15	1150	8.9×10^{9}
NW Pacific	3.5	5	779	6.0×10^{9}
NW Pacific	3.5	15	1816	1.4×10^{10}
NW Pacific	3; 1	5 km; 5-15 km	1001	7.8×10^{9}
Global	2	5	2153	8.3×10^{10}
Global	2	15	4453	1.7×10^{11}
Global	3.5	5	3016	1.2×10^{11}
Global	3.5	15	7041	2.7×10^{11}
Global	3; 1	5 km; 5-15 km	3878	1.4×10^{11}

11. Figures

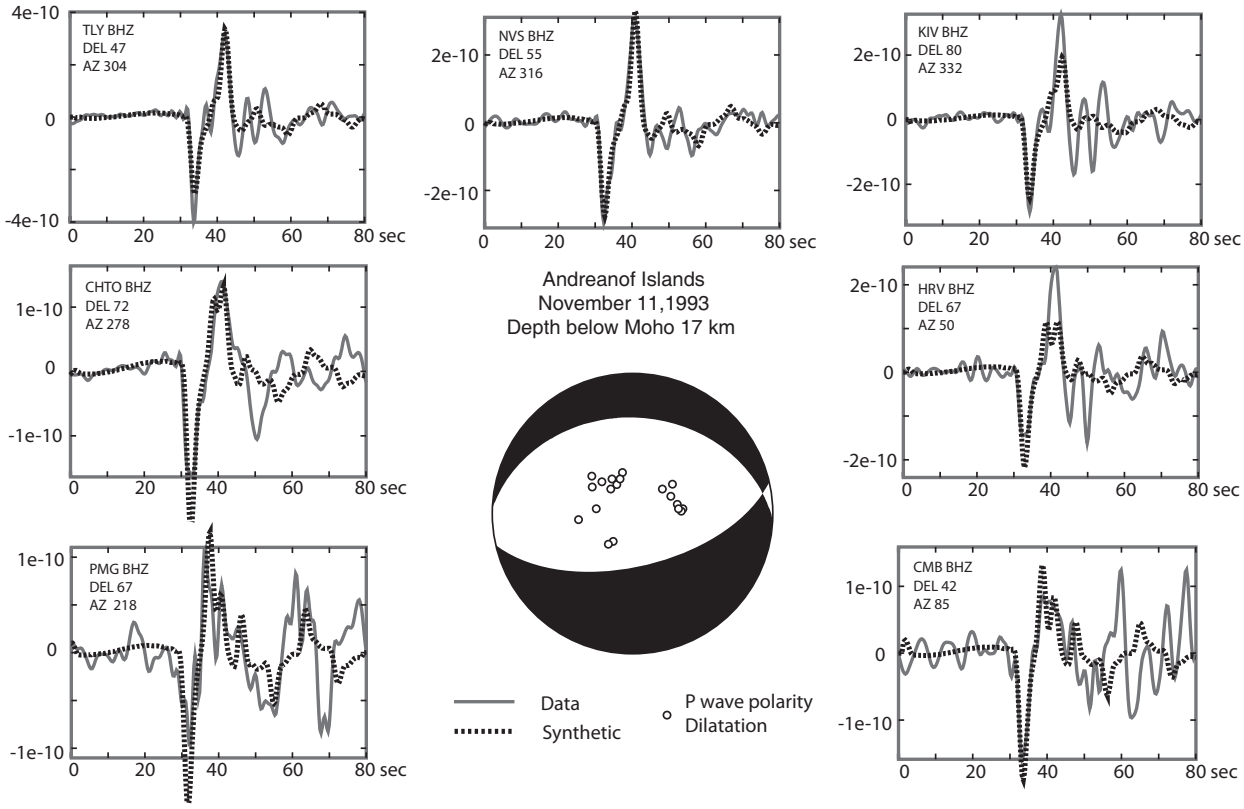

Figure 1 – Waveforms for 11 November 1993 Event

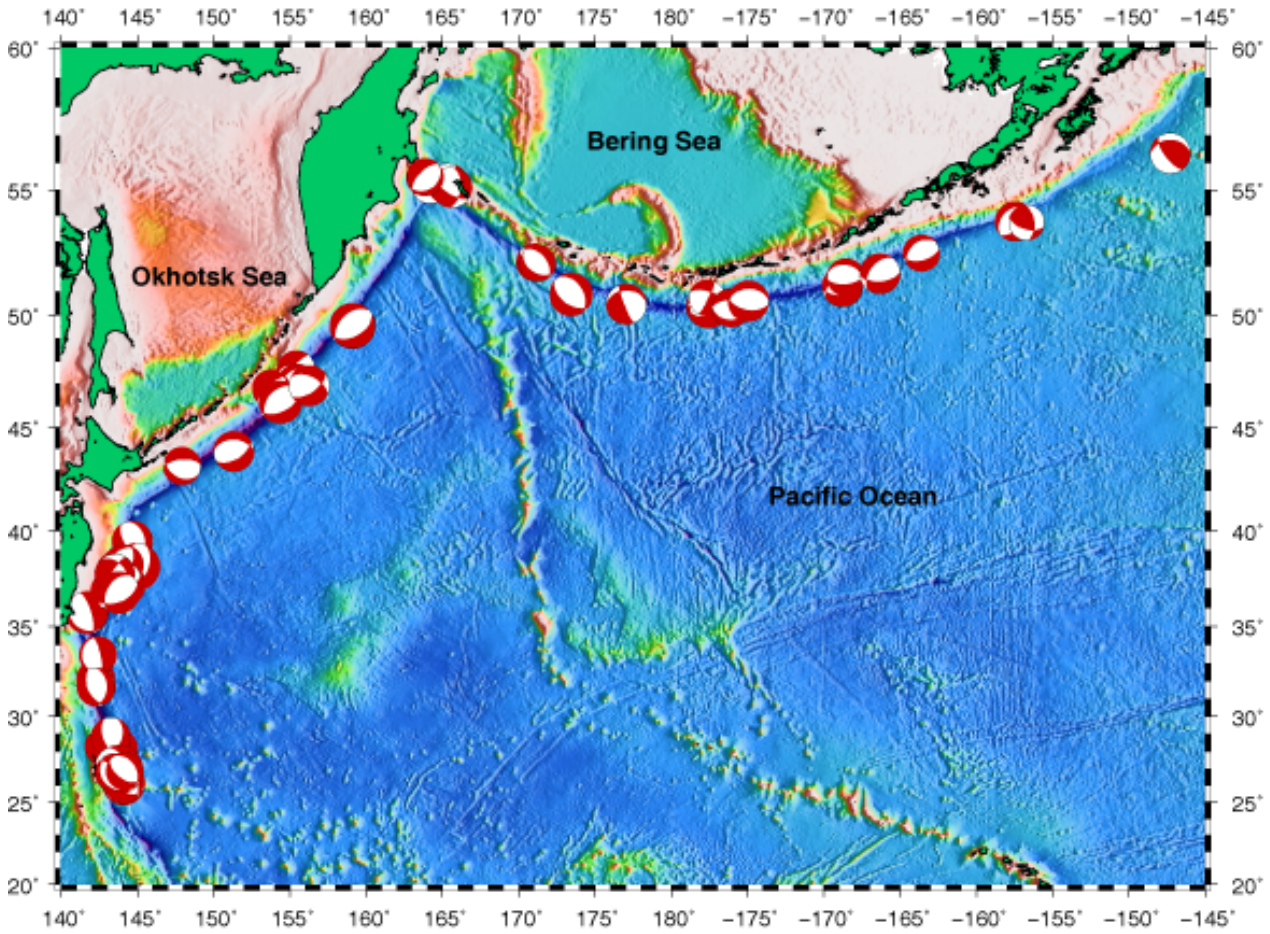

Figure 2 – Outer Rise Earthquakes around the Pacific Basin

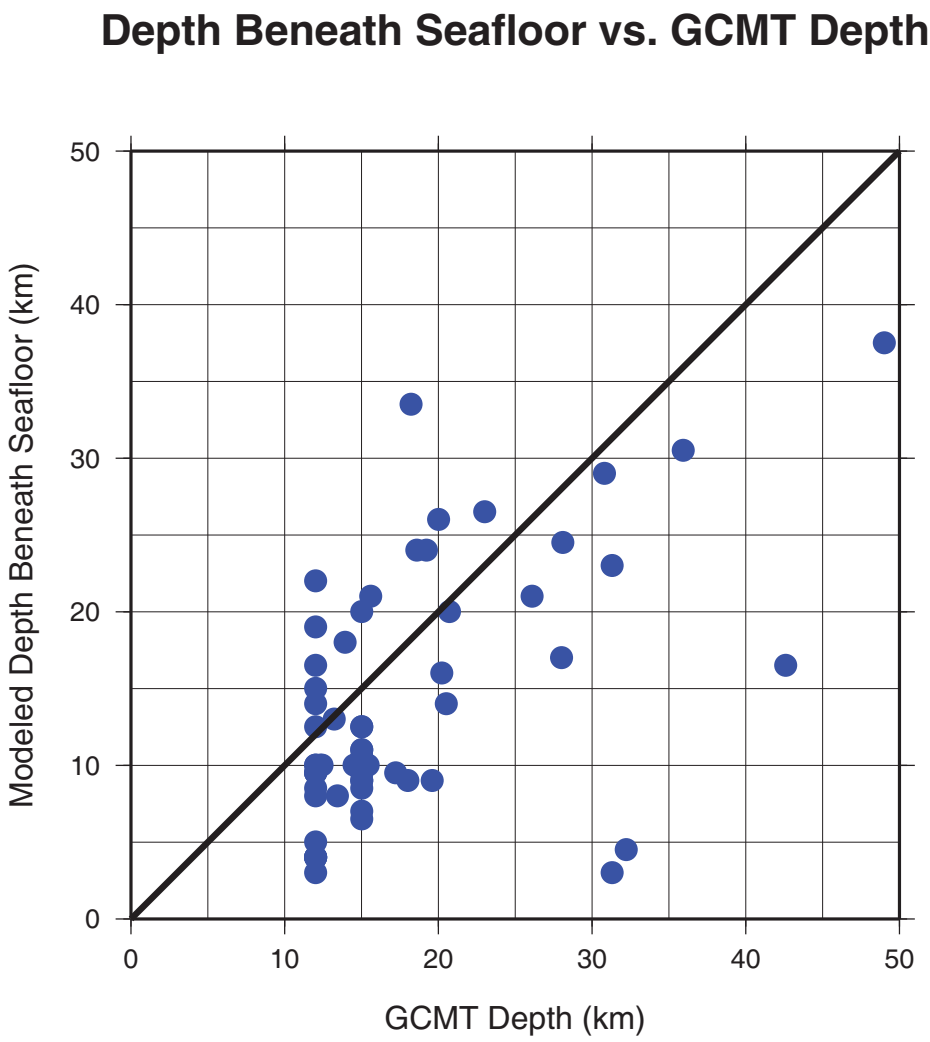

Figure 3 – Modeled depths vs. CMT depths

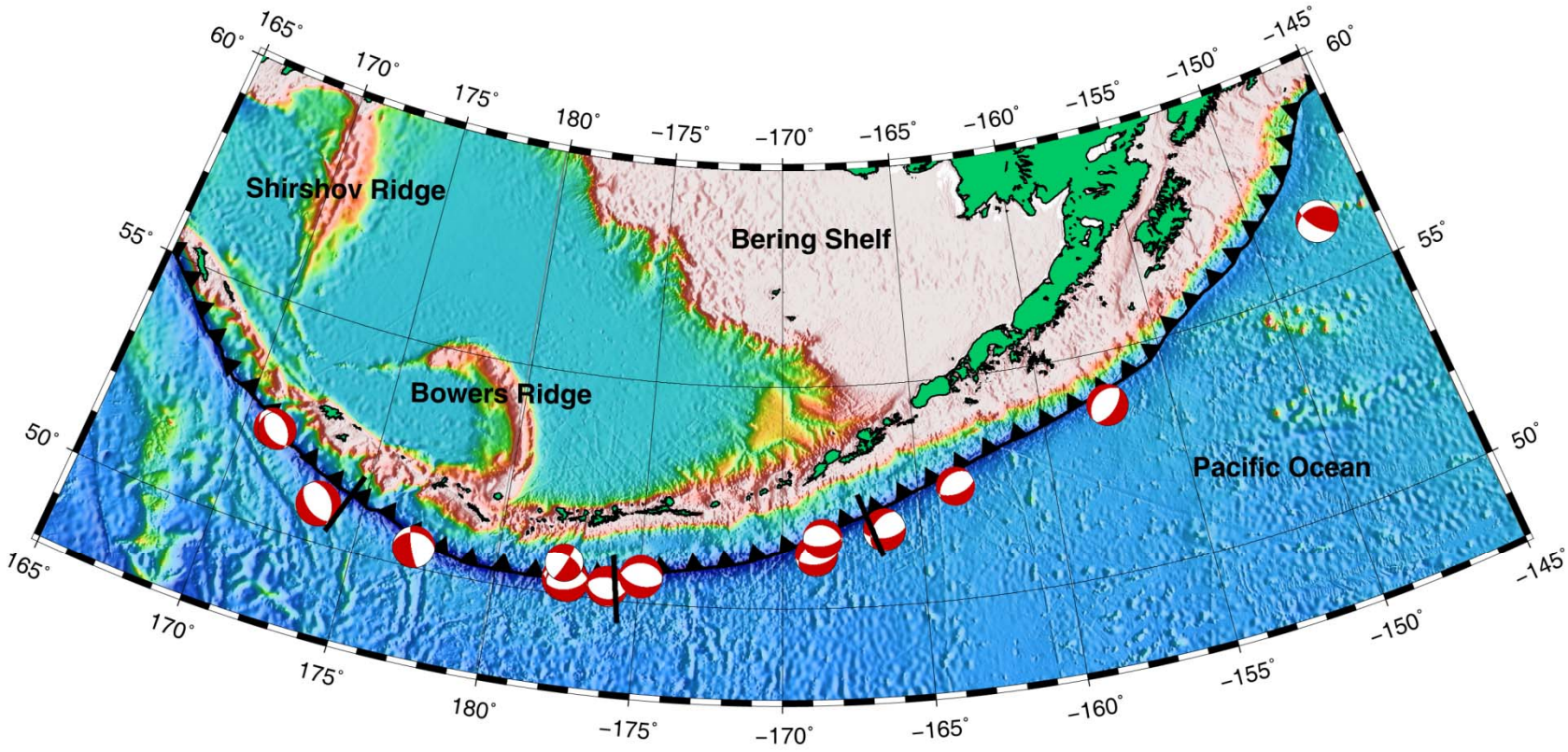

Figure 4 – Map of Alaskan and Aleutian Trench Seismicity

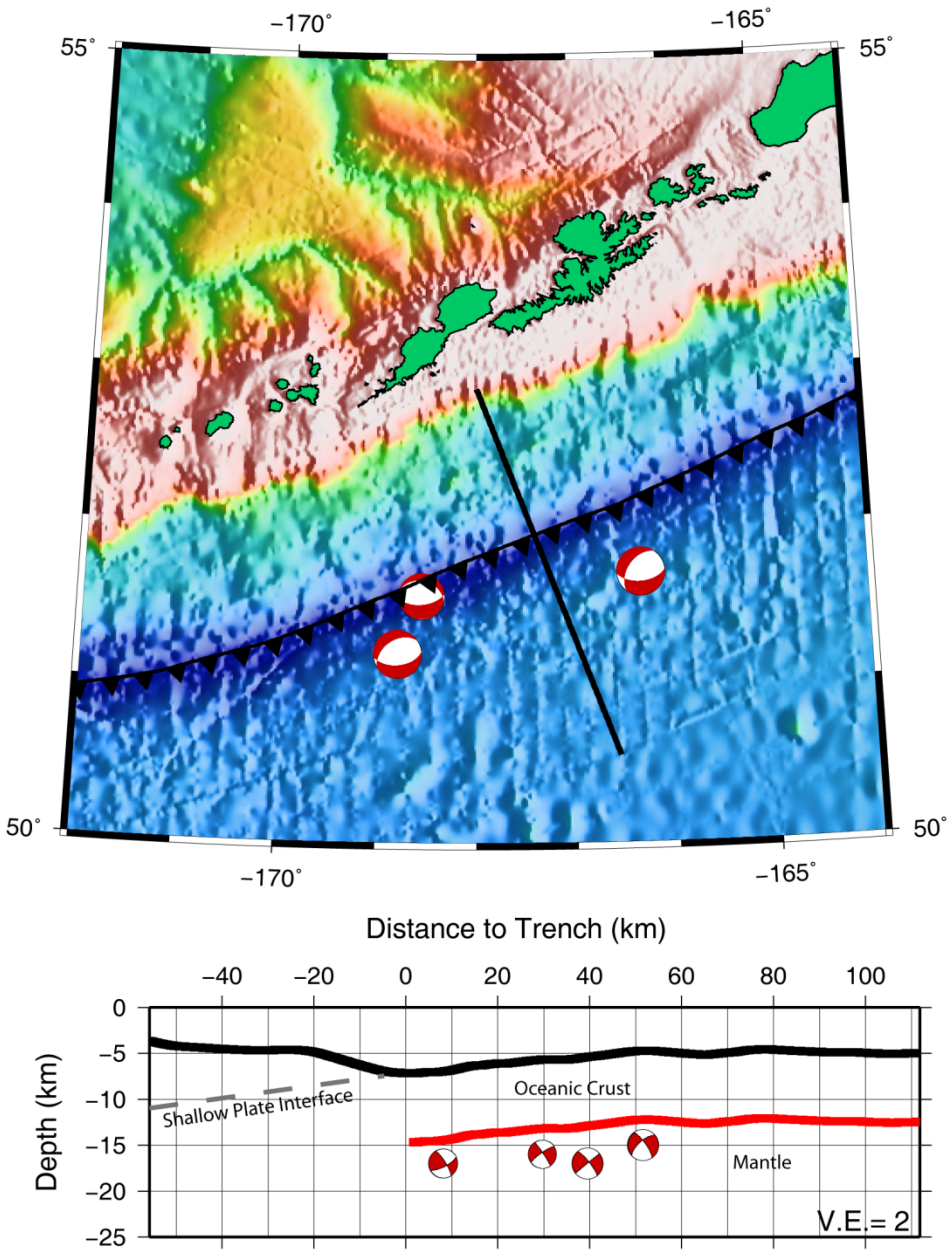

Figure 5 – Fox Islands: Map and Cross-Section

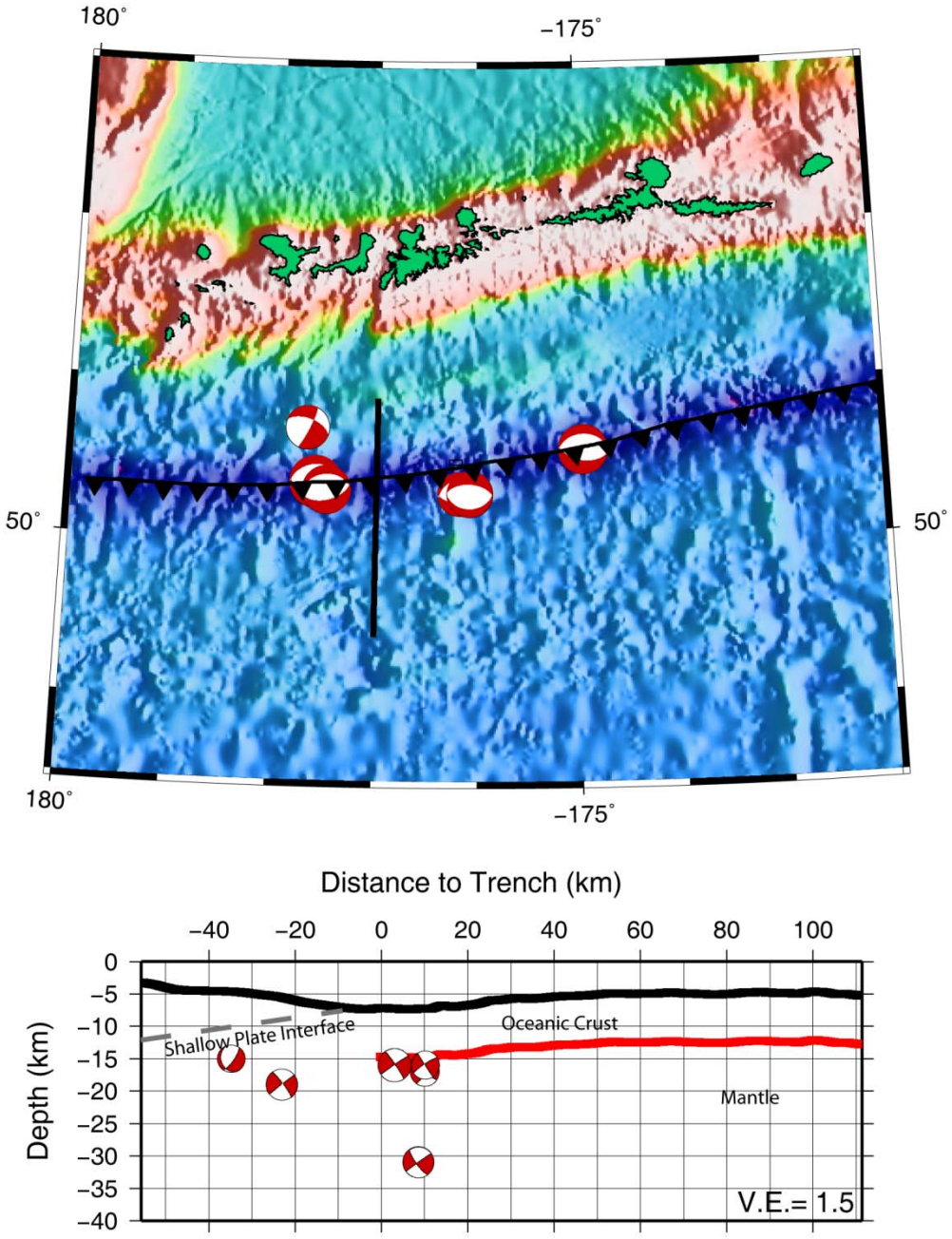

Figure 6 - Andreanof Islands: Map and Cross-Section

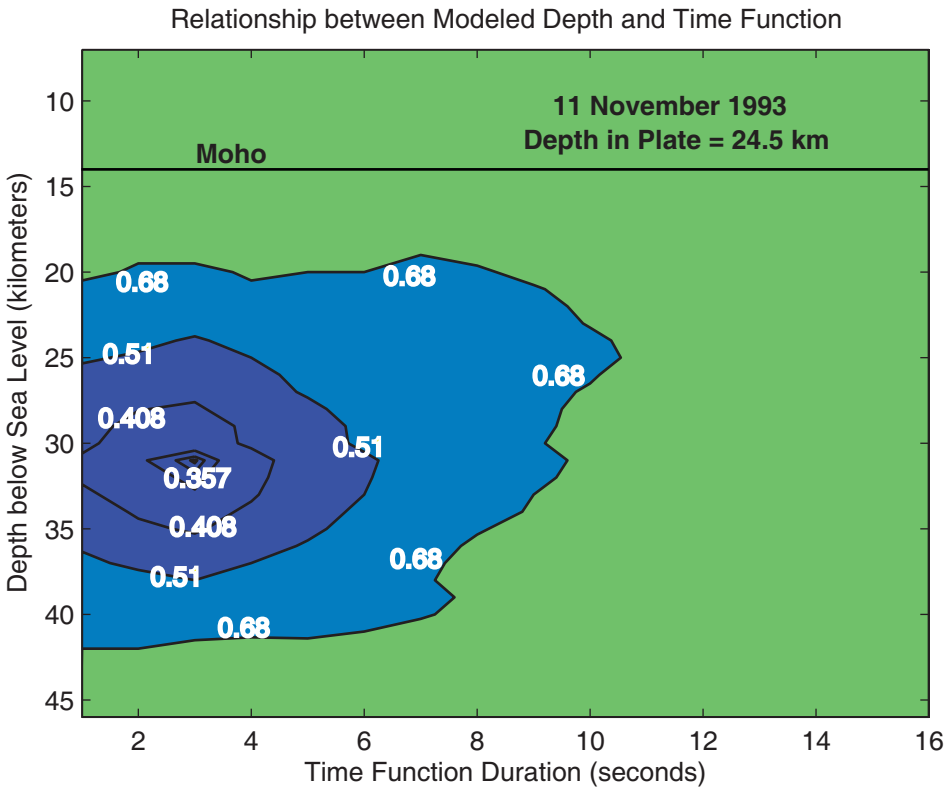

Figure 7 – Misfit Contours for 11 November 1993 Event

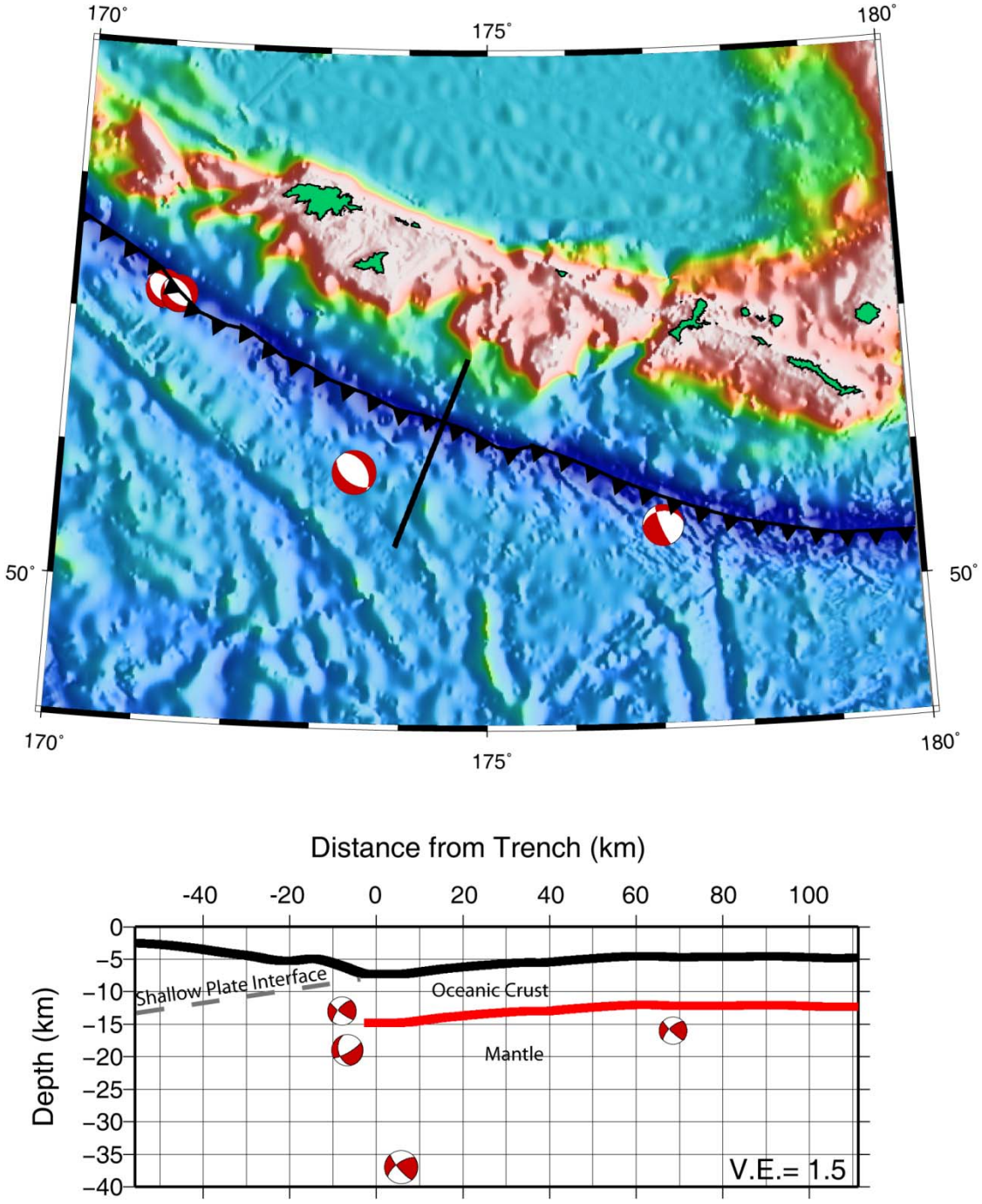

Figure 8 - Near and Rat Islands: Map and Cross-Section

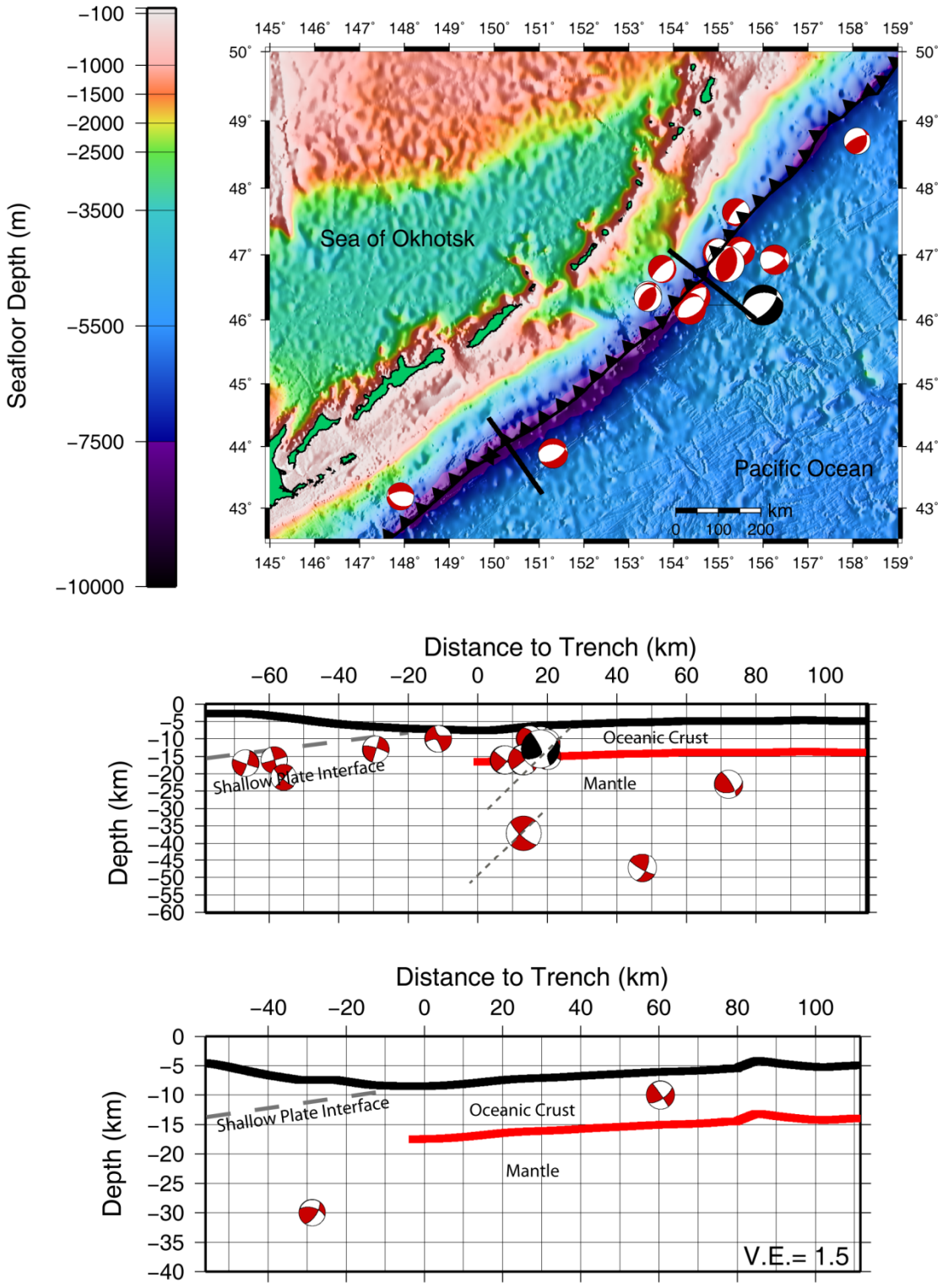

Figure 9 – Kuril Trench: Map and Cross-Section

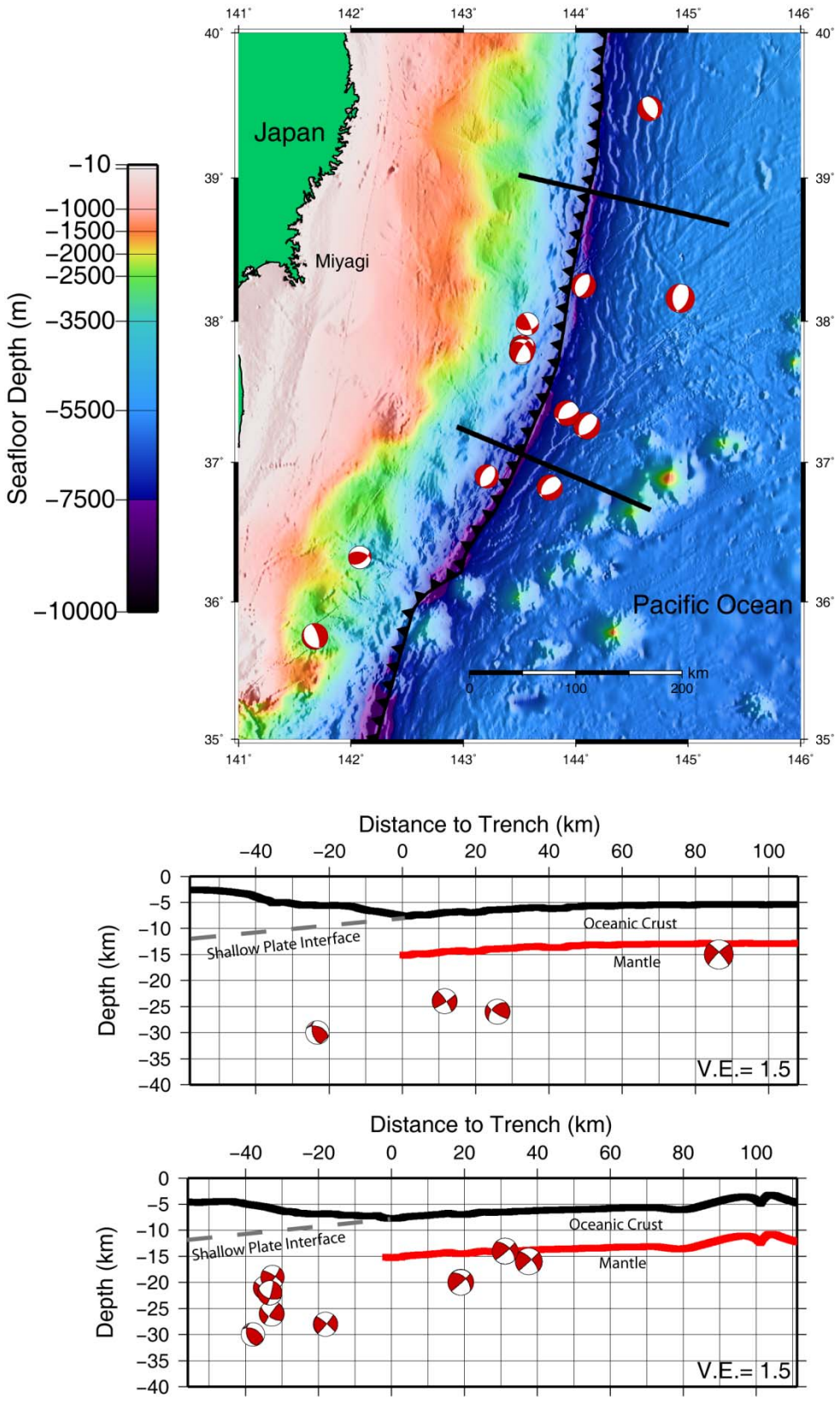

Figure 10 – Northern Japan: Map and Cross-Section

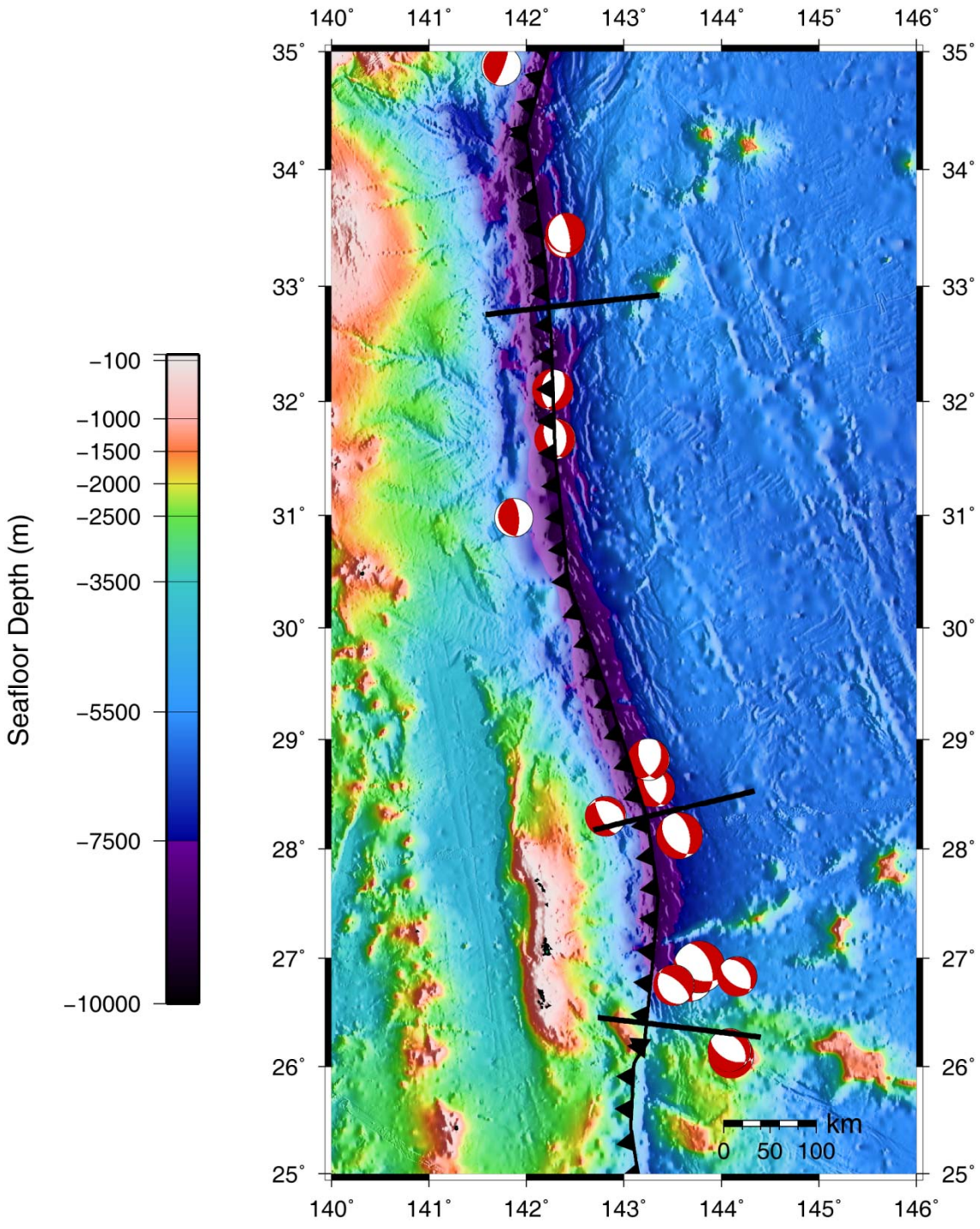

Figure 11 – Map of Izu-Bonin Trench Seismicity

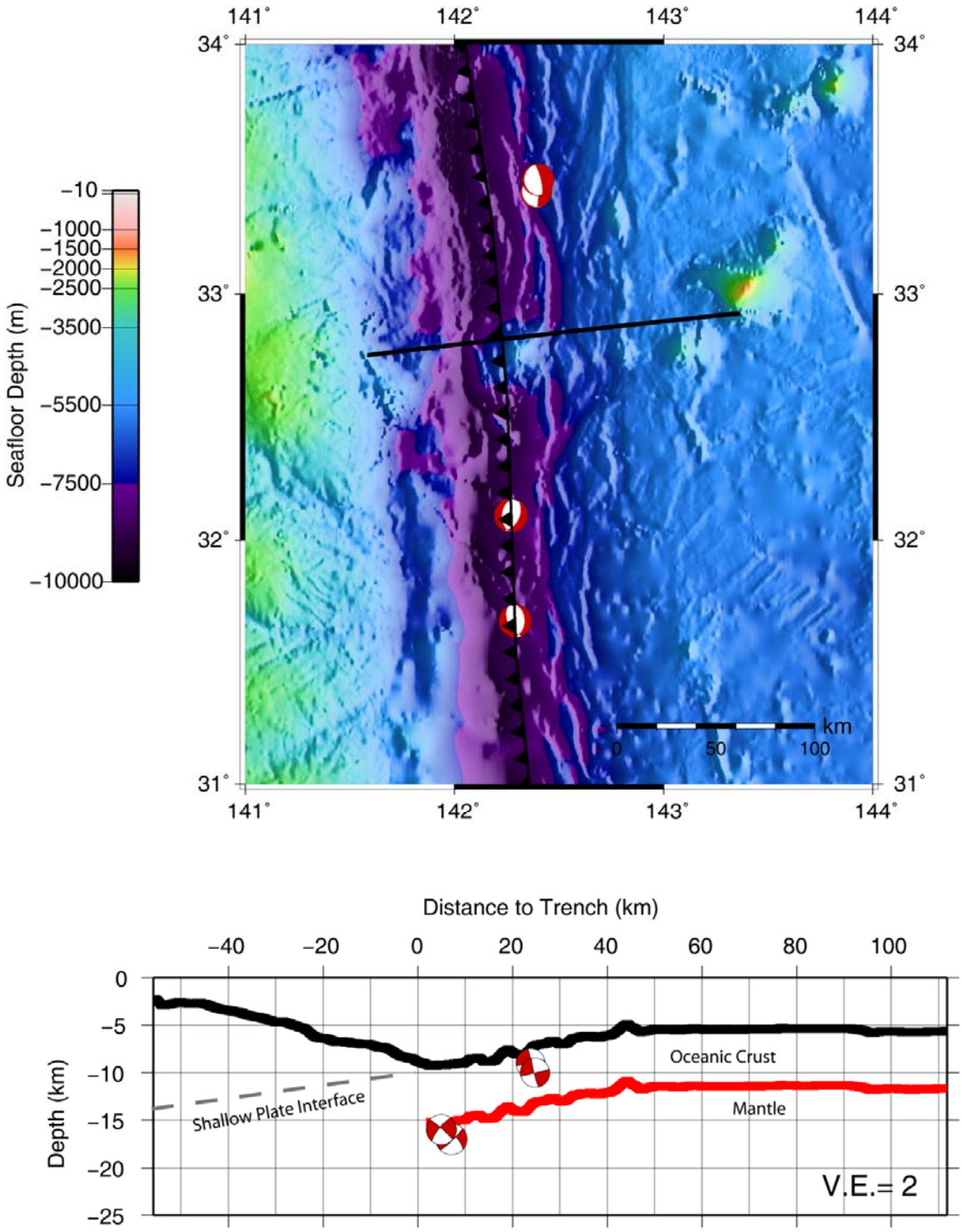

Figure 12 – Izu: Map and Cross-Section

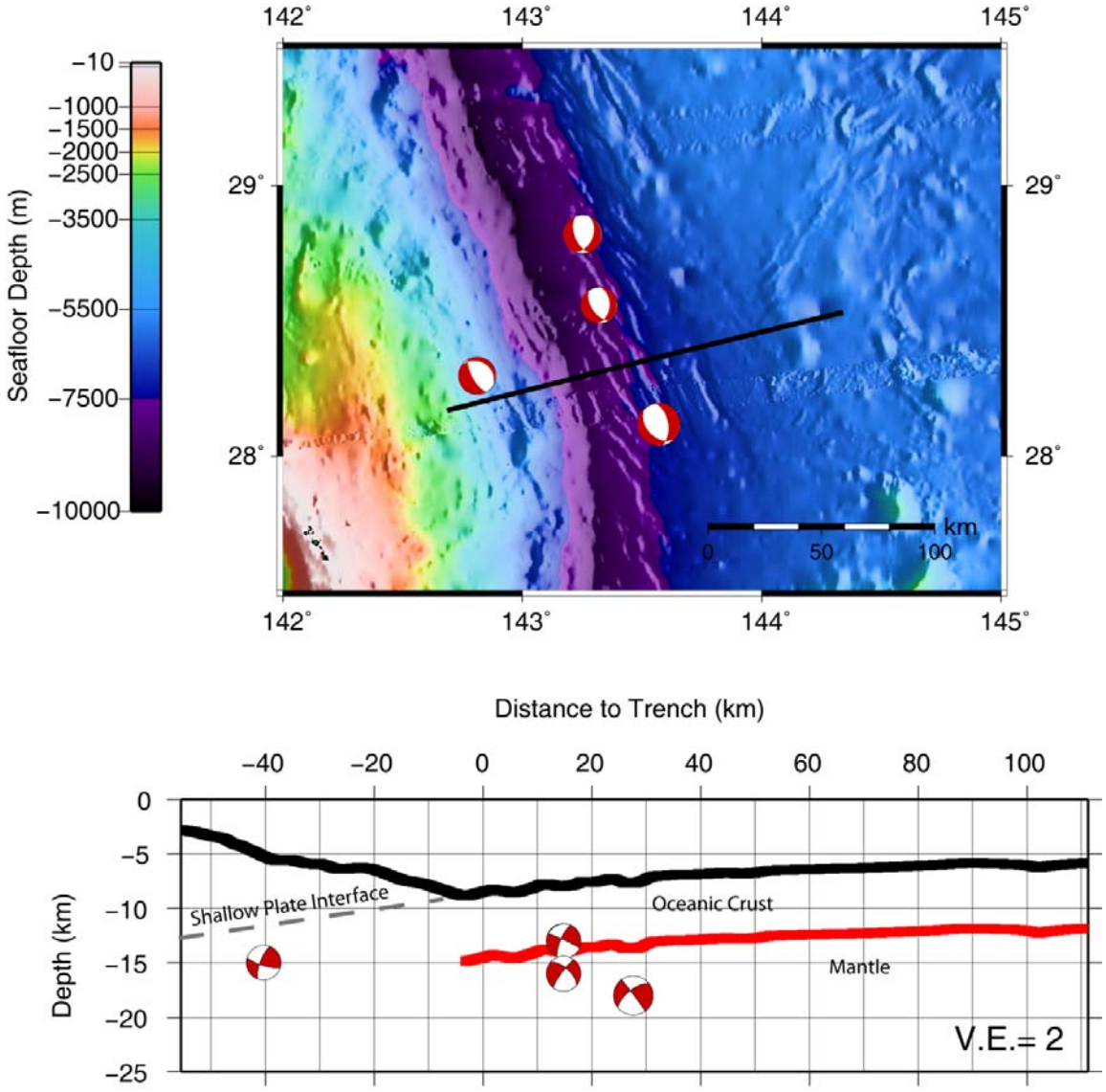

Figure 13 - Northern Bonin: Map and Cross-Section

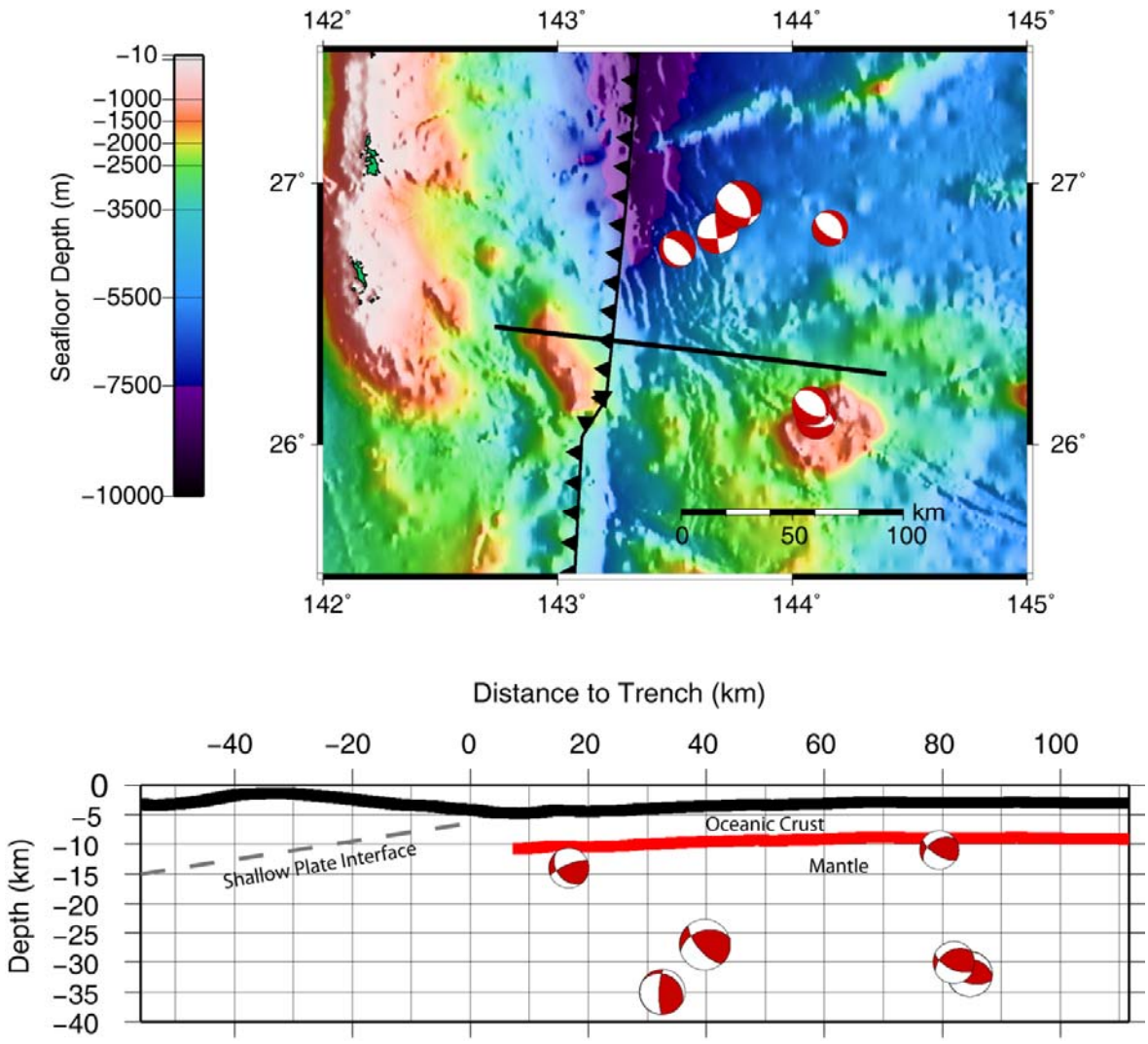

Figure 14 - Southern Bonin: Map and Cross-Section

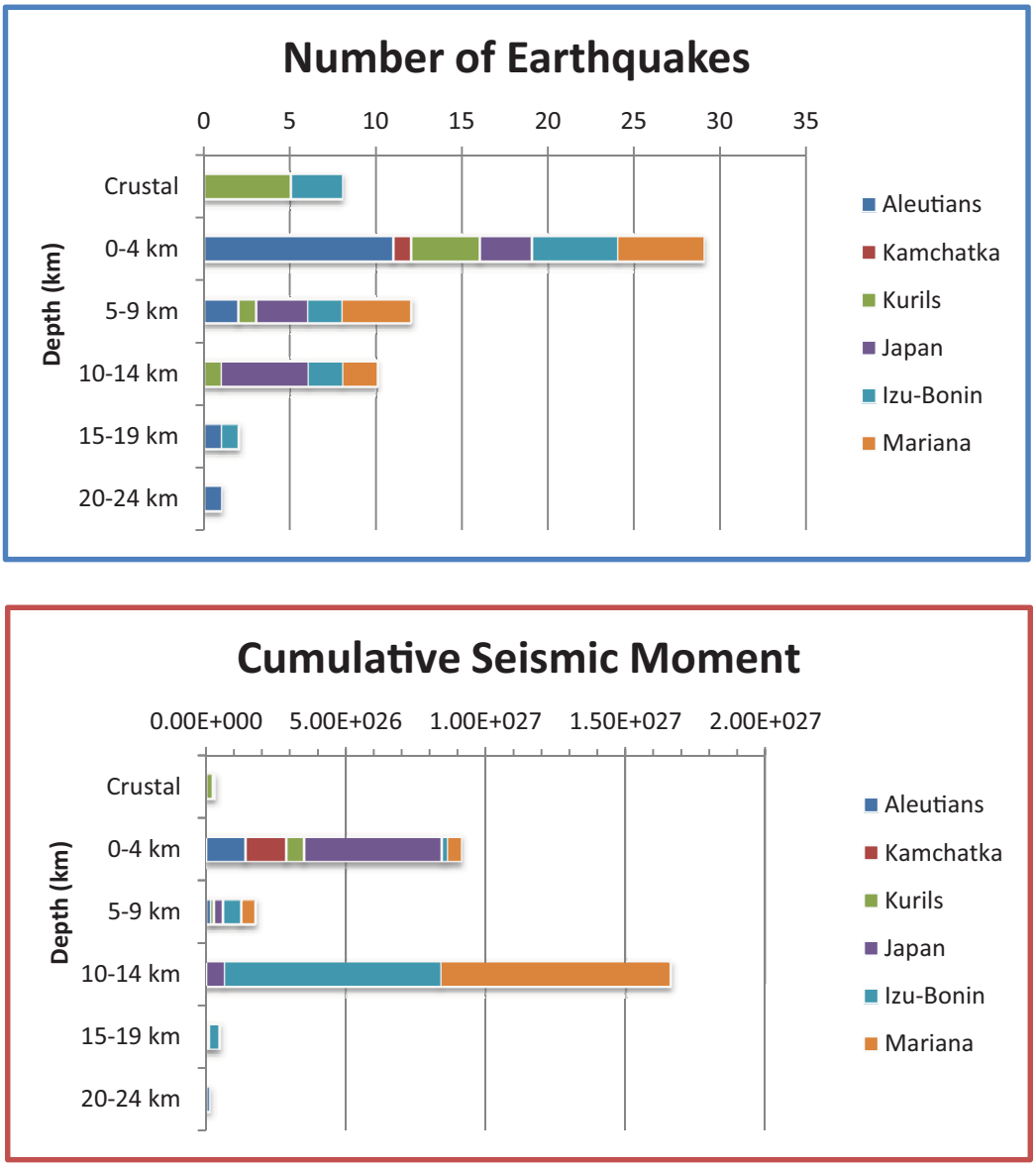

Figure 15 – Depth of Extensional Earthquakes: Histogram

CHAPTER 5

CONCLUSIONS

This research makes clear that the state of stress along the shallow plate interface and within the outer rise of subduction zones is not only necessary to understand earthquake and tsunami hazard at subduction zones, but it also informs our understanding of mechanisms of earthquake nucleation and slip, our understanding of the materials present at depth within the subduction zone mantle wedge, and our understanding of material transport into the subduction zone and even into the Earth's deep mantle.

In chapter 2, I have used the presence of very small earthquakes and their sense of slip to help us understand more about how some subduction zones may or may not be susceptible to great, tsunamigenic, disastrous slip along the shallow plate boundary. Results from this project have illustrated that the subduction zone plate interface at the Northern Mariana Subduction Zone exhibits significant variation along the strike of the subduction zone; this observation may help us to better understand if the Marianas is in fact 'aseismic' and if so, why this aseismicity might exist. Furthermore, the presence of these earthquakes provides us with a better understand of the materials present and their behavior at depth within the mantle wedge and plate interface.

In chapter 3, I have studied moderate-sized outer rise earthquakes which occur along the length of the Mariana Subduction Zone. Along the length of the subduction zone, I identify patterns of purely tension in the outer rise and a region where both tension and compression occur in the outer rise. This observation is significant, particularly in regards to issues of plate interface coupling, stress within the outer rise,

and potential for great damaging earthquakes at this subduction zone. Accurate depths for these outer rise events allow us to better constrain models for stress distribution within the bending plate and whether additional regional compression is necessary to explain the pattern exhibited by the earthquakes. The understanding of stress within the outer rise not only allows us to better understand seismic hazard at the subduction zone, but it also helps us to image the depth to which extensional faulting occurs. This extensional faulting may be a key contributor to hydration of the bending plate prior to subduction and transport of water into the Earth.

In chapter 4, I have explored the seismicity of the outer rise at several Northern and Western Pacific Basin subduction zones in order to better understand the depth extent to which extension occurs within the bending plate prior to subduction. As discussed for the Mariana outer rise, this extensional faulting is a major contributor to the subduction of water into the Earth and is unconstrained for at most subduction zones. This research resolves that extension occurs at least in the top 10-15 km of the bending oceanic plate. If this entire region within the bending plate is hydrated to that depth, then significantly more water may be input into subduction zones than previously thought. Furthermore, if this water is transported beyond the subduction zone and into the deep Earth, it has important implications for what we know about the evolution of our Earth through time.